PRELIMINARY

CENTER FOR VOLCANIC AND TECTONIC STUDIES[1]
DEPARTMENT OF GEOSCIENCE

University of Nevada, Las Vegas
Las Vegas, Nevada 89154

Report No. 41

ANNUAL REPORT for the Period 10/1/89 to 9/30/90 Submitted to
the Nuclear Waste Project Office
State of Nevada

November 1, 1990

RECEIVED
NOV 27 1990
NUCLEAR WASTE PROJECT OFFICE

[1]Eugene I. Smith-Principal Investigator
Daniel Feuerbach-Research Associate
Terry Naumann-Research Associate
James E. Faulds, Research Associate
Tracey Cascadden, Research Assistant

TABLE OF CONTENTS

INTRODUCTION 6

STRUCTURAL FRAMEWORK OF THE YUCCA MOUNTAIN/CRATER FLAT REGION, NEVADA: POSSIBLE CONTROLS ON PLIOCENE/QUATERNARY VOLCANISM NEAR THE PROPOSED HIGH-LEVEL RADIOACTIVE WASTE REPOSITORY 8

INTRODUCTION 8

REGIONAL SETTING 9

STRUCTURAL FRAMEWORK OF THE YUCCA MOUNTAIN/CRATER FLAT 12

TIMING OF DEFORMATION 16

PLIOCENE/QUATERNARY VOLCANISM 19

DISCUSSION 21

REFERENCES CITED 28

CRATER FLAT 35

CONTENT OF THIS REPORT 35

INTRODUCTION 35

THE 1.1 Ma CYCLE 36

THE 3.7 Ma CYCLE 42

10.5 Ma BASALT 43

GEOCHEMISTRY AND GEOCHRONOLOGY 43

ISOTOPES 46

GEOCHRONOLOGY 47

REFERENCES 48

FORTIFICATION HILL AND CALLVILLE MESA VOLCANIC FIELDS 49

INTRODUCTION 49

GEOLOGIC SETTING 51

VOLCANOLOGY AND STRATIGRAPHY 53

PETROGRAPHY 59

MINERAL CHEMISTRY 61

GEOCHEMISTRY 62

DISCUSSION AND PRELIMINARY MODELS FOR THE EVOLUTION OF THE MAGMA 64

ISOTOPIC STUDIES 69

REFERENCES 70

MAGMATISM, EXTENSIONAL TECTONICS AND SEDIMENTATION IN THE LAKE MEAD AREA, NEVADA AND ARIZONA: A NEW MODEL 77

INTRODUCTION 77

MAGMATISM, EXTENSION AND SEDIMENTATION 78

IMPLICATIONS OF MODEL 81

ACKNOWLEDGMENTS 81

REFERENCES CITED 81

GEOLOGY AND GEOCHEMISTRY OF PLIOCENE BASALTS IN THE REVEILLE RANGE, CENTRAL NEVADA 83

ABSTRACT 83

INTRODUCTION 83

VOLCANIC CENTERS AND STRATIGRAPHY 85

PETROGRAPHY 86

MINERAL CHEMISTRY 88

GEOCHEMISTRY 89

ISOTOPIC ANALYSIS 91

REFERENCES 92

THE EASTERN BOUNDARY OF THE EXTENSIONAL ALLOCHTHON IN THE EASTERN BASIN AND RANGE: VOLCANIC AND STRUCTURAL GEOLOGY OF THE NORTHERN WHITE HILLS, ARIZONA.

..... 92

APPENDIX I AND II 94

QUICK REFERENCE TABLE OF CONTENTS

INTRODUCTION 6

STRUCTURAL FRAMEWORK OF THE YUCCA MOUNTAIN/CRATER FLAT REGION, NEVADA: POSSIBLE CONTROLS ON PLIOCENE/QUATERNARY VOLCANISM NEAR THE PROPOSED HIGH-LEVEL RADIOACTIVE WASTE REPOSITORY 8

CRATER FLAT 35

FORTIFICATION HILL AND CALLVILLE MESA VOLCANIC FIELDS 49

MAGMATISM, EXTENSIONAL TECTONICS AND SEDIMENTATION IN THE LAKE MEAD AREA, NEVADA AND ARIZONA: A NEW MODEL 77

GEOLOGY AND GEOCHEMISTRY OF PLIOCENE BASALTS IN THE REVEILLE RANGE, CENTRAL NEVADA 83

THE EASTERN BOUNDARY OF THE EXTENSIONAL ALLOCHTHON IN THE EASTERN BASIN AND RANGE: VOLCANIC AND STRUCTURAL GEOLOGY OF THE NORTHERN WHITE HILLS, ARIZONA 92

INTRODUCTION

This report summarizes our activities during the period October 1, 1989 to September 30, 1990. Our goal was to develop an understanding of late-Miocene and Pliocene volcanism in the Great Basin by studying Pliocene volcanoes in the vicinity of the proposed high-level nuclear waste repository at Yucca Mountain, Nevada. Field studies during this period concentrated on the Quaternary volcanoes in Crater Flat, Yucca Mountain, Fortification Hill, at Buckboard Mesa and Sleeping Butte, and in the Reveille Range. Also, a study was initiated on structurally disrupted basaltic rocks in the northern White Hills of Mohave County, Arizona.

As well as progress reports of our work in Crater Flat, Fortification Hill and the Reveille Range, this paper also includes a summary of model that relates changing styles of Tertiary extension to changing magmatic compositions, and a summary of work being done in the White Hills, Arizona. In the Appendix, we include copies of published papers not previously incorporated in our monthly reports.

In this annual report we:

(1) address several aspects of the structural framework of Yucca Mountain that have formerly received little attention. These include evidence for a protracted period of extension from Oligocene time to present, slip data from major normal faults, assessment of strain rates, possible explanations for the en echelon pattern of normal faults and attendant sharp displacement gradients, and potential structural controls on Pliocene/Quaternary volcanoes. Finally, we consider the possible implications of these data on the proposed high-level nuclear waste repository.

(2) provide new geochemical data for the Fortification Hill field that documents the transition from older subalkalic to younger alkalic volcanism. This transition occurred between 5.71 and 5.42 Ma and may reflect a change from lithospheric to asthenospheric mantle sources with time. This change may reflect lithospheric erosion due to regional extension.

(3) propose a four stage model for the late-Tertiary (18-4.7 Ma) evolution of the Lake Mead area, Nevada and Arizona that relates extensional style, magmatism and sedimentation.

(4) report on the results of a detailed stratigraphic, petrologic and geochemical investigation of alkali basalts from the Reveille Range, Nevada. Major, trace and rare-earth element geochemistry was determined on 62 samples collected from a stratigraphic section defined on the basis of geologic mapping and K-Ar dating. Alkali-basalt lavas occur as shallow intrusions, domes, flow stacks up to 100 m thick and over 50 dissected cinder cones. Activity spans 3 million years, beginning with alkali basalts and hawaiites erupted between 5.9 and 5.1 Ma (Episode 1), followed by a smaller volume of lava ranging in composition from picrite to trachybasalt that erupted between 4.6 and 3.0 Ma (Episode 2). Explosive eruptions of trachyte and tristanite occurred at 4.4 and 4.2 Ma. Geochemical modeling indicates that lavas formed through a process of partial melting of asthenospheric mantle with small amounts of crustal contamination.

(5) describe late-Tertiary volcanism along the eastern boundary of the extensional allochthon in the White Hills, Arizona.

(6) present a review of our work in Crater Flat. This report duplicates information presented the CVTS annual report for 1989. We believed that it would be beneficial to include this text because of the intense interest in the origin of Crater Flat and large number of additional individuals now involved in the evaluation of the Yucca Mountain site who have not read this contribution. This contribution also reviews the work of the CVTS in Crater Flat during 1989-90.

STRUCTURAL FRAMEWORK OF THE YUCCA MOUNTAIN/CRATER FLAT REGION, NEVADA: POSSIBLE CONTROLS ON PLIOCENE/QUATERNARY VOLCANISM NEAR THE PROPOSED HIGH-LEVEL RADIOACTIVE WASTE REPOSITORY

(James E. Faulds)

INTRODUCTION

Investigations to assess the suitability of Yucca Mountain, Nevada, as a site for the permanent isolation of high-level radioactive waste began in 1977. In 1987, the U.S. Congress mandated the termination of studies at other sites, leaving Yucca Mountain as the only potential high-level repository under investigation. Yucca Mountain lies 140 km northwest of Las Vegas, Nevada, on the extreme western margin of the Nevada test site and approximately 50 km north-northeast of Death Valley, California. Crater Flat is a small intermontane basin directly west of Yucca Mountain that contains several Pliocene to Quaternary basaltic volcanic complexes.

This paper focuses on the detailed structural evolution of the Yucca Mountain/Crater Flat area and possible structural controls on Pliocene/Quaternary volcanism. On the basis of geologic mapping, structural analysis, and a synthesis of

previous investigations, we address several aspects of the structural framework that have formerly received little attention. These include evidence for a protracted period of extension from Oligocene time to present, slip data from major normal faults, assessment of strain rates, possible explanations for the en echelon pattern of normal faults and attendant sharp displacement gradients, and potential structural controls on Pliocene/Quaternary volcanoes. Finally, we consider the possible implications of these data on the proposed high-level nuclear waste repository.

REGIONAL SETTING

A series of generally north-south-trending, gently east-tilted fault blocks, which are bounded by west-dipping normal faults, constitute the Yucca Mountain/Crater Flat region (Scott and Bonk, 1984; Carr, 1988; Scott, 1990). The fault blocks are largely composed of Miocene tuffs, which range in age from 14.5 to 11.3 Ma (Scott and Bonk, 1984; Carr, 1988). The tuffs, which locally exceed 3 km in thickness, accumulated within a large volcano-tectonic depression, consisting of several nested calderas, within the southern part of the southwestern Nevada volcanic field (Byers and others, 1976b; Christiansen and others, 1977; Carr, 1988). The southwestern Nevada volcanic field occupies a region of right-stepping in the Walker Lane belt (Carr, 1984) (Fig. 1), which corresponds to a 75 to 125-km-wide northwest-trending zone of dominantly dextral displacement (Carr, 1984; Stewart, 1986). Tertiary and Quaternary rocks in the Yucca Mountain/Crater Flat region have been mapped and described by Christiansen and Lipman (1965), Lipman and McKay (1965), McKay and Sargent (1970), Orkild and

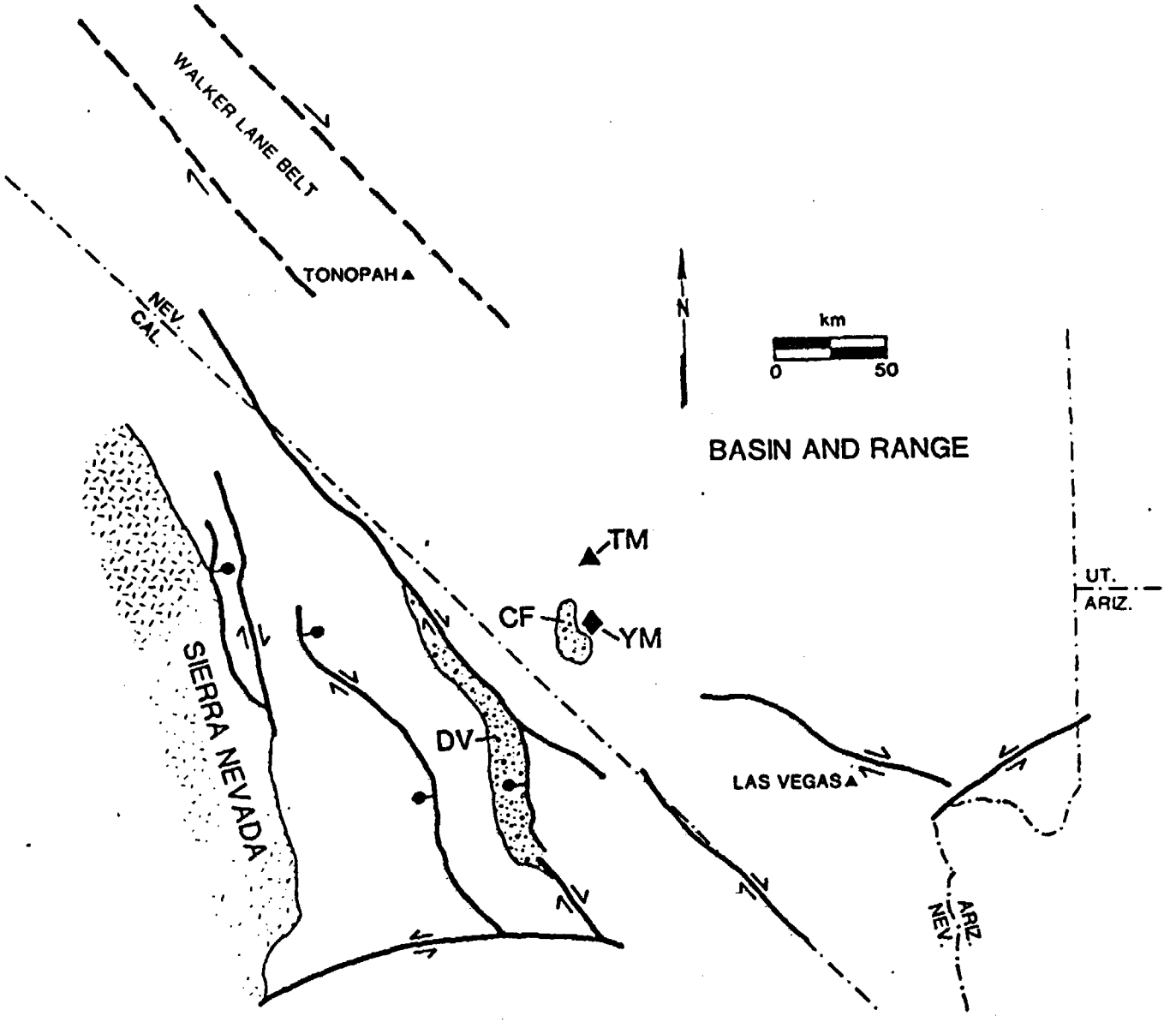

Figure 1. Regional geologic map showing major normal fault systems (e.g., Bullfrog Hills detachment system), strike-slip faults, southwest Nevada volcanic field, Yucca Mountain, Bare Mountain, and extension direction.

O'Connor (1970), Byers and others (1976a); Christiansen and others (1977); Scott and Bonk (1984), Swadley and others (1984); Swadley and Carr (1987), Maldonado (1985), Scott (1990), and Faulds and Feuerbach (in prep.). The Miocene rocks presumably rest on folded and thrust-faulted Proterozoic and Paleozoic sedimentary and metamorphic rocks, similar to that exposed at Bare Mountain (e.g., Carr and Monsen, 1988) (Fig. 1).

Extension in the Yucca Mountain region probably began during Oligocene time (Schweickert and Caskey, 1990) and has continued, perhaps episodically, to the present. The regional extension direction has apparently rotated from west-southwest/east-northeast in early to middle Miocene time to northwest/southeast in late Miocene to Quaternary time (Zoback and others, 1981; Stock and Healy, 1988; Wernicke and others, 1988).

During late Cenozoic time, Yucca Mountain has bordered one of the most tectonically active parts of the Basin and Range province on the north and east. Less than 20 km west of Yucca Mountain, the Bullfrog Hills area experienced more than 100% extension 8 to 10 Ma, including unroofing of middle Miocene mylonites (Maldonado, 1990). Moreover, to the southwest of Yucca Mountain in the Death Valley region, a system of kinematically related normal and predominantly dextral strike-slip faults has accommodated many kilometers of displacement since middle Miocene time (Wright and others, 1974; Burchfiel and others, 1987; Butler and others, 1988; Wernicke and others, 1988), denuding some of the youngest and possibly deepest structural levels of Cordilleran metamorphic core complexes (Holm and Wernicke, 1990). Stewart (1983) proposed that during late Cenozoic time the Panamint Range was translated 80 km

northwestward along gently west-dipping normal faults from an original position atop the Black Mountains. Wernicke and others (1988) suggested that the Panamint, Nopah, and Resting Springs Ranges restore into a narrow crustal sliver less than 10 km wide adjacent to the Spring Mountains. Most of the dismemberment of this narrow crustal sliver in the western part of the Death Valley region probably occurred since 4 Ma (Wernicke and others, 1986, 1988; Burchfiel and others, 1987; Butler and others, 1988). Although minimized by other interpretations (Prave and Wright, 1986; Wright and Troxel, 1973) and observed geometries on seismic reflection profiles (Serpa and others, 1988), large-magnitude extension of the Death Valley region in late Cenozoic time is not disputed. The Death Valley region may represent the only region in the Basin and Range province where recent strain rates have been sufficient to unroof mylonites as young as late Miocene in age (cf., Asmerom and others, 1990; Holm and Wernicke, 1990). Such high strain rates were more typical of the Basin and Range province during early to middle Miocene time.

Basaltic volcanism accompanied late Cenozoic extension in the Yucca Mountain/Crater Flat region (Fig. 2). Basaltic volcanic complexes in the immediate vicinity of Yucca Mountain include both Pliocene and Quaternary centers in Crater Flat and an isolated late Quaternary center directly south of Yucca Mountain (Vaniman and others, 1982; Smith and others, 1990; Wells and others, 1990) (Fig. 2). The Plio-Pleistocene volcanic centers in the Yucca Mountain/Crater Flat region represent a small fraction of post-6 Ma basaltic volcanism in the southern Great Basin and adjacent areas (Fig. 3). Ascertaining the structural controls on these volcanic centers may have

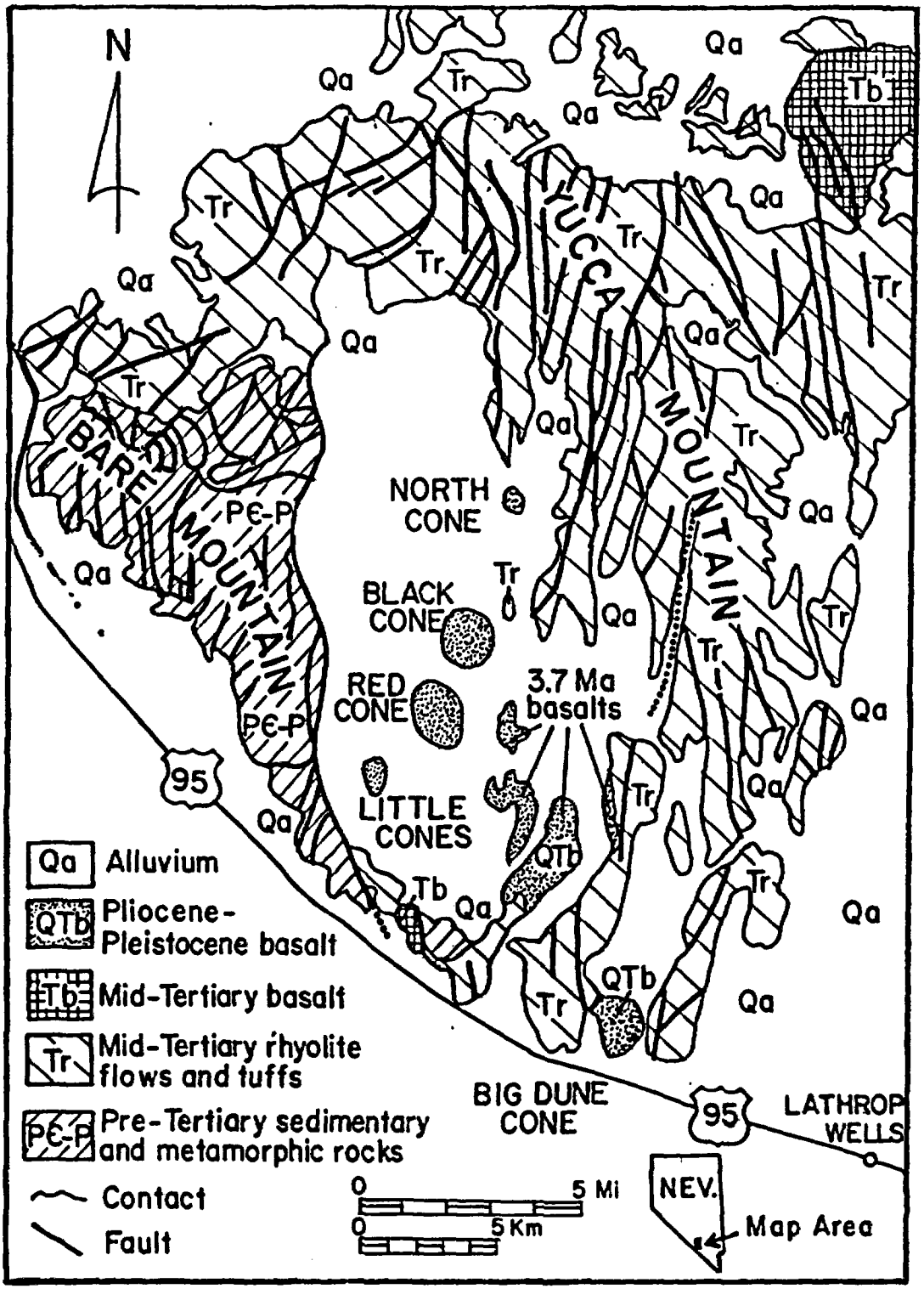

Figure 2. Generalized geologic map of Yucca Mountain/Crater Flat region showing Yucca Mountain, Crater Flat, Pliocene and Quaternary volcanic centers, major normal faults, Bare Mountain, Amargosa basin.

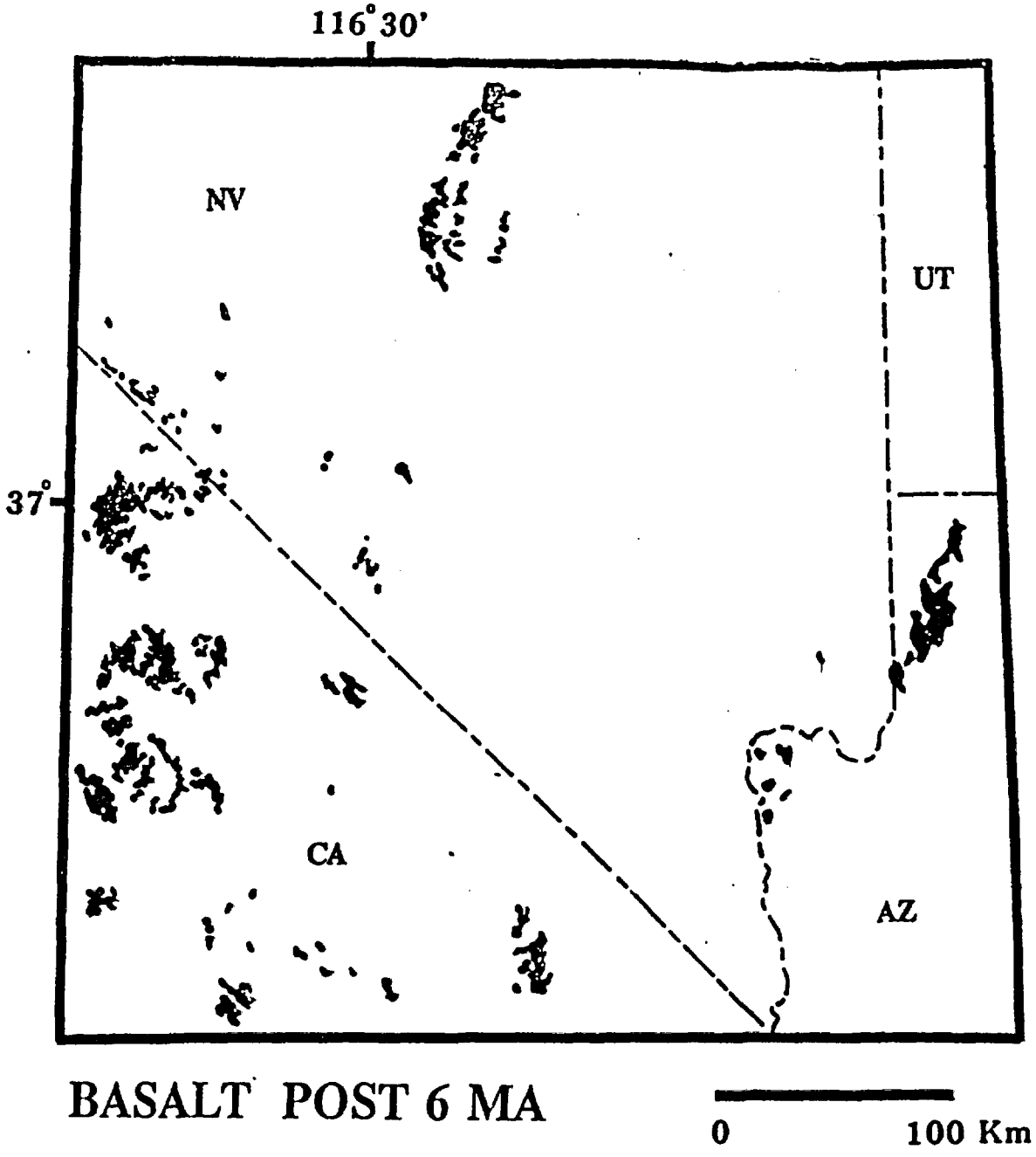

Figure 3. Distribution of post 6 Ma basalts.

important implications for assessing the potential volcanic hazard of the proposed repository site.

STRUCTURAL FRAMEWORK OF THE YUCCA MOUNTAIN/CRATER FLAT AREA

Closely-spaced, moderately to steeply dipping, north- to northeast-trending normal faults fragment Yucca Mountain into an array of relatively narrow fault blocks (Plate 1 and Fig. 4). The average fault attitude in the northwestern part of Yucca Mountain is N14°E, 68°NW (Fig. 5). Most faults dip westward and accommodate east-tilting, but east-dipping normal faults and west-tilted fault blocks characterize small areas. Stratal tilts generally range from 3 to 15°. Older units are more steeply tilted. The magnitude of tilting increases slightly to the south across Yucca Mountain commensurate with an increase in displacement on several major faults and decrease in average fault dip (Scott, 1986, 1990).

The faults are arranged in an en echelon pattern and display significant along-strike displacement gradients. In many cases, displacement varies by orders of magnitude either between or within individual fault segments. For example, displacement along a northeast-trending, west-dipping segment of the Windy Wash fault decreases from 300 m to 0 in less than 1.5 km (Figs. 4 and 5). Northeast-trending fault segments commonly link longer north-striking segments. Displacement does not vary systematically with fault trend. Minor northwest-trending dextral and northeast-trending sinistral strike-slip faults also cut Yucca Mountain (Scott and Whitney, 1987).

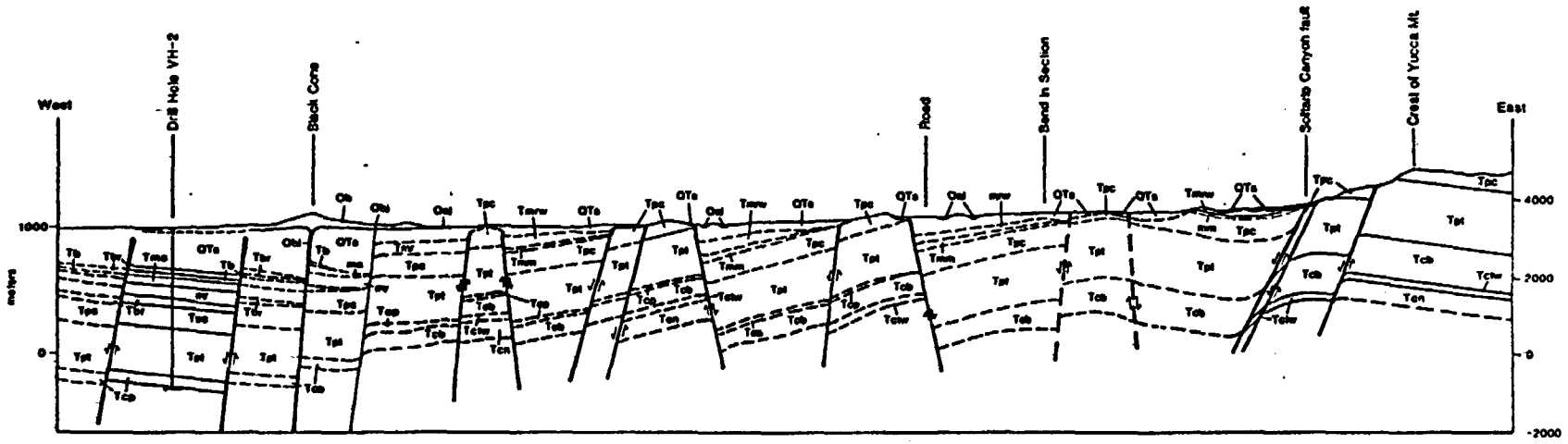

Figure 4. Cross sections of Yucca Mountain/Crater Flat area.

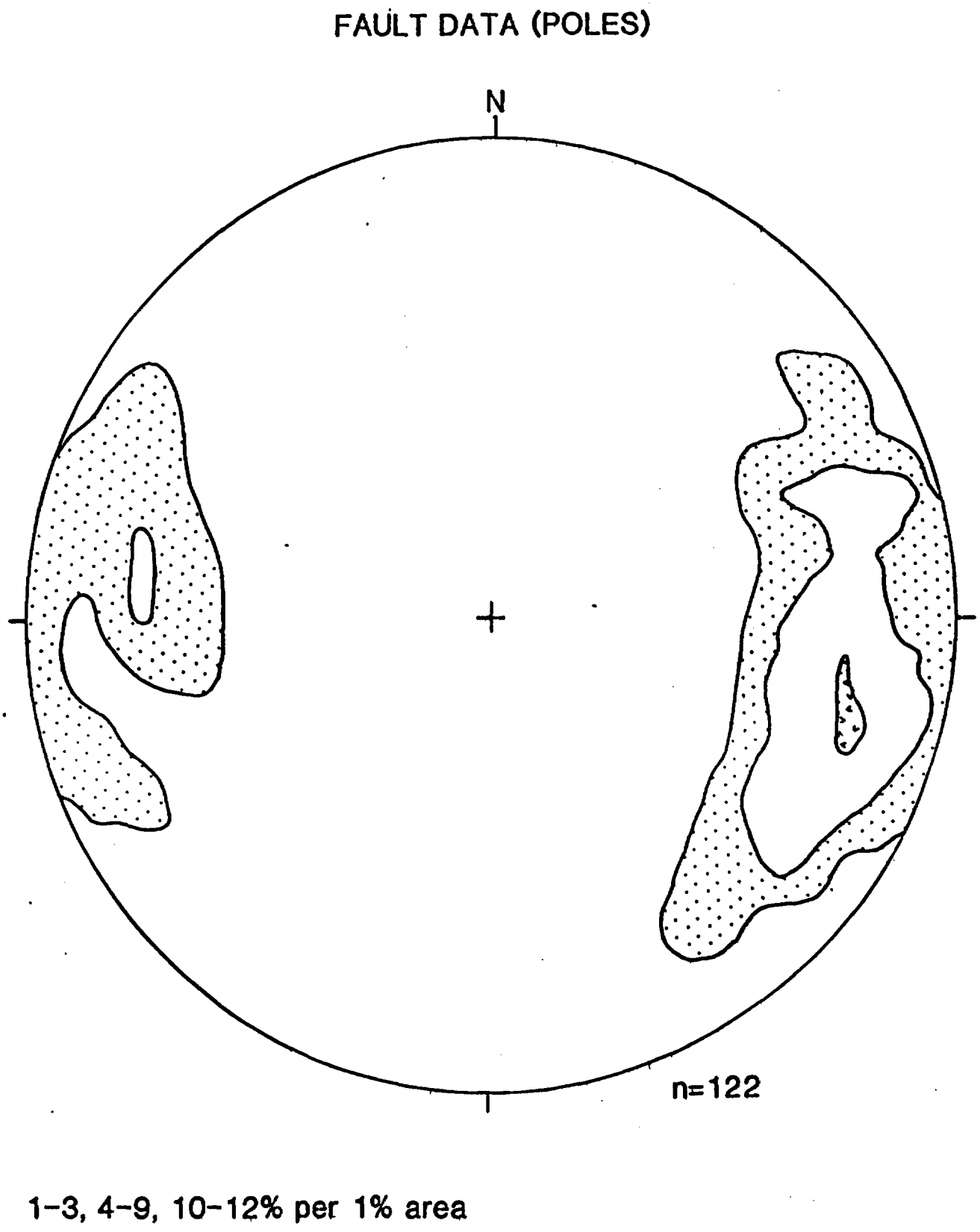

Figure 5. Poles to faults, northwestern Yucca Mountain.

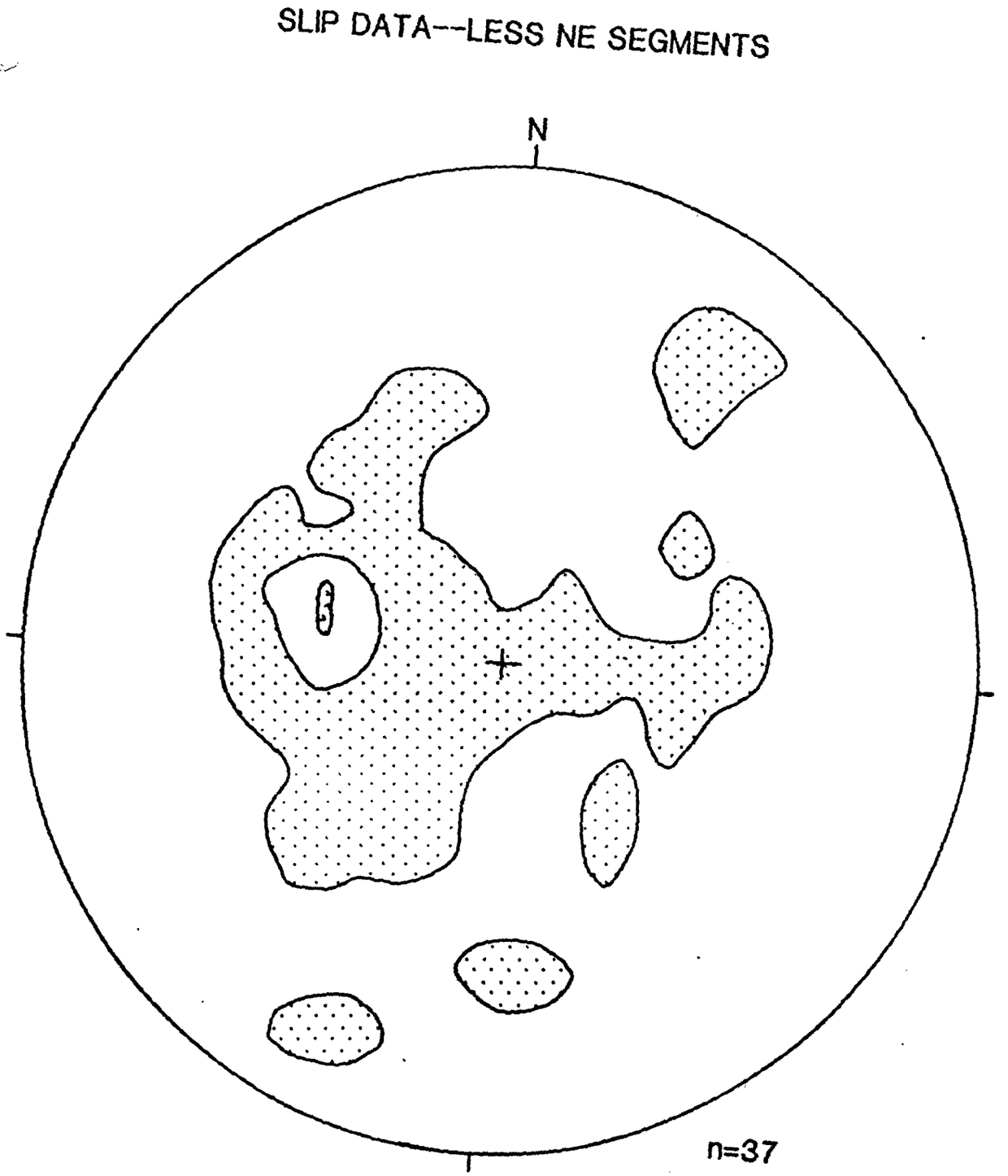

Figure 6. Sliplines, north-striking normal faults.

Northeast-striking faults and tilts increase in abundance southward across the Yucca Mountain/Crater Flat region. Paleomagnetic data from the 12.9 Ma Tiva Canyon Member of the Paintbrush Tuff indicate that the change in structural grain may result from approximately 30° of vertical-axis clockwise rotation of the southern part of Yucca Mountain relative to the northern part (Rosenbaum and Hudson, in press; Rosenbaum and others, in press). On the basis of 26 km of apparent right separation of a north- to northwest-vergent Mesozoic thrust and overturned fold system, Schweickert (1989) proposed that a major north-northwest-trending strike-slip fault in the vicinity of Amargosa Valley and Crater Flat may be responsible for the apparent clockwise rotation of Miocene strata. However, surface expressions of this fault have not been observed.

The margins of Yucca Mountain are irregular and poorly defined because of the lack of major range-front faults (Figs. 2 and 4). En echelon north- to northeast-striking, west-dipping normal faults flank Yucca Mountain on the west. To the east, several east-tilted ridges comprising Yucca Mountain project beneath Jackass Flats, which may correspond to a small half graben situated on the downthrown parts of the east-tilted Yucca Mountain structural blocks. As displacement on many faults decreases, Yucca Mountain merges northward with the Timber Mountain/Oasis Valley caldera complex, the source for much of the ash-flow tuff that forms Yucca Mountain (e.g., Byers and others, 1976b). The northwest-trending Amargosa basin borders Yucca Mountain on the south (Fig. 2).

Crater Flat is a structural depression that bounds Yucca Mountain on the west. Geologic mapping and drill core demonstrate that more than 1 km of structural relief

exists in the Miocene tuffs between the crest of Yucca Mountain and Crater Flat near Black Cone (Fig. 4). In addition, seismic-refraction (Ackermann and others, 1988) and gravity data (Snyder and Carr, 1984) have been interpreted to indicate that more than 2 km of relief exists on the prevolcanic surface. The depth of the prevolcanic surface ranges from 3.2 km beneath the center of Crater Flat to 1.3 km below southern Yucca Mountain. Drill core show that more than 360 m of late Tertiary to Quaternary sedimentary rocks locally accumulated within the Crater Flat basin (Carr and Parrish, 1985). Thus, the Miocene volcanic section in the central part of Crater Flat approaches 3 km in thickness, far exceeding that in the southern part of Yucca Mountain. Carr (1988) therefore concluded that the Crater Flat structural depression resulted primarily from middle Miocene caldera collapse related to the 14.5 Ma Crater Flat Tuff. However, the continuation of several normal faults in the northwestern part of Yucca Mountain into Crater Flat, where they cut Quaternary sediments (Swadley and others, 1984), and the Miocene stratigraphy displayed in two shallow drill holes in Crater Flat (Carr, 1982; Carr and Parrish, 1985) demonstrate that the bedrock geology of Yucca Mountain extends beneath the alluvial fill of Crater Flat. Crater Flat comprises a series of structurally depressed fault blocks that were buried by late Tertiary to Quaternary sedimentary and volcanic rocks rather than a discrete graben or half-graben. Whether this structural depression originated primarily through caldera collapse or the vagaries of displacement patterns on major normal faults is difficult to resolve without additional subsurface data.

The western margin of Crater Flat is defined by a discrete north-northwest-trending, east-dipping range-front normal fault, here referred to as the Bare Mountain fault. The depth of the prevolcanic surface in Crater Flat, as inferred from seismic-refraction data, suggest a minimum of 2600 m of Tertiary displacement along the Bare Mountain fault (Ackermann and others, 1988). The Bare Mountain fault has facilitated recurrent late Quaternary movements (Reheis, 1988). As displacement along the Bare Mountain fault decreases to the north and south, the Crater Flat basin terminates. Thus, the Bare Mountain fault appears to be the single most important feature controlling the location of the Crater Flat basin. Snyder and Carr (1984) suggested that the Bare Mountain fault may represent a reactivated ring-fracture zone of a "trap-door" type caldera situated in Crater Flat.

The gently west-dipping Bullfrog Hills detachment system bounds the Bare Mountain block on the west and north (Reynolds, 1986; Carr and Monsen, 1988; Maldonado, 1990). The Bare Mountain structural block appears to correspond to a culmination in the lower plate of the Bullfrog Hills detachment system. The Proterozoic and Paleozoic sedimentary and metamorphic rocks in the footwall of the Bare Mountain fault are laced by both thrust faults and gently dipping normal faults.

Slip data collected from fault surfaces in the northwestern part of Yucca Mountain indicate a steeply plunging west-northwest-trending slipline on the predominant set of north- to northeast-trending normal faults. These data reflect measurements of several microstructures, including R_1 Riedel shears, slickenside striae, tension gashes, hard rock fragments and associated grooves, and mullions (e.g., Angelier

and others, 1985). Slickenside striae were only used if geologic relations (e.g., offset Tertiary strata) implied movement subparallel to the striae. Most fault surfaces exhibit one prominent slipline. Sliplines from north- to north-northeast-trending faults average 60-->283, whereas those from northeast-trending faults trend 66-->297 (Figs. 7 and 8). Slickenside orientations from the northeastern part of Yucca Mountain (U.S. Geological Survey, 1984) show similar orientations. Thus, dip-slip normal movement dominated most faults. However, northeast- and north-northwest-trending faults commonly show small components of left and right slip, respectively. These data are suggestive of a west-northwest/east-southeast extension direction. The sliplines on individual faults cannot, however, be clearly attributed to a discrete episode of deformation. For example, the data collected from the bedrock faults may reflect deformation from both Miocene and Quaternary episodes of extension.

TIMING OF DEFORMATION

Extension in the Yucca Mountain/Crater Flat region has probably been operative from late Oligocene/early Miocene to late Quaternary time. Oligocene to middle Miocene normal faults, coarse basin-fill deposits, and unconformities exposed in surrounding ranges suggest that extension may have disrupted the Yucca Mountain/Crater Flat area prior to eruption of the 14.5 Ma Crater Flat tuff (Schweickert and Caskey, 1990). On the basis of map relations indicating deposition of the 11.3 Ma Rainier Mesa Member of the Timber Mountain Tuff across small fault scarps developed in the 12.9 Ma Tiva Canyon Member of the Paintbrush Tuff and older tuffs, Carr (1988)

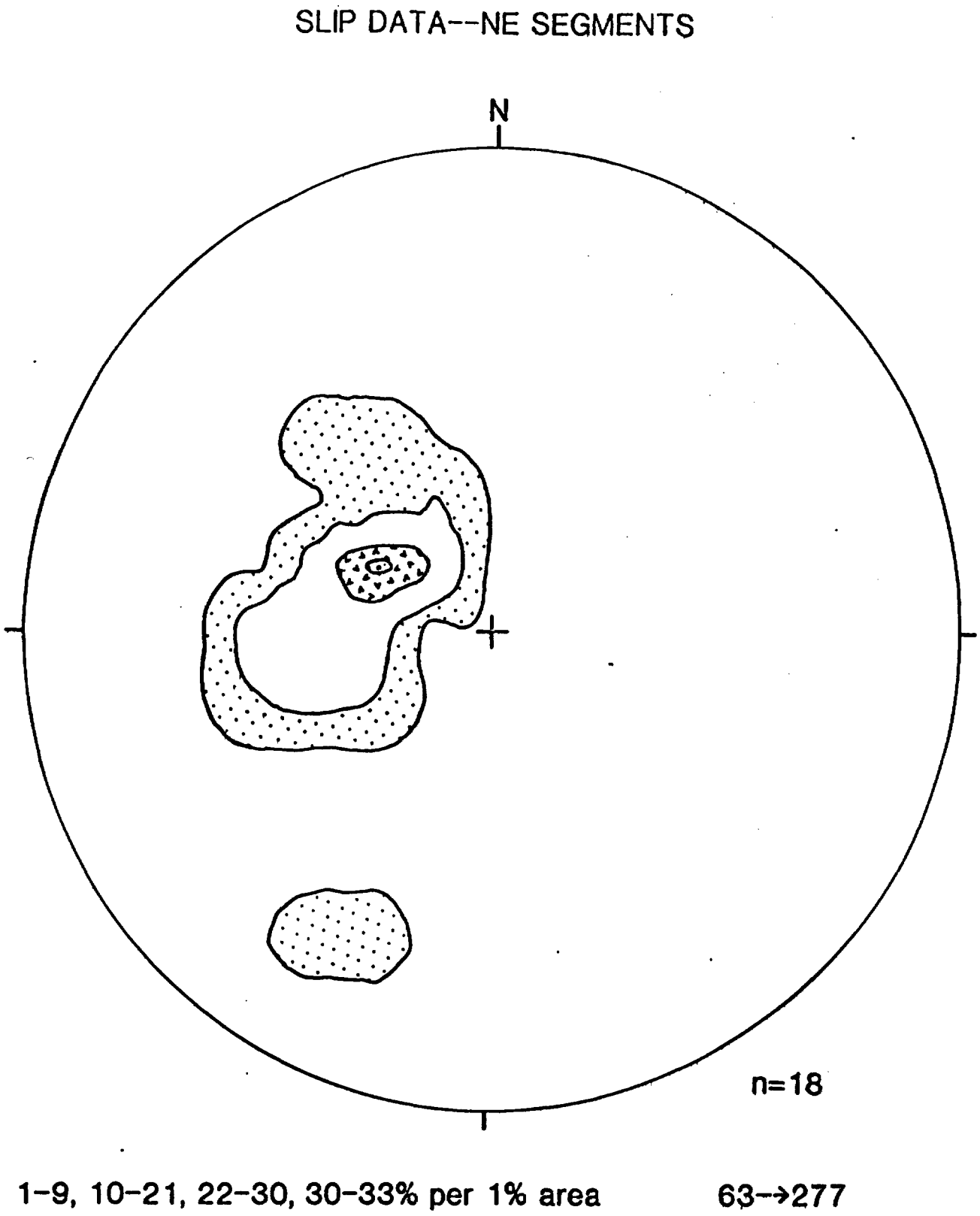

Figure 7. Sliplines, northeast-striking normal faults.

IRREGULAR DISPLACEMENT PATTERNS

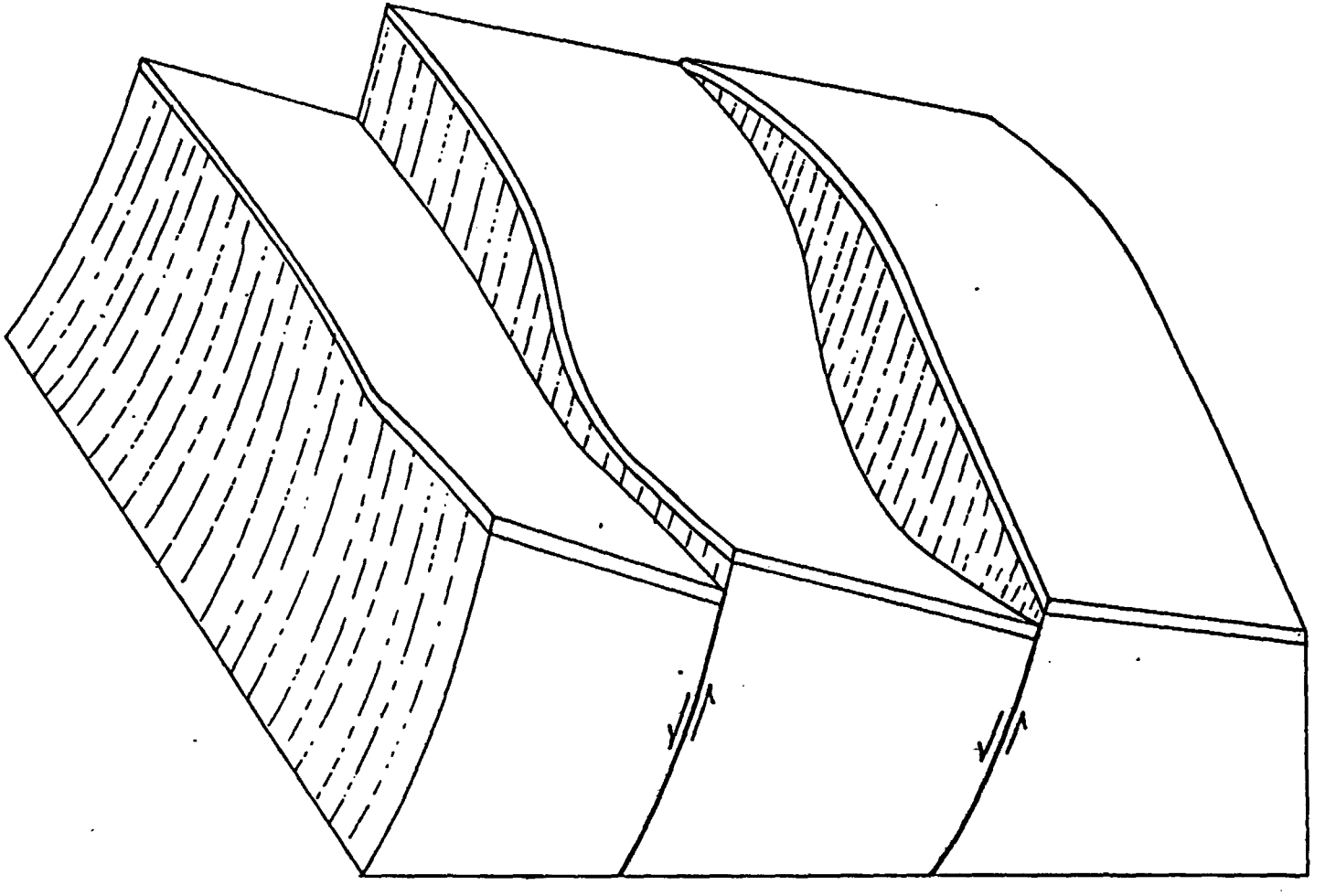

Figure 8. Schematic block diagram showing broad folds produced by irregular displacement gradients along major normal faults.

concluded that the major episode of extension occurred between 11.3 to 12.9 Ma. We concur that significant displacement took place during this time interval. For example, the Rainier Mesa Member of the Timber Mountain Tuff is appreciably thicker on the downthrown side of many normal faults in the northwestern part Yucca Mountain. In addition, the Tiva Canyon tuff is commonly more highly tilted than the Rainier Mesa Member of the Timber Mountain Tuff (Figs. 4 and 5). Megabreccias of Paleozoic rock occur at two intervals in drill hole USW VH-2, the oldest of which is situated between the 12.9 Ma Tiva Canyon Member of the Paintbrush Tuff and 11.3 Ma Rainier Mesa Member of the Timber Mountain Tuff (Carr and Parrish, 1985). The Bare Mountain block represents the only probable source area for the megabreccias. Thus, unroofing of the Bare Mountain block and significant displacement along the Bullfrog Hills detachment system and/or Bare Mountain fault must have occurred prior to 11.3 Ma.

However, in many areas, the Rainier Mesa Member of the Timber Mountain Tuff and Tiva Canyon Member of the Paintbrush Tuff exhibit little discordance in the magnitude of tilting. Erosional relicts of the Timber Mountain Tuff on several ridges in the northwestern part of Yucca Mountain (Plate 1) demonstrate that the Timber Mountain Tuff was not originally confined to structural basins, as suggested by the U.S. Department of Energy (1988) and Scott (1990), but instead was widely distributed across the Yucca Mountain/Crater Flat region. Moreover, significant faulting and tilting disrupt the Timber Mountain Tuff throughout the Yucca Mountain/Crater Flat area. We therefore propose that the major pulse of extension in the Yucca Mountain/Crater Flat region postdated eruption of the Timber Mountain Tuff. The mildly faulted 3.7 Ma

basalts in Crater Flat place a younger age constraint on this episode of extension. Major extension in the Yucca Mountain/Crater Flat region may have coincided with the 8 to 10 Ma pulse of extension (Maldonado, 1990) in the Bullfrog Hills area to the west. Extension has continued into late Quaternary time, as evidenced by displaced Pleistocene and Holocene deposits in and along the margins of Crater Flat and in the northeastern part of Yucca Mountain (Swadley and others, 1984; U.S. Department of Energy, 1988; Reheis, 1988; Ramelli and Bell, unpublished mapping).

The slipline data and estimates of stratigraphic throw permit assessment of long-term slip rates and subsidence rates in the Yucca Mountain/Crater Flat region. On the basis of apparent offset of Pliocene basalts in the southeastern part of Crater Flat, Bell (unpublished data) calculated slip rates ranging from .01 to .04 mm/yr over the past 2.5 to 3.7 Ma. In this case, most of the strain was accommodated by a single fault along the southeastern margin of Crater Flat (Figs. 2 and 4). Based on stratigraphic throw and estimates of net slip of the base of the Timber Mountain Tuff, the subsidence rate of Crater Flat near Black Cone relative to the western margin of Yucca Mountain was approximately .05 mm/yr between 11.3 and 0.8 Ma (cross section). The thickness of the Rainier Mesa tuff varies little between drill hole USW VH-2 and the southwestern margin of Yucca Mountain. The subsidence rate of Crater Flat relative to the crest of Yucca Mountain was estimated at 0.1 mm/yr between 12.9 and 0.8 Ma on the basis of apparent sliplines and stratigraphic throw of the base of the Tiva Canyon tuff, the thickness of which differs little across cross section A-A′ (Fig. 4). It is important to note that the estimates of subsidence rates incorporate offset along a series of faults, rather

than an individual fault. Thus, the subsidence rates essentially reflect slip rates on the *zone* of en echelon, west-dipping faults that bounds Yucca Mountain on the west, which fortuitously averages out the effects of irregular displacement patterns along individual faults. Furthermore, the estimated subsidence rates may obscure episodic movement along the faults (e.g., possible pulse of extension 8 to 10 Ma). However, the estimated subsidence rates are in close accord with Quaternary and Pliocene-Quaternary displacement rates along the Bare Mountain fault (Swadley and others, 1984) and southeastern margin of Crater Flat, respectively. An intriguing possibility is that, since middle Miocene time, much of the Yucca Mountain/Crater Flat region has experienced a long protracted period of relatively mild extension during which displacement rates have changed little.

Preliminary estimates of the magnitude of extension since middle Miocene time, using the base of the Tiva Canyon Member of the Paintbrush Tuff as a structural datum, range from 2 to 5 percent. Most of the extension probably took place after deposition of the Timber Mountain Tuff.

PLIOCENE/QUATERNARY VOLCANISM

In the immediate vicinity of Yucca Mountain, Pliocene and Quaternary basalts erupted from three major areas: (1) a 4-km-long north-trending fissure in the southeastern part of Crater Flat 2.5 to 3.7 Ma (Vaniman and Crowe, 1981; Vaniman and others, 1982); (2) a 12-km-long northeast-trending arcuate belt in Crater Flat 0.7 to 1.1 Ma (Crowe and Carr, 1980; Vaniman and Crowe, 1981; Vaniman and others, 1982;

Crowe and others, 1983; Feuerbach and others, 1990; Smith and others, 1990); and (3) the isolated Lathrop Wells center on the southern flank of Yucca Mountain less than 20 ka (Crowe and others, 1988; Wells and others, 1990). Most of the volcanoes in the Yucca Mountain region show evidence of polycyclic activity (Wells and others, 1990), involving multiple eruptive cycles over 10^4 to 10^5 years (Turrin and Renne, 1987; Renault and others, 1988; Crowe and others, 1989).

The Pliocene/Quaternary basalts are generally alkalic in composition (Vaniman and Crowe, 1981; Farmer and others; 1989; Crowe, 1990). Major rock types include Hy- to Ne-normative alkali basalt and hawaiite. Nd, Sr, and Pb isotopic signatures suggest derivation from mantle lithosphere, potentially of pre-extension origin (Farmer and others, 1989). Geochemical and petrologic characteristics further indicate little fractionation and residence time within the crust. Derivation from lithospheric mantle and little residence time in crustal magma chambers imply that the basaltic magmas were tapped by crustal-penetrating channelways (e.g., Anderson, 1988). Pliocene/Quaternary basalts in nearby regions originated similarly (Anderson, 1988; Cole, 1989; Smith and others, in prep.).

Alignments of the Pliocene/Quaternary volcanic centers in Crater Flat mimics the structural grain within Yucca Mountain. Dikes in the Pliocene fissure system strike north-south to north-northeast, whereas dikes, scoria mounds, and volcanic complexes are aligned along a N35°E to N50°E trend in the Pleistocene belt. Unfortunately, the Tertiary bedrock geology is not exposed at any of the Quaternary/Pliocene volcanic centers. Geologic mapping of nearby Tertiary bedrock and drill core data (Carr, 1982;

Carr and Parrish, 1985) suggest, however, that both the Pliocene and Pleistocene volcanic centers in Crater Flat occur near major west-dipping normal faults. The Lathrop Wells center is situated near the intersection of major west-dipping, northeast- and north-northwest-striking faults.

DISCUSSION

Implications of Structural Framework

One of the most critical structural features of Yucca Mountain is the en echelon pattern of faults and attendant irregular displacement patterns. For example, appreciable strain gradients over distances of less than 1.5 km along many faults, including some that have accommodated Quaternary displacement, indicate that late Tertiary/Quaternary displacement rates have also varied significantly along some faults. Consequently, slip data from isolated trenches may not adequately depict Quaternary or late Tertiary displacement rates. In addition, the irregular displacement patterns locally produced tilting about non-horizontal axes, which in turn created broad folds that trend oblique to the predominant north-south structural grain (Fig. 8). Strata within an east-tilted fault block on the northwestern part of Yucca Mountain are warped into a broad northeast-trending syncline (Figs. 4 and 5). The abrupt northern limb of the syncline occurs directly east of a sharp southward decrease in displacement on a major west-dipping normal fault (Plate 1). The more subtle southern limb of the syncline lies directly west and within the hanging wall of a northward increase in offset along a west-dipping normal fault. Adjacent to particularly sharp displacement gradients, the folds

essentially represent north- or south-facing monoclines. These folds may be relevant to the proposed repository, as they may affect near-surface patterns of ground water flow in the Yucca Mountain/Crater Flat region.

Although a convincing origin for the closely-spaced en echelon pattern of faults cannot be determined with the available data, any feasible explanation must take into account preexisting structural fabrics. The segmentation and arcuate traces of some faults (e.g., Bare Mountain fault) led Carr (1988) to propose that the en echelon pattern of faults in the Crater Flat area results primarily from the reactivation of caldera ring-fractures, which originated during the eruption of the Crater Flat Tuff. However, segmented faults and arcuate traces of faults are common in many areas of the Basin and Range province devoid of calderas. Nonetheless, the emplacement of silicic plutons at relatively shallow levels and associated hydrothermal alteration and hydrolytic fracturing of surrounding country rocks may have greatly influenced the mechanical behavior of the Yucca Mountain/Crater Flat region during subsequent regional extension. For example, closely-spaced fractures in Paleozoic and Proterozoic basement rocks, if favorably oriented in the regional stress field, may have precipitated partitioning of strain along an array of closely-spaced en echelon faults rather than large magnitude displacement on widely-spaced, regionally extensive normal faults.

The origin of the northeast-trending fault segments may be related to northeast-trending basement structures. For example, steeply dipping bedding generally strikes east-west within a large overturned fold of Paleozoic and late Proterozoic rock in the southern part of Bare Mountain. If the fold continues to the east beneath Crater Flat,

the strike of bedding might be expected to swing northeastward as part of the large oroclinal flexure associated with the Las Vegas Valley shear zone and Walker Lane belt. Thus, northeast-striking Proterozoic and Paleozoic bedding may have locally influenced the structural grain in the Yucca Mountain/Crater Flat region. Interpretations involving the continuation of the west-vergent Mesozoic fold and thrust system beneath Crater Flat and Yucca Mountain favor models entailing dismemberment of the Mesozoic system by normal faults (e.g., Wernicke and others, 1988) rather than a right-lateral strike-slip fault projecting beneath Crater Flat (e.g., Schweickert, 1989).

Alternatively, the northeast-trending fault segments may be secondary in origin, perhaps resulting from dextral strain and clockwise rotation of preexisting north-striking faults. This scenario could account for the more northwesterly trend of sliplines on northeast-trending faults, as compared to north-striking faults (Figs. 7 and 8). However, paleomagnetic data reveal little clockwise rotation and distributed dextral strain across the southwestern Nevada volcanic field (Hudson and Rosenbaum, 1990). Furthermore, slip data from these faults is a small data base and may not be representative of northeast-striking faults throughout the region. The lack of tight constraints on the timing of slip is also a critical problem along most faults, as the orientation of the principal stress directions have changed significantly since late Miocene time (Zoback and others, 1981). We therefore favor the former explanation for the origin of the northeast-striking fault segments.

Possible Controls on Pliocene/Quaternary Volcanism

Basaltic volcanism has been an important component of the Pliocene/Quaternary tectonic regime throughout much of the Great Basin and adjoining regions. However, the detailed structural controls on basaltic volcanism remain unresolved in most areas. In the Yucca Mountain/Crater Flat region, alignments of scoria mounds, dikes, and volcanic complexes demonstrate that the Pliocene/Quaternary basalts were extruded along both north-south and northeast trends.

North- to northeast-trending normal faults probably controlled the alignment of the Pliocene/Quaternary volcanic centers in Crater Flat. Drill core and geologic mapping indicate that the north-trending Pliocene fissure system and at least the three northern Quaternary volcanic complexes are situated very close to major west-dipping normal faults. In addition, the late Quaternary Lathrop Wells center lies near the intersection of north-northwest- and northeast-striking, west-dipping normal faults. However, direct observation of the controlling structures in the Yucca Mountain/Crater Flat region is precluded by both a lack of Tertiary bedrock exposures and little dissection in the immediate vicinity of the volcanic centers. Analogue studies of older, more highly dissected basaltic volcanic centers in nearby regions may therefore shed some light on the controlling structures near Yucca Mountain (e.g., Smith and others, 1990). For example, although commonly near faults of parallel trend, Pliocene/Quaternary volcanic centers in southwestern Utah and northwestern Arizona generally do not lie directly on faults (Anderson, 1988; Feuerbach and others (CVTS), unpublished mapping). Anderson (1988) concluded that steep joints controlled the alignment of volcanic centers in southwestern Utah. We suspect that steep joints, as opposed to actual fault planes, may

have also governed the *near-surface* ascent of basaltic magmas in the Yucca Mountain/Crater Flat region.

The petrologic and geochemical characteristics of the basalts suggest, however, control by crustal-penetrating channelways. Because the distribution of joints may change significantly across any mechanical contrast (e.g., lithologic contacts or variations in welding), it is difficult to imagine systems of joints that would penetrate the entire crust. We therefore conclude that *at depth*, north- to northeast-trending faults ultimately controlled the location and alignment of Pliocene and Quaternary volcanic centers in the Yucca Mountain/Crater Flat region. Deep seismic reflection profiles in the Death Valley region have been interpreted to indicate that a moderately dipping normal fault links a subhorizontal magma chamber near the ductile-brittle transition at 15 km depth to a 0.69 Ma cinder cone (deVoogd and others, 1986). We further speculate that preexisting fabrics in Proterozoic and Paleozoic rocks influenced the location and trend of many normal faults, especially those that strike northeast, and thus indirectly controlled the location of some volcanic centers.

Northeast-trending faults and/or joints provided favorable conduits for basaltic magmas during Quaternary time, as they were oriented perpendicular to the least principal stress. Hydraulic fracturing stress measurements performed in 4 drill holes indicate that the least principal stress trends N60°W and that Yucca Mountain is currently under high extensional stress (Stock and Healy, 1988). Earthquake focal mechanisms and in situ stress measurements indicate a least principal stress trending west-northwest/east-southeast throughout the Basin and Range province (Zoback and

others, 1981). Preferentially oriented dike swarms and fault slip data from the Great Basin, including the Death Valley region, also suggest a least principal stress direction of approximately N60°W over the past several million years (i.e., less than 5 Ma) (Zoback and others, 1981; Wernicke and others, 1988). The north-northeast-trend of the entire Pliocene/Quaternary Death Valley-Pancake Range basaltic volcanic belt probably reflects the orientation of this stress field.

In contrast, the north- to north-northeast-trending dikes within the 2.5 to 3.7 Ma fissure system in Crater Flat imply a least principal stress oriented roughly east-west. The configuration of the modern stress field does differ significantly from that 20 to 10 Ma, when the least principal stress was directed west-southwest/east-northeast (Zoback and others, 1981). Thus, the Pliocene basalts may have been erupted during the clockwise rotation of the regional stress field. Zoback and others (1981) suggested, however, that the major change in stress orientation took place approximately 10 Ma. Variations in the alignments of Pliocene/Quaternary volcanic centers may reflect changes in the underlying structural grain or perhaps local and/or brief permutations in the regional stress field. Such permutations in the Yucca Mountain/Crater Flat region may result from dextral shear along or near the tips of the Walker Lane belt and Las Vegas Valley shear zone.

The clockwise rotation of the southern part of Yucca Mountain, as inferred from paleomagnetic data (Rosenbaum and others, in press), may be related to dextral strain along the Las Vegas Valley shear zone, which may continue into Amargosa Valley. Some of the right-lateral offset along the hypothetical western extension of the Las

Vegas Valley shear zone may be transferred into normal displacement along the Bullfrog Hills detachment system in the vicinity of Bare Mountain. This may account for the apparent termination of the Bullfrog Hills detachment system in the eastern part of Bare Mountain (Carr and Monsen, 1988).

The presence of major strike-slip faults in the Yucca Mountain/Crater Flat region may have important implications on the Pliocene/Quaternary basaltic volcanism. The structures responsible for tapping basaltic magmas presumably penetrate the entire crust (e.g., Farmer and others, 1989) and provide clear channelways to the surface. It is questionable whether this can be accomplished by moderately or gently dipping normal faults. Small pull-aparts along major strike-slip fault zones may, however, produce relatively unobstructed channelways between the lithospheric mantle and surface. The right step between the Las Vegas Valley shear zone and Walker Lane belt in the Yucca Mountain/Crater Flat region may essentially correspond to a large crustal pull-apart zone. Basaltic volcanism along the entire Death Valley/Pancake Range volcanic belt may be associated with the crustal pull-apart. Many strike-slip faults that simply link two extensional domains are probably thin-skinned and restricted to the upper plate of an individual detachment system (Burchfiel and others, 1989). However, strike-slip fault zones that track across several extensional domains, such as the Walker Lane belt and Las Vegas Valley shear zones, are probably not confined to the upper plate of an individual detachment system and may penetrate the entire crust. Such thick-skinned strike-slip shear zones may, at least initially, tap the basaltic magmas, especially within pull-apart zones. The basaltic magmas may rise along sigmoidally shaped cylinders at

deep crustal levels before spreading out, at shallow levels, along structures favorably oriented in the regional stress field (e.g., north- to northeast-trending normal faults and joints in the Yucca Mountain/Crater Flat region) (Fig. 9). The Pliocene Fortification Hill volcanic field in northwestern Arizona may have also emerged along a pull-apart zone directly south of the intersection of the left-lateral northeast-trending Lake Mead and right-lateral northwest-trending Las Vegas Valley shear zones.

Concerns for Proposed Repository

Our main concerns for the proposed repository are (1) possible inadequate estimates of slip rates due to the irregular displacement gradients and en echelon pattern of normal faults; (2) effect that "second order" folds produced by the irregular displacement patterns may have on local ground water flow; and (3) lack of control on subsurface bedrock structures, which is needed for regional reconstructions and better assessment of structural controls on recent volcanism. Additional trenching along clear-cut Quaternary scarps, as well as along the projection of Quaternary faults, and structural analysis of microstructures in the fault rocks should afford comprehensive estimates of slip rates. The "second order" folds can seemingly be incorporated into future models of ground water flow without great difficulty. The lack of subsurface control represents the greatest dilemma, for its resolution requires regional-scale, seismic-reflection profiles and several additional deep drill holes.

REFERENCES CITED

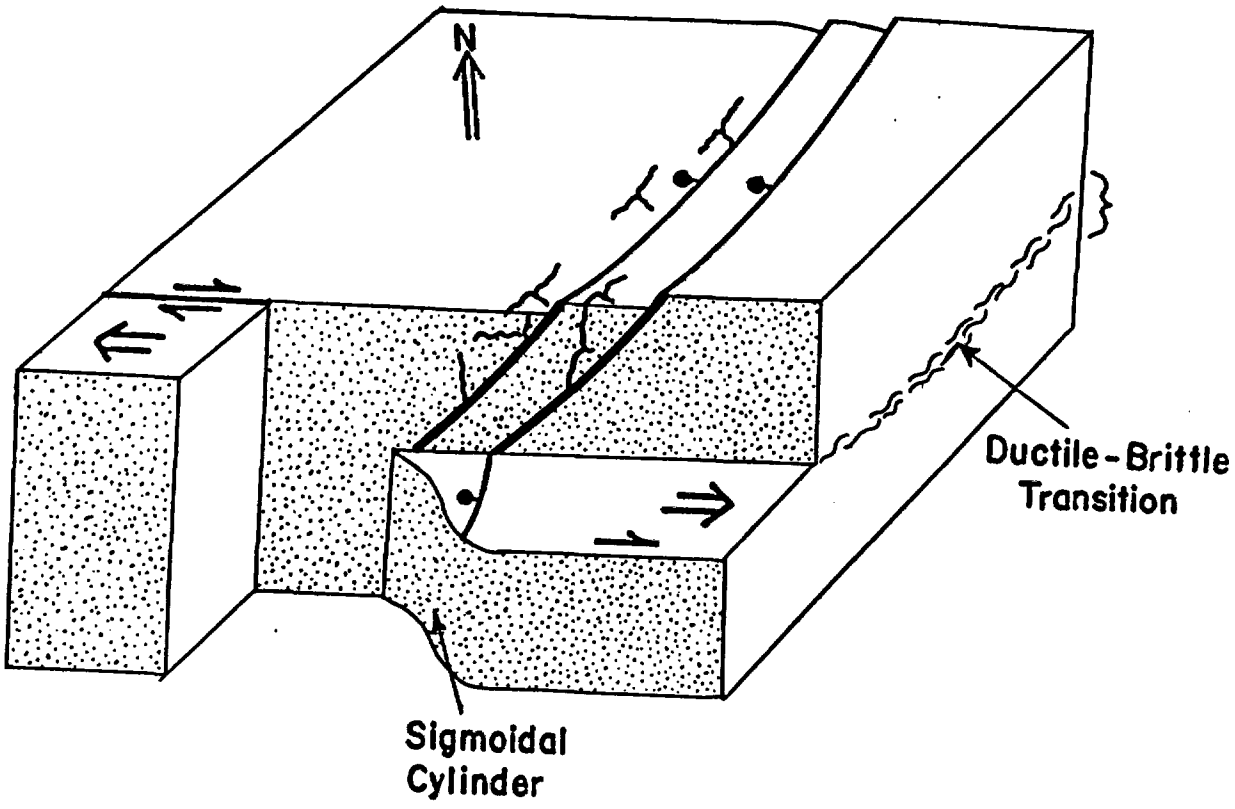

Figure 9. Model for ascent of basalts, showing rise along sigmoidal cylinders at deep crustal levels, spreading out along normal faults oriented perpendicular to extension direction at intermediate to shallow crustal levels, and final near-surface ascent along joints, minor faults and bedding planes.

Ackermann, H. D., Mooney, W. D., Snyder, D. B., and Sutton, V. D., 1988, Preliminary interpretation of seismic-refraction and gravity studies west of Yucca Mountain, Nevada: U.S. Geological Survey Bulletin 1790, p. 23-34.

Anderson, R. E., 1988, Hazard implications of joint-controlled basaltic volcanism in southwestern Utah: Geological Society of America Abstracts with Programs, v. 20, p. A115.

Angelier, J., Colletta, B., and Anderson, R. E., 1985, Neogene paleostress changes in the Basin and Range: A case study at Hoover Dam, Nevada-Arizona: Geological Society of America Bulletin, v. 96, p. 347-361.

Asmerom, Y., snow, J. K., Holm, D. K., Jacobsen, S. B., Wernicke, B. P., and Lux, D. R., 1990, Rapid uplift and crustal growth in extensional environments: An isotopic study from the Death Valley region, California: Geology, v. 18, p. 223-226.

Burchfiel, B. C., Hodges, K. V., and Royden, L. H., 1987, Geology of the Panamint Valley-Saline Valley pull apart system, California: Palinspastic evidence for low-angle geometry of a Neogene range-bounding fault: Journal of Geophysical Research, v. 92, p. 10,422-10,426.

Burchfiel, B. C., and 6 others, 1989, Intracrustal detachment within zones of continental deformation: Geology, v. 17, p. 748-752.

Butler, P. R., Troxel, B. W., and Verosub, K. L., 1988, Late Cenozoic history and styles of deformation along the southern Death Valley fault zone, California: Geological Society of America Bulletin, v. 100, p. 402-410.

Byers, F. M., Carr, W. J., Christiansen, R. L., Lipman, P. W., Orkild, P. P., and Quinlivan, W. d., 1976a, Geologic map of the Timber Mountain caldera area, Nye County, Nevada: U.S. Geological Survey Miscellaneous Investigations Map, I-891, scale 1:48,000.

Byers, F. M., Carr, W. J., Orkild, P. P., Quinlivan, W. D., and Sargent, K. A., 1976b, Volcanic suites and related cauldrons of the Timber Mountain-Oasis Valley caldera complex, southern Nevada: U.S. Geological Survey Professional Paper 919.

Carr, M. D., and Monsen, S. A., 1988, Field trip guide to the geology of Bare Mountain, in Weide, D. L., and Faber, M. L., eds., This extended land--Geological journeys in the southern Basin and Range: Geological Society of America, Cordilleran Section, Field Trip Guidebook, p. 50-57.

Carr, W. J., 1982, Volcano-tectonic history of Crater Flat, southwestern Nevada, as suggested by new evidence from drill hole USW-VH-1 and vicinity: U.S. Geological Survey Open-File Report 82-457, 23 p.

Carr, W. J., 1984, Regional structural setting of Yucca Mountain, southwestern Nevada, and late Cenozoic rates of tectonic activity in part of the southwestern Great Basin, Nevada and California: U.S. Geological Survey Open-File Report 84-854, 109 p.

Carr, W. J., 1988, Volcano-tectonic setting of Yucca Mountain and Crater Flat, southwestern Nevada, in Carr, M. D., and Yount, J. C., eds., Geologic and hydrologic investigations of a potential nuclear waste disposal site at Yucca Mountain, southern Nevada: U.S. Geological Survey Bulletin 1790, p. 35-49.

Carr, W. J., and Parrish, L. D., 1985, Geology of drill hole USW-VH-2, and structure of Crater Flat, southwestern Nevada: U.S. Geological Survey Open-File Report 85-475, 41 p.

Christiansen, R. L., and Lipman, P. W., 1965, Geologic map of the Topopah Spring NW quadrangle, Nye County, Nevada: U.S. Geological Survey Quadrangle Map GQ-444, scale 1:24,000.

Christiansen, R. L., Lipman, P. W., Carr, W. J., Byers, F. M., Orkild, P. P., and Sargent, K. A., 1977, Timber Mountain-Oasis Valley caldera complex of southern Nevada: Geological Society of America Bulletin, v. 88, p. 943-959.

Cole, E. D., 1989, Petrogenesis of late Cenozoic alkalic basalt near the eastern boundary of the Basin-and-Range: Upper Grand Wash trough, Arizona and Gold Butte, Nevada: M.S. thesis, University of Nevada, Las Vegas, 68 p.

Crowe, B. M., 1990, Basaltic volcanic episodes of the Yucca Mountain region, in Proceedings of the International Nuclear Waste Symposium: American Nuclear Society and American Society of Civil Engineers, v. 1, p.

Crowe, B. M., and Carr, W. J., 1980, Preliminary assessment of the risk of volcanism at a proposed nuclear waste repository in the southern Great Basin: U.S. Geological Survey Open-File Report 80-357.

Crowe, B. M., Vaniman, D. T., and Carr, W. J., 1983, Status of volcanic hazard studies for the Nevada Nuclear Waste Storage Investigations: Los Alamos National Laboratory Report LA-9325-MS.

Crowe, B. M., Harrington, C., McFadden, L., Perry, F., Wells, S. Turrin, B., and Champion, D., 1988, Preliminary geologic map of the Lathrop Wells volcanic center: Los Alamos National Laboratory Report LA-UR-88-4155.

Crowe, B. M., Turrin, B., Wells, S. G., McFadden, L., Renault, C. Perry, F., Harrington, C., and Champion, D., 1989, Polycyclic volcanism: A common eruption mechanism of small basaltic centers in the western U.S.A.: New Mexico Bureau of Mines and Mineral Resources Bulletin 131, p. 63.

deVoogd, B., and 8 others, 1986, Death Valley bright spot: A midcrustal magma body in the southern Great Basin, California?: Geology, v. 14, p. 64-67.

Farmer, G. L., Perry, F. V., Semken, S., Crowe, B., Curtis, D., and DePaolo, D. J., 1989, Isotopic evidence on the structure and origin of subcontinental lithospheric mantle in southern Nevada: Journal of Geophysical Research, v. 94, p. 7885-7898.

Feuerbach, D. L., Smith, E. I., and Shafiqullah, M., 1990, Structural control of Pleistocene volcanism in Crater Flat, Nevada: Geological Society of America Abstracts with Programs, v. 22, no. 3, p. 23.

Holm, D. K., and Wernicke, B., 1990, Black Mountains crustal section, Death Valley extended terrain, California: Geology, v. 18, p. 520-523.

Hudson, M. R., and Rosenbaum, J. G., 1990, Paleomagnetism of the southwestern Nevada volcanic field: Absence of vertical-axis rotation (Abstract): EOS (Transactions of the American Geophysical Union), in press.

Lipman, P. W., and McKay, E. J., 1965, Geologic map of the Topopah Spring SW quadrangle, Nye County, Nevada: U.S. Geological Survey Geologic Quadrangle Map, GQ-439, scale 1:24,000.

Maldonado, F., 1985, Geologic map of the Jackass Flats area, Nye County, Nevada: U.S. Geological Survey Miscellaneous Investigations Series Map I-1519, scale 1:48,000.

Maldonado, F., 1990, Structural geology of the upper plate of the Bullfrog Hills detachment fault system, southern Nevada: Geological Society of America Bulletin, v. 102, p. 992-1006.

McKay, E. J., and Sargent, K. A., 1970, Geologic map of the Lathrop Wells quadrangle, Nye County, Nevada: U.S. Geological Survey Geologic Quadrangle Map, GQ-883, scale 1:24,000.

Orkild, P. P., and O'Connor, J. T., 1970, Geologic map of the Topopah Spring quadrangle, Nye County, Nevada: U.S. Geological Survey Geologic Quadrangle Map, GQ-849, scale 1:24,000.

Prave, A. R., and Wright, L. A., 1986, Isopach pattern of the lower Cambrian Zabriskie Quartzite, Death Valley region, California-Nevada: How useful in tectonic reconstructions: Geology, v. 14, p. 251-254.

Reheis, M. C., 1988, Preliminary study of Quaternary faulting on the east side of Bare Mountain, Nye County, Nevada: U.S. Geological Survey Bulletin 1790, p. 103-112.

Renault, C. E., Wells, S. G., and McFadden, L. D., 1988, Geomorphic and pedologic evidence for polygenetic volcanism in late Quaternary cinder cones: Examples from Cima volcanic field, California and Crater Flat/Lathrop Wells volcanic field, Nevada: Geological Society of America Abstracts with Programs, v. 20, p. A115.

Reynolds, M. W., 1986, Geometry and chronology of late Cenozoic detachment faulting, Funeral and Grapevine Mountains, Death Valley, California: Geological Society of America Abstracts with Programs, v. 18, p. 175.

Rosenbaum, J. G., and Hudson, M. R., in press, Paleomagnetic investigations of Tertiary structural rotations at Yucca Mountain: Focus '89, Nuclear Waste Isolation in the Unsaturated Zone, American Nuclear Society.

Rosenbaum, J. G., Hudson, M. R., and Scott, R. B., in press, Paleomagnetic constraints on the geometry and timing of deformation at Yucca Mountain, Nevada: Journal of Geophysical Research.

Schweickert, R. A., 1989, Evidence for a concealed dextral strike-slip fault beneath Crater Flat, Nevada: Geological Society of America Abstracts with Programs, v. 21, p. A90.

Schweickert, R. A., and Caskey, S. J., 1990, Pre-middle Miocene extensional history of the Nevada Test Site (NTS) region, southern Nevada: Geological Society of America Abstracts with Programs, v. 22, no. 3, p. 81.

Scott, R. B., 1986, Extensional tectonics at Yucca Mountain, southern Nevada: Geological Society of America Abstracts with Programs, v. 18, no.5, p. 411.

Scott, R. B., 1990, Tectonic setting of Yucca Mountain, southwest Nevada, in Wernicke, B., ed., Basin and Range extensional tectonics near the latitude of Las Vegas, Nevada: Geological Society of America Memoir 176, in press.

Scott, R. B., and Bonk, J., 1984, Preliminary geologic map of Yucca Mountain, Nye County, Nevada, with geologic sections: U.S. Geological Survey Open-File Report 84-494, scale 1:12,000.

Scott, R. B., and Whitney, J. W., 1987, The upper crustal detachment system at Yucca Mountain, SW Nevada: Geological Society of America Abstracts with Programs, v. 19, no.5, p. 332-333.

Serpa, L., de Voogd, B., Wright, L., Willemin, J. Oliver, J., Hauser, E., and Troxel, B., 1988, Structure of the central Death Valley pull-apart basin and vicinity from COCORP profiles in the southern Great Basin: Geological Society of America Bulletin, v. 100, p. 1437-1450.

Smith, E. I., Feuerbach, D. L., Naumann, T. R., and Faulds, J. E., 1990, The area of most recent volcanism near Yucca Mountain, Nevada: Implications for volcanic risk assessment, in Proceedings of the International Nuclear Waste Symposium: American Nuclear Society and American Society of Civil Engineers, v. 1, p. 81-90.

Snyder, D. B., and Carr, W. J., 1984, Interpretation of gravity data in a complex volcano-tectonic setting, southwestern Nevada: Journal of Geophysical Research, v. 89, p. 10,193-10,206.

Stewart, J. H., 1983, Extensional tectonics in the Death Valley area, California: Transport of the Panamint Range structural block 80 km northwestward: Geology, v. 11, p. 153-157.

Stewart, J. H., 1986, Tectonics of the Walker Lane belt, western Great Basin--Mesozoic and Cenozoic deformation in a zone of shear: Metamorphism and crustal evolution of the western United States, v. 7, Prentice-Hall, Inc., Englewood Cliffs, New Jersey.

Stock, J. M., and Healy, J. H., 1988, Stress field at Yucca Mountain, Nevada: U.S. Geological Survey Bulletin 1790, p. 87-94.

Swadley, W. C., and Carr, W. J., 1987, Geologic map of the Quaternary and Tertiary deposits of the Big Dune quadrangle, Nye County, Nevada, and Inyo County, California: U.S. Geological Survey Miscellaneous Investigations Series, Map I-1767, scale 1:24,000.

Swadley, W. C., Hoover, D. L., and Rosholt, J. N., 1984, Preliminary report on late Cenozoic faulting and stratigraphy in the vicinity of Yucca Mountain, Nye County, Nevada: U.S. Geological Survey Open-File Report 84-788, 42 p.

Turrin, B. D., and Renne, P. R., 1987, Multiple basaltic eruption cycles from single vents, Cima volcanic field, California; evidence for polygenetic basaltic volcanism: Geological Society of America Abstracts with Programs, v. 19, p. 458-459.

U.S. Department of Energy, 1988, Site characterization plan, Yucca Mountain site, Nevada research and development area, Nevada, v. 1, part A, 353 p.

U.S. Geological Survey, 1984, A summary of geologic studies through January 1, 1983, of a potential high-level radioactive waste repository site at Yucca Mountain, southern Nye County, Nevada: Open-File Report 84-792, 103 p.

Vaniman, D. T., and Crowe, B. M., 1981, Geology and petrology of the basalt of Crater Flat: Applications to volcanic risk assessment for the Nevada Nuclear Waste Storage Investigations: Los Alamos National Laboratory Report LA-8845-MS.

Vaniman, D., Crowe, B., and Gladley, E. S., 1982, Petrology and geochemistry of hawaiite lavas from Crater Flat, Nevada: Contributions to Mineralogy and Petrology, v. 80, p. 341-357.

Wells, S. G., McFadden, L. D., Renault, C. E., and Crowe, B. M., 1990, Geomorphic assessment of late Quaternary volcanism in the Yucca Mountain area, southern Nevada: Implications for the proposed high-level radioactive waste repository: Geology, v. 18, p. 549-553.

Wernicke, B. P., Hodges, K. v., and Walker, J. D., 1986, Geological setting of the Tucki Mountain area, Death Valley National Monument, California, in Dunne, G. C., ed., Mesozoic and Cenozoic structural evolution of selected areas, east-central California: Geological Society of America, Cordilleran Section, Los Angeles, p. 67-80.

Wernicke, B. P.., Axen, G. J., and Snow, J. K., 1988, Basin and Range extensional tectonics near the latitude of Las Vegas, Nevada: Geological Society of America Bulletin, v. 100, p. 1738-1757.

Wright, L. A., and Troxel, B. W., 1973, Shallow-fault interpretation of Basin and Range structure, southwestern Great Basin, in DeJong, K. A., and Scholten, R., eds., Gravity and tectonics: New York, John Wiley & Sons, p. 397-407.

Wright, L. A., Otton, J. K., and Troxel B. W., 1974, Turtleback surfaces of Death Valley viewed as phenomena of extensional tectonics: Geology, v. 2, p. 53-54.

Zoback, M. L., Anderson, R. E., and Thompson, G. A., 1981, Cainozoic evolution of the state of stress and style of tectonism of the Basin and Range province of the western United States: Philosophical Transactions of the Royal Society of London, v. A300, p. 407-434.

CRATER FLAT
(D.L. Feuerbach)

CONTENT OF THIS REPORT

This report duplicates information presented the CVTS annual report for 1989. We believed that it would be benefical to include this text because of the intense interest in the origin of Crater Flat and large number of additional individuals now involved in the evaluation of the Yucca Mountain site who have not read this contribution. This contribution also reviews the work of the CVTS in Crater Flat during 1989-90.

INTRODUCTION

The possibility of basaltic volcanism is recognized as a potential hazard when evaluating the suitability of placing a high-level nuclear waste repository at Yucca Mountain, Nye County, Nevada. The reason for concern is that during the last 4 m.y., basalt has periodically erupted in or near Crater Flat, a basin that borders the west flank of Yucca Mountain. Volcanism at Crater Flat occurred in three episodes (Vaniman et al, 1982) (Figure 1): (1) 3.7 Ma basalt that erupted from a north-south trending fissure in southeastern Crater Flat; (2) 1.1 Ma basalt, comprised of four cinder cone complexes in the center of Crater Flat; and (3) 300 to 5 Ka basalt at the Big Dune cinder cone (Lathrop Wells cone), located 15 km south of the repository block. Basalt also erupted along the southern flank of Crater Flat 10.5 Ma (Tb) (Figure 1).

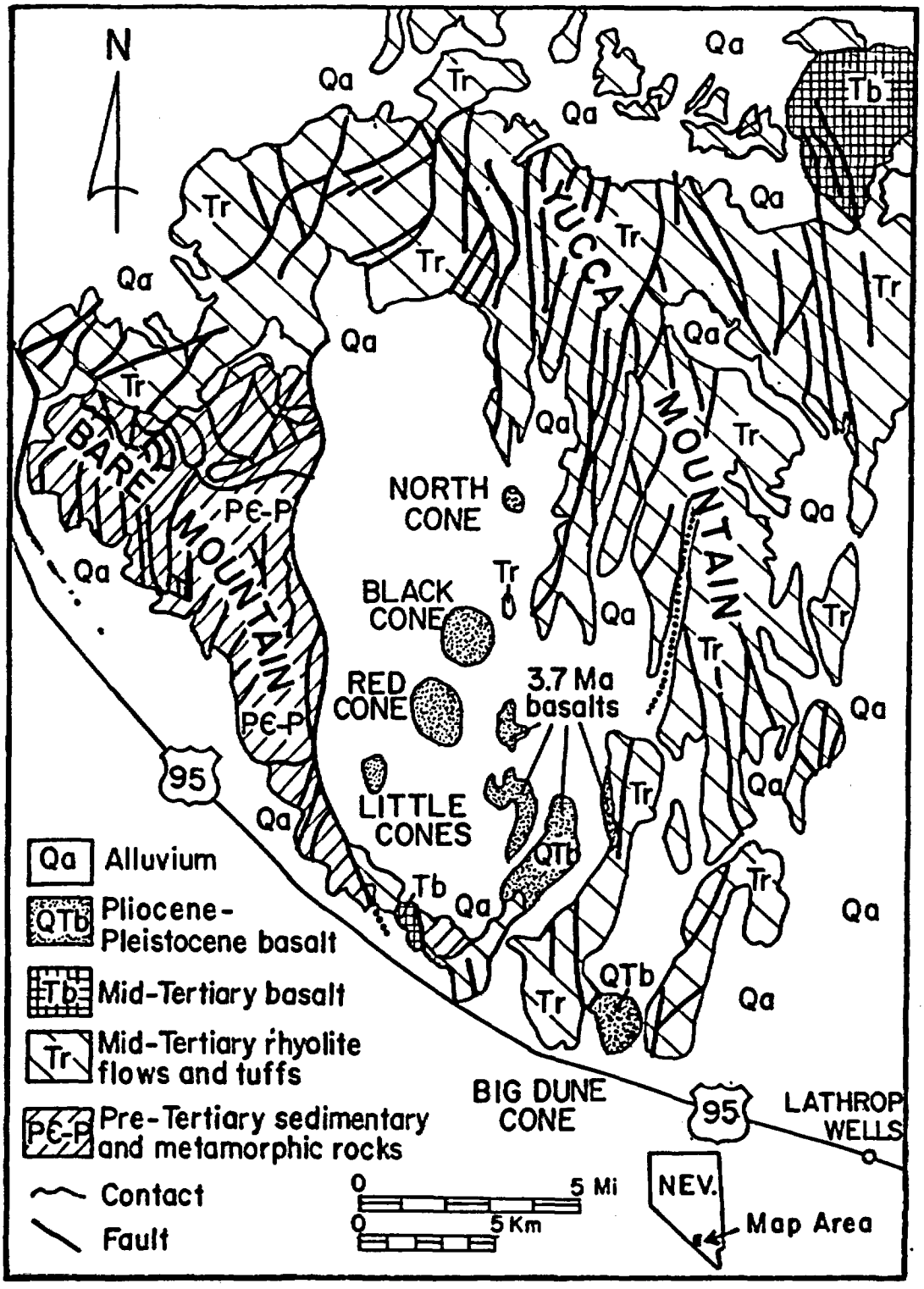

Figure 1. Location map for the Crater Flat-Yucca Mountain area (modified from Cornwall, 1972).

Geologic Setting

Crater Flat and Yucca Mountain are located in the south-central Great Basin. Crater Flat is a southward-sloping valley that is bordered to the west by Bare Mountain and to the east by Yucca Mountain (Figure 1). Bare Mountain is composed of a highly faulted and rotated upper Precambrian and Paleozoic section. Yucca Mountain consists of a faulted section of the Tertiary Paintbrush and Crater Flat tuffs. The surface of the Crater Flat is composed of Quaternary alluvium containing clasts of Tertiary tuff and Paleozoic sediments. Beneath the veneer of alluvium is a thick package of Miocene ash-flow tuff that is overlain by a thin section of basalt, and a landslide deposit composed of clasts of Paleozoic rocks (Carr, 1988).

THE 1.1 Ma CYCLE

Flows and pyroclastic rocks of the 1.1 Ma cycle are alkali-basalts that erupted from four cinder cone complexes in the central part of Crater Flat. They are called from south to north, Little Cones, Red Cone, Black Cone and Northern Cone (Figure 1). We have mapped Black Cone and Red Cone at a scale of 1:1500.

Black Cone

Lava and scoria from Black Cone covers nearly 4 km^2. The center is composed of alkali-basalt flows and pyroclastic deposits of scoria, agglutinate, ash and bombs that erupted from at least 10 separate vents (Figure 2). Lava was deposited on alluvium sloping to the south. As a result, basalt flowed preferentially to the south.

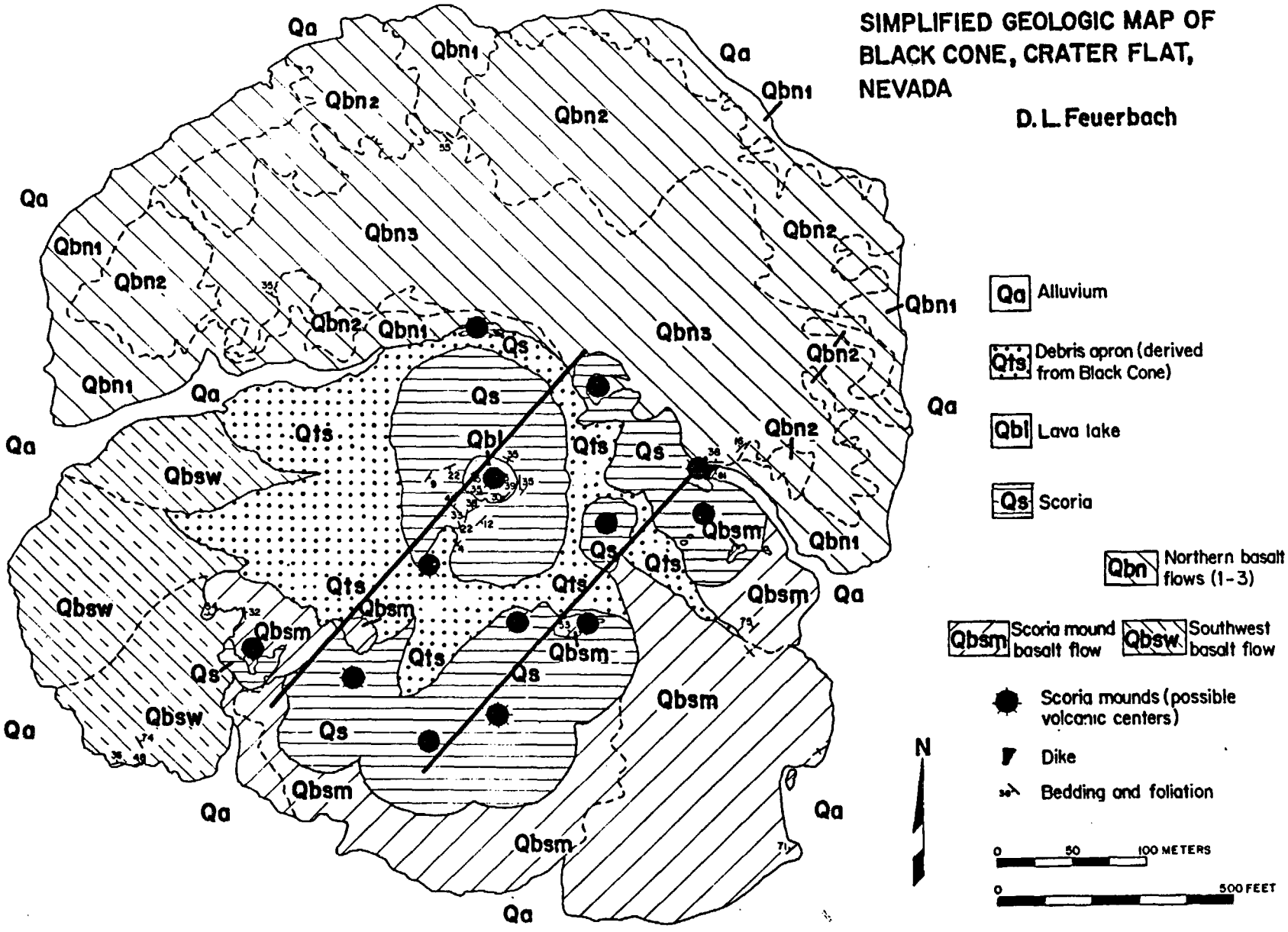

Figure 2. Geologic map of Black Cone.

Black Cone Cinder Cone

The most prominent landform at Black Cone is a cinder cone that stands approximately 60 m above the surrounding flows. The cone is oval in plan view with a long axis oriented north-south. Except for a well developed lava lake at its summit and numerous rootless lava flows, the cone is composed of pyroclasts of scoria, agglutinated scoria, ash and bombs. The northwest half of the cone retains its mantle of scoria and has a near-pristine profile. This slope is slightly modified by rills and has a distinct cone apron. Erosion has removed the scoria mantle from the southeast side of Black Cone revealing the internal stratigraphy of the cone.

In a section from the southern base of Black Cone to its summit, there are four packages of scoria exposed (Figure 3). The lowest scoria unit (Sc1) appears to represent the lower flanks of the cone. The unit dips gently away from the summit (9 to 12 degrees). Locally Sc1 contains concentrations of large (>0.5 m in size) bombs. These beds may represent deposits at the base of the cone where bombs rolled down the cone and accumulated (McGetchin et al, 1974).

The next higher package of scoria (Sc2) is a cliff forming section that may have been deposited outside and below the crater rim. The unit strikes N45E and dips away from the crater rim (20 degrees). Within this unit, bedded scoria reflects as many as 10 pulses of Strombolian eruption. In addition to bedded scoria, the deposit contains bombs and zones of agglutinated and welded scoria and rootless flows. These deposits suggest that the style of volcanism fluctuated between mildly explosive Strombolian to Hawaiian-type lava fountaining.

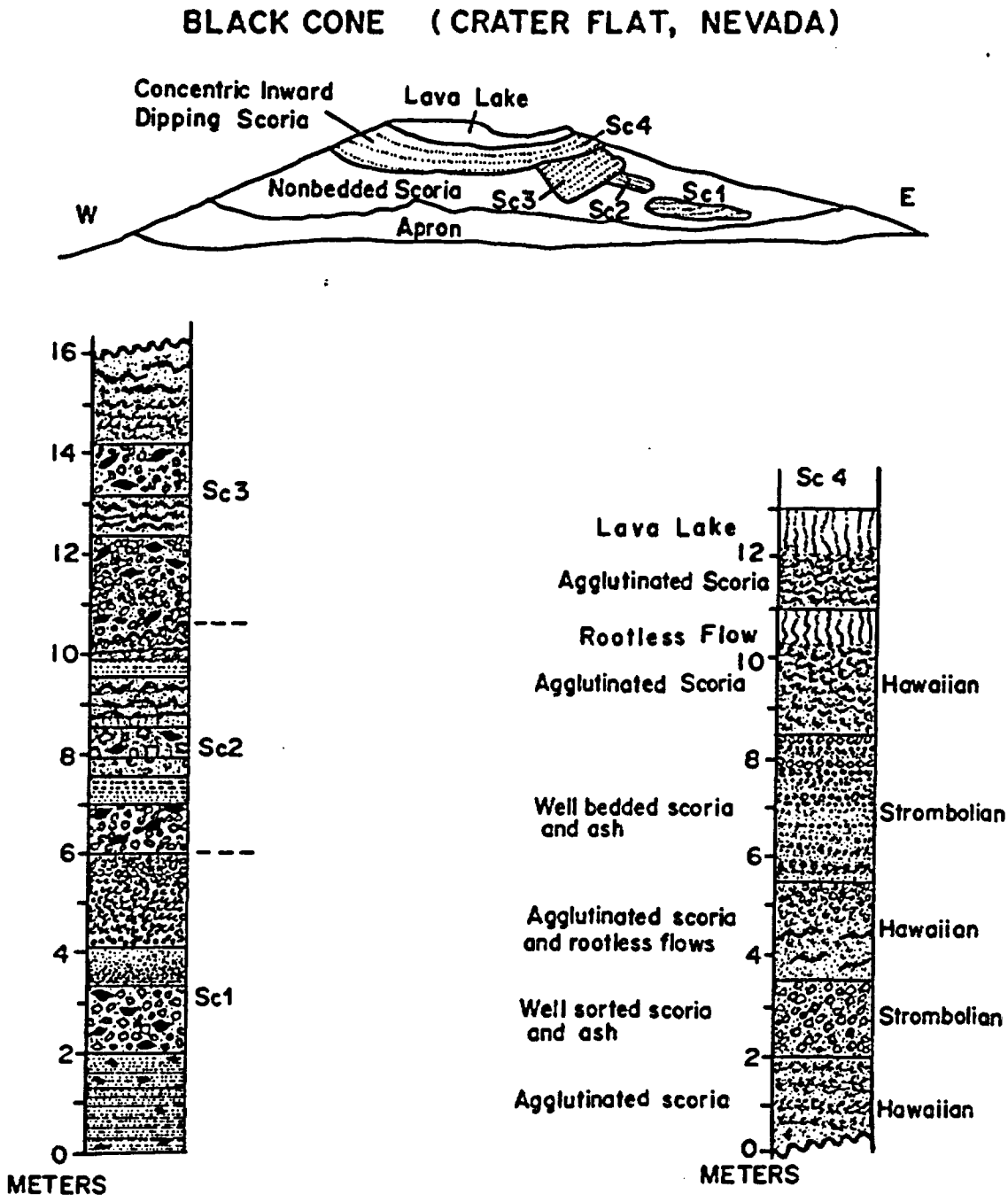

Figure 3. Stratigraphic sections of the four scoria units (Sc1, Sc2, Sc3 and Sc4) exposed at Black Cone and location of the scoria units on the south flank of Black Cone.

Separating Sc2 from Sc3 is an angular unconformity marked by a 2 cm thick zone of caliche. Sc3, a 4 m thick section of scoria, similar in lithology to Sc2, strikes toward the summit crater and dips 22 to 33 degrees to the west-southwest. Sc3 may be a section of Sc2 that collapsed during an event that over steepened the walls of the summit crater or the flank of the cinder cone (possibly a crater breaching event).

Another unconformity separates Sc3 from Sc4, the uppermost section of scoria. This unconformity can be traced around the south and east sides of the cone and may represent the lip of a pre-Sc4 crater. Bedding in Sc4 dips radially inward, toward the summit, and represents pyroclastic deposition in a summit crater. Sc4 records a style of eruption that fluctuated between Strombolian and Hawaiian-type lava fountaining; bedded scoria is interbedded with rootless flows and agglutinated spatter. The ratio of flow to scoria increases upward suggesting that lava fountaining became more important late in the eruption of Sc4. Sc4 is capped by a 2-3 m thick lava lake formed by massive flows of olivine basalt.

Other Vents

Even though the cinder cone is the most prominent topographic feature associated with the Black Cone complex, it may only account for a small volume of flows. A larger volume of flows erupted from at least 10 vents located north, south and east of Black Cone (Figure 2). These vents are commonly represented by scoria mounds that are composed of cinder, ash and large bombs. Vents are aligned along two sub-parallel zones that strike approximately N40E. One zone includes Black Cone and 4 scoria mounds (Black Cone zone); the other zone lies 300 m to the southeast of Black Cone and

contains at least 7 mounds (Southeast zone). A feeder dike within the Southeast zone is exposed in the interior of a scoria mound cut by a wash. The dike is 3 m wide and strikes N36E and dips 81 degrees to the south. The attitude of the dike at this locality reflects the northeast trend of the Southeast zone.

Lava Flows

Block and Aa olivine-basalt flows surround Black Cone. The basalt flows are vesicular to massive and contain olivine as the dominant phenocryst. Flow ramps and topographic benches are the major features on the surface of the flows. We subdivided the flows into three groups based on spatial relationships and stratigraphy (Plate 1). They are the northern flows, scoria-mound flows, and southwest flows.

The northern flows are composed of at least three flow units (Figure 2). They may have erupted from two scoria mounds near the northern base of Black Cone. These flows traveled nearly a kilometer from their source toward the north, east and west. Some of the older northern flows may have erupted from the northernmost part of the Southeast zone.

The scoria-mound flows are exposed south and southeast of Black Cone. These short and stubby flows can be traced back to seven coalescing cinder mounds which lie along the Southeast zone. Flows travelled primarily to the south. The longest unit flowed nearly 1 km from its source.

The southwest flows traveled approximately 0.75 km to the south and west from their probable source near the western base of Black Cone. The source for these flows is

not exposed, however, flow direction indicators such as ramp structures allow these flows to be traced toward their source.

Flow direction of lava flows from the Black Cone complex was controlled by the south dipping slope of the floor of Crater Flat. Only the northern flows travelled to the north. We suggest that the northern flows erupted after a substantial mound of scoria and flows formed to the south; related to the eruption of the scoria mounds and the Black Cone cinder cone. The northern flows travelled down a reversed topographic slope off the northern flank of this mound to the north, northeast and northwest. At this time we suggest that the northern flows are younger than the scoria mound and southwestern flows.

Red Cone

The Red Cone complex is composed of a large cone (Red Cone), 13 scoria mounds, and basalt flows that cover about 3 km^2 (Figure 4).

Red Cone proper is a highly eroded block and scoria cone built primarily of blocks of lava that are locally welded together, and minor amounts of scoria, bombs and ash. The top of the cone is capped by numerous rootless flows that may have ponded in a summit crater. A dike exposed on the west side of the summit may be the feeder for some of the summit eruptions. Small pods of amphibole-bearing lava crop out on the west flank of Red Cone. These lavas are either intrusive into the cone or are flows that erupted from the western flank of the cone.

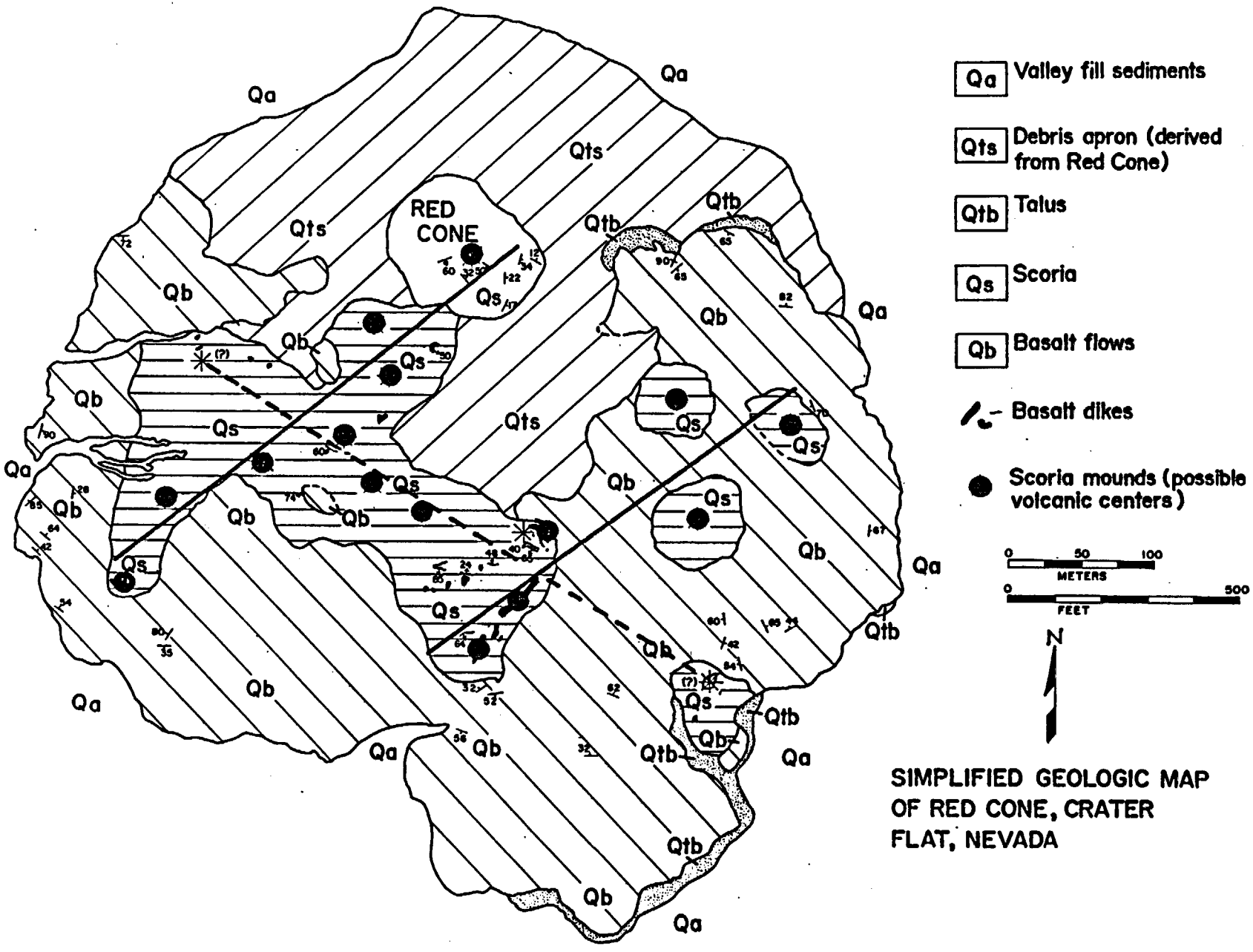

Figure 4. Geologic map of Red Cone.

Red Cone proper did not serve as a source for any of the major lava flows at the center. Most of the lava flows originated from vents expressed by scoria mounds that crop out south and east of Red Cone. The scoria mounds contain cinder, scoria, ash, bombs and zones of agglutinated scoria. These units were deposited by Strombolian eruptions and by lava fountaining of the Hawaiian type. Dikes are exposed in the interiors of some of the more highly eroded scoria mounds. The scoria mounds are aligned in three zones: two trend approximately N45E and a third subordinate zone strikes N50W (Figure 4). The two northeast trends may represent two sub-parallel fissures that are approximately 200 m apart. Red Cone lies on the northernmost of these trends. A degraded scoria mound at the intersection of the southernmost northeast striking fissure and the northwest trend may have been the source for many of the flows which lie southeast of Red Cone. Directly south of this locality, along strike of the fissure is a linear outcrop of agglutinated scoria and dikes in scoria. This appears to be a zone where lava fountaining occurred.

Basalt flows crop out west, east and south of Red Cone. They are primarily vesicular to massive block and Aa flows that contain varying amounts of olivine phenocrysts. We have divided the flows into three units based on spatial relationships and stratigraphy (Plate 1): Qb1, a stack of flows that erupted from scoria mounds southwest of Red Cone; Qb2, flows that erupted from the mounds south and southeast of Red Cone; Qb3, a small flow that erupted from the base of Red Cone; Using topographic benches as indicators of flow fronts, suggests that at least three pulses of lava formed the Qb1 stack of flows. Contacts between flows are usually covered by

blocky talus making it difficult to determine if soil horizons exist between flows. The southward topographic gradient of the floor of Crater Flat may explain the southerly flow of lava and the lack of flows to the north of Red Cone. Stratigraphy of the flow units is ambiguous because of poor exposure of the contacts, however Qb3 flowed toward the north because of the volcanic barrier produced by the eruption of Qb2 so we feel that Qb3 represents the latest flow unit.

THE 3.7 Ma CYCLE

Basalts of the 3.7 Ma cycle are the most voluminous in Crater Flat. Outcrops cover at least 20 km^2 (Figure 5). This area is a minimum value, because many exposures are covered by alluvium. Olivine basalt of the 3.7 Ma cycle flowed to the east and west from a 4 km long north-south-striking fissure (Figure 5). Strombolian eruptions became localized at numerous points along the fissure, forming scoria cones containing cinder, ash and bombs. The basalt flows were later cut and displaced by north-south striking high-angle normal faults.

The fissure has been eroded to the point where dikes are exposed. The dikes are high-angle (dips from 75-90 degrees) and range in strike from N20W to N20E, however, the dominant strike is north-northeast. In scoria, dikes have offshoots that strike nearly due west. Dikes are apparently not constrained by pre-existing structure once they intrude scoria. In one locality, a dike is exposed on the valley floor. Here, the dike strikes N20E and dips 85 degrees to the south. Unfortunately, the area is covered by

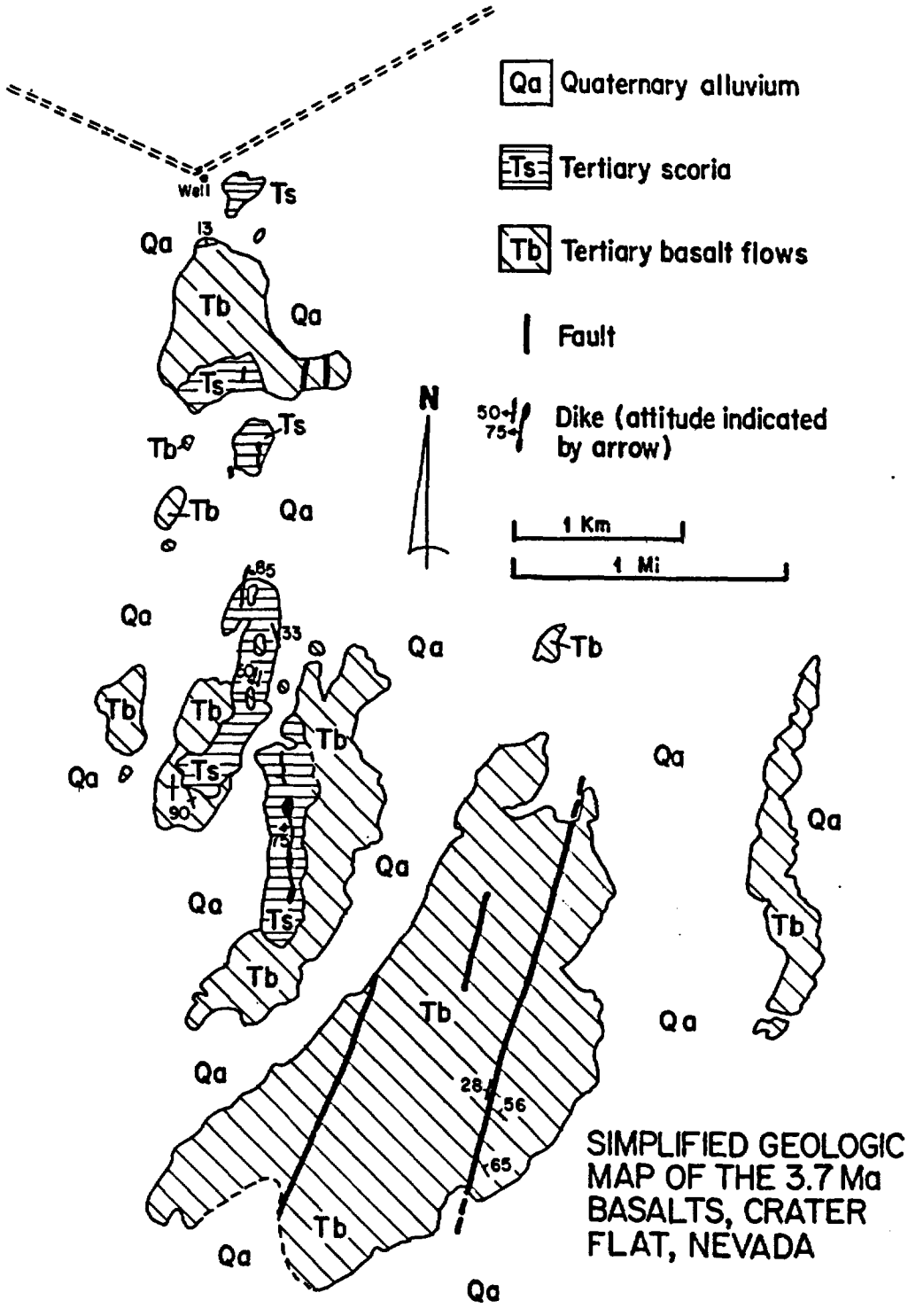

Figure 5. Generalized geologic map of the 3.7 Ma basalt in eastern Crater Flat.

fragments of alluvium on the valley floor so the actual contact with country rock is not exposed.

10.5 Ma BASALT

Basalt flows and eroded cinder cones (10.5 Ma) (Swadley and Carr, 1987) are exposed at the southern margin of Crater Flat (Figure 1). The flows are deposited on the Ammonia Tanks Member of the Timber Mountain Tuff and are overlain by a landslide block composed of relatively intact slabs of carbonate of the Bonanza King and Carrara Formations. The 10.5 basalts flows are tilted approximately 30 degrees to the east-northeast.

The basalt is composed of olivine, and clinopyroxene phenocrysts in a pilotaxitic to trachytic groundmass of plagioclase microlites, olivine, clinopyroxene and iron oxide. Glomeroporphiritic clots of pyroxene are scattered within the flows. Lava flowed to the east from at least three cinder cones that are composed of scoria and bombs and are intruded by plugs and meandering dikes. Basalt equivalent to these units lies approximately 400 m below the surface of Crater Flat in drillhole USW VH-2 (Carr, 1988).

GEOCHEMISTRY AND GEOCHRONOLOGY

Chemical Classification

Based on 51 major element analyses (Table 1), the basalts of Crater Flat were classified according to the chemical classification scheme of Irvine and Baragar (1971).

Sample #	Group	SiO2	Al2O3	Fe2O3	MgO	TiO2	CaO	Na2O	K2O	P2O5	MnO	Total
C8-1-1-LN	BC	49.49	16.63	10.51	5.08	1.36	8.44	3.19	1.50	1.09	0.16	97.96
C8-1-2-LN	BC	49.82	16.63	10.73	5.11	1.38	8.34	3.16	1.53	1.10	0.17	98.02
C8-1-3-LN	BC	49.61	16.67	10.84	5.12	1.39	8.34	3.12	1.52	1.13	0.17	98.36
C8-1-4-LN	BC	49.00	16.71	10.53	4.73	1.43	8.36	3.06	1.51	1.10	0.16	97.38
C8-1-5-LN	BC	49.30	16.65	10.60	5.39	1.42	8.23	2.87	1.64	1.15	0.17	97.80
C9-1-06-LN	BC	49.59	16.60	10.64	4.92	1.39	8.45	3.09	1.61	0.85	0.17	97.78
C9-1-07-LN	BC	49.89	16.93	10.99	5.05	1.45	8.47	3.32	1.63	0.91	0.17	98.82
C9-1-08	BC	48.63	16.59	11.03	5.11	1.45	8.87	3.23	1.58	0.92	0.17	98.01
C9-1-09	BC	48.89	16.76	11.22	5.19	1.45	8.39	3.26	1.62	0.91	0.18	98.13
C9-1-10-LN	BC	49.68	17.09	11.03	5.16	1.46	8.39	3.32	1.71	0.90	0.18	99.19
C9-1-11-LN	BC	49.39	17.17	10.45	4.91	1.43	8.80	3.37	1.67	0.93	0.17	98.49
C9-1-12-LN	BC	49.77	16.93	10.63	5.45	1.44	8.19	3.03	1.70	0.93	0.17	98.57
C9-1-13-LN	BC	49.35	17.22	11.01	5.14	1.45	8.55	3.29	1.67	0.92	0.17	99.01
C9-1-14-LN	BC	49.91	17.38	10.97	5.19	1.46	8.44	3.38	1.75	0.95	0.17	99.61
C9-1-15-LN	BC	48.96	16.97	10.76	5.17	1.44	8.39	3.28	1.76	0.92	0.17	97.83
C9-1-16-LN	BC	50.24	17.31	11.47	5.32	1.46	8.64	3.35	1.73	0.88	0.18	100.70
C9-1-19-LN	BC	51.12	17.39	10.51	5.28	1.38	8.62	3.46	1.42	0.81	0.17	100.39
C9-1-26-LN	BC	49.32	17.03	10.64	5.03	1.48	8.52	3.24	1.89	1.00	0.19	98.54
C9-2-27-LN	RC	49.26	17.29	10.69	5.07	1.54	8.57	3.51	1.74	1.11	0.18	99.18
C9-2-28-LN	RC	49.66	17.25	10.22	4.78	1.38	8.56	3.53	1.74	1.01	0.19	98.53
C9-2-29-LN	RC	49.22	17.04	10.64	4.85	1.48	8.38	3.30	1.96	1.06	0.21	98.31
C9-2-30-LN	RC	49.00	16.93	10.44	4.75	1.45	8.50	3.40	1.75	1.45	0.18	98.01
C9-2-31-LN	RC	49.54	17.17	10.24	4.60	1.39	8.57	3.63	1.77	1.09	0.20	98.44
C9-2-32-LN	RC	50.54	17.53	10.84	5.25	1.45	8.86	3.55	1.83	1.20	0.21	101.50
C9-2-33-LN	RC	49.03	16.94	10.61	4.83	1.44	8.43	3.35	1.93	1.04	0.17	97.99
C9-2-34-LN	RC	50.33	17.29	10.89	5.13	1.48	8.85	3.48	1.76	1.20	0.18	100.85
C9-2-35-LN	RC	48.90	16.96	10.53	4.67	1.42	8.60	3.41	1.82	1.05	0.18	97.74
C9-2-36-LN	RC	49.05	16.89	10.78	4.74	1.47	8.42	3.46	1.76	1.03	0.17	98.26
C9-2-37-LN	RC	48.90	16.68	10.59	5.35	1.50	8.35	3.37	1.82	1.06	0.18	97.99
C9-2-38-LN	RC	48.69	16.89	10.15	4.52	1.35	8.81	3.48	1.66	1.01	0.19	97.97
C9-2-39-LN	RC	49.42	16.97	10.34	4.86	1.37	8.58	3.40	1.86	0.98	0.19	98.22
C9-2-40-LN	RC	49.48	17.04	10.33	4.88	1.38	8.52	3.49	1.80	1.00	0.20	98.35
C9-2-41-LN	RC	49.38	17.15	10.80	5.02	1.53	8.49	3.34	2.00	1.08	0.21	99.19
C9-2-42-LN	RC	49.21	17.00	10.45	4.69	1.48	8.50	3.28	1.85	1.05	0.19	98.15
C9-2-43-LN	RC	50.51	17.71	10.98	4.96	1.54	8.68	3.56	1.99	1.16	0.21	101.50
C9-2-44-LN	RC	49.24	17.16	10.51	4.72	1.51	8.32	3.43	1.84	1.14	0.20	98.35
C9-2-45-LN	RC	49.86	17.19	10.47	4.36	1.48	8.38	3.55	1.72	1.08	0.20	98.80
C9-2-46-LN	RC	49.68	17.02	10.37	5.09	1.40	8.78	3.55	1.68	1.17	0.19	99.15
C9-3-47-LN	NC	48.87	17.34	11.23	5.42	1.75	8.65	3.46	2.08	1.09	0.19	100.30
C9-4-48-LN	LC	45.91	16.39	12.38	5.17	2.38	9.74	3.97	1.34	1.54	0.19	99.84
C9-4-49-LN	LC	45.78	16.34	13.22	4.87	2.79	9.04	3.88	1.53	1.40	0.18	99.90
C9-5-50-LN	LW	47.26	16.92	11.92	5.86	2.02	8.62	3.52	1.07	1.30	0.19	98.69
C9-6-51-LN	3.7p	45.97	15.17	12.43	6.79	2.02	8.86	2.97	1.92	0.54	0.18	99.10
C9-6-52-LN	3.7p	47.18	15.75	12.84	6.66	1.92	9.77	3.16	0.85	0.88	0.19	100.33
C9-6-53-LN	3.7	44.66	15.37	13.60	7.19	2.14	10.04	2.87	1.00	0.78	0.21	101.26
C9-6-54-LN	3.7	47.82	16.46	12.80	6.37	2.07	9.91	3.35	1.00	0.91	0.20	101.31
C9-6-55-LN	3.7	46.48	15.06	12.59	8.11	1.81	9.23	2.99	1.34	0.79	0.21	98.90
C9-7-56-LN	10.5	49.09	15.90	10.12	7.21	1.65	8.60	3.23	1.47	0.74	0.16	99.59
C9-7-57-LN	10.5	48.38	15.75	10.12	6.94	1.64	8.66	3.13	1.37	0.70	0.15	99.18
C9-7-58-LN	10.5	48.76	15.85	10.03	7.90	1.60	8.79	3.12	1.39	0.69	0.16	99.50
C9-6-59-LN	3.7	47.62	15.65	11.98	6.61	1.82	8.55	3.08	1.44	0.85	0.18	99.36
CO-1-68-LN												0.00

Table 1. Major element data in Wt% for the basalt in Crater Flat.

Basalt from Black Cone (18 samples), Red Cone (20 samples), the 10.5 cycle (three samples), the 3.7 Ma cycle (six samples) and Northern Cone (one sample) are alkali basalts. Little Cones (two samples) and Big Dune Cone (one sample) are classified as hawaiites. Rocks from Black Cone, Red Cone, Northern Cone and the 10.5 cycle fall within the potassic series and rocks from Little Cones, Big Dune Cone and the 3.7 Ma cycle fall within the sodic series.

Chemical Variation

Major Elements

The range of SiO_2 for the different volcanic centers in Crater Flat is 44.7-47.8% (3.7 Ma basalt); 45.9% (Little Cones); 47.9-49.7% (Black Cone); 48.7-50.5% (Red Cone); 48.9% (Northern Cone); 47.3% (Big Dune Cone). To determine the nature of chemical variation in the basalts from Crater Flat, Harker variation diagrams were plotted for each major element (Figure 6). Preliminary results for Black, Red, Big Dune and Little Cones include:

(1) A flow from the Big Dune Cone contains normative hypersthene (7%) (Figure 7). Vaniman et al. (1982) indicated that basalt from the Big Dune Cone is in general nepheline normative. However, they report one sample of flow rock with 1.4% normative hypersthene.

(2) Basalt from Little Cones, when compared to the other samples from the 1.1 Ma basalts of Crater Flat, are lower in SiO_2 and higher in P_2O_5, TiO_2 and Fe_2O_3 (Figure 6). Little Cones contain the only rocks of the 1.1 Ma cycle that are nepheline normative (Figure 7).

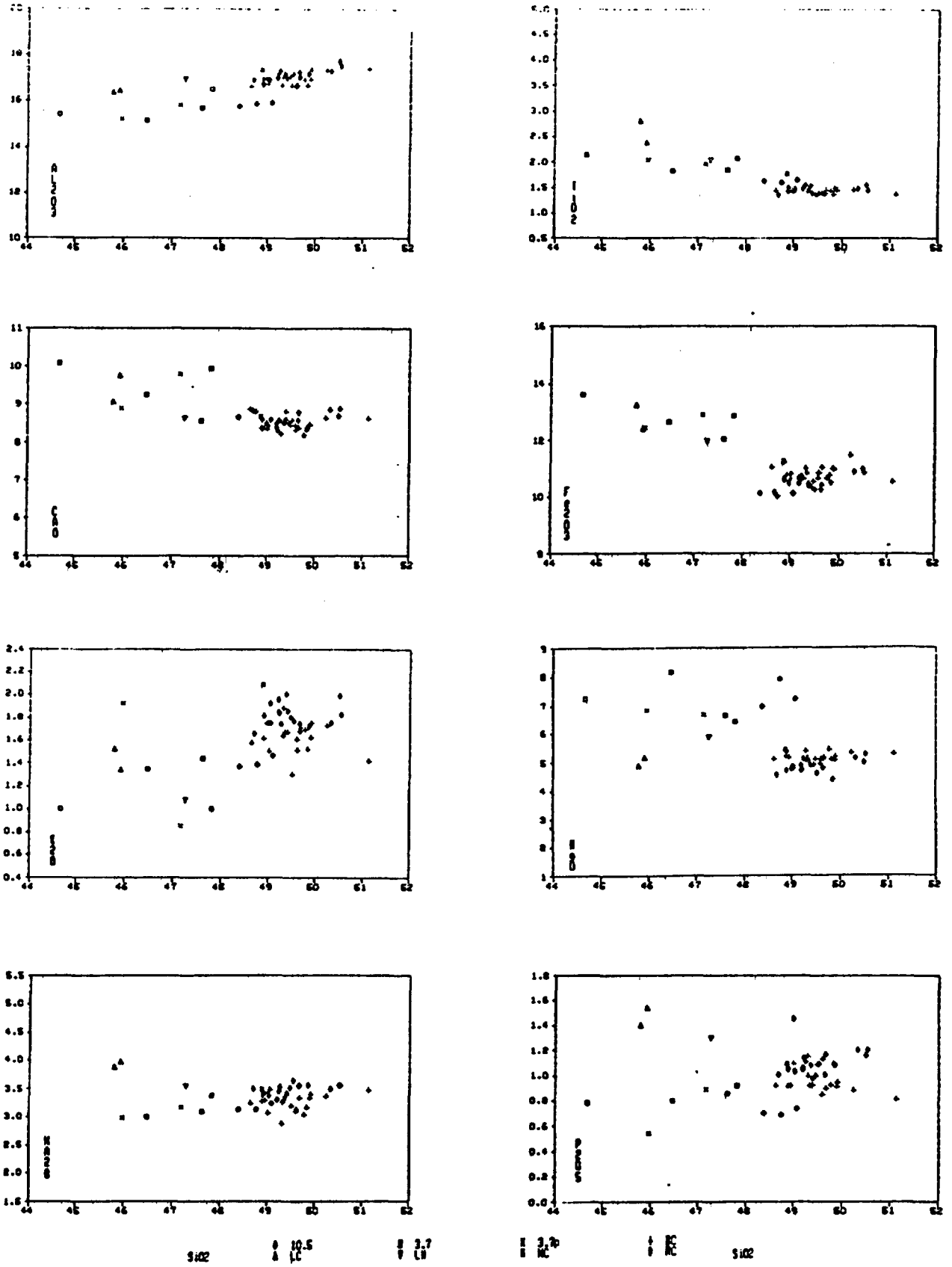

Figure 6. Harker variation diagrams of major elements (Wt %) plotted vs. SiO_2 for the basalt in Crater Flat. 10.5 = 10.5 Ma basalt, 3.7 = 3.7 Ma basalt, 3.7p = 3.7 Ma basalt on western flank of Yucca Mountain, BC = Black Cone, RC = Red Cone, NC = northern cone, LC = Little Cone, LW = Lathrop Wells.

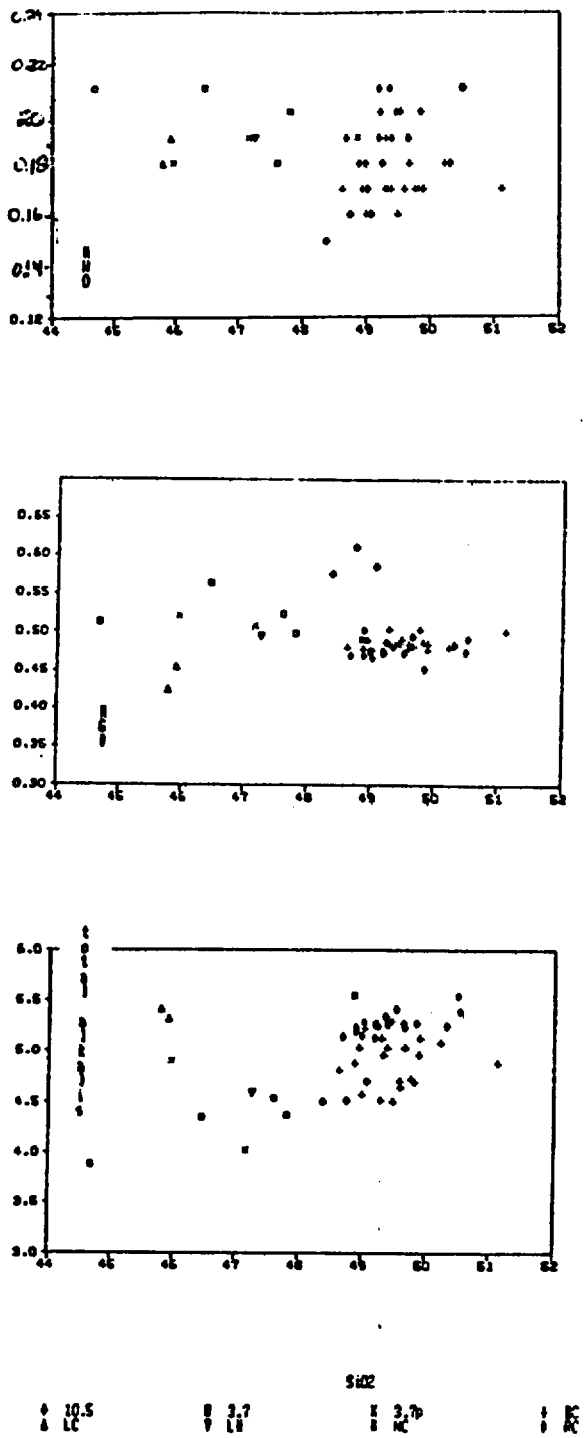

Figure 6. (continued) Harker variation diagrams of major elements (Wt %) plotted vs. SiO_2 for the basalt in Crater Flat. 10.5 = 10.5 Ma basalt, 3.7 = 3.7 Ma basalt, 3.7p = 3.7 Ma basalt on western flank of Yucca Mountain, BC = Black Cone, RC = Red Cone, NC = northern cone, LC = Little Cone, LW = Lathrop Wells.

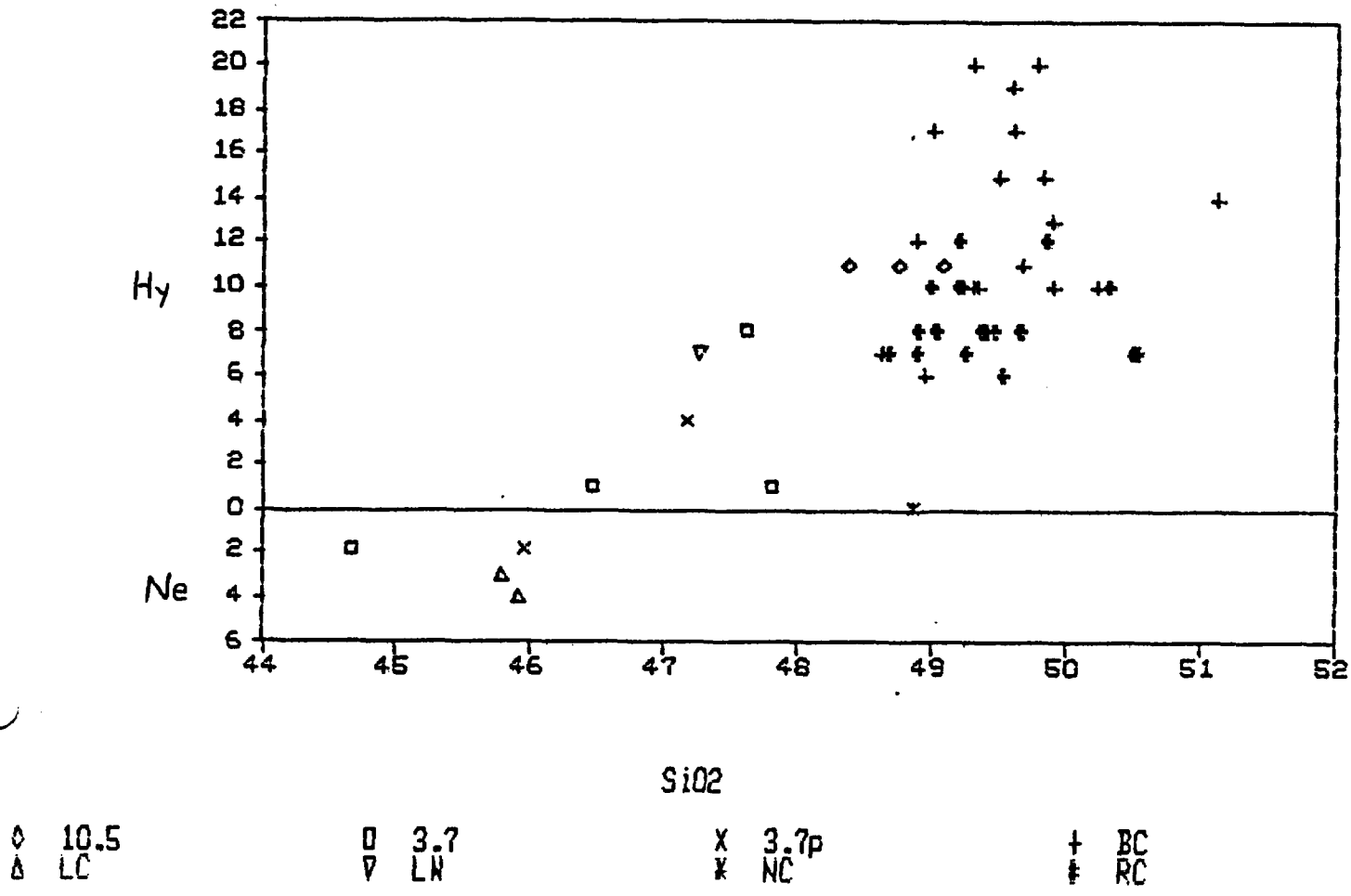

Figure 7. Normative Ne and hy+Q content vs. SiO_2 for the basalt from Crater Flat. 10.5 = 10.5 Ma basalt, 3.7 = 3.7 Ma basalt, 3.7p = 3.7 Ma basalt on western flank of Yucca Mountain, BC = Black Cone, RC = Red Cone, NC = northern cone, LC = Little Cone, LW = Lathrop Wells.

(3) Samples for the Northern Cone plot in the fields for samples of Black Cone and Red Cone (Figures 6 and 7).

(4) A comparison of 3.7 Ma basalt with 1.1 Ma basalt shows that:

a. the 3.7 Ma basalt contains lower SiO_2, Al_2O_3, P_2O_5 and BaO,and higher MgO, Fe_2O_3, TiO_2 and CaO (Figure 6).

b. The 3.7 Ma basalts may contain either normative nepheline or hypersthene. Basalts of Black and Red Cones are only hypersthene normative (Figure 7).

c. Red Cone, Black Cone and the 3.7 Ma basalts display increasing BaO and Al_2O_3 and constant to slightly decreasing abundances of TiO_2 with increasing SiO_2 (Figure 6).

d. The 3.7 Ma basalts display increasing Na_2O with increasing SiO_2, but Black and Red Cones have constant Na_2O concentrations (Figure 6).

e. K_2O concentrations are scattered on Harker diagrams for Crater Flat basalts (Figure 6).

(5) When comparing basalts from Black Cone to those from Red Cone, fields overlap. Black Cone basalts are slightly lower in SiO_2, P_2O_5, Na_2O, BaO and MnO and higher in Fe_2O_3. MgO, Fe_2O_3. CaO and P_2O_5 increase with increasing SiO_2 at Red Cone but decrease at Black Cone (Figure 7).

(6) The 10.5 Ma basalt have SiO_2 content between 48.5 and 49.5. When compared to basalts from the other cycles the 10.5 Ma lavas are lower in Fe_2O_3

and P_2O_5. The 10.5 Ma lava has a higher Mg# (0.57-0.61) than lava from the other cycles (Figure 6).

Trace Elements

Trace and rare earth data is presented in Table 2. The 1.1 Ma cycle and Lathrop Wells lavas are strongly enriched in light rare-earth elements (LREE), immobile elements and large-ion-lithophile (LIL) elements and are slightly depleted in the transition elements (Sc, V, Cr and Co) when compared to MORB (Figure 8). The 3.7 Ma and 10.5 Ma lavas are also enriched in LREE, LIL and immobile elements but not to the same degree as the 1.1 Ma and Lathrop Wells lavas. The 3.7 and 10.5 Ma lavas are not depleted in the transition elements. The 10.5 Ma lava are the least enriched in LIL, REE and immobile elements and are the least depleted in the transition elements (Figure 8). REE plots show a steep negative slope for the 1.1 Ma and Lathrop Wells lavas with La enriched 200-400 times over chondrite abundances (Figure 9). The 3.7 and 10.5 Ma basalts are enriched in La 100 to 200 times chondrite.

ISOTOPES

Crater Flat basalts have high initial $^{87}Sr/^{86}Sr$ (0.707), very low epsilon Nd (-9 to -12) and have slighlty elevated $^{207}Pb/^{206}Pb$ and $^{208}Pb/^{204}Pb$ contents (15.6 and 38.5 respectively) (Table 3 and Figure 10). The combination of high $^{87}Sr/^{86}Sr$ and low epsilon Nd has been attributed to crustal contamination (Semken, 1984) and to the partial melting of a mature lithospheric mantle component (Farmer et al., 1989). The lack of

Sample #	Group	La	Ce	Nd	Eu	Tb	Yb	Lu	Sm	Cr	Co	Sr	Ba	Sc	Hf	Ta	Th	V
C8-1-1-LN	BC	111.00	209.00		2.54		1.57	0.55	11.00	97.80	24.30	1420.00	1180.00	17.40	7.43	1.61	11.80	152.00
C8-1-2-LN	BC	119.00	226.00	18.60	2.71	1.22	3.29	0.24	12.00	103.00	26.30	1900.00	1610.00	18.60	7.64	1.71	12.60	168.00
C8-1-3-LN	BC	114.00	213.00		2.52		3.03	0.36	11.30	100.00	24.60	1350.00	1630.00	17.30	7.35	1.45	12.20	156.00
C8-1-4-LN	BC	125.00	218.00		2.66		3.26	0.41	12.70	88.20	23.80	1800.00	1640.00	17.40	7.38	1.43	12.20	146.00
C8-1-5-LN	BC	116.00	223.00		2.62	1.78	3.33	0.25	11.60	102.00	24.70	1670.00	1890.00	17.10	7.69	1.79	12.20	147.00
C9-1-06-LN	BC	120.00	233.00	90.10	2.68	1.55	2.79	0.31	11.90	117.00	28.10	16.10	1380.00	19.20	7.91	1.40	27.00	176.00
C9-1-07-LN	BC	118.00	213.00	94.00	2.41		1.54	0.23	11.70	100.00	25.60	1490.00	1620.00	17.20	7.24	1.66	15.60	158.00
C9-1-08	BC	121.00	233.00		2.74		2.69	0.34	12.10	119.00	27.90	1820.00	1900.00	19.10	8.01	1.82	13.00	161.00
C9-1-09	BC	118.00	219.00	143.00	2.54	1.19	2.42	0.15	11.90	106.00	25.30	1610.00	1370.00	17.40	7.47	1.60	12.40	176.00
C9-1-10-LN	BC	122.00	223.00		2.65	1.62	3.09	1.01	12.20	104.00	27.20	1870.00	1650.00	17.90	7.62	1.72	13.30	168.00
C9-1-11-LN	BC	116.00	210.00		2.51	1.40	2.29	0.34	11.50	79.70	23.40	2110.00	1490.00	16.60	7.19	1.53	11.80	162.00
C9-1-12-LN	BC	121.00	223.00		2.66	0.95	3.23	0.39	12.20	95.40	25.70	1850.00	1660.00	17.90	7.55	1.58	12.70	191.00
C9-1-13-LN	BC	117.00	220.00		2.54		2.87	0.31	11.90	97.40	25.50	1780.00	1470.00	17.70	7.74	1.66	12.80	161.00
C9-1-14-LN	BC	123.00	233.00	87.60	2.81	2.40	2.71	0.25	12.30	109.00	26.10	1900.00	1580.00	18.20	8.02	1.56	13.00	174.00
C9-1-15-LN	BC	117.00	220.00	78.20	2.65	1.20	3.40	0.21	11.30	104.00	25.10	1630.00	1640.00	17.50	7.68	1.33	12.00	169.00
C9-1-16-LN	BC	122.00	221.00	122.00	2.70	1.36	1.80	0.38	12.30	115.00	26.30	2170.00	1440.00	17.90	7.88	1.44	12.80	163.00
C9-1-19-LN	BC	111.00	206.00		2.45	1.21	3.14	0.41	11.20	91.00	24.70	1530.00	1830.00	17.50	7.33	1.45	11.80	168.00
C9-1-26-LN	BC																	
C9-2-27-LN	RC	125.00	232.00		2.95	1.04	2.00	0.34	12.80	97.90	25.70	1520.00	1240.00	18.10	7.97	1.49	12.80	167.00
C9-2-28-LN	RC	143.00	277.00		3.13	1.61	1.72	0.38	13.10	77.80	23.80	2480.00	1980.00	17.80	7.42	1.19	15.20	150.00
C9-2-29-LN	RC	126.00	234.00		2.70	1.13	2.57		12.50	78.00	24.30	2090.00	1600.00	16.90	7.73	1.70	12.00	162.00
C9-2-30-LN	RC	128.00	243.00	98.00	2.90		2.03		12.70		24.20	1930.00	1410.00	17.10	77.70		12.90	155.00
C9-2-31-LN	RC	156.00	277.00	95.60	2.85	1.09	3.13		14.30		23.10	2630.00	1960.00	16.40	63.20	1.41	14.70	162.00
C9-2-32-LN	RC	154.00	276.00	94.60	2.84	1.42	3.20	0.31	13.90	71.70	23.20	2440.00	1460.00	16.40	6.94	1.42	14.80	172.00
C9-2-33-LN	RC	139.00	272.00	82.20	3.05	1.45	3.35	0.31	13.20	74.30	24.70	1960.00	1570.00	17.10	7.79	1.48	13.80	
C9-2-34-LN	RC	141.00	268.00	74.70	2.92		2.10	0.29	13.10	72.50	24.00	2130.00	1890.00	16.90	7.98	1.65	13.80	158.00
C9-2-35-LN	RC	143.00	262.00	80.50	2.92	1.16	2.97	0.36	13.60	69.50	24.00	2070.00	1650.00	17.00	8.28	1.65	13.80	174.00
C9-2-36-LN	RC	136.00	248.00	90.40	2.79	1.07	2.67	0.29	12.80	75.40	24.60	2040.00	1580.00	16.90	7.81	1.67	12.80	176.00
C9-2-37-LN	RC	120.00	214.00	108.00	2.61	1.14	2.49	0.33	11.80	108.00	25.20	1370.00	1460.00	17.70	7.38	1.59	11.80	168.00
C9-2-38-LN	RC	157.00	277.00	84.00	2.98	1.83	3.15	0.46	13.90	77.90	24.30	2720.00	1620.00	17.40	7.63	1.35	15.60	153.00
C9-2-39-LN	RC	151.00	276.00	98.70	3.02	1.67	2.23		13.40	73.20	23.60	2290.00	1420.00	17.20	7.17	1.53	15.30	159.00
C9-2-40-LN	RC	149.00	25.00	95.60	2.87	1.35	3.20		13.60	74.00	22.20	2200.00	1660.00	16.40	7.36	1.65	14.50	164.00
C9-2-41-LN	RC	122.00	209.00	107.00	2.52	1.56	2.91	0.28	11.90	79.50	23.10	1490.00	1280.00	16.30	7.51	1.39	11.60	171.00
C9-2-42-LN	RC	127.00	232.00	94.50	2.82	1.36	3.68	0.37	12.80	73.50	23.80	1560.00	1740.00	16.90	7.57	1.47	12.70	173.00
C9-2-43-LN	RC	126.00	226.00	97.90	2.78	1.23	3.20	0.53	12.30	72.40	22.80	1940.00	1830.00	16.60	8.06	1.48	12.50	166.00
C9-2-44-LN	RC	121.00	212.00	101.00	2.43	0.87	3.31		11.50	59.70	21.10	1270.00	1280.00	14.60	6.65	1.45	10.50	834.00
C9-2-45-LN	RC	137.00	254.00	89.10	3.08		3.03	0.41	13.60	86.60	26.50	1800.00	1610.00	18.80	8.34	1.70	13.40	26.40
C9-2-46-LN	RC	154.00	295.00	110.00	3.05	1.32	2.56	0.29	14.10	76.40	25.10	2100.00	1930.00	17.60	8.32	1.67	15.60	167.00
C9-3-47-LN	NC	119.00	237.00	88.80	2.99	1.31	2.85	0.31	12.70	84.30	26.90	1940.00	1560.00	18.20	8.21	1.29	11.60	180.00
C9-4-48-LN	LC	137.00	271.00	122.00	3.27	1.49	2.70	0.40	16.10	74.80	25.70	2760.00		16.80	7.73	1.60	9.96	204.00
C9-4-49-LN	LC	91.10	194.00	86.20	2.84	1.54	2.90	0.32	12.80	65.80	27.70	2250.00	1270.00	18.10	7.25	1.76	6.51	244.00
C9-5-50-LN	LW	98.60	199.00	76.00	2.76	1.08	2.43	0.33	12.30	107.00	28.40	1490.00	1580.00	19.30	7.47	1.33	7.98	192.00
C9-6-51-LN	3.7p	68.20	138.00	60.20	2.11		2.75	0.37	8.86	189.00	35.00	1240.00	878.00	24.40	6.15	0.91	5.93	258.00
C9-6-52-LN	3.7p	70.10	134.00	60.40	2.07	6.08	3.04	0.29	9.01	248.00	35.50	170.00	1150.00	24.10	5.61	0.99	6.08	231.00
C9-6-53-LN	3.7	65.20	134.00	61.90	2.10	0.88	2.90	0.36	9.51	237.00	39.20	1220.00	1010.00	26.70	5.66	1.38	5.21	266.00
C9-6-54-LN	3.7	72.60	148.00	76.50	2.20	1.33	2.92	0.41	10.10	125.00	30.90	1320.00	927.00	24.70	6.00	1.33	6.76	271.00
C9-6-55-LN	3.7	64.50	130.00	68.20	2.32		2.49	0.37	8.75	269.00	41.90	1500.00	900.00	25.20	5.25	1.30	6.23	229.00
C9-7-56-LN	10.5	50.80	106.00		2.35	1.10	1.80	0.34		245.00	33.40	1290.00	1030.00	21.10	4.73	1.26	6.86	200.00
C9-7-57-LN	10.5	48.50		56.70	2.23	0.91	1.97	0.32	8.21		32.40	1580.00	965.00	20.70	5.03	0.83	5.98	190.00
C9-7-58-LN	10.5	45.10	83.70	61.30	2.07		1.94	0.32	7.81	286.00	33.90	1230.00	989.00	20.30	4.78	1.11	4.76	210.00
C9-6-59-LN	3.7	83.60		87.90	2.56	1.27	2.13	0.34	10.10	175.00	43.10	1680.00	977.00	21.50	6.12	0.95	6.16	229.00
CO-1-68-LN		109.00	178.00	78.30	2.54	1.16	2.23	0.30	9.88	163.00	25.80	1490.00	1240.00	16.00	7.04	1.31	10.60	148.00

Table 2. Rare earth and trace element data for the basalt in Crater Flat.

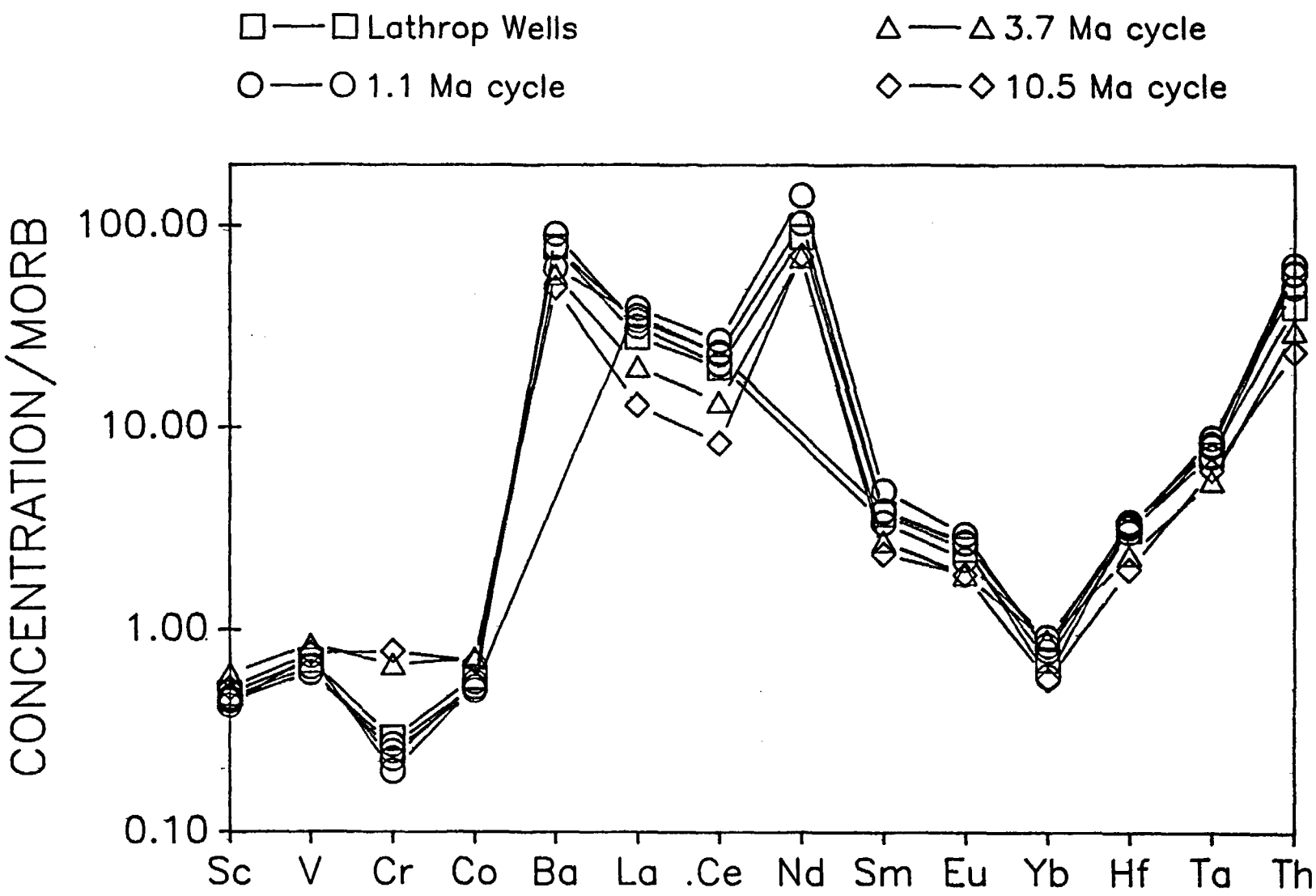

Figure 8. Spider diagram showing trace element abundances relative to MORB in the basalt from Crater Flat.

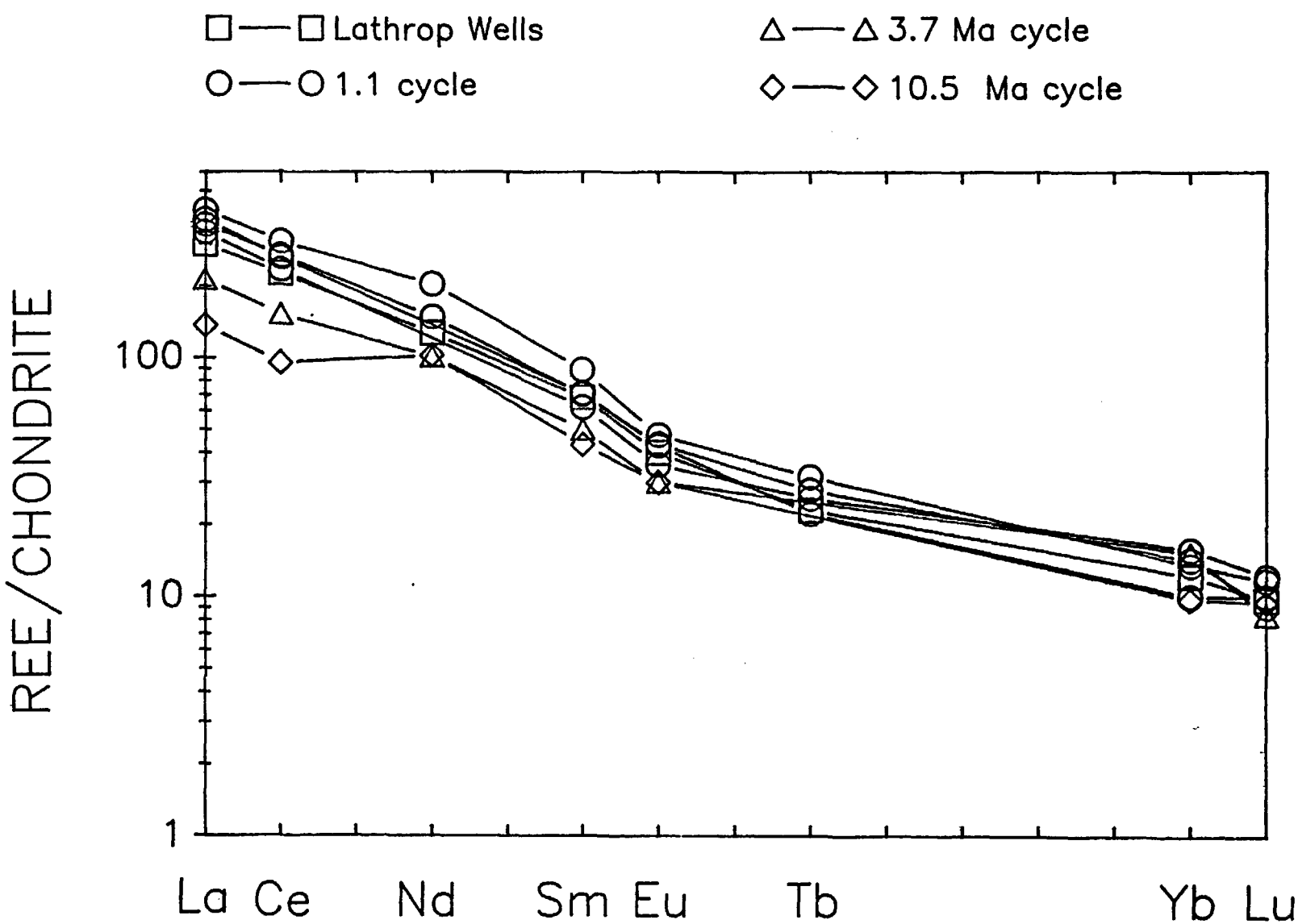

Figure 9. REE diagram for the basalt in Crater Flat.

Table 3. New Sr, Nd and Pb isotope data for the basal

	Black Cone C9-1-16	Red Cone C9-2-39	North Cone C9-3-47
Sr(87/86)i	.70981	.70706	.70687
(143Nd/144Nd)m	.512142	.512180	.512178
E(Nd,0)	-9.68	-8.93	-8.97
Pb206/204	18.515	18.533	18.482
Pb207/204		15.574	15.583
Pb208/204		38.501	38.496

	Little Cone C9-4-48	Lath. Wells C9-5-50	3.7 Ma basal C9-6-54
Sr(87/86)i	.70718	.70697	.70722
(143Nd/144Nd)m	.512173	.512127	.512049
E(Nd,0)	-9.07	-9.97	-11.49
Pb206/204	18.616	18.365	18.285
Pb207/204	15.570	15.563	15.568
Pb208/204	38.628	38.342	38.640

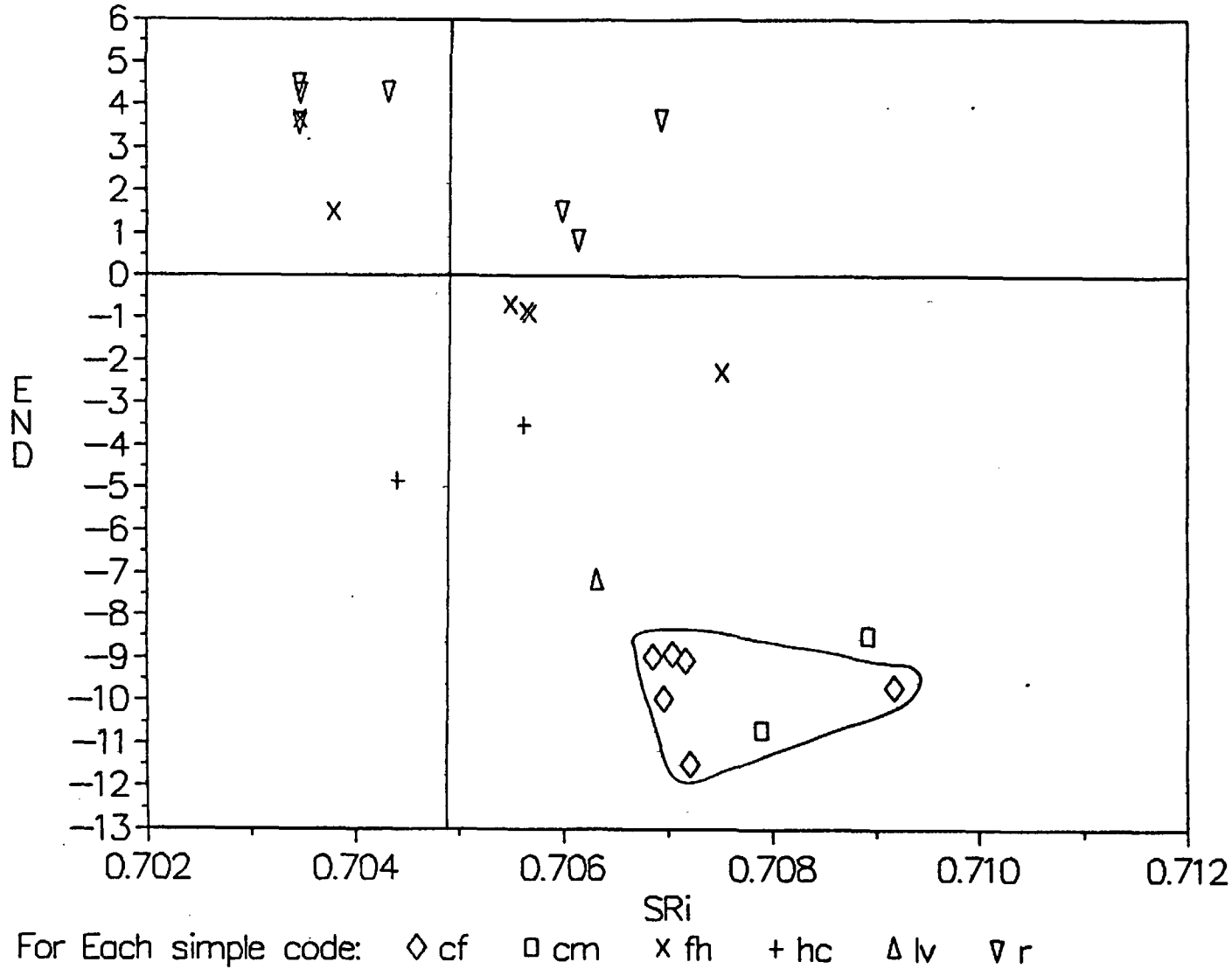

Figure 10. Epsilon Nd-initial $^{87}Sr/^{86}Sr$ plot for basalts in the southern Basin and Range province. Crater Flat basalts (circled field of diamonds) are characteristically low in epsilon Nd and high in $^{87}Sr/^{86}Sr$.

feldspar phenocrysts, a low pressure liquidus phase, the lack of any petrographic or field evidence of mixing, and low of high field strength element concentration suggests that Crater Flat basalt was derived by the melting of lithospheric mantle with little or no crustal component.

GEOCHRONOLOGY

K-Ar plagioclase separate dates are presented in Table 4.

Table 4. Potassium-Argon dates for basalts in the Crater Flat area.

Cycle	Volcanic Center	K-Ar date (Ma)
	Lathrop Wells	0.06 +/- 0.03
1.1 Ma	Little Cones	0.77 +/- 0.04
	Red Cone (dike)	0.98 +/- 0.10
	Red Cone (amphibole-bearing unit)	1.01 =/- 0.06
	Red Cone (basalt on top of Red Cone)	0.95 +/- 0.08
	Black Cone (cinder mound flow)	0.71 +/- 0.06
	Black Cone (lava lake)	1.09 +/- 0.12
	Northern Cone	1.05 +/- 0.07
3.7 Ma	dike in rift zone	2.54 +/- 0.09

REFERENCES

Carr, W.J., 1988, Volcano-tectonic setting of Yucca Mountain and Crater Flat, southwestern Nevada: U.S. Geological Survey Bulletin 1790, p. 35-49.

Cornwall, H.R., 1972, Geology and mineral deposits of southern Nye County, Nevada: Nevada Bureau of Mines and Geology Bulletin 77, 49 p.

Farmer, G.L., Perry, F.V., Semken, S., Crowe, B., Curtis, D., and DePaolo, D.J., 1989, Isotopic evidence on the structure and origin of subcontinental lithospheric mantle in southern Nevada: Journal of Geophysical Research, v. 94, p. 7885-7898.

Irvine, T.N., and Baragar, W.R.A., 1971, A guide to the chemical classification of the common volcanic rocks: Canadian Journal of Earth Sciences, v. 8, p. 523-548.

Kleinhampl, F.J., and Ziony, J.I., 1985, Geology of northern Nye County, Nevada: Nevada Bureau of Mines and Geology Bulletin 99A, 172 pp.

McGetchin, T.R., Settle, M. and Clouet, B.A., 1974, Cinder cone growth modelled after Northeast Crater, Mount Etna, Sicily: Journal of Geophysical Research, v. 79, no. 23, p. 3257-3272.

Semken, S.C., 1984, A neodymium and strontium isotopic study of late Cenozoic basaltic volcanism in the southwestern Basin and Range province: M.S. thesis, UCLA, 68 p.

Swadley, W. C., and Carr, W. J., 1987, Geologic map of the Quaternary and Tertiary deposits of the Big Dune quadrangle, Nye County, Nevada, and Inyo County, California: U.S. Geological Survey Miscellaneous Investigations Series, Map I-1767, scale 1:24,000.

Vaniman, D., Crowe, B., and Gladney, E.S., 1982, Petrology and geochemistry of hawaiite lavas from Crater Flat, Nevada: Contributions to Mineralogy and Petrology, v. 80, p. 341-357.

FORTIFICATION HILL AND CALLVILLE MESA VOLCANIC FIELDS

(D.L. FEUERBACH)

INTRODUCTION

There is a wealth of information concerning mid-Tertiary calc-alkaline silicic to intermediate volcanism in the Basin and Range. Most of this volcanism occurred either prior to or during active upper crustal extension. There are also numerous studies discussing late-Pliocene to Quaternary alkalic mafic volcanism. In most cases mafic volcanism post-dates major block rotation associated with Basin and Range extension. These studies have demonstrated that there is a fundamental chemical difference between volcanic rocks formed during and prior to regional extension and volcanic rocks produced in the last 4 Ma. One topic that has not been discussed is whether there is a gradual transition from earlier (mid-Tertiary) calc-alkaline intermediate to Pliocene-Quaternary volcanism or whether the transition is abrupt. We document the nature of this transition in the Lake Mead area of Nevada and Arizona, where Tertiary volcanism provides an almost continuous record of changing magmatic composition from calc-alkaline intermediate volcanism that occurred during active extension (18-12 Ma) to alkali basalt volcanism that occurred after the major phase of extension (after 9 Ma).

There are several well-studied volcanic centers in the Lake Mead area that formed during the active extension. These include volcanic and plutonic rocks located at Boulder Wash (Naumann, 1987; Naumann and Smith, 1988 and Smith et al., 1989), the River Mountains (Smith, 1982 and Smith et al., 1989), the McCullough Range (Smith et al., 1988), Wilson Ridge (Feuerbach, 1986; Feuerbach and Smith, 1986; Larson, 1989; Larson and Smith, 1990) and the Hamblin-Cleopatra volcano (Anderson, 1973; Thompson, 1985, Barker and Thompson, 1989). These rocks are calc-alkalic or alkali-calcic andesites and dacites, and are associated with diorite to quartz monzonite plutons. Processes proposed for the generation of these intermediate igneous rocks are attributed to complex open-system processes involving assimilation and/or mixing of a felsic component with a fractionated mafic phase (Naumann, 1987; Smith et al., 1990; Larson and Smith, 1990). These processes are similar to those described by Nielson and Dungan (1985), McMillan and Dungan (1986), and Novak and Bacon (1986).

For this study we concentrated on the younger mafic volcanic rocks that erupted during and after the latest upper crustal extensional event in the Lake Mead area. We investigated the Callville Mesa field that formed between 8.5 and 10.3 Ma during the latest period of active upper crustal extension and block rotation, and the Fortification Hill field that formed between 4.7 to 5.9 Ma after the main phase of upper crustal extension. The objective of this study is to document this fundamental change in volcanism during waning extension in the Lake Mead area. We report on volcanology, petrography, geochemistry and isotope geochemistry of these volcanic rocks and model their magmatic evolution.

GEOLOGIC SETTING

The Callville Mesa and Fortification Hill volcanic fields lie in the southern part of the Basin-and-Range physiographic province in the Lake Mead area of Nevada and Arizona (Figure 1). Major structures in the Lake Mead area are low-angle and high-angle normal faults and strike-slip faults that may have formed during at least two mid-Miocene episodes of detachment faulting (Duebendorfer et al., 1989). The major strike-slip systems are the Lake Mead Fault Zone (LMFZ), a series of west-southwest trending left-lateral strike-slip faults and the Las Vegas Valley Shear Zone, a series of east-southeast trending right-lateral strike-slip faults (Figure 1). These strike-slip zones are interpreted to be coeval with normal faults and may have formed as transfer zones between two differentially extending upper-plate blocks (Bohannon, 1983; Weber and Smith, 1987; Duebendorfer and Wallin, in press). The Lake Mead Fault Zone serves as a boundary between two geologically different blocks. North-northwest trending high-angle normal faults south of the Lake Mead Fault zone cut low-angle faults, Miocene volcanic and plutonic rocks, and Miocene to Pliocene clastic intrabasinal sediments of the Horse Spring and Muddy Creek Formations (Anderson, 1978; Mills, 1985; Feuerbach, 1986). Movement along these faults resulted in a series of horsts and grabens and half grabens. Small allocthonous blocks of tilted Paleozoic carbonate, shale and sandstone also crop out in the grabens. Fortification Hill basalt crops out mainly south of Lake Mead (Figure 2).

The area north of the Lake Mead Fault Zone is composed of highly tilted Mesozoic sediments and Miocene intrabasinal sediments of the Horse Spring and Muddy

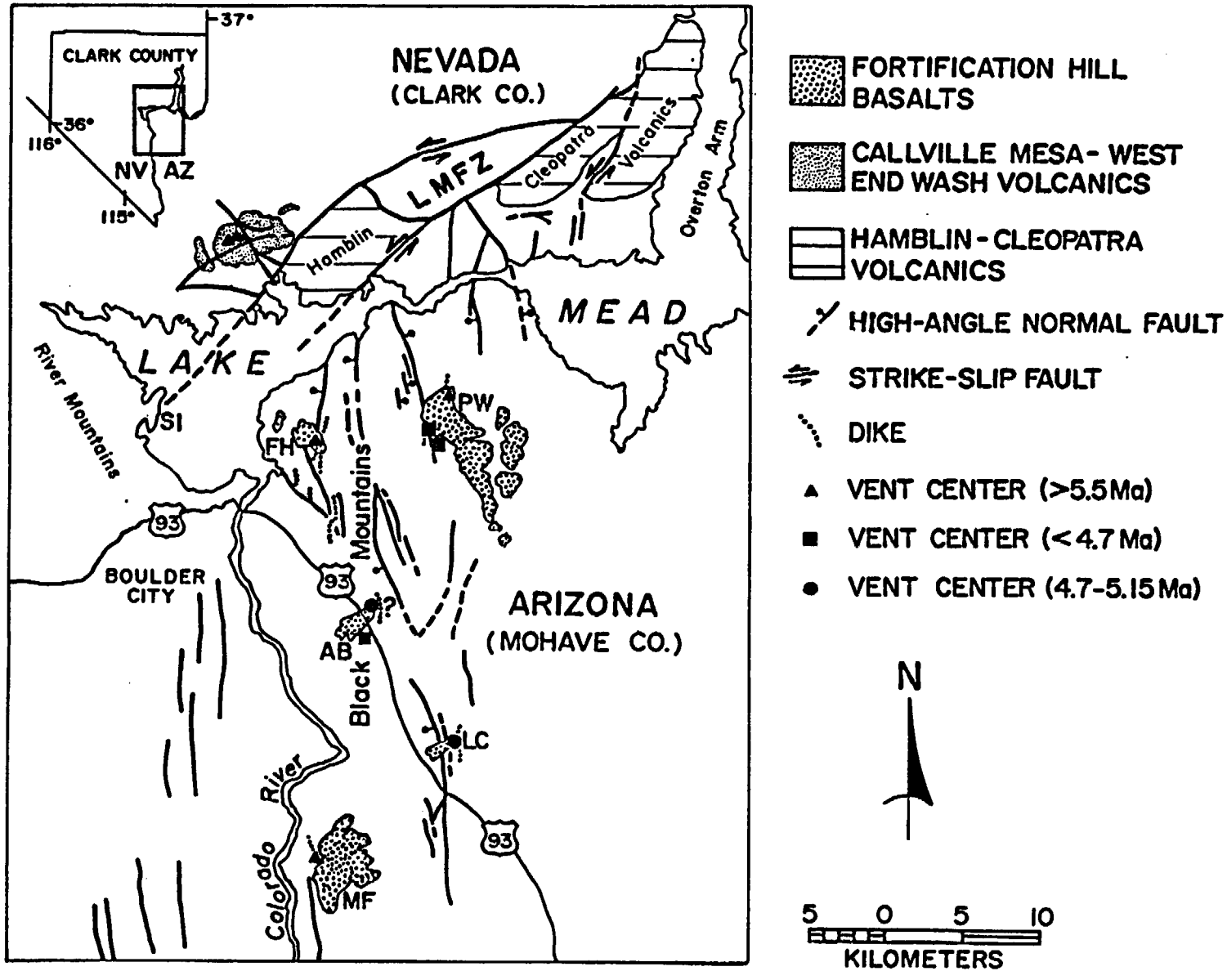

Figure 2. Generalized geoiogic map of the Lake Mead area.

Creek Formations (Bohannon, 1983). The area north of the fault zone is devoid of any major igneous activity although minor amounts of Fortification Hill basalt crop out at Black Point, Nevada.

Basin and Range tectonism is often recorded in Tertiary clastic sediments. The origin of these sediments is usually related to the opening of a basin that is then infilled with debris from the surrounding ranges. There are three unconformable units of Tertiary intra-basin clastic deposits in the Lake Mead area. They are the Horse Spring Formation (20-13 Ma), Red Sandstone Unit (11-8.5 Ma) (Bohannon, 1982; Duebendorfer and Wallin, in press) and the Muddy Creek Formation (8.5-4.7) Ma). It is important to note that the only the Muddy Creek Formation is not appreciably affected by faulting and rotation. Duebendorfer and Wallin (in press) have suggested that the Red Sandstone Unit was deposited in a tectonic basin formed from large-scale detachment faulting. The northern boundary for this basin is the Las Vegas Valley Shear Zone which they interpret as the transfer structure separating the highly extended terrane to the south from a less extended terrane to the north. The Callville Mesa volcanic rocks were erupted during development of this basin and are confined to the Red Sandstone basin. The Fortification Hill basalts are time-equivalent to the relatively undeformed Muddy Creek Formation.

VOLCANOLOGY AND STRATIGRAPHY

Callville Mesa Volcanic Field

The Callville Mesa (CM) volcanic field is exposed primarily on Black and Callville Mesas which lie adjacent to the LMFZ (Figure 2). Flows locally lie on and are interbedded with a conglomerate that is correlative with the Red Sandstone unit first recognized by Bohannon (1984).

Volcanic activity at Callville Mesa and West End Wash lasted from 10.3 to 8.5 Ma. Basaltic andesite erupted from two volcanoes that lie on Callville Mesa and in West End Wash (Figure 3). Lavas on Callville Mesa erupted from a compound cinder cone on the footwall of an east-west striking down-to-the-south normal fault (Figure 3). This cone is composed of interbedded scoria and olivine bearing basaltic andesite flows. A lava lake sequence occupies the summit area. Within West End Wash, two sequences of lava flows are exposed. Although, both areas are nearly identical in mineralogy and chemistry, they are separated by an angular unconformity. Lavas at West End Wash are tilted 20 to 50 degrees to the west and are concordant with underlying sediments. Flows of the West End Wash volcano are overlain by nearly horizontal flows that erupted from the Callville Mesa volcano.

Fortification Hill Basalt Field

The Fortification Hill basalt field forms a 75 km long north-northeast trending zone that extends from Malpais Flattop, Arizona to Black Point, Nevada (Figure 1). The field is composed of flows of tholeiite, calc-alkalic basalt and alkalic basalt that

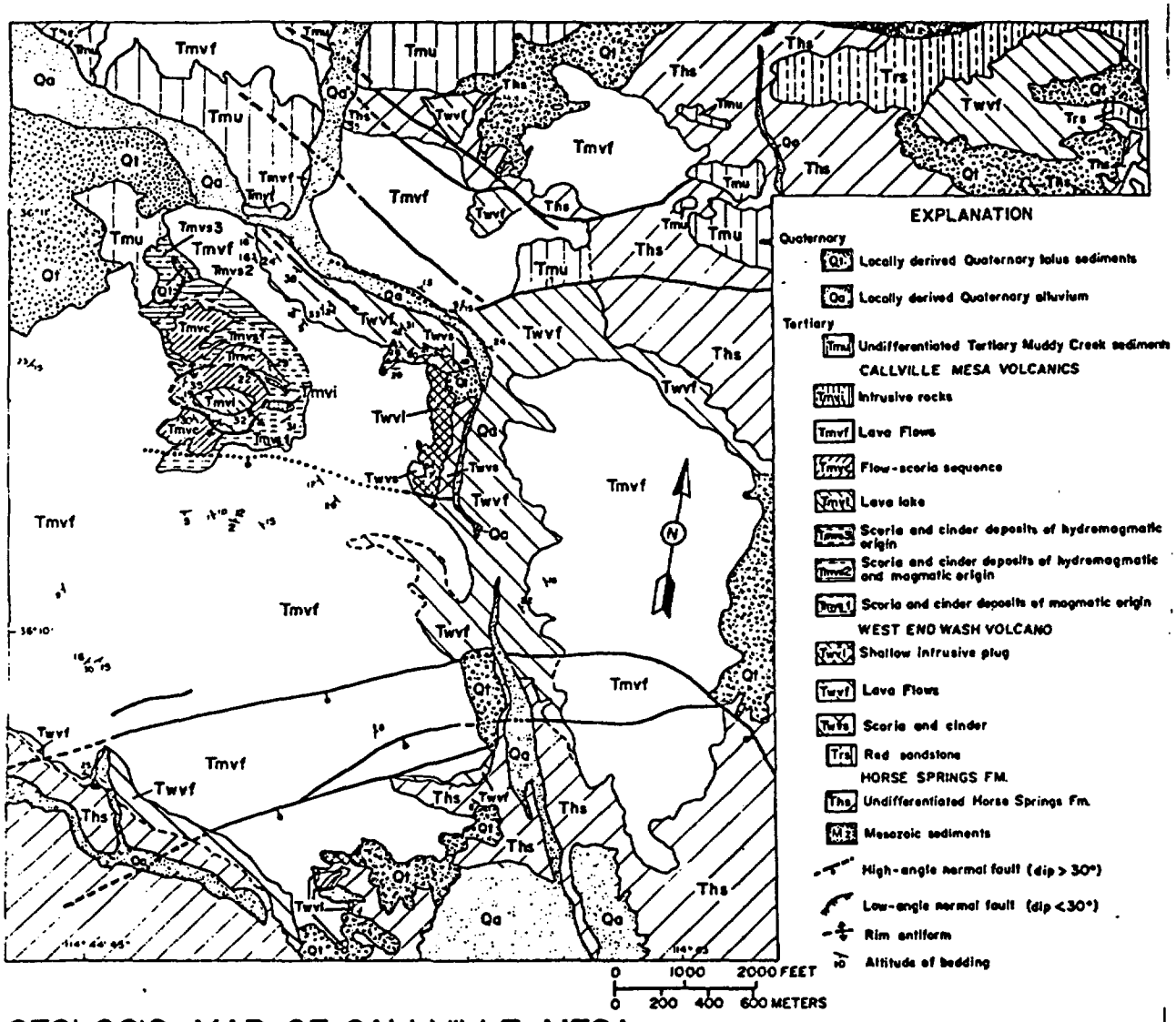

GEOLOGIC MAP OF CALLVILLE MESA

Figure 3. Geologic Map of the Callville Mesa volcanic field.

periodically erupted from eight separate volcanic centers from 6.02 to 4.3 Ma. The earliest eruptions occurred at Black Point (6.02 Ma). Initial eruptions occurred at 5.88 Ma both at Fortification Hill (FH) and Malpais Flattop (MF). As volcanism was waning at Fortification Hill, eruptions were occurring at Petroglyph Wash (PW) (5.42 Ma). Volcanic activity was initiated 5.13 m.y. ago at the Lava Cascade (LC) and lasted till 4.74 Ma. Alkali basalt bearing large kaersutite megacrysts occur south of Hoover Dam along U.S. 93 as dikes, plugs and a small flow (Campbell and Schenk, 1950). Intrusions of the same magma type crop out in the Petroglyph Wash area (Feuerbach, 1986) and near Saddle Island (Smith, 1984). The emplacement of this alkalic-basalt magma (YAB) occurred at about 4.7 Ma (Scott et al., 1971 and this study). These are the youngest basalts of the Fortification Hill field.

Subalkalic and alkalic basalts occur in the Fortification Hill field (FH). We divide FH basalt into three groups: (1) Tholeiitic two pyroxene basalt (6.02-5.71 Ma) (SAB) at Black Point and Malpais Flattop and subalkalic basalt at Fortification Hill (lower section). (2) Alkali basalt (5.42 to 4.74 Ma) (OAB) at Fortification Hill (upper section), Petroglyph Wash and Lava Cascade. (3) Alkali basalt (4.61 to 4.3 Ma) (YAB) along U.S. 93 near Hoover Dam, Saddle Island and in Petroglyph Wash.Black Point

Black Point, Nevada is located along the eastern shore of the Overton Arm of Lake Mead approximately 10 km south of Overton Beach, Nevada (Figure 1). The Black Point volcanic center is composed of SAB flows and dikes and thin ash beds that are intercalated with fine-grained and gypsiferous facies of the Muddy Creek Formation. The

basalt erupted from three en echelon north-trending dikes. In two locations, dikes feeding flows are clearly observed.

Eruptions at Black Point were relatively quiet as evidenced by the lack of scoria and bombs. However, there is a light-colored silicic ash of variable thickness (0 to 2 m) at the base of the flows that locally displays cross-bedding. This unit is interpreted as a pyroclastic surge deposit and its presence suggests that mafic volcanism may have initiated by silicic explosive hydroclastic eruptions (Figure 4).

Malpais Flattop

Malpais Flattop is composed of a thick stack of SAB flows located just south of Willow Beach (Figure 2). Two sections of basalt are recognized. Intercalated within Muddy Creek conglomerate is a 15 to 20 m thick stack of highly altered olivine basalt. This section of basalt is conformable with the Muddy Creek sediments and dips gently (20 degrees) toward the east. The upper section caps Malpais Flattop and is separated from the lower basalt flows by a thick section of Muddy Creek conglomerate. This basalt is relatively unaltered and dips gently (<5 degrees) to the east.

Fortification Hill

Fortification Hill is a steep sided mesa on the southeast side of Lake Mead in Mohave County, Arizona (Figure 2). The escarpment that forms the cap of Fortification Hill is composed of over 100 flows of olivine basalt and scoria (Mills, 1986). SAB Flows travelled predominately toward the west and north and form a complex set of cinder

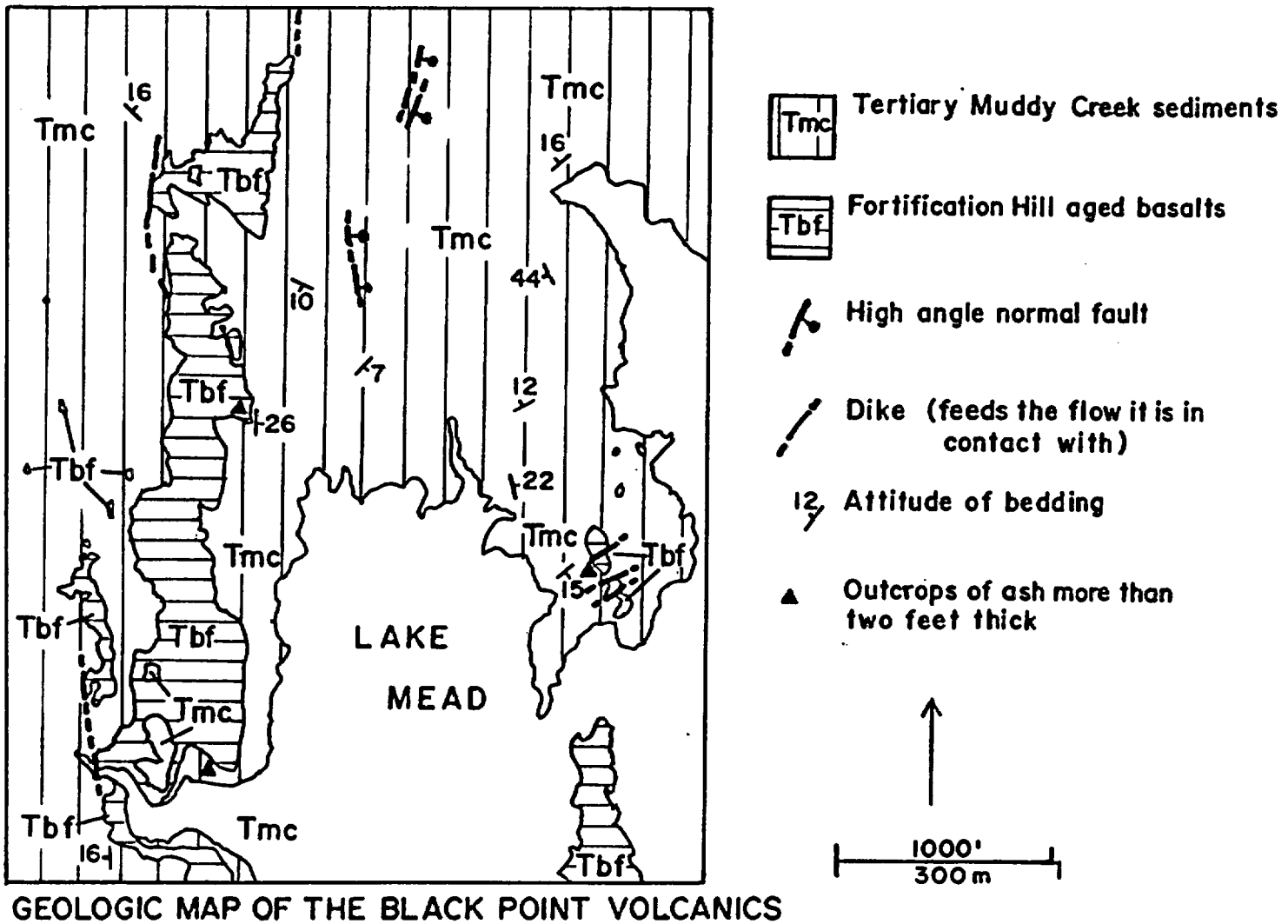

Figure 4. Geologic map of the Black Point area.

cones. The cones are related to a north-trending en echelon dike system that parallels the east-dipping mid-Miocene Fortification fault zone (Figure 2).

Cinder cones are highly eroded. Cones are composed of massively bedded red to brown scoria, bedded cinder, bombs, spatter, agglutinated scoria, loose scoria and ash that was deposited by Strombolian eruptions. OAB Pyroxene-olivine-plagioclase and olivine basalt plugs and associated dikes intrude scoria. Six plugs are aligned in a north-south direction, parallel to the elongation of the vent center (Figure 5). Plugs are sub-round to oval shaped with their long axes parallel to that of the vent center. Many dikes intrude the scoria, some of which feed flows on the flanks of the cinder cones.

Petroglyph Wash

The Petroglyph Wash basalt exposures lie directly east of Wilson Ridge south of Lake Mead in Mohave County Arizona (Figure 2). Three vent areas are exposed in the area. Most of the OAB flows erupted from a large cinder cone complex located at Gilbert Wash (5.42 Ma). Two late-stage intrusions of highly alkalic-basalt (YAB) are located west of the flows in Petroglyph Wash. These plugs were emplaced at 4.64 Ma. A minor volume of lava may have been erupted from the plug/scoria vents. Fortification Hill basalt is also exposed 10 km south of Petroglyph Wash along the western margin of the Black Mountains. The vents for these flows have not been identified.

The cinder cone in Gilbert Wash is deeply dissected and intruded by meandering feeder dikes and a plug. Vent facies contain scoria, cinder, ash and bombs. A 1-2 m wide

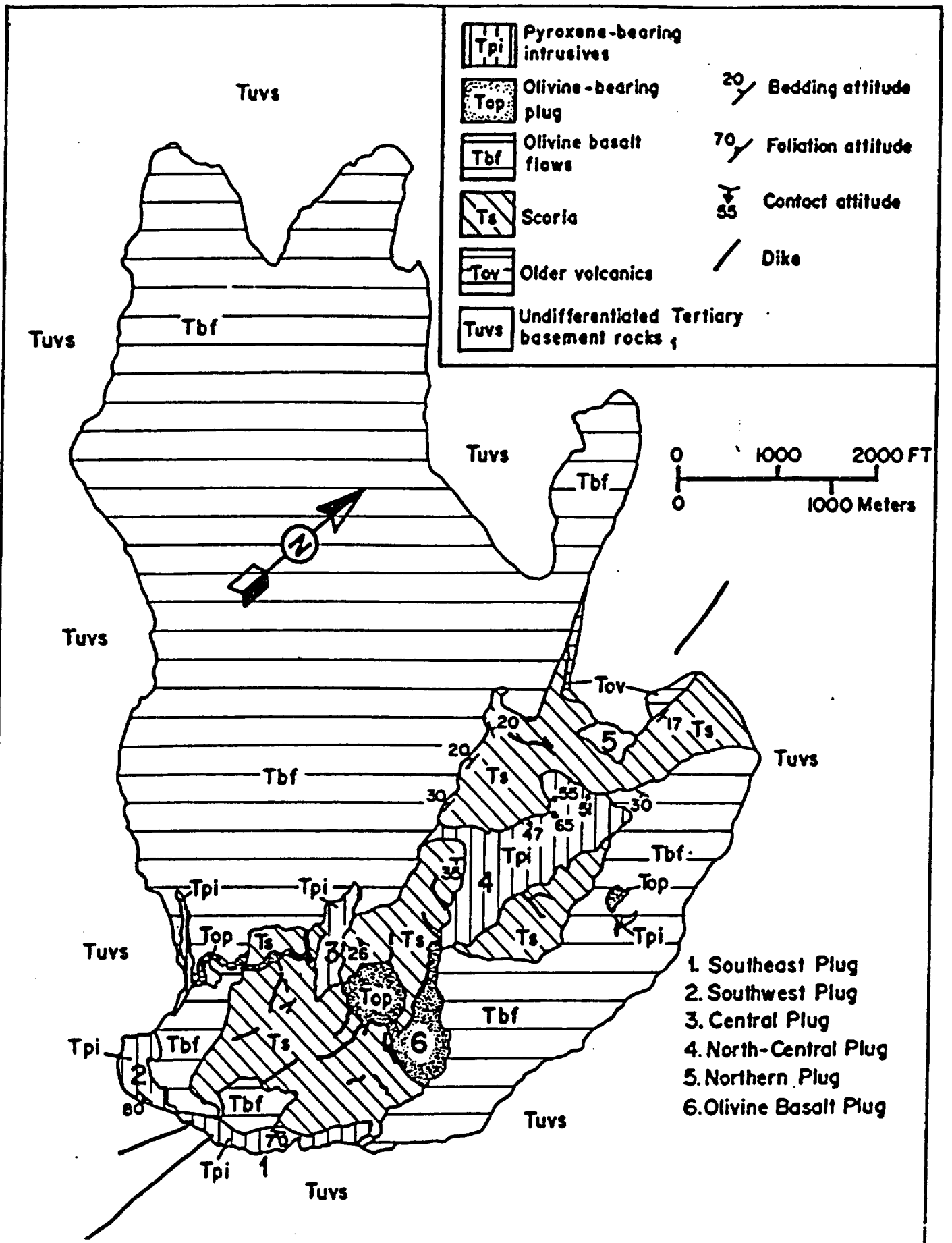

Figure 5. GEOLOGIC MAP OF FORTIFICATION HILL

dike which can be traced from the country rock into the cinder cone may be part of the conduit system which fed the center.

The Lava Cascade

OAB eruptions from cinder cones (5.13-4.74 Ma) near the summit of the Black Mountains produced lava that flowed nearly two kilometers to the west down a steep canyon cut in Precambrian basement rock toward the Colorado River (Figure 2). Flows crossed range bounding faults and tilted late-Tertiary Muddy Creek conglomerates (Figure 6).

Olivine-pyroxene-bearing basalt plugs and olivine-basalt plugs intrude scoria. The scoria deposits are composed of spatter, agglutinated scoria, loose scoria, cinder and ash, and rare blocks which resulted from Strombolian eruptions. Feeder dikes extend north and south from the vent center into the Precambrian basement. Olivine-plagioclase basalt flows erupted from the flanks of scoria-cinder cones early in the formation of the Lava Cascade.

Young Alkalic Basalt

Black Canyon

The youngest volcanism in the Fortification Hill field is represented by megacryst and xenolith bearing alkali basalt dikes and flows which crop out 10 to 15 km south of Hoover Dam along U.S. 93 (Figure2). Basalt erupted during deposition of Muddy Creek

Geologic Map of Lava Cascade

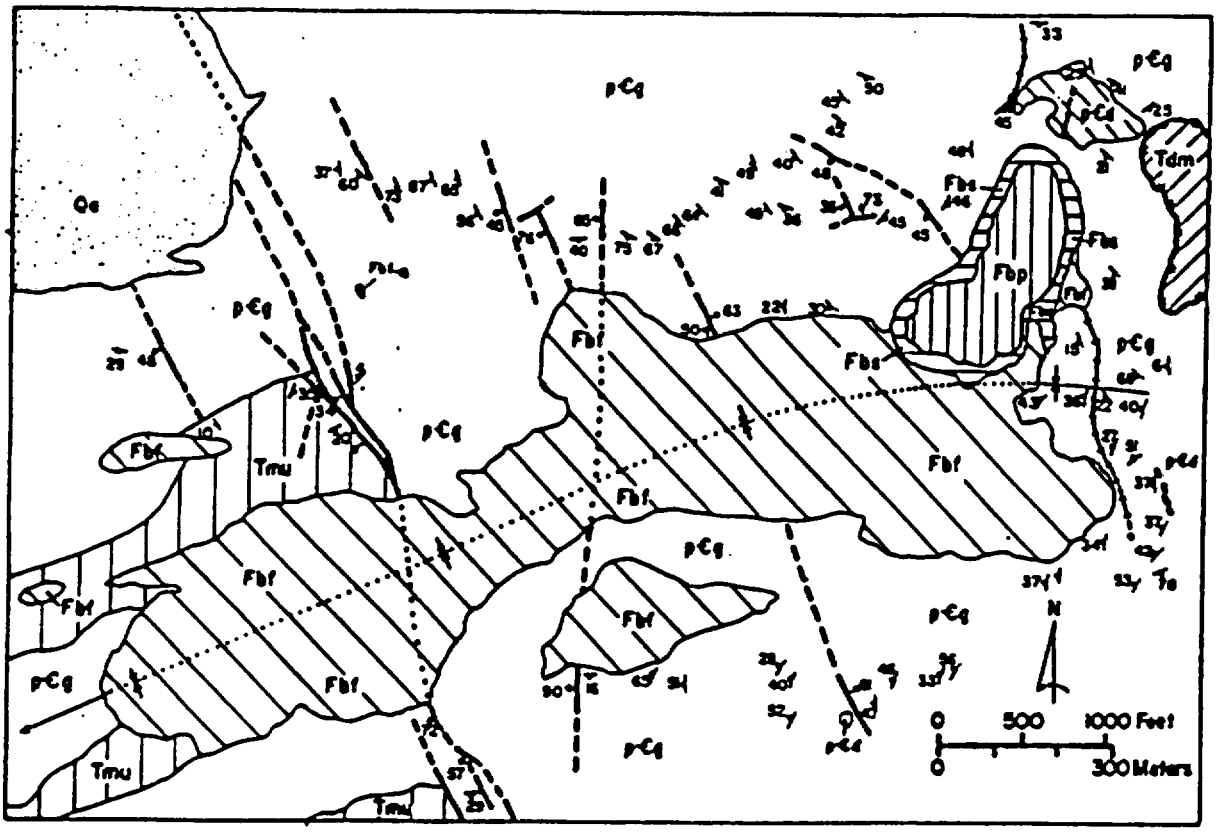

Explanation

- Qa — Quaternary alluvium
- Fbp — Intrusive plugs
- Fbf — Olivine basalt flows
- Fbs — Scoria, spatter, ash and cinder
- Tmu — Muddy Creek Formation
- Tdm — Mount Davis volcanic rocks
- p€d — Precambrian diorite
- p€g — Precambrian gneiss and granite

- High-angle normal fault- dashed where inferred, dotted where covered, arrow indicates direction of dip, ball and bar on hanging wall
- Low-angle normal fault- teeth point to upper plate
- Basalt Dike
- Attitude of foliation
- Attitude of bedding
- Synform axis- dotted where covered, arrow points in direction of plunge

Figure 6. Geologic Map of the Lava Cascade area.

fanglomerate. These dikes and flows were first identified as camptonite by Campbell and Schenk (1950) because of the large kaersutite crystals which are carried in the basalt. Nielson (manuscript in preparation) suggested that the kaersutite is part of a mantle derived xenocryst and xenolith assemblage that was transported to the surface by the alkalic basalt.

Intrusive Plugs at Petroglyph Wash

Two plugs (the diatreme and scoria/plug center) intrude the Wilson Ridge Pluton in the western part of Petroglyph Wash. The diatreme is composed of a tuff breccia intruded by a 50 m wide YAB plug and a smaller 4 m diameter pipe of alkali basalt. Pyroxene megacrysts are contained in the smaller pipe of basalt. The breccia contains matrix supported clasts of scoria and angular fragments of mid-Tertiary Wilson Ridge quartz monzonite (country rock) in a buff colored tuffaceous matrix.

The basalt/plug occupies a topographic high west of the flows in Petroglyph Wash. The YAB plug is surrounded by scoriaceous unit that is composed of agglutinated cinder, ash and scoria and contains angular clasts of Wilson Ridge quartz monzonite. The plug rock is alkali-basalt and the outer portions of the plug contain the same quartz monzonite inclusions as the scoria. This plug is fed by a north-trending dike which is exposed directly south of the plug.

PETROGRAPHY

Callville Mesa Volcanics

CM volcanism produced basaltic-andesite which contains phenocrysts of euhedral to subhedral partially resorbed and iddingsitized olivine (Fo 57-83) (1-5%); subhedral, zoned, and resorbed andesine and labradorite (An 30-70) (10-30%); subhedral, poikilitic clinopyroxene (diopsidic-augite) (2-9%); and subhedral orthopyroxene (pigeonite and hypersthene) (3% to trace amounts) (Table 1). Quartz and alkali-feldspar (sanidine) occur as xenocrysts that are rimmed by glass and acicular clinopyroxene (diopsidic-augite). Glomeroporphyritic clots (1-1.5 mm in size) of olivine, diopsidic-augite, and plagioclase; and rare pyroxenite xenoliths containing both clinopyroxene and orthopyroxene occur in basaltic-andesite flows.

Fortification Hill Basalt

Flows

All of the basalt flows in the Fortification Hill field except those from Malpais Flattop contain porphyritic iddingsitized olivine phenocrysts (Fo 49) in a trachytic to pilotaxitic groundmass of olivine, andesine, labradorite, diopsidic-augite and iron oxide (Table 1). Some flows may also contain labradorite, diopsidic-augite and orthopyroxene (probably hypersthene) in the phenocryst phase. Flows from Malpais Flattop contain iddingsitized olivine in a ophitic to subophitic matrix. Diopsidic-augite, pigeonite and hypersthene contain poikilites of labradorite and andesine.

Selected modal mineral percents and Cr values

	Lava Cascade														
	*Flow (6)**	*Plug (5)*	*Dikes (1)*	*114*	*102*	*Flow (2)*	*Plug (6)*	*Dikes (4)*	*13*	*143*	*144*	*Flow (9)*	*Plug (2)*	*46*	*50*
Phenocrysts															
Plagioclase	trace	16	24	trace	trace	4	6	5	6	4	3	21	17	13	25
Olivine	6	7	10	7	6	6	3	3	10	trace	2	3	3	4	3
Clinopyroxene	---	2	1	---	---	---	3	trace	trace	1	trace	5	4	3	5
Magnetite	---	trace	---	---	---	---	trace	---	trace	1	1	---	---	---	---
Orthopyroxene	---	---	---	---	---	---	---	---	---	---	---	1	trace	---	---
Xenocrysts															
Quartz	---	---	trace	---	---	---	---	---	---	---	---	trace	trace	---	trace
Alkali Feldspar	---	---	trace	---	---	---	---	---	---	---	---	trace	trace	---	trace
Xenoliths															
Pyroxenite	---	---	---	---	---	---	---	---	---	---	---	trace	---	---	---
Granite	---	---	trace	---	---	---	---	---	---	---	---	trace	trace	---	---
Cr (ppm)				322	301				361	70	173			149	106

* number of samples averaged for each column in parentheses

Table 1. Selected modal mineral percents and Cr values for representative rocks from the Fortification Hill and Callville Mesa volcanic fields.

Plugs

Late-stage plugs are coarse-grained compared to flows and contain olivine phenocrysts (Fo 45-50) in a coarse-grained interstitial groundmass of andesine, labradorite, diopsidic-augite and olivine. Xenoliths of coarse-grained pyroxene-olivine-plagioclase basalt appear as glomeroporphyritic clots scattered randomly in the matrix. Plagioclase in the xenoliths display penetration twins. Feldspars in the plug rock are more sodic than those in the flows. Some plugs carry subhedral to euhedral phenocrysts of iron oxide that contain inclusions of plagioclase.

Young Alkali Basalt

Matrix of the young alkalic-basalt (YAB) ranges from glassy to interstitial or pilotaxitic containing microlites of plagioclase laths, altered olivine, altered diopsidic-augite and magnetite. Olivine is the primary phenocryst phase. Ubiquitous to YAB are ultramafic inclusions and megacrysts of augite and kaersutite. These phases are best preserved at the Black Canyon exposures.

Black Canyon lavas contain the megacrysts that are resorbed subhedral xenocrysts of kaersutite (up to 5 cm in length) along with lesser amounts of clinopyroxene. Other minerals present in the rock are sodic plagioclase and anorthoclase (Campbell and Schenk, 1950; Neilson, manuscript in preparation).

Ultramafic xenoliths include: 1) altered lherzolite containing fresh chrome-diopside and orthopyroxene; 2) altered wehrlite containing altered olivine poikilites

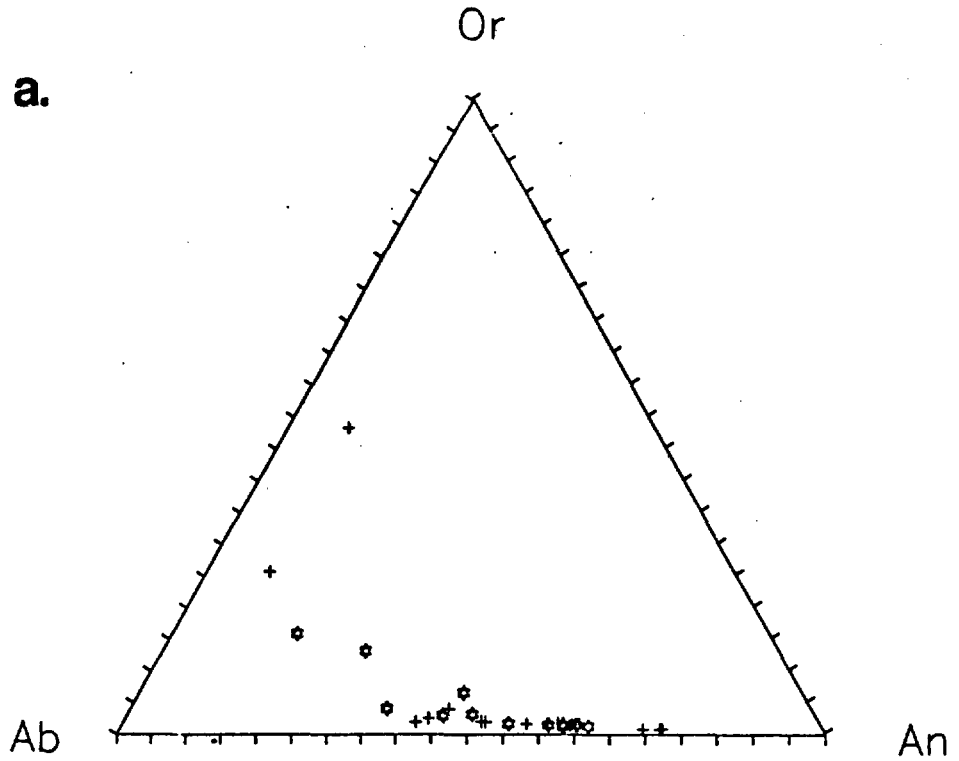

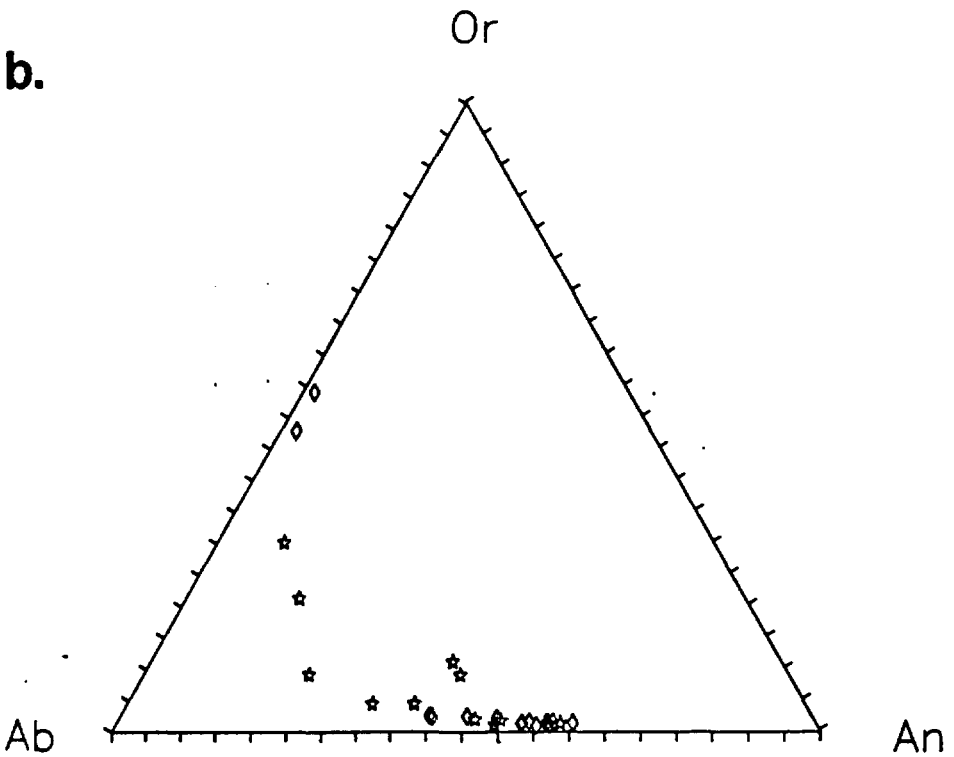

Figure 7. Plagioclase compositions plotted on an Or-Ab-An diagram (a) SAB lava from Malpais Flattop (stars) and Fortification Hill(+); (b) OAB (diamonds) and YAB (stars) lava from Petroglyph Wash.

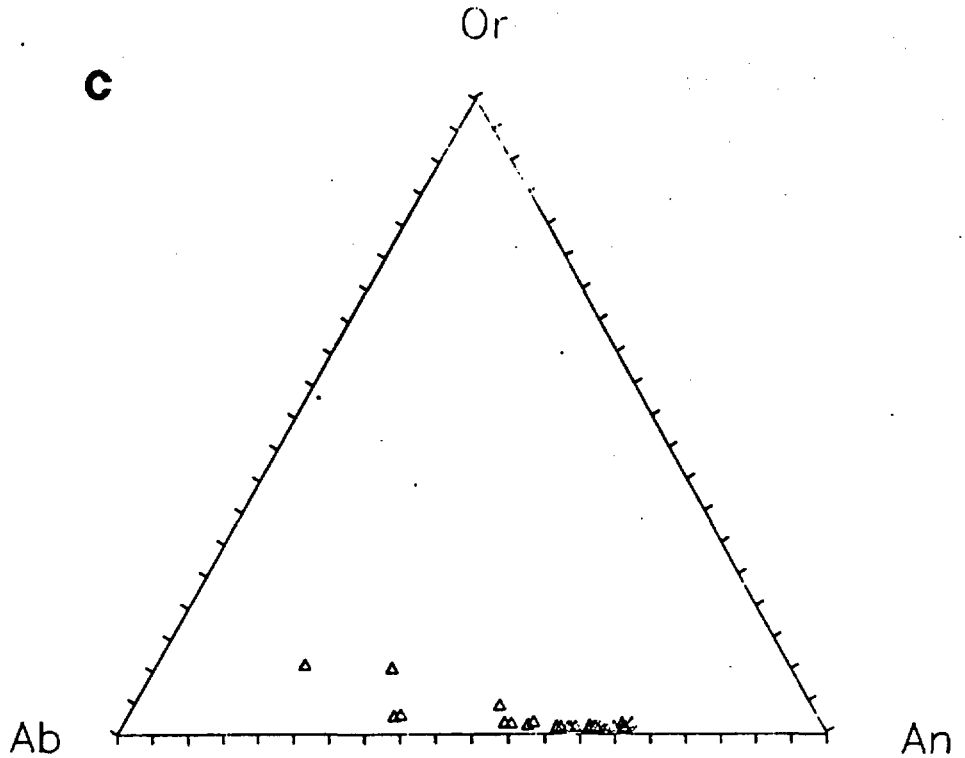

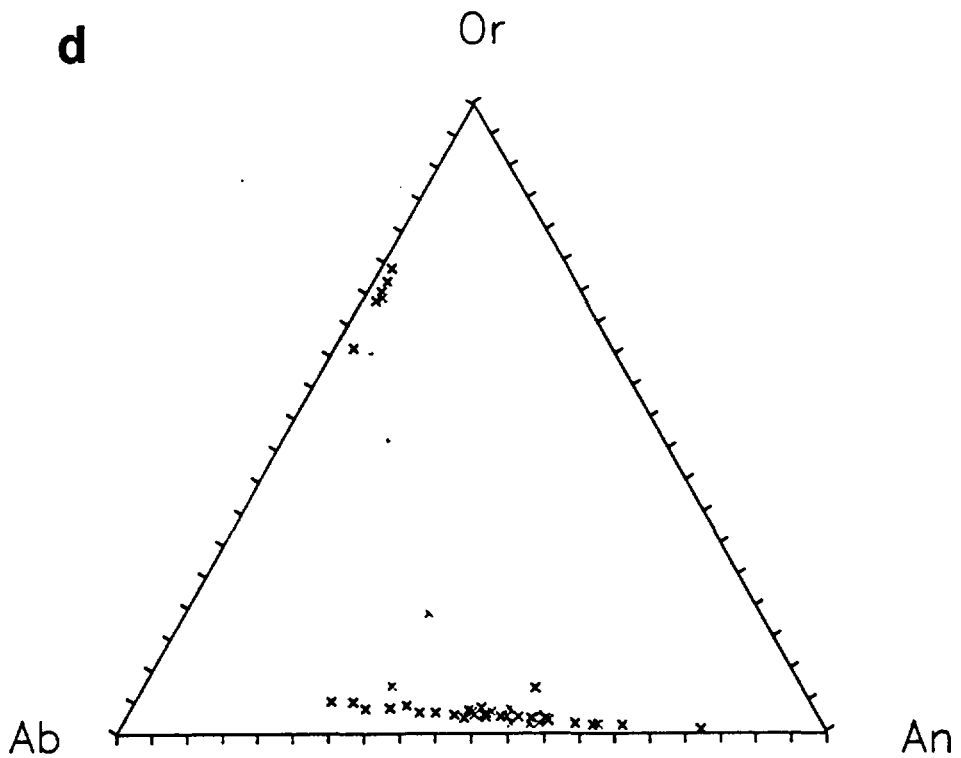

Figure 7. (cont) Plagioclase compositions on an Or-Ab-An diagram. (c) OAB rocks from Lava Cascade; (d) CM basaltic andesite.

enclosed by Ti-clinopyroxene; 3) Al-augite pyroxenites and; 4) poikilites of apatite and biotite enclosed by kaersutite (Nielson, manuscript in preparation).

MINERAL CHEMISTRY

Mineral chemistry was obtained from the University of New Mexico using a Camica 4 spectrometer superprobe.

Plagioclase

There is a considerable range of plagioclase compositions within individual samples. This variation is attributed to single crystal compositional zoning and not to the presence of a disequilibrium assemblage of phenocrysts. The SAB lava from Fortification Hill and Malpais Flattop contain the widest range of plagioclase compositions (An 40-78) (Figure 7a). YAB plagioclase clusters between An 50-60, however there is a population of anorthoclase present as well (Figure 7b). OAB plagioclase ranges in composition from An 45 to An 73, however the plagioclase from Petroglyph Wash has a lower average An content than those from the Lava Cascade (Figure 7b and c). The plug at Lava Cascade contains the widest range of any of the OAB lavas analyzed (An 40-73) (Figure 7c). Two populations of feldspar are present in the CM lava (Figure 7d); plagioclase phenocrysts zoned from An 85-30 and xenocrysts of sanidine.

Pyroxene

All of the lava from the CM and FH contain diopsidic augite as the dominant pyroxene. Diopsidic augite in the CM lava have compositions that cluster about $Wo_{45}En_{45}Fs_{15}$. Hypersthene (En_{70-55}) and pigeonite ($Wo_{5-10}En_{55-60}Fs_{30-40}$) are also present in the CM lavas (Figure 8a). Diopsidic augite in the OAB lava have compositions which fall into the range from $Wo_{37-49}En_{35-50}Fs_{9-18}$ (Figure 8b and c). The OAB rocks from Lava Cascade (Figure 8b) have diopsidic augite compositions that cluster about $Wo_{47}En_{37}Fs_{15}$ and are higher in the Wo component than augite from Petroglyph Wash (Figure 8c). The diopsidic augite compositions from the SAB lava have the largest variation with respect to Ca ($Wo_{30-45}En_{40-45}Fs_{10-25}$) Figure 8d). SAB lavas also contain hypersthene (En_{64}) and pigeonite ($Wo_{5-15}En_{33-60}Fs_{30-56}$). YAB pyroxene clusters about $Wo_{50}En_{37}Fs_{13}$ (Figure 8c).

Olivine

Olivine in the FH lavas is more iron rich in groundmass crystals (Fo 45-50) than in phenocryst phases (Fo 75-85). The most Mg rich olivine occurs in the OAB and YAB lavas (Figure 8b and c). Olivine in CM lavas range from Fo 57-83 (Figure 8d).

GEOCHEMISTRY

Analytical Methods

Whole rock major element concentrations were determined by Inductively Coupled Plasma techniques (ICP) at Chemex Labs, Inc. (Sparks, NV). Rare-earth elements and Cr, V, Sc, Rb, Sr, Ba, Ta, Hf, Th were analyzed by Instrumental Neutron

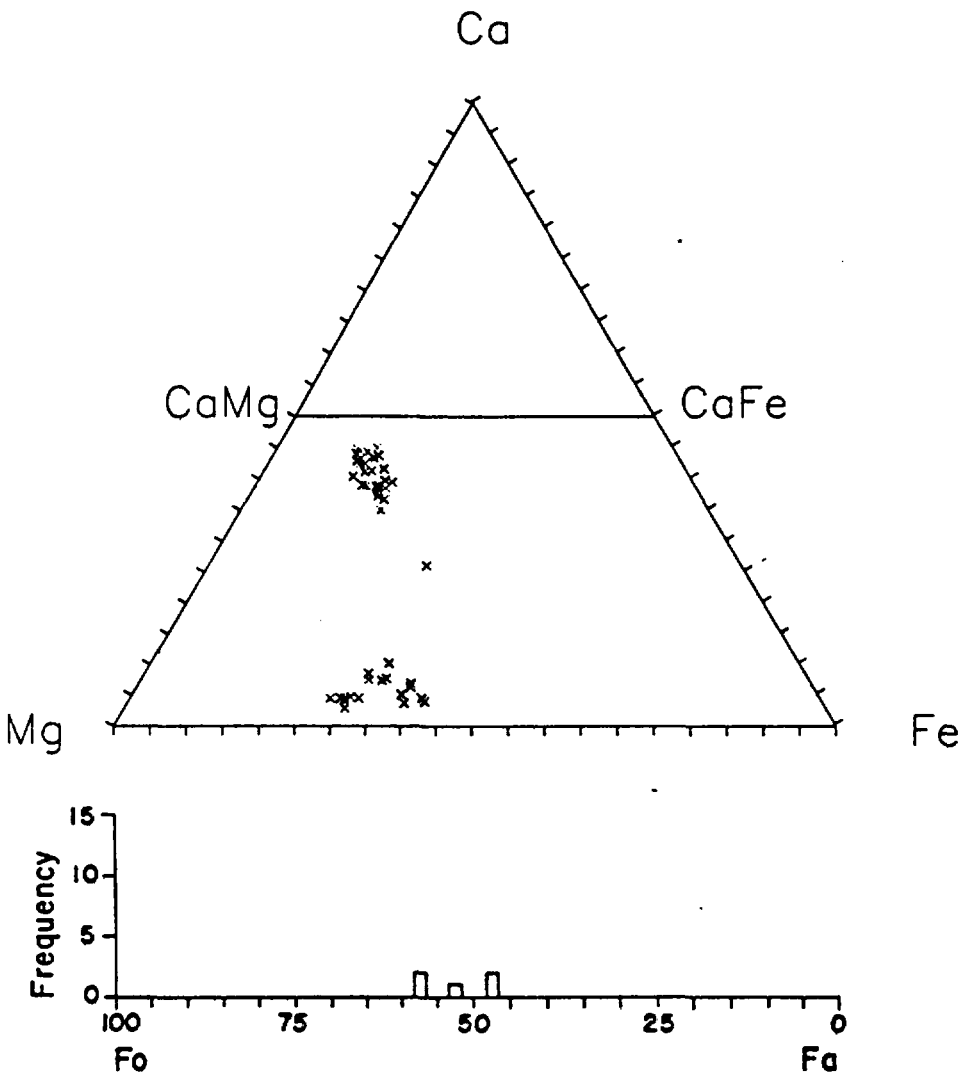

Figure 8a. Mineral chemistry for pyroxene and olivine in the basaltic-andesite from Callville Mesa.

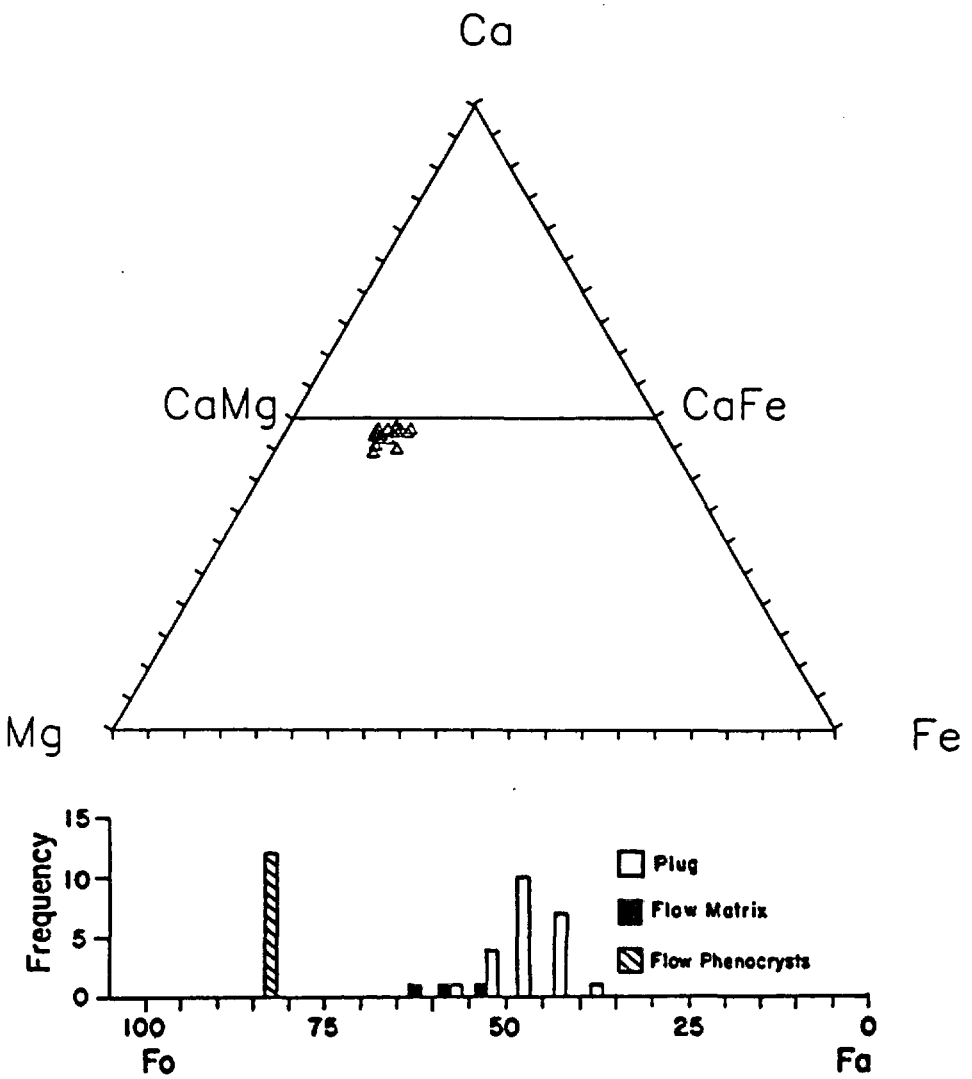

Figure 8b. Mineral chemistry for pyroxene and olivine in the OAB rocks from Lava Cascade.

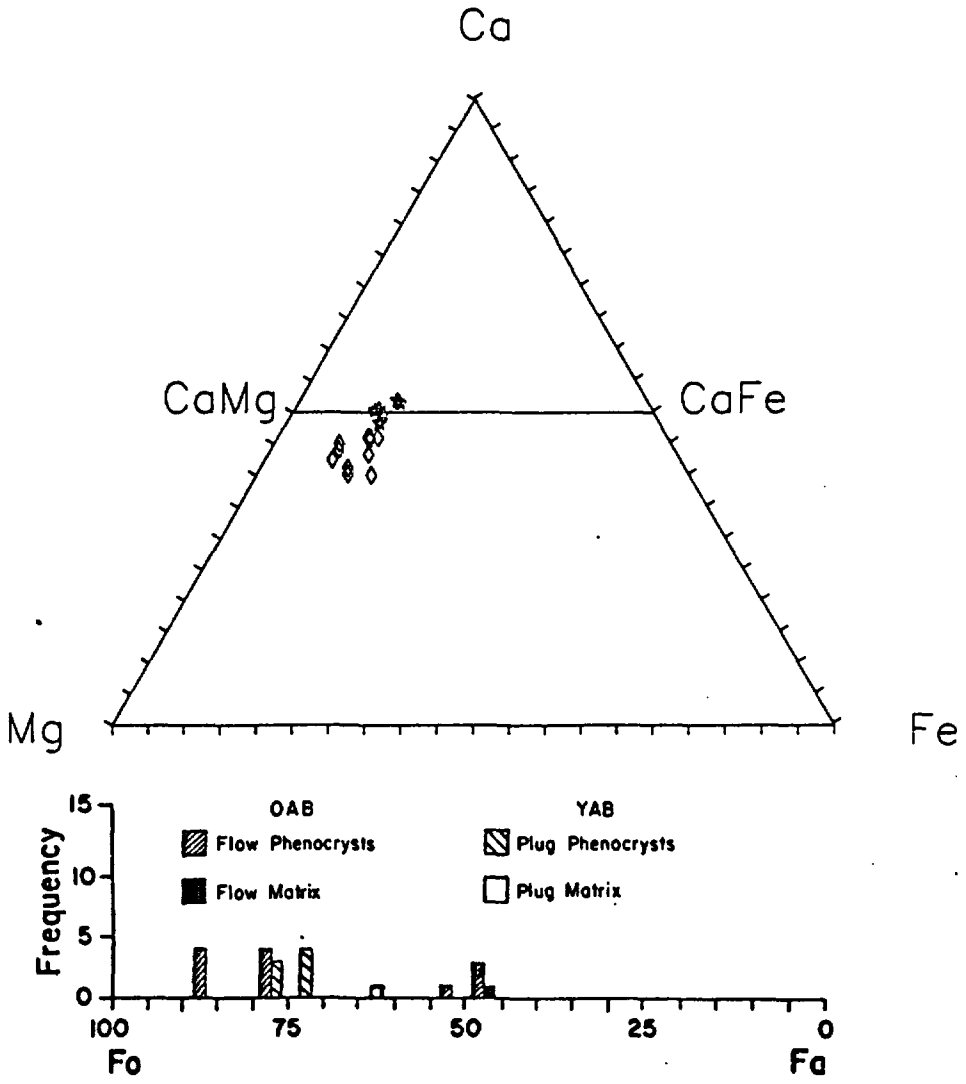

Figure 8c. Mineral chemistry for pyroxene and olivine in the OAB rocks from Lava Cascade. Olivine in the OAB (diamonds) and YAB lava from Petroglyph Wash (star).

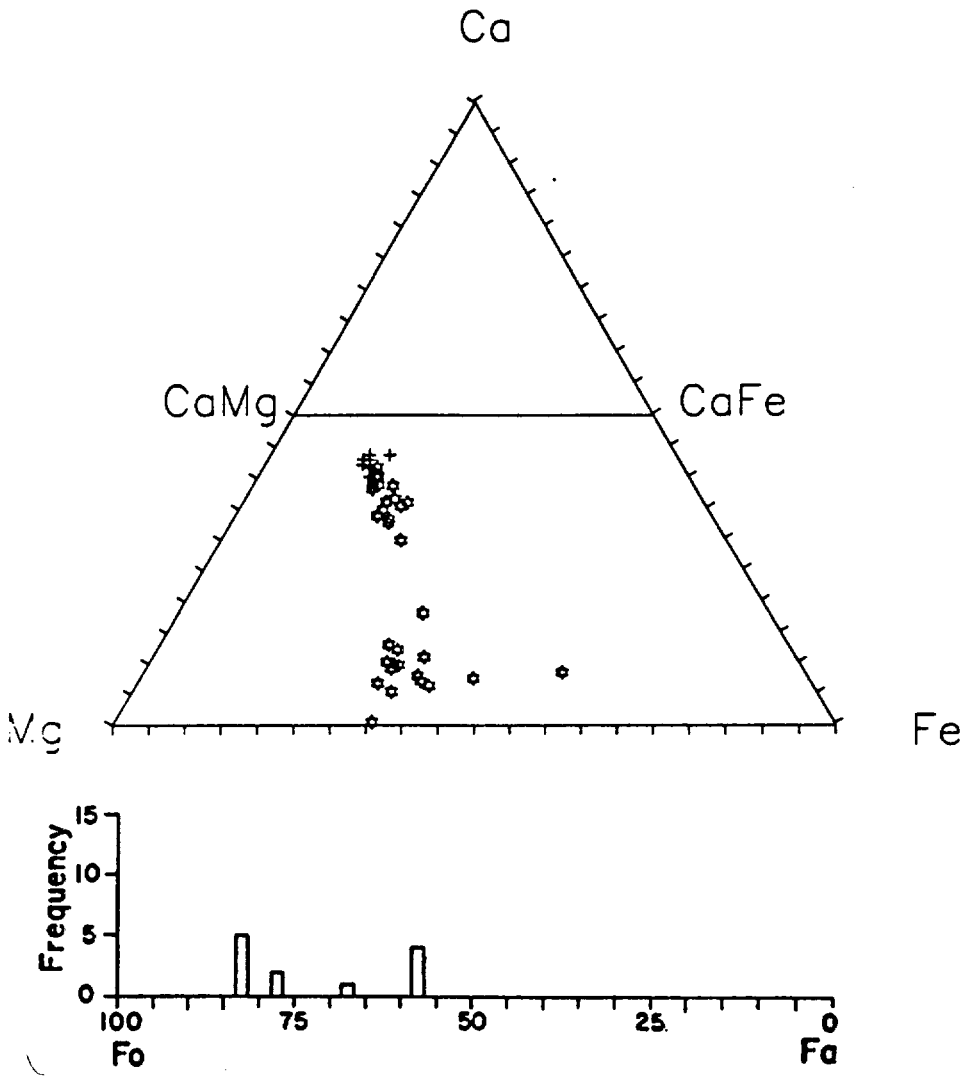

Figure 8d. Mineral chemistry for pyroxene and olivine in the SAB lava from Malpais Flattop (stars) and Fortification Hill (+).

Activation Analysis (INAA) at the Phoenix Memorial Laboratory, University of Michigan. The multi-element standards G-2, GSP-1, BHVO-1, and RGM-1 were used as internal standards.

Major Elements

Major elements are shown in Table 2. Various major oxides are plotted against SiO_2 in Figure 9. CM volcanic rocks vary in SiO_2 content from 52-57% and are mainly calc-alkalic basaltic-andesites. Fe_2O_3, MgO, TiO2, CaO and MnO decrease with increasing SiO_2, while P_2O_5, Na_2O and Al_2O_3 remain constant (Figure 12). All but three of the Callville Mesa volcanic rocks are quartz normative (1-7%) (Table 2). All samples contain normative hypersthene and andesine.

In the FH field the SAB and OAB lava have the widest range of SiO_2 (44-50). The YAB rocks cluster near 45% SiO_2. YAB rocks are enriched in TiO_2, P2O5, total alkalis and normative nepheline and depleted in Fe2O3, MgO when compared to the SAB and OAB rocks (Figure 9). Mg# for the FH field range from 0.45 to 0.6. Basalts from Lava Cascade and Fortification Hill are nepheline and olivine, or hypersthene and olivine normative. Labradorite is the normative plagioclase.

Sample #	Group	SiO2	Al2O3	Fe2O3	MgO	TiO2	CaO	Na2O	K2O	P2O5	MnO	Total
F8-24-51-LN	CM	53.91	16.19	9.48	4.55	1.19	7.24	3.62	2.02	0.26	0.15	98.97
87-24-146	CM	57.45	15.12	7.59	3.64	0.93	5.56	3.28	2.40	0.32	0.12	97.97
F8-24-43-LN	CM	53.09	16.16	9.32	4.89	1.18	7.53	3.53	2.27	0.27	0.15	98.36
F8-24-53-LN	CM	53.92	16.35	10.06	5.28	1.49	7.63	3.40	1.46	0.29	0.15	100.90
F8-24-55-LN	CM	54.26	15.59	8.99	5.06	1.05	6.75	3.55	2.03	0.27	0.12	100.85
F8-24-56-LN	CM	54.96	16.29	9.32	4.28	1.25	7.31	3.68	2.55	0.35	0.14	100.55
F8-24-57-LN	CM	55.00	16.30	9.42	4.74	1.19	7.34	3.57	2.46	0.35	0.14	100.75
F8-24-58-LN	CM	57.25	15.97	8.72	4.31	1.04	6.46	3.56	2.49	0.28	0.12	100.55
F8-24-59-LN	CM	57.80	15.78	8.47	4.07	1.02	6.28	3.57	2.49	0.26	0.12	100.55
F8-24-60-LN	CM	55.56	15.91	8.66	4.40	1.06	6.91	3.38	2.35	0.28	0.11	100.60
F8-24-61-LN	CM	55.73	15.84	9.09	4.24	1.13	6.88	3.54	2.74	0.30	0.12	100.60
F8-24-62-LN	CM	56.27	15.88	8.88	4.33	1.06	6.77	3.62	2.24	0.28	0.12	100.90
F8-24-63-LN	CM	54.52	16.22	8.68	4.43	1.12	7.23	3.48	1.72	0.29	0.12	99.92
F8-24-64-LN	CM	53.50	16.13	9.55	4.92	1.20	7.17	3.58	1.80	0.32	0.14	99.05
F8-24-65-LN	CM	56.53	15.99	9.17	4.44	1.08	6.53	3.57	2.30	0.30	0.13	100.55
F8-24-66-LN	CM	53.84	16.16	8.55	4.64	1.11	7.13	3.56	1.99	0.33	0.11	99.81
F8-24-67-LN	CM	55.55	16.42	9.11	4.43	1.19	7.28	3.75	2.39	0.34	0.12	101.75
F8-24-68-LN	CM	55.18	15.84	8.49	4.33	1.07	6.64	3.52	2.54	0.30	0.10	100.25
F8-24-69-LN	CM	53.61	15.91	8.89	4.99	1.06	7.15	3.36	2.33	0.31	0.11	100.65
F8-24-70-LN	CM	57.32	15.87	8.80	4.15	1.09	6.74	3.51	2.48	0.25	0.13	100.90
F8-24-71-LN	CM	54.91	17.19	8.14	2.69	1.28	7.85	3.90	3.08	0.39	0.09	101.15
F8-24-72-LN	CM	55.58	15.87	9.24	4.96	1.14	6.77	3.59	2.69	0.31	0.14	101.30
F8-24-85-LN	CM	54.65	16.47	9.60	4.76	1.20	7.50	3.55	2.96	0.38	0.14	101.40
F8-24-86-LN	CM	53.27	16.45	10.14	5.56	1.23	7.86	3.58	2.42	0.36	0.15	101.25
F8-23-91-LN	CM	54.05	16.51	10.21	3.22	1.81	6.47	4.21	2.01	0.50	0.14	99.30
F8-24-100-LN	CM	46.83	14.78	11.34	6.25	2.18	9.03	3.45	1.19	0.45	0.13	98.20
F8-24-50-LN	CM	56.87	15.49	8.61	4.27	1.01	6.32	3.48	2.37	0.20	0.15	99.24
F8-24-44-LN	CM	53.57	15.80	9.57	4.45	1.20	7.18	3.56	2.18	0.27	0.15	98.11
F8-24-45-LN	CM	53.17	16.32	9.78	4.99	1.21	7.45	3.51	2.00	0.25	0.15	99.02
F8-24-46-LN	CM	53.26	15.71	10.46	5.08	1.15	7.07	3.46	1.82	0.21	0.15	98.54
F8-24-47-LN	CM	53.87	15.65	9.34	4.92	1.16	6.96	3.36	1.79	0.23	0.14	98.33
F8-24-48-LN	CM	52.11	15.73	9.91	5.45	1.22	7.56	3.43	1.54	0.24	0.15	98.07
F8-24-49-LN	CM	55.24	15.98	8.97	4.10	1.13	6.90	3.55	2.33	0.25	0.14	99.17
F8-24-54-LN	CM	54.24	15.58	9.27	4.95	1.12	6.91	3.44	2.08	0.26	0.11	98.97
F7-38-14-LN	OAB	47.62	15.28	11.73	7.78	1.39	8.94	3.39	1.29	0.27	0.17	99.51
87-38-134	OAB	49.77	16.81	10.54	5.72	1.55	9.66	3.39	0.90	0.51	0.16	99.72
87-38-137	OAB	49.37	16.29	10.42	5.91	1.49	9.42	3.28	0.90	0.49	0.16	99.15
87-38-133	OAB	47.29	15.58	12.54	6.03	1.63	10.07	3.14	1.30	0.49	0.17	99.06
87-38-135	OAB	47.60	15.70	12.57	5.84	1.61	9.98	3.30	1.40	0.49	0.18	99.38
87-38-136	OAB	48.25	15.96	12.26	5.82	1.53	10.27	3.34	1.40	0.48	0.18	99.70
87-38-139	OAB	49.02	16.51	10.80	5.15	1.45	10.00	3.54	1.20	0.51	0.16	98.82
87-38-141	OAB	47.08	15.33	12.41	6.54	1.36	9.46	3.02	1.30	0.44	0.16	99.19
87-38-142	OAB	48.09	15.41	11.50	5.86	1.56	10.17	3.19	1.00	0.48	0.17	98.39
87-38-143	OAB	47.97	16.05	11.87	5.32	1.46	10.16	3.26	1.40	0.49	0.17	98.64
87-38-144	OAB	47.34	15.87	11.66	5.84	1.41	10.24	3.18	1.40	0.48	0.16	98.70
87-42-127	OAB	45.36	14.34	11.56	9.41	1.28	9.34	2.90	1.40	0.53	0.16	97.44
87-42-128	OAB	47.95	16.41	11.33	4.78	1.61	10.02	3.39	1.60	0.55	0.16	98.58
87-57-105	OAB	43.54	15.10	13.10	8.71	1.71	10.57	2.39	1.00	0.49	0.18	99.37
87-57-106	OAB	44.46	16.64	13.01	5.52	1.95	10.77	3.08	1.10	0.53	0.18	98.30
87-57-107	OAB	45.35	16.71	13.81	5.54	2.07	11.13	3.15	1.20	0.53	0.19	100.27
87-57-108	OAB	45.06	16.25	12.68	5.57	1.99	10.92	3.20	1.00	0.54	0.18	97.99
87-57-109	OAB	42.84	15.09	12.90	7.17	1.73	10.96	2.74	1.00	0.49	0.17	96.93

Table 2. Major element data in Wt% for the CM basaltic andesite and FH basalt.

Sample #	Group	SiO2	Al2O3	Fe2O3	MgO	TiO2	CaO	Na2O	K2O	P2O5	MnO	Total
87-57-110	OAB	44.65	14.72	12.06	7.54	1.77	10.39	2.49	1.00	0.56	0.17	96.83
87-57-111	OAB	44.41	15.81	13.42	6.79	1.90	10.89	3.12	1.10	0.52	0.18	98.19
87-57-112	OAB	44.28	15.20	13.78	8.33	1.78	10.54	3.01	1.10	0.53	0.19	98.94
87-57-113	OAB	44.15	15.22	13.38	8.06	1.76	10.69	2.88	1.10	0.52	0.18	98.46
87-57-114	OAB	44.89	14.59	12.64	8.53	1.76	9.78	2.62	0.80	0.47	0.17	97.98
87-57-132	OAB	45.43	15.67	13.96	8.59	1.81	10.87	2.98	1.20	0.53	0.19	101.88
f7-57-09-1n	OAB	43.47	15.15	12.53	8.64	1.76	11.06	2.84	1.20	0.33	0.18	98.07
f7-57-10-1n	OAB	43.48	15.24	12.70	9.14	1.75	10.46	2.76	1.16	0.30	0.18	98.06
F8-42-79-LN	OAB	48.58	16.75	11.12	5.13	1.98	9.68	3.68	1.81	0.50	0.16	100.80
F8-42-77-LN	OAB	48.46	16.69	10.54	5.37	1.69	9.73	3.56	2.54	0.60	0.15	101.15
F8-42-78-LN	OAB	48.22	16.24	11.70	5.93	1.89	9.72	3.49	2.58	0.57	0.17	101.05
F8-42-81-LN	OAB	48.58	17.00	10.58	5.00	1.79	9.73	3.61	1.93	0.57	0.16	100.50
F8-42-82-LN	OAB	47.52	16.61	10.56	5.35	1.76	9.79	3.57	2.11	0.57	0.16	99.50
F8-42-83-LN	OAB	48.24	16.76	10.50	5.38	1.72	9.92	3.56	2.12	0.58	0.16	100.75
F8-42-84-LN	OAB	47.66	16.70	11.45	6.10	1.71	10.07	3.57	1.81	0.51	0.17	100.75
84-60	SAB	48.87	15.25	10.11	7.15	1.53	9.52	3.19	1.23	0.37	0.17	97.41
84-59	SAB	48.58	15.80	10.40	6.41	1.60	10.30	3.12	1.09	0.44	0.17	97.93
84-54	SAB											0.00
F7-38-13-LN	SAB	45.79	14.50	12.80	8.78	1.41	8.38	2.86	0.84	0.28	0.16	97.34
F7-38-15-LN	SAB	44.62	14.29	11.93	8.55	1.29	7.92	2.81	1.10	0.28	0.15	96.45
F7-60-5-LN	SAB	47.64	16.31	11.07	7.91	1.40	7.24	3.16	1.02	0.16	0.17	97.07
87-10-120	SAB	46.32	15.30	13.39	8.92	1.16	7.93	2.97	0.90	0.34	0.19	101.53
87-38-138	SAB	48.89	16.73	10.44	5.47	1.51	10.87	3.30	0.80	0.49	0.16	100.08
87-57-101	SAB	47.24	15.18	12.07	8.16	1.89	10.12	2.87	1.15	0.46	0.23	100.75
87-57-102	SAB	47.17	14.90	12.58	8.35	1.94	10.17	2.98	1.02	0.36	0.26	100.26
87-59-103	SAB	49.81	15.75	10.05	8.04	1.46	7.48	3.10	1.08	0.25	0.23	98.58
87-10-115	SAB	45.34	14.35	14.02	8.67	1.17	7.86	3.07	0.60	0.32	0.19	96.40
87-10-116	SAB	44.19	14.02	13.92	9.04	1.12	7.45	3.03	0.70	0.29	0.19	96.60
87-10-119	SAB	45.04	14.47	13.68	8.71	1.15	7.57	2.68	0.90	0.30	0.18	98.22
87-10-121	SAB	44.58	14.35	13.82	8.76	1.10	6.55	4.17	0.70	0.30	0.19	97.66
f7-60-031n	SAB	46.99	0.00	13.19	8.75	1.18	8.38	2.72	0.81	0.22	0.19	98.34
f7-60-04-1n	SAB	47.28	14.95	12.38	6.82	1.40	8.90	2.92	1.07	0.24	0.19	96.98
f7-60-06-1n	SAB	47.87	14.67	13.34	6.95	1.53	9.29	2.80	1.21	0.25	0.20	98.76
F7-25-01-LN	YAB	44.57	16.34	10.44	5.52	2.46	8.77	4.15	1.94	0.68	0.19	99.50
f7-25-2-1n	YAB	44.90	16.53	11.14	5.73	2.40	7.68	4.73	1.04	0.72	0.16	98.06
87-45-124	YAB	45.50	16.89	10.04	5.94	2.52	8.53	4.78	2.20	0.77	0.19	98.48
F8-42-73-LN	YAB	44.79	17.42	12.23	6.36	2.11	10.86	3.11	1.89	0.71	0.19	101.20
F8-42-74-LN	YAB	45.02	17.59	12.28	6.53	2.01	10.76	3.32	2.25	0.76	0.18	101.30
F8-42-75-LN	YAB	44.90	17.57	11.68	6.28	1.97	10.68	3.42	2.27	0.75	0.18	100.95
F8-42-76-LN	YAB	45.00	16.79	10.88	6.21	2.54	8.78	4.94	3.70	0.88	0.18	100.65
F8-93-93-LN	YAB	44.31	15.87	9.80	3.26	2.77	8.34	3.89	2.85	0.82	0.14	101.55
F8-93-94-LN	YAB	47.01	16.77	10.57	4.12	2.82	7.31	4.85	4.18	0.87	0.15	101.30
F8-93-96-LN	YAB	44.05	15.52	10.46	5.88	3.02	9.07	3.08	2.80	0.78	0.15	101.40

TABLE 2 (continued)

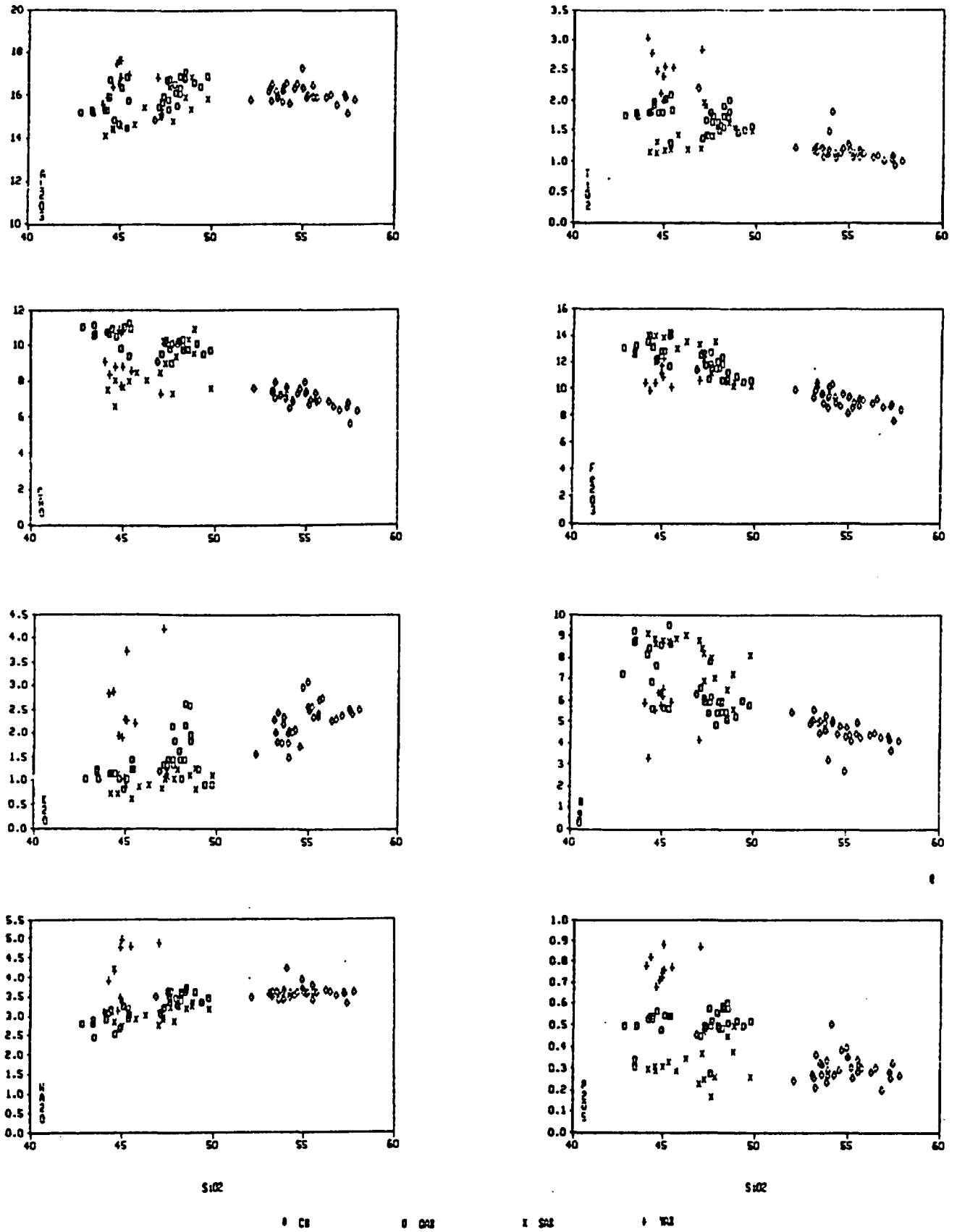

Figure 9. Harker variation diagrams for the lava from the Callville Mesa (CM) and Fortification Hill (SAB, OAB, YAB) volcanic fields.

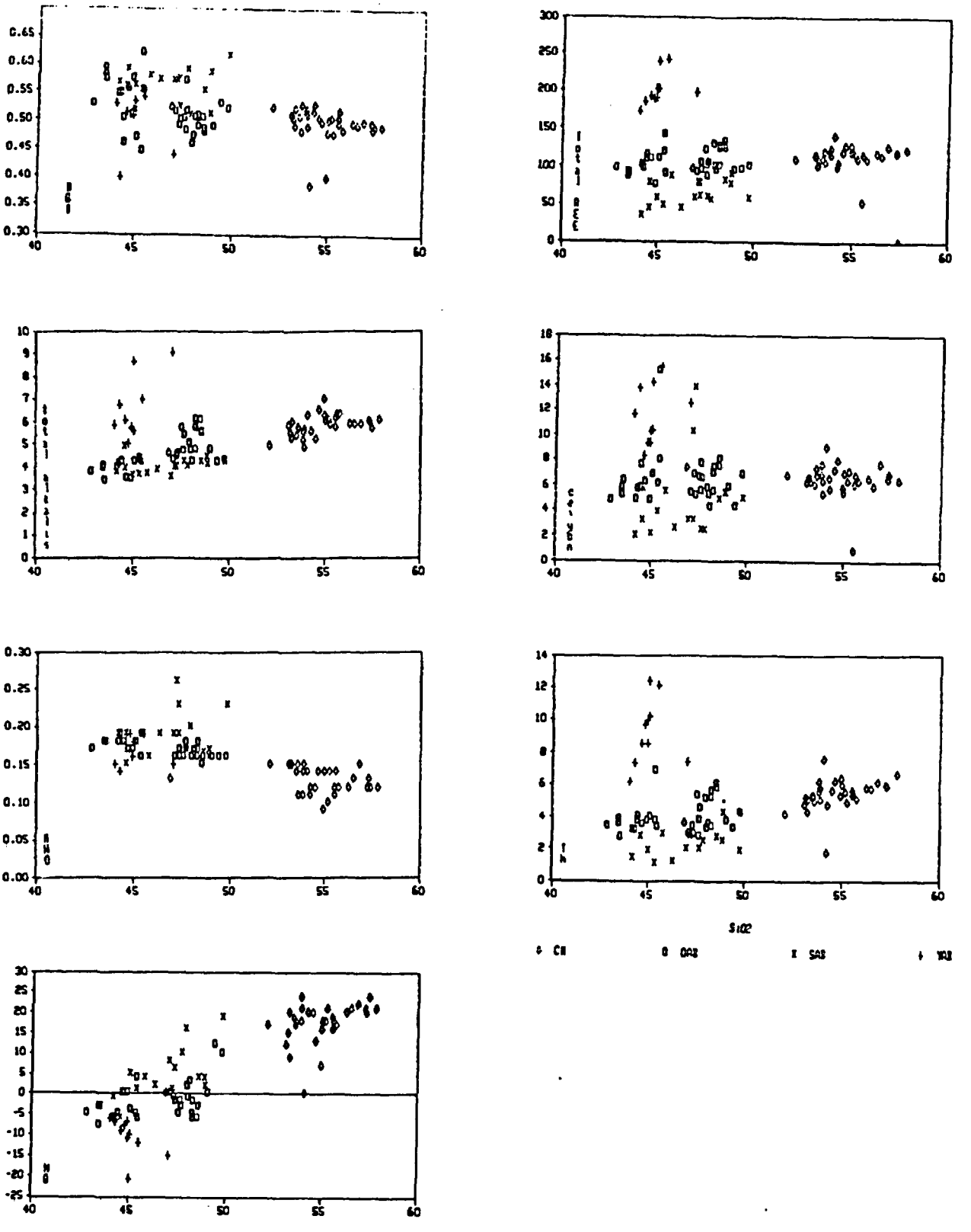

Figure 9. (cont.) Harker variation diagrams for the lava from the Callville Mesa (CM) and Fortification Hill (SAB, OAB, YAB) volcanic fields.

Trace elements

Trace and REE data is presented in Table 3. In the FH field, the OAB and YAB rocks are depleted in transition elements such as V, Cr and Co and enriched in the LREE (La and Ce) and high field-strength elements (Hf and Ta) relative to MORB (Figure 10a). Th is enriched in all of the FH rocks but is more enriched in YAB. Rare-earth elements are normalized to chondrite and plotted on Figure 11a. YAB rocks are enriched in the LREE and show a steeper slope than the SAB rocks The OAB rocks are intermediate in LREE enrichment to the YAB and SAB lava.

Trace element abundances in the CM lavas are nearly the same throughout the suite of rocks. LREE are enriched nearly 100 times chondrite while HREE are enriched about 10 times. This produces a moderately steep slope for the REE plot (Figure 11b). CM lavas are strongly enriched in K, Ba and Th and moderately enriched in the LREE with respect to MORB (Figure 10b). CM lavas are slightly depleted in the transitional elements.

DISCUSSION AND PRELIMINARY MODELS FOR THE EVOLUTION OF THE MAGMA

Callville Mesa

CM basaltic andesite has isotopic, chemical and textural evidence of crustal contamination (initial $^{87}Sr/^{86}Sr$ = 0.708-0.709, epsilon Nd= -8.49 to -10.69 and $^{206}Pb/^{204}Pb$ = 17.173 to 17.332) (Figures 12, 13 and 14). We suggest that Callville

Sample #	Group	La	Ce	Nd	Eu	Tb	Yb	Lu	Sm	Cr	Co	Sr	Ba	Sc	Hf	Ta	Th	V
F8-24-51-LN	CM	38.39	76.02	17.43	1.46		2.73	0.29	5.80	109.33	26.61		882.28	21.11	6.06	1.28	5.76	184.88
87-24-146	CM																	
F8-24-43-LN	CM	35.76	68.30	13.18	1.50	1.35	2.52	0.36	5.45	123.74	26.61	905.46	629.41	20.34	4.55	1.62	4.73	170.71
F8-24-53-LN	CM	35.10	70.10		1.43		3.00	0.44	5.35	130.00	30.10		755.00	23.20	3.97	1.42	5.06	189.00
F8-24-55-LN	CM	32.00	63.50		1.23		2.52	0.32	4.90	150.00	26.70	804.00	998.00	16.80	3.65	1.11	4.71	141.00
F8-24-56-LN	CM	39.10	77.70	28.90	1.56	1.13	3.29	0.32	5.81	107.00	28.20		875.00	21.90	5.32	1.78	6.31	175.00
F8-24-57-LN	CM	36.90	74.40	31.00	1.47		2.44	0.41	5.68	107.00	27.60	891.00	881.00	20.90	4.50	1.30	5.95	177.00
F8-24-58-LN	CM	38.60	71.00	27.70	1.28		2.48	0.40	5.60	113.00	24.10		976.00	16.40	4.31	1.07	5.92	146.00
F8-24-59-LN	CM	38.20	75.40	44.30	1.25		2.68	0.29	5.34	116.00	24.90	719.00	1080.00	17.00	4.67	1.13	6.59	144.00
F8-24-60-LN	CM	35.50	7.51		1.34		2.15	0.34	5.26	115.00	24.20		895.00	17.30	4.21	0.96	5.61	141.00
F8-24-61-LN	CM	36.30	64.00	35.40	1.22	0.85	2.32	0.34	5.57	113.00	25.20	720.00	961.00	17.60	4.18	0.87	5.14	163.00
F8-24-62-LN	CM	36.20	71.20		1.36		2.49	0.34	5.26	124.00	24.90		874.00	17.60	4.51	0.88	5.79	139.00
F8-24-63-LN	CM	35.40	73.90		1.58	1.59	2.33	0.33	5.45	121.00	26.60		968.00	19.00	4.79	1.10	5.65	162.00
F8-24-64-LN	CM	33.30	68.40		1.39		2.56	0.37	5.29	135.00	30.10		809.00	20.50	4.46	1.16	5.24	153.00
F8-24-65-LN	CM	35.30	69.90	31.80	1.37		2.71	0.26	5.25	112.00	24.60		818.00	17.20	4.43	1.32	5.69	146.00
F8-24-66-LN	CM	35.90	74.80	30.40	1.42		2.48	0.34	5.43	160.00	28.80		864.00	19.50	4.60	1.12	5.57	155.00
F8-24-67-LN	CM	34.70	71.60	29.40	1.35	1.58	2.67	0.32	5.38	155.00	28.40	846.00	910.00	19.20	4.60	0.95	5.31	153.00
F8-24-68-LN	CM	34.20	72.10		1.40		2.60	0.34	5.22	134.00	27.70		781.00	18.20	4.29	0.96	5.46	153.00
F8-24-69-LN	CM	31.80	65.10		1.21		2.18	0.30	4.87	156.00	27.20	931.00	848.00	17.50	3.91	1.03	4.96	151.00
F8-24-70-LN	CM	37.90	72.40	31.80	1.23		2.39	0.33	5.48	115.00	24.60		964.00	17.30	4.77	1.12	5.90	143.00
F8-24-71-LN	CM	36.50	73.00	32.30	1.43	1.11	2.88	0.32	5.66	142.00	32.10		882.00	21.20	4.37	1.36	5.26	172.00
F8-24-72-LN	CM	34.90	71.00	30.20	1.27		2.37	0.27	5.14	158.00	28.40		773.00	18.90	4.60	0.86	5.47	155.00
F8-24-85-LN	CM	37.50	79.90	28.90	1.39		2.29	0.32	5.52	115.00	28.50	903.00	976.00	21.70	4.76	1.66	6.19	169.00
F8-24-86-LN	CM	33.00	65.10	35.10	1.34		2.36	0.30	5.14	124.00	31.70		748.00	21.40	4.13	0.88	5.06	170.00
F8-23-91-LN	CM	42.90	87.50	37.70	1.63		2.20	0.31	6.23	23.10	24.60	2490.00	1240.00	15.80	4.67	1.67	7.53	182.00
F8-24-100-LN	CM	27.30	59.80	28.40	1.70		1.84	0.26	5.87	312.00	38.20		431.00	24.10	4.45	1.68	3.61	226.00
F8-24-50-LN	CM	38.28	77.29	20.62	1.03		2.31	0.36	5.78	105.64	24.01		971.85	17.29	4.20	0.97	6.11	126.78
F8-24-44-LN	CM	35.59	75.24	13.49	1.47		2.32	0.33	5.44	113.54	28.07		645.47	21.22	5.11		5.25	181.24
F8-24-45-LN	CM	34.41	70.58	40.67	1.59		2.44	0.31	5.50	121.09	29.07	0.00	857.04	21.20	5.09	1.79	5.16	183.60
F8-24-46-LN	CM	30.89	61.16	23.47	1.23		2.13	0.32	5.01	149.00	29.50		724.56	18.66	3.94		4.29	162.33
F8-24-47-LN	CM	36.54	74.22	20.03	1.43	1.46	2.20	0.32	5.46	91.77	22.54	1675.30	850.69	18.65	5.06	1.72	6.20	156.72
F8-24-48-LN	CM	32.28	68.55	15.94	1.46		2.32	0.29	5.29	135.51	30.53		823.20	20.77	5.50	1.26	4.14	171.95
F8-24-49-LN	CM	33.95	67.61	22.47	1.38		2.18	0.34	5.32	144.50	28.79		1054.60	19.62	3.86	0.97	4.89	170.80
F8-24-54-LN	CM	31.60	59.40		1.21		2.05	0.31	4.78	153.00	28.80		1110.00	18.10	4.04	1.18	1.68	168.00
F7-38-14-LN	OAB	23.82	52.27		1.47	1.73	2.17	0.29	4.77	270.04	40.46		582.98	24.53	3.11	1.18	2.75	226.87
87-38-134	OAB	33.05	57.44		1.51		1.92	0.29	5.48	127.13	33.77	683.87		26.80	4.08	1.46	4.18	165.50
87-38-137	OAB	30.08	54.86		1.50		2.95	0.48	5.37	122.06	36.39		700.00	28.46	3.40	1.77	3.24	214.15
87-38-133	OAB	31.22	62.18		1.44		2.08	0.36	5.27	176.04	35.15	676.81	600.00	27.83	3.60	1.31	3.33	255.07
87-38-135	OAB	31.71	58.57		1.47		1.75	0.30	5.40	112.39	36.92	642.89	640.00	28.70	3.55	1.22	3.72	238.63
87-38-136	OAB	33.06	56.00		1.64		2.33	0.32	5.57	116.94	35.35		806.61	28.75	3.45	1.69	3.34	243.81
87-38-139	OAB	30.27	53.32		1.56		2.10	0.25	5.10	75.79	38.60			28.67	3.53	1.65	3.67	246.61
87-38-141	OAB	29.22	52.95		1.34		2.28	0.15	4.96	268.33	41.48		510.00	25.99	3.41	1.64	2.90	207.85
87-38-142	OAB	30.83	53.35		1.26		2.85	0.19	5.24	169.47	34.07			28.26	2.83	1.78	3.52	225.96
87-38-143	OAB	32.69	57.45		1.53		2.52	0.37	5.53	70.47	32.70		690.00	26.32	4.18	1.31	3.23	235.79
87-38-144	OAB	29.52	54.15		1.40		2.41	0.23	5.08	172.98	34.17		570.00	27.29	2.72	1.60	2.86	204.80
87-42-127	OAB	48.05	83.91		1.40		1.26	0.34	5.99	454.06	43.98		890.79	27.77	3.10	2.05	6.77	198.35
87-42-128	OAB	40.02	78.46		1.56		3.13	0.21	6.32	62.75	30.63		826.17	24.85	3.27	1.97	5.10	197.43
87-57-105	OAB	28.89	52.91		1.37		1.88	0.27	4.93	325.31	45.64			30.07	3.55	1.68	2.65	257.52
87-57-106	OAB	36.46	67.25		1.63		2.04	0.40	5.92	81.01	34.31	717.49		27.41	2.88	1.97	3.98	232.49
87-57-107	OAB	37.21	69.70		1.61		2.59	0.35	5.95	79.71	34.69			28.63	4.51	2.07	3.66	245.43
87-57-108	OAB	34.15	64.89		1.72		2.17	0.32	5.81	96.20	35.78			28.87	3.60	2.39	3.91	238.52
87-57-109	OAB	30.15	56.23		1.48		2.73	0.32	5.50	257.73	42.05			30.78	3.69	1.69	3.34	233.82

Table 3. Trace and rare earth data in ppm for the CM basaltic andesite and FH basalt.

Sample #	Group	La	Ce	Nd	Eu	Tb	Yb	Lu	Sm	Cr	Co	Sr	Ba	Sc	Hf	Ta	Th	Y
87-57-110	OAB	35.78	63.47		1.62		2.34	0.25	5.61	278.27	42.80	705.69		29.90	3.32	1.45	3.48	231.31
87-57-111	OAB	32.92	64.56		1.59	1.87	2.53	0.24	5.63	187.35	41.18			31.80	3.96	1.73	3.64	281.88
87-57-112	OAB	32.20	54.67		1.51		2.21	0.22	5.50	301.01	45.91			30.01	3.26	1.54	3.13	229.81
87-57-113	OAB	32.11	59.18		1.46		2.79	0.26	5.27	268.08	43.12			30.22	3.26	1.66	3.15	229.06
87-57-114	OAB	23.35	42.85		1.23		2.06	0.21	4.47	321.55	43.94			30.37	3.42	1.34	3.68	235.18
87-57-132	OAB	29.00	51.61		1.48		1.48	0.39	5.11	296.45	43.83			29.72	3.50	1.17	3.31	243.77
f7-57-09-1n	OAB	27.20	55.61	15.70	1.64	1.59	2.17	0.23	5.06	313.29	47.09		499.04	31.23	3.65	1.57	3.80	237.27
f7-57-10-1n	OAB	23.34	52.72	15.54	1.38		2.30	0.27	4.55	307.74	45.14		354.24	31.30	4.02	1.53	3.52	262.53
F8-42-79-LN	OAB	37.90	74.40	32.00	1.76		2.27	0.32	6.25	38.90	30.30	1160.00	1090.00	26.70	4.87	2.26	5.69	262.00
F8-42-77-LN	OAB	39.40	82.00	31.70	1.82		2.51	0.39	6.46	49.60	33.00	1270.00	772.00	27.00	4.85	2.01	5.98	251.00
F8-42-78-LN	OAB	38.10	77.10	37.30	1.68		2.39	0.32	6.29	61.80	34.40	1070.00	921.00	26.90	4.48	2.43	5.54	251.00
F8-42-81-LN	OAB	37.40	78.70	27.00	1.93		2.22	0.25	6.15	47.50	32.90		777.00	26.70	4.53	1.92	5.72	233.00
F8-42-82-LN	OAB	37.70	72.30	39.50	1.61		2.49	0.37	6.16	50.00	31.80		793.00	25.00	4.00	1.87	5.28	281.00
F8-42-83-LN	OAB	37.20	74.90		1.65		2.45	0.35	6.06	59.80	32.80		911.00	26.20	4.44	1.95	5.16	232.00
F8-42-84-LN	OAB	32.40	61.70	39.20	1.36		2.18	0.33	5.27	138.00	33.20		579.00	26.80	3.61	1.76	4.52	238.00
84-60	SAB	27.77	39.67	0.00	1.62	0.00	1.70	0.31	4.56	221.14	23.60	498.10	600.00	28.31	2.94	1.49	2.49	
84-59	SAB	29.99	40.52	0.00	1.56	0.00	1.90	0.35	5.39	186.14	23.50	481.20	590.00	30.77	2.87	1.42	2.71	
84-54	SAB	84.79	115.12	58.19	2.40	2.93	1.91	0.30	10.20	28.87		ERROR	1708.20	13.37	5.95	0.91	10.45	
F7-38-13-LN	SAB	24.58	52.42		1.59		2.20		4.83	361.25	52.58		475.00	26.50	3.38	1.69	2.87	212.82
F7-38-15-LN	SAB	23.33	45.73		1.36		1.85		4.45	321.84	43.69		400.00	23.08	2.56	1.80	2.73	209.23
F7-60-5-LN	SAB	15.62	33.24		1.44		3.22	0.41	4.37	254.49	39.83			36.43	3.93		1.90	226.00
87-10-120	SAB	11.79	24.73		1.05		2.30	0.17	3.07	326.47	53.70			24.68	2.83		1.16	176.98
87-38-138	SAB	29.03	50.29		1.51		2.14	0.36	5.25	161.78	34.29			27.37	3.46	1.65	4.19	234.15
87-57-101	SAB	24.92	43.52		1.64		0.72	0.24	4.74	256.92	43.80			31.93	5.56	1.58	2.95	
87-57-102	SAB	26.03	42.92		1.62		0.96	0.43	4.57	300.89	49.02			34.18	6.86	1.89	2.75	
87-59-103	SAB	15.59	32.37		1.58		1.50	0.54	4.22	269.36	42.89			38.83	7.14	0.70	1.82	
87-10-115	SAB	13.59	26.59		0.98		1.59	0.23	3.22	289.46	57.62			27.59	2.03	0.53	1.01	199.05
87-10-116	SAB	11.13	16.52		0.91		2.01	0.17	2.80	270.98	54.42			25.23	2.20		1.37	215.40
87-10-119	SAB	28.96	18.26		0.84		2.01	0.24	4.88	267.19	51.58			24.29	2.53	0.78	1.86	198.42
87-10-121	SAB	12.61	24.27		0.93		1.75	0.28	3.07	271.13	56.33			24.53	1.70	0.95		194.46
f7-60-031n	SAB	13.22	34.82	11.51	1.27		2.50	0.30	3.56	337.30	52.33			25.62	2.71		1.90	214.10
f7-60-04-1n	SAB	14.86	35.70	11.67	1.07	1.44	2.58	0.29	3.93	241.73	41.07		440.86	29.98	3.57			220.94
f7-60-06-1n	SAB	15.49	29.93		1.28		2.81	0.35	4.00	227.46	42.30			32.98	3.21		2.45	246.61
F7-25-01-LN	YAB	60.56	116.23		2.38	1.11	3.16		9.03	151.37	28.12	1254.20	1237.20	18.93	6.73	3.50	8.50	178.89
f7-25-2-1n	YAB	59.91	116.34	52.90	2.38		2.84	0.30	8.84	139.39	29.12	779.37	818.06	18.03	6.45	4.02	8.51	185.81
87-45-124	YAB	85.51	140.88		2.35		2.08	0.40	8.94	391.48	28.20	1041.40	12.79	17.44	6.98	5.68	12.05	191.77
F8-42-73-LN	YAB	61.40	116.00	51.40	1.84		2.85	0.36	7.14	46.60	35.80	1210.00	1380.00	26.60	4.73	3.13	9.62	308.00
F8-42-74-LN	YAB	65.80	124.00	73.80	2.01		2.73	0.36	7.71	49.00	36.60		1480.00	26.90	5.11	2.74	10.20	278.00
F8-42-75-LN	YAB	65.60	124.00	47.80	1.89		2.74	0.37	7.68	48.70	35.00	1300.00	1150.00	26.60	4.83	2.78	9.96	259.00
F8-42-76-LN	YAB	75.10	151.00	40.30	2.30	1.33	2.43	0.22	8.61	113.00	29.60	1240.00	1340.00	18.60	7.22	6.01	12.40	216.00
F8-93-93-LN	YAB	55.80	118.00	46.30	2.41		1.95	0.30	7.91	76.30	22.80	2370.00	798.00	12.70	7.33	5.01	7.28	142.00
F8-93-94-LN	YAB	58.90	124.00	53.10	2.43	1.34	2.26	0.31	8.37	98.50	23.30	1980.00	1050.00	13.10	7.80	5.48	7.38	153.00
F8-93-96-LN	YAB	53.10	107.00	43.70	2.27		2.09	0.30	8.46	103.00	25.40	950.00	664.00	15.20	7.16	4.81	6.08	193.00

TABLE 3 (continued)

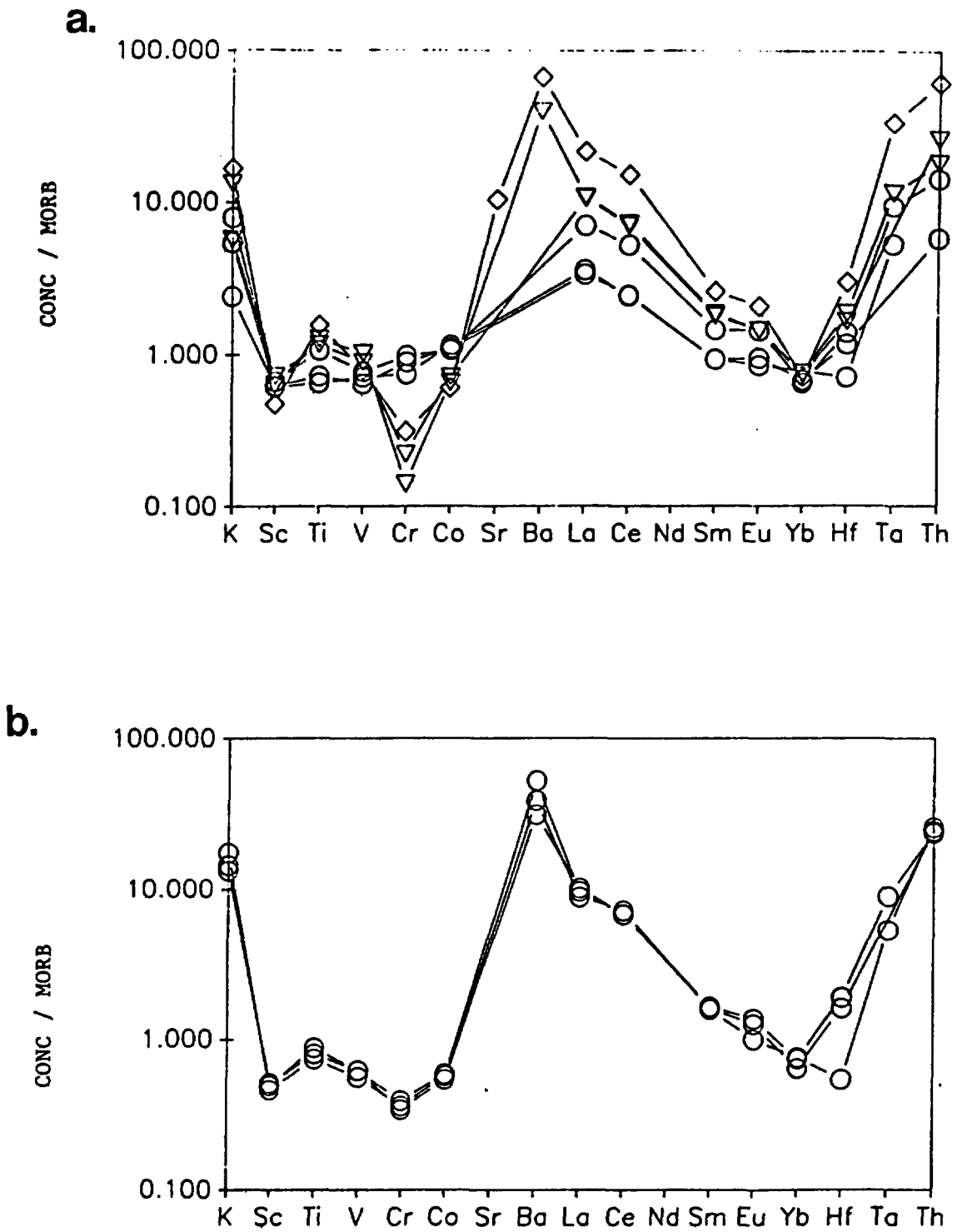

Figure 10. Spider diagrams showing trace element abundances relative to MORB in the: (a) FH basalt (circles = SAB; inverse triangles = OAB; diamonds = YAB lava); (b) CM basaltic andesite.

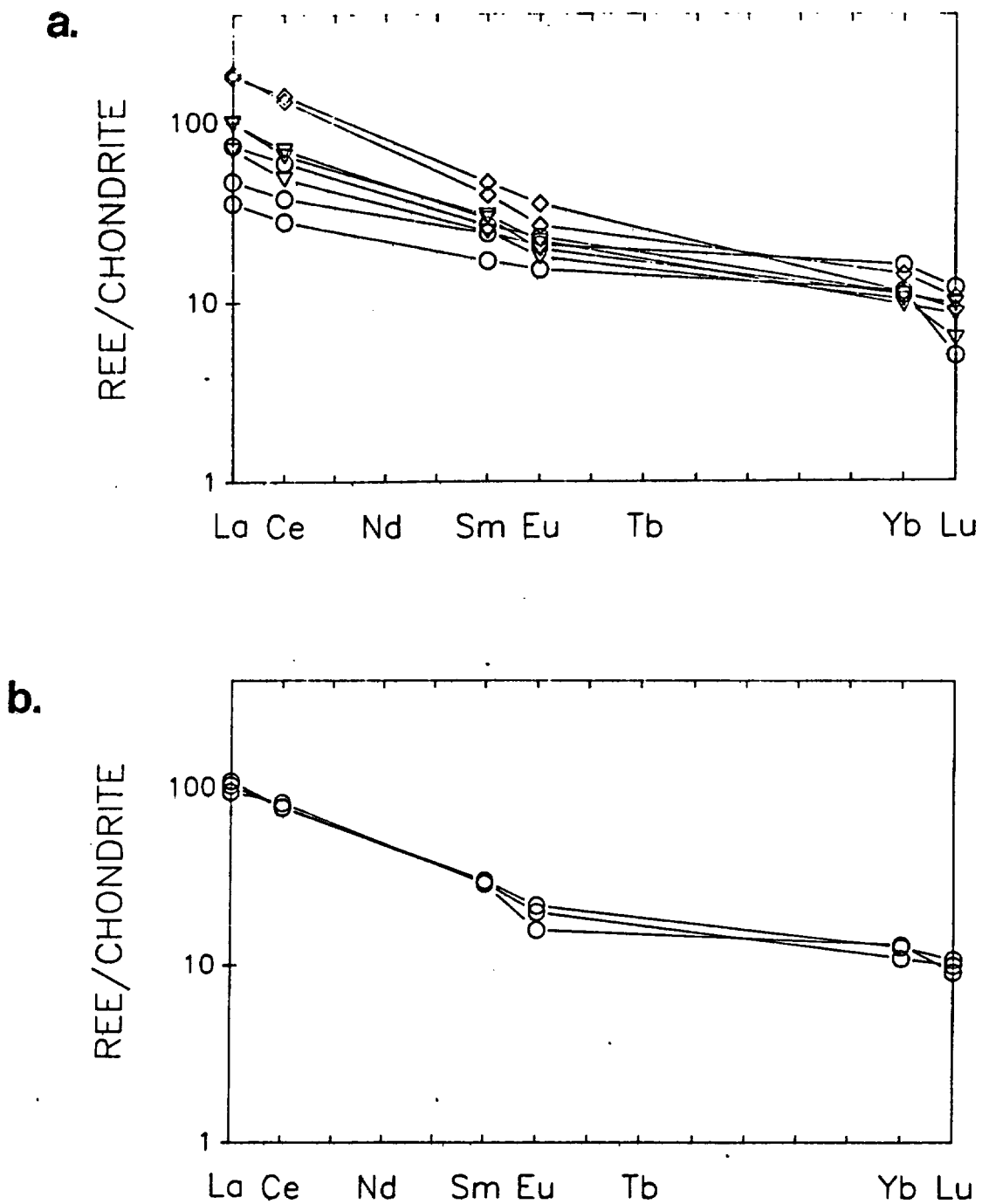

Figure 11. REE diagrams for: (a) FH basalt (circles= SAB; inverse triangles=OAB; diamonds=YAB lava); (b) CM basaltic andesite.

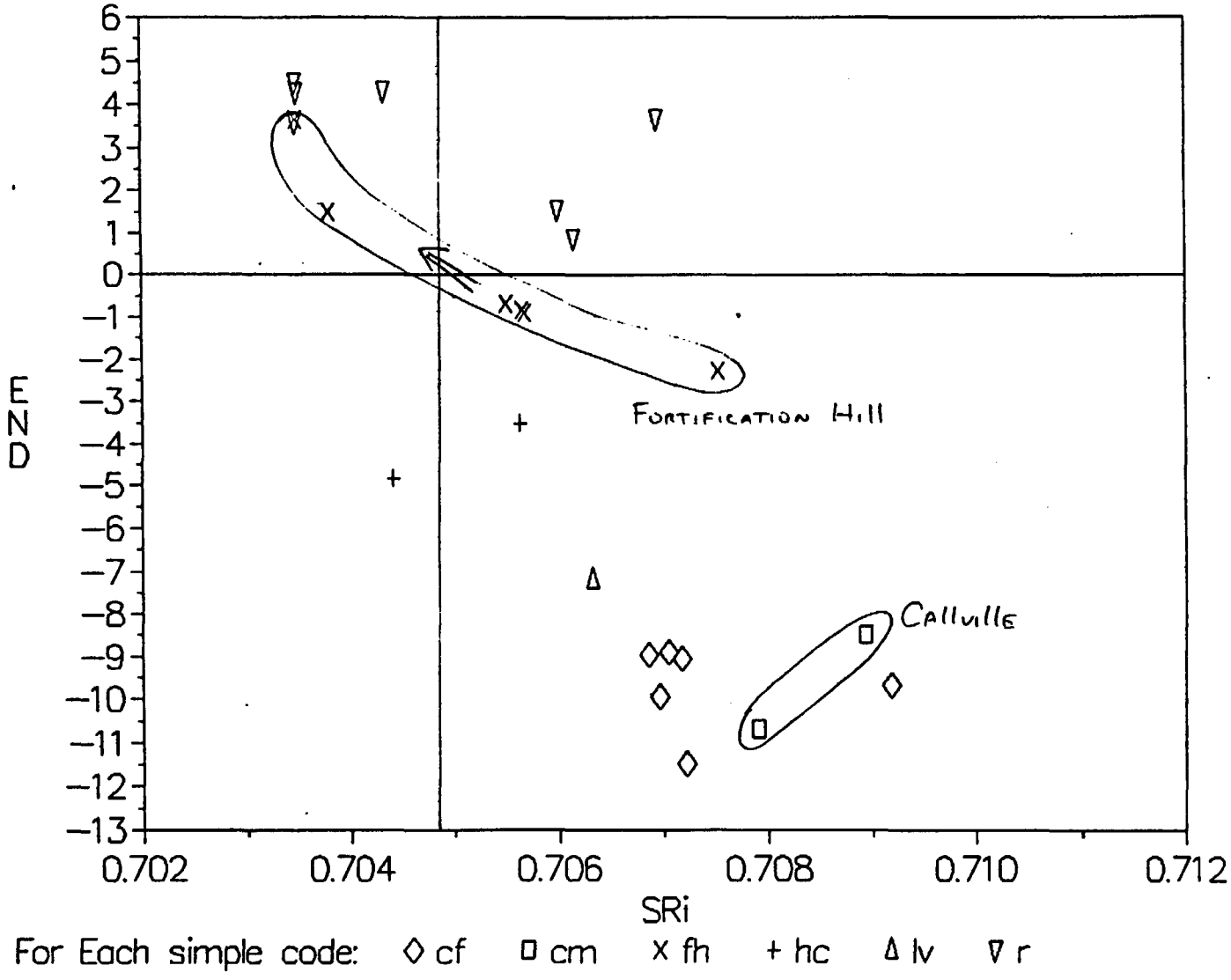

Figure 12. Epsilon Nd-initial $^{87}Sr/^{86}Sr$ plot for basalts in the southern Basin and Range province. Fortification Hill basalts form a linear array with a negative slope and show lower $^{87}Sr/^{86}Sr$ and epsilon Nd with time (arrow is a time vector).

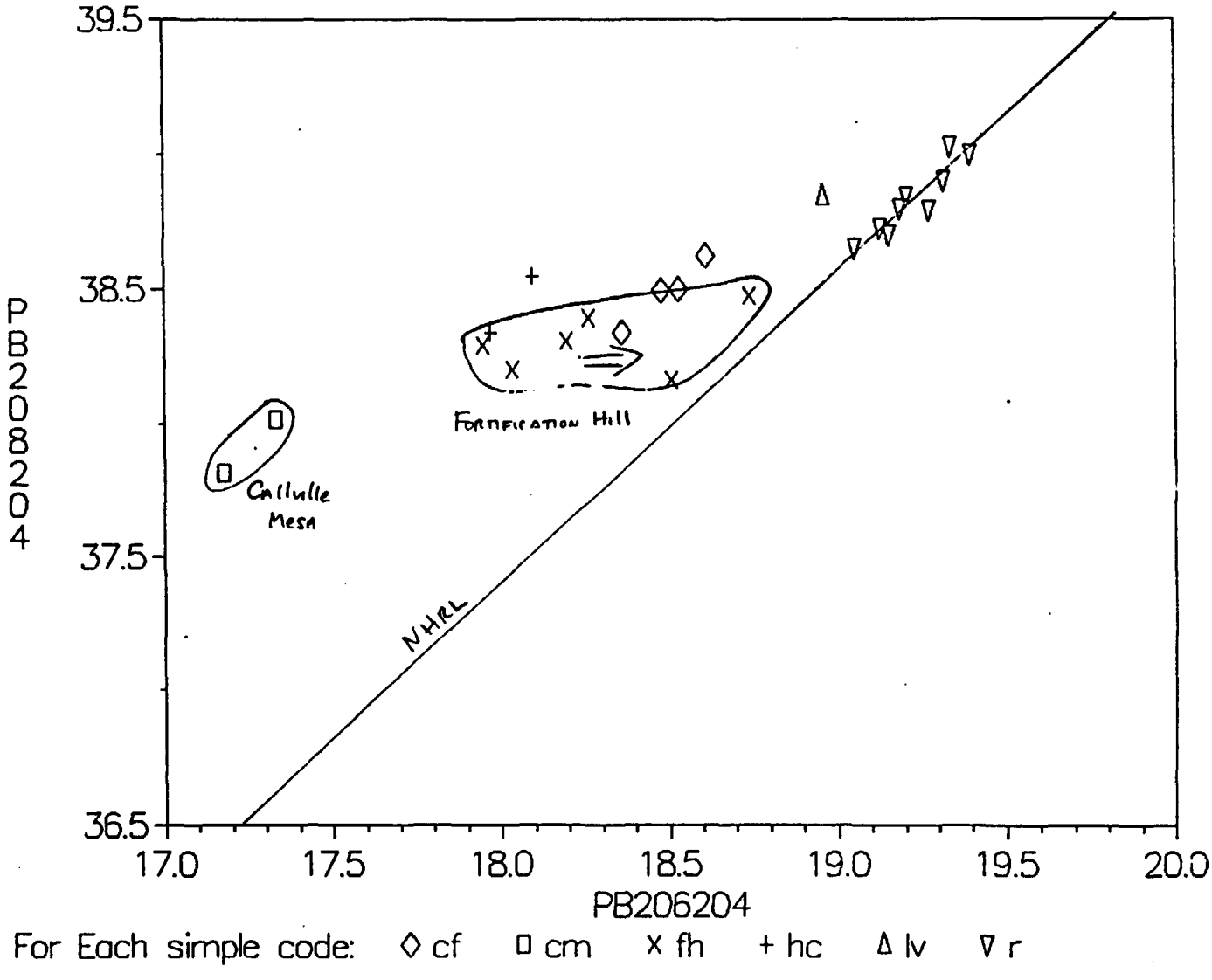

Figure 13. $^{208}Pb/^{204}Pb$ vs. $^{206}Pb/^{204}Pb$ plot for basalts in the southern Basin and Range province. Fortification Hill basalts lie above the northern hemisphere reference line (NHRL) and become more radiogenic with time (arrow is a time vector). Callville Mesa lavas have low $^{206}Pb/^{204}Pb$ values.

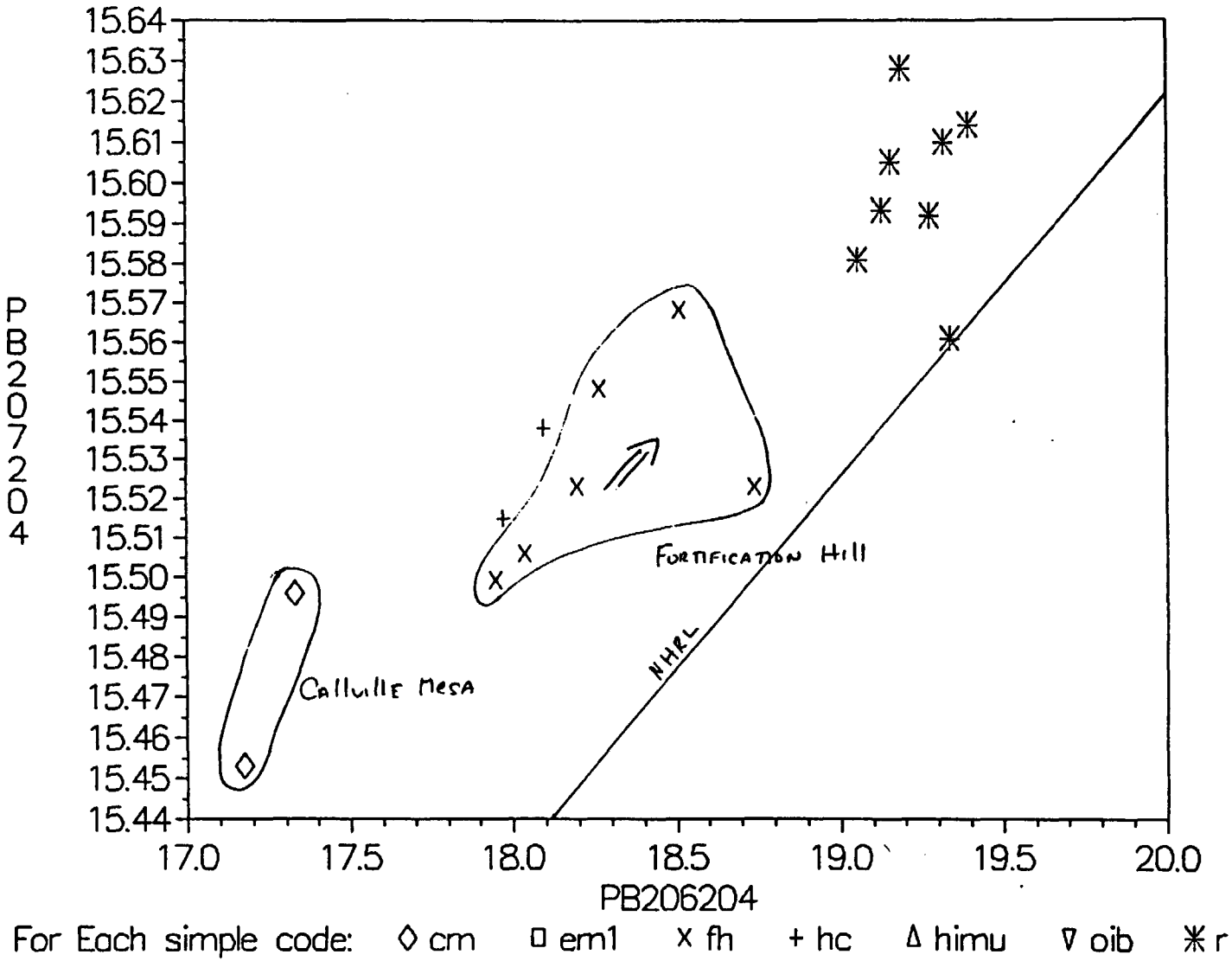

Figure 14. $^{207}Pb/^{206}Pb$ vs. $^{206}Pb/^{204}Pb$ plot for basalts in the southern Basin and Range province. Fortification Hill basalt lie above the NHRL and become more radiogenic with age (arrow is a time vector). Callville Mesa lavas are low in both $^{207}Pb/^{206}Pb$ and $^{206}Pb/^{204}Pb$.

magmas were generated in the lithospheric mantle as basalt similar in composition to basalt in Callville Wash (10.6 Ma) and younger Fortification Hill basalt, but were contaminated in the crust during ascent.

To evaluate the relative importance of mixing and fractionation, major elements were modelled by using the program XLFRAC (Stormer and Nicholls, 1978); trace and REE were modelled using Rayleigh fractionation and by techniques that determine the change of the concentration of an element as a system undergoes concurrent mixing and fractionation (Depaolo, 1981; Thompson et al., 1986). We suggest that the most primitive lavas at Callville Mesa (sample 46) were generated by the mixing of magma with the composition of the olivine basalt of Fortification Hill (sample 144) with an upper crustal contaminant such as the quartz monzonite of the Tertiary Wilson Ridge Pluton (sample 368) (Smith et al., 1989). Mixing may have been accompanied by fractionation of clinopyroxene and plagioclase. The R value (mass assimilated component/mass crystallizing phase) is 0.7 for major-element models (Table 5) and 0.15 for trace-element models (Table 6). Further differentiation (sample 46 to 50) is modelled by fractionation of olivine, Fe-Ti oxide, clinopyroxene, and plagioclase (Table 5 and 6).

Fortification Hill Basalt

The SAB, OAB and YAB lavas of FH field record a transition from subalkalic to alkalic volcanism with time (Table 7). This transition occurred between 5.71 and 5.42 Ma during the formation of Fortification Hill. Chemically, the change from SAB to YAB is

Table 5. **Summary of Major Element Models**

	Model 1				Model 2			
	Parent	Differentiate	Model	Residuals	Parent	Differentiate	Model	Residuals
SiO2	49.21	54.34	53.97	0.39	54.34	57.78	57.63	0.15
Al2O3	16.46	16.03	15.84	0.18	16.03	15.74	15.69	0.05
Fe2O3	12.18	10.67	10.42	0.26	10.67	8.75	8.64	0.11
CaO	10.42	7.21	7.1	0.12	7.21	6.42	6.31	0.05
MgO	5.46	5.18	5.03	0.16	5.18	4.34	4.28	0.05
Na2O	3.34	3.53	3.89	-0.37	3.53	3.54	3.45	-0.07
K2O	1.44	1.86	2.47	-0.61	1.86	2.41	2.53	-0.12
TiO2	1.5	1.17	1.3	0.12	1.17	1.03	1.3	-0.27
Minerals Fractionated								
Olivine				0				4.85
Clinopyroxene				11.03				4.65
Plagioclase				14.58				15.76
Magnetite				2.43				2.76
Mixed Component			(368)	+19.51				0
Total Fractionated				28.08				28.01
R value				0.7				0
Residuals				0.811				0.147

Model 1- Callville Mesa least evolved by
Mixing of Fortification Hill type magma (144) with
upper crust (Wilson Ridge 368) plus fractionation.
R value of model is 0.15.
Model 2-Callville Mesa basaltic andesites (46 to 50).

Table 6. **Fractional Crystallization Models - Selected Trace and Rare Earth Elements/1**

Element	1	2
Ce	-5.71	+3.58
Sm	-1.05	+0.75
Eu	-0.38	+0.57
Yb	-0.65	+0.45
Lu	+0.04	+0.06
Cr	-22.1	+28.55
V	----	+77.13
Sc	-9.2	+5
Co	----	+11.36

Numbers above are difference in ppm between model and actual rock.

Phases	-0.1 Plag	-0.05 Plag
	-0.05 Cpx	-0.15 Cpx
	-0.05 Ol	-0.05 Ol
	+0.03 (368)	

Model 1- Callville Mesa least evolved by
Mixing of Fortification Hill type magma (144) with upper crust (Wilson Ridge 368) plus fractionation.
R value of model is 0.15.

Model 2-Callville Mesa basaltic andesites (46 to 50).

Note:
1- All models use Depaolo Equation.

marked by an increase in Na_2O+K_2O (3.5 to 7%), Ce/Yb(n) (3.5-12), Th (2.5 to 9 ppm), P_2O_5 (0.35 to 0.8%), TiO_2 (1.3 to 2.5%), and normative nepheline (all values are means). OAB lavas are intermediate in composition between SAB and YAB. Isotopically, the change from SAB to YAB is marked by a decrease in initial $^{87}Sr/^{86}Sr$ from 0.7079-0.7056 in SAB lavas to 0.7055 in OAB to 0.7035 in YAB. Epsilon Nd increases from -2.28 to -0.84 in SAB to -0.64 in OAB to 3.68 in YAB (Figure 12). These chemical and isotopic variations reflect a change in source with time from the lithospheric mantle to the asthenosphere.

Similar initial Sr 87/86 epsilon Nd values for the SAB and OAB basalt at Fortification Hill suggest that both magma types were generated from the same source. The geochemical differences observed between these two magma types must be caused by crystal fractionation. Low MgO contents (6 to 9 wt. %) and Mg numbers (0.6 to 0.45), and low Cr and V (marginally low) suggest that even the most primitive basalts in the FH field are evolved when compared to primitive alkali-olivine basalt magmas (Basaltic Volcanism Study Project, 1981). This too suggests that crystal fractionation must have taken place between the time magma was melted and when it reached the surface.

Preliminary models for the evolution of the magma in the FH field were produced for basalt at Fortification Hill and Lava Cascade. The models suggest that differing degrees of batch melting combined with crystal fractionation produce the variations

Table 7. Summary of Sub-Alkalic and Alkalic Suites in the Lake Mead Area.

Alkalic	Sub-alkalic	Age (Ma)
	Callville Mesa (CM)	10.3-8.5
	Black Point (SAB)	6.02
	Malpais Flattop (SAB)	5.8
Fortification Hill (OAB)	Fortification Hill (SAB)	5.89-5.42
Petroglyph Wash (OAB)		5.43
Lava Cascade (OAB)		5.16-4.74
Young Alkalic Basalt (YAB)		4.6-4.3

CM-Callville Mesa, SAB-Subalkaline basalt, OAB-Older alkaline basalt, YAB-Younger alkaline basalt

observed at both Fortification Hill and Lava Cascade. A number of possible mantle sources could have produced basaltic magma in the Lake Mead area. We selected a spinel lherzolite for modelling the basalts since this rock type is found as xenoliths in alkali olivine basalts to the east and south of Lake Mead in the western Colorado Plateau (northwestern Arizona) (Alibert et al., 1986) and in alkali basalt dikes near Hoover Dam (Wilshire et al., 1988). Spinel bearing peridotite is also found in alkali basalts of the Big Pine volcanic field south of Bishop, California (Ormerod et al., 1988). Spinel lherzolite used in our models is assumed to contain 20% clinopyroxene, 20% orthopyroxene, 7% spinel and 53% olivine. This mineralogy is similar to primitive natural spinel lherzolites (Jagoutz et al., 1979). The source material is assumed to contain 2.7 ppm Ce (about 3 X chondrite and on the high end of the range reported by Wilshire et al., 1988), 0.3 ppm Yb (about 1 x chondrite) and 3000 ppm Cr (a typical primitive mantle value; Taylor and McLennan, 1985). As shown on Figures 15 and 16, batch melts of a spinel lherzolite source do not match the observed compositions. However, fractional crystallization of olivine and Fe-Ti oxide from these batch melts produces differentiation curves that intersect the observed data points. Less highly evolved magmas at both the Fortification Hill and Lava Cascade volcanoes were formed by 25 to 40% fractional crystallization (23 to 38% olivine + Fe-Ti oxide) of a 5% batch melt (Figure 15). More evolved olivine basalt, and pyroxene basalt may have formed by progressively smaller degrees of batch melting and fractionation (Figure 16). Plagioclase

Figure 15. Ce/Yb vs. Ce process diagram suggest a two-stage evolution for Fortification Hill and Lava Cascade basalts. (1) Batch melting of spinel peridotite with 20% clinopyroxene, 20% orthopyroxene, 7% spinel and 53% olivine assumed to contain 2.7 ppm Ce and 0.3 ppm Yb (3 and 1 X chondrite, respectively). (2) fractional crystallization of olivine and magnetite form these batch melts. Numerical labels on evolution vectors indicate the percent of either fractional crystallization or partial melting.

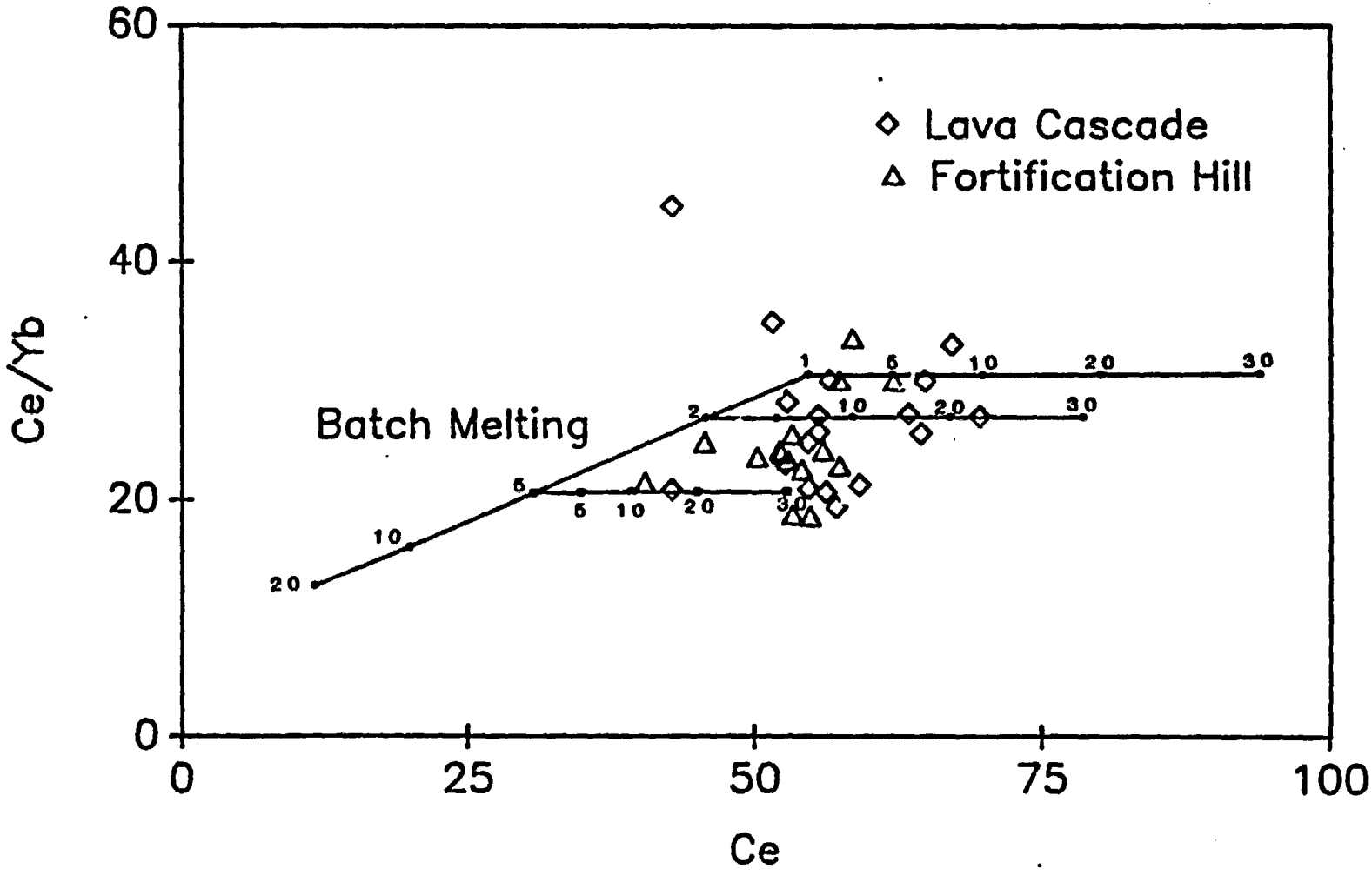

Figure 16. A plot of a rare-earth element vs. a transition element (Ce vs. Cr) also suggests a two-stage evolution for Fortification Hill and Lava Cascade basalts. Source composition and mineralogy are discussed in the capion to Figure 14. Numerical labels on evolution vectors indicate the percent of either fractional crystallization or partial melting.

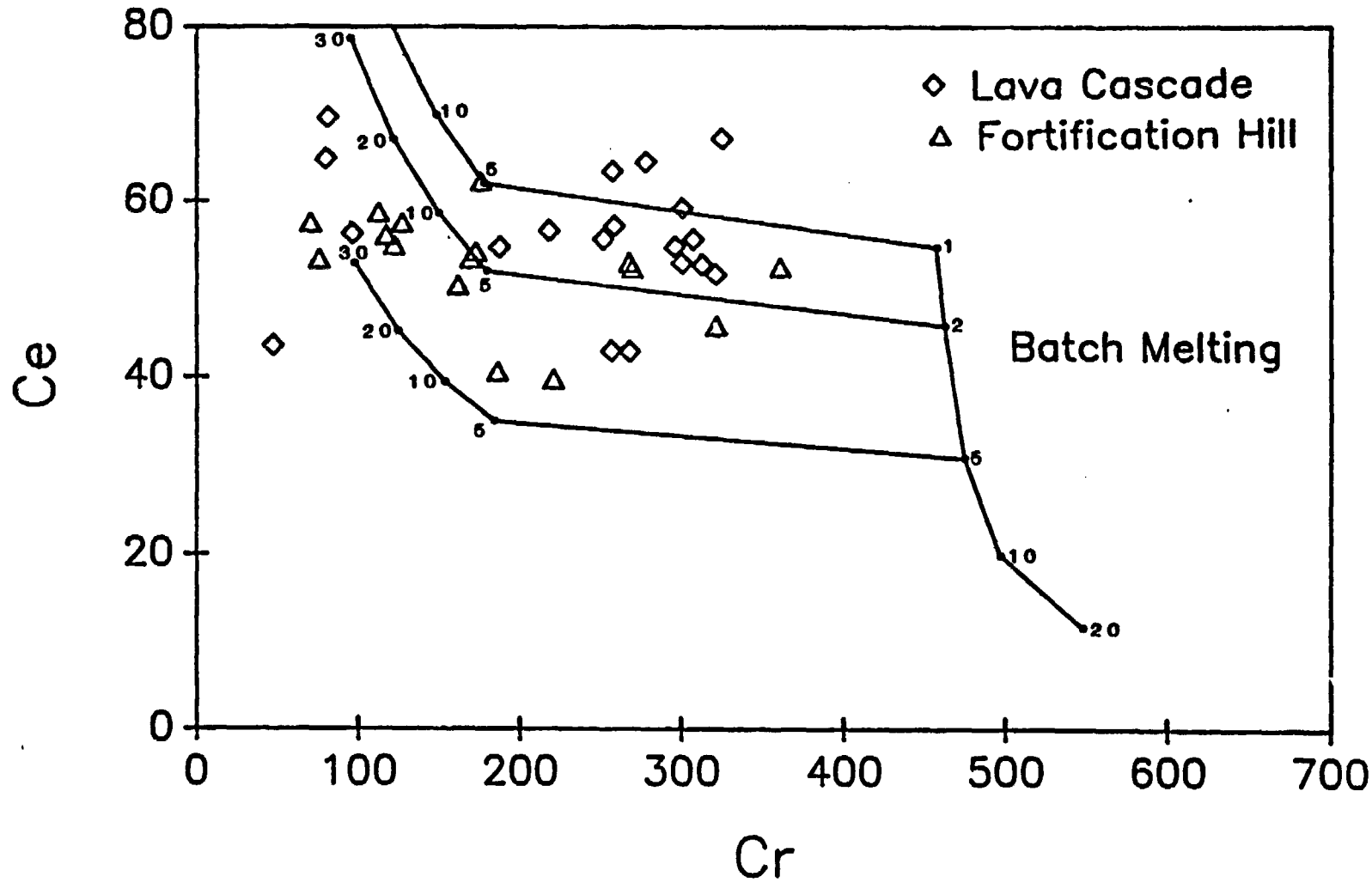

and clinopyroxene in glomeroporphritic clots may have crystallized under higher pressure conditions.

ISOTOPIC STUDIES

Fortification Hill basalts show an inverse relationship between epsilon Nd and initial $^{87}Sr/^{86}Sr$. Basalt from Black Point has the lowest epsilon Nd (-3.5) and the highest initial $^{87}Sr/^{86}Sr$ (0.708) (Table 3). Alkali basalt in Petroglyph Wash and along U.S. 93 has the highest epsilon Nd (+3.5) and the lowest initial $^{87}Sr/^{86}Sr$ (0.704). Subalkalic basalt from Fortification Hill and Petroglyph Wash have intermediate values. Callville Mesa lavas show very high epsilon Nd (-9 to -12) and initial $^{87}Sr/^{86}Sr$ (0.708-0.709) (Figure 12). Fortification Hill basalts lie above the NHRL (northern hemisphere reference line) and have a Pb isotopic signature more typical of basalt on the Colorado Plateau in northwestern Arizona than in the southern Basin and Range (Figures 13 and 14)(compare with data in Farmer et al., 1989). Callville Mesa basaltic andesite shows unusually low Pb ratios ($^{206}Pb/^{204}Pb=17.3$, $^{207}Pb/^{204}Pb=15.45$-15.5, $^{208}Pb/^{204}Pb=37.75$ (Figures 13 and 14).

When viewing the Pb and Sr systems together (Figure 17), there is a negative linear corelation between Pb and initial $^{87}Sr/^{86}Sr$ for Fortification and Callville Mesa volcanics. Alkali basalts lie near the radiogenic Pb end-member mantle component HIMU (Zindler and Hart, 1986) close to a mixing line between HIMU and the nonradiogenic enriched mantle component EMI (Zindler and Hart, 1986). Therefore the Pb and Sr isotopic systems suggest that the alkali basalts were derived from

Table 4. New Sr, Nd and Pb isotope data for Fortification Hill and Callville Mesa volcanic fields.

	CM F8-24-49	CM F8-24-68	OAB 87-38-143	OAB 87-57-107	OAB 87-57-113
Sr(87/86)i	.70893	70.790	.70567		
(143Nd/144Nd)m	0.512203	.512090	.512592	.512711	.512751
E(Nd,0)	-8.49	-10.69	-.90	1.42	2.20
Pb206/204	17.332	17.173			
Pb207/204	15.496	15.453			
Pb208/204	38.010	37.814			

	OAB F8-42-82	SAB 87-10-120	SAB 87-10-121	SAB F7-38-13	YAB F8-42-76
Sr(87/86)i	.70550	.70753	.70793	.70565	.70347
(143Nd/144Nd)m	.512603	.512520		.512595	.512824
E(Nd,0)	-.69	-2.30		-.84	3.63
Pb206/204	18.263	18.033	17.947	18.194	18.741
Pb207/204	15.548	15.506	15.499	15.523	15.523
Pb208/204	38.397	38.203	38.291	38.309	38.476

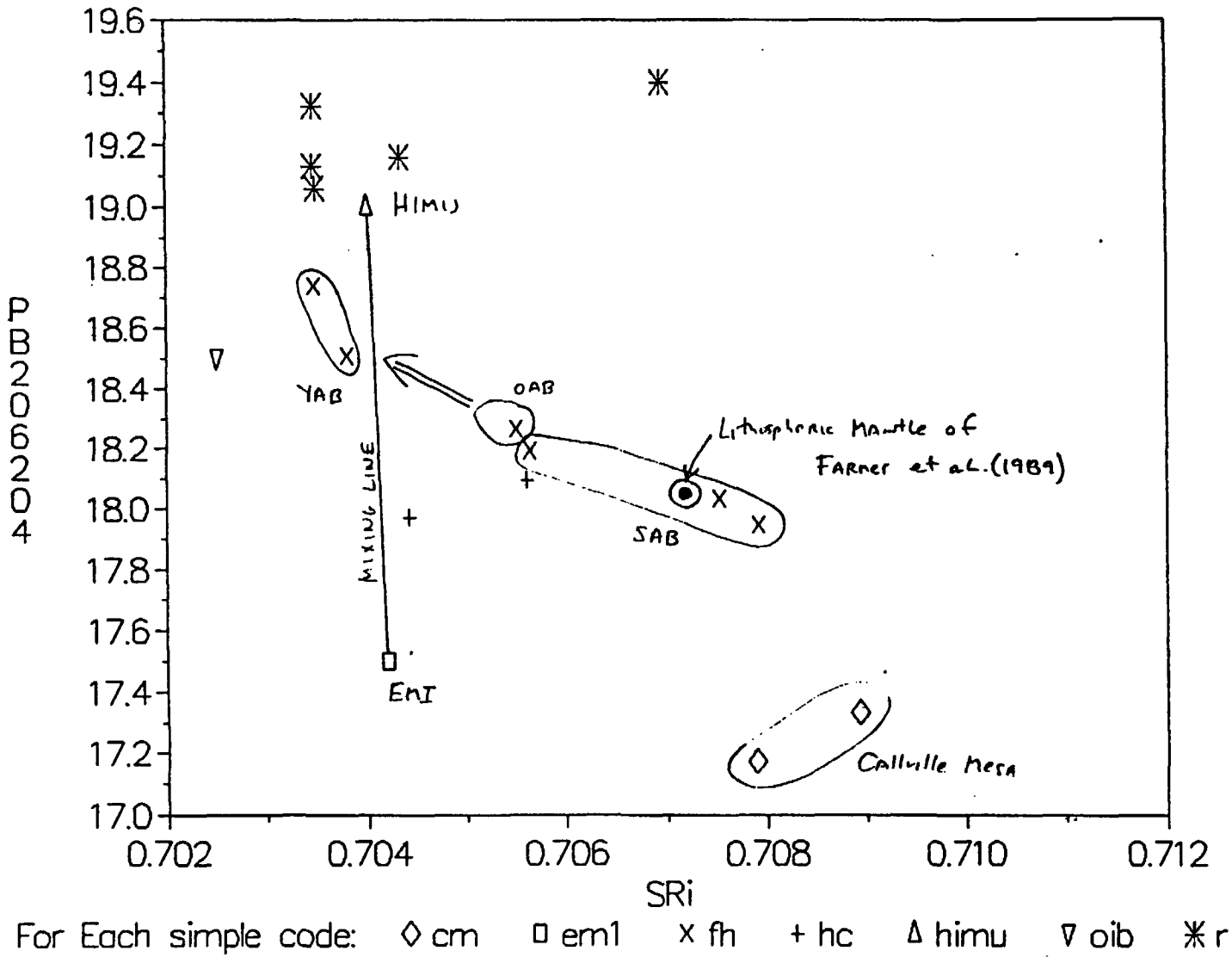

Figure 17. $^{206}Pb/^{204}Pb$ vs. initial $^{87}Sr/^{86}Sr$ plot for basalts in the southern Basin and Range province. Younger alkali basalts (YAB) lie near a mixing line between a HIMU and EMI mantle components. Older alkali basalts (OAB) and subalkalic basalts (SAB) represent the addition of a third component. We suggest that this component is lithospheric mantle.

asthenospheric mantle representing a two component mixture of HIMU and EMI. However, since the OAB and SAB basalts, and Callville Mesa basaltic andesites do not fall along this mixing line, at least one additional component is required. We suggest that this component is similar to the radiogenic lithospheric mantle component proposed as the source for southern Nevada basalts by Farmer et al. (1989) or some type of crust. Callville Mesa lavas show clear evidence for contamination. We suggest that the contaminating component is low U crust (lower crust).

REFERENCES

Alibert, C., Michard, A., and Albarede, F., 1986, Isotope and trace element geochemistry of Colorado Plateau volcanics: Geochemica et Cosmochimca Acta, v. 50, p. 2735-2750.

Anderson, R.E., 1973, Large-magnitude late Tertiary strike-slip faulting north of Lake Mead, Nevada: U.S. Geological Survey Professional Paper 794, 18 p.

Anderson, R.E., 1978, Geological Map of the Black Canyon 15′ Quadrangle, Arizona and Nevada: U.S. Geological Survey Map GQ-1394.

Basaltic Volcanism Study Project, 1981, Basaltic volcanism on the terrestrial planets: New York, Pergamon Press, 1286 p.

Bohannon, R.G., 1983, Geologic map, tectonic map and structure sections of the Muddy and northern Black Mountains, Clark County, Nevada: U.S. Geological Survey, Map I-1406.

Campbell, Ian and Schenk, E.T., 1950, Camptonite dikes near Boulder Dam, Arizona: American Mineralogist, v. 35, nos. 9-10, p. 671-692.

Depaolo, D.J., 1981, Trace element and isotopic effects of combined wall-rock assimilation and fractional crystallization: Earth and Planetary Science Letters, v. 53, p.189-202.

Deubendorfer, E.M., Sewall, A.J., and Smith, E.I., 1989, The Saddle Island detachment: an evolving shear zone in the Lake Mead area, Nevada: Geological Society of America Special Paper (in press).

Duebendorfer, E.M. and Wallin, E.T., (1990), Basin development and syntectonic sedimentation associated with kinematically coupled strike-slip and detachment faulting, southern Nevada: Geology (in press).

Farmer, G.L., Perry, F.V., Semken, S., Crowe, B., Curtis, D., and DePaolo, D.J., 1989, Isotopic evidence on the structure and origin of subcontinental lithospheric mantle in southern Nevada: Journal of Geophysical Research, v. 94, p. 7885-7898.

Feuerbach, D.L., 1986, Geology of the Wilson Ridge pluton; a mid-Miocene quartz monzonite intrusion in the northern Black Mountains, Mohave County, Arizona and Clark County, Nevada: (M.S. Thesis): Las Vegas, University of Nevada, 79 p.

Feuerbach, D.L., and Smith, E.I., 1987, Late-Miocene Fortification Hill basalt, Lake Mead area, Nevada and Arizona: source areas and conduit geometry: Geological Society of America Abstracts with Programs, v. 19, no. 6, p. 376-377.

Feuerbach, D.L., and Smith, E.I., 1988, Changes in volcanism during declining stages of regional extension in the Lake Mead area, Nevada and Arizona: Geological Society of America Abstracts with Programs, v. 100, p. A114.

Glazner, A.F. and Ussler, W., 1989, Crustal extension, crustal density, and the evolution of Cenozoic magmatism in the Basin and Range of the western United States: in Leeman, W.P. and Fritton, J.G., Magmatism associated with lithospheric extension: Journal of Geophsical Research, in press.

Larsen, L.L. and Smith, E.I., 1990, Mafic enclaves in the Wilson Ridge pluton, northwestern Arizona: Implications for the generation of a calc-alkaline intermediate pluton in an extensional environment: Journal of Geophysical Research, v. 95, p. 17,693-17,716.

McMillan, N.J. and Dungan, M.A., 1986, Magma mixing as a petrogenetic process in the development of the Taos Plateau volcanic field, New Mexico: Journal of Geophysical Research, v. 91, p. 6029-6045.

Mills J.G., 1985, The geology and geochemistry of volcanic and plutonic rocks in the Hoover Dam 7 1/2 quadrangle, Clark County, Nevada and Mohave County, Arizona (M.S. Thesis): Las Vegas, University of Nevada, 119 p.

Naumann, T.R., 1987, Geology of the central Boulder Canyon Quadrangle, Clark County, Nevada: M.S. Thesis, Univ. Nevada, Las Vegas, 68 p.

Naumann, T.R. and Smith, E.I., Evidence for magma mixing in mid-Tertiary volcanic rocks: Lake Mead region, Nevada: Geological Society of America Abstracts with Programs, v. 19, no. 6, p. 435.

Nielsen, R.L. and Dungan, M.A., 1985, The petrology and geochemistry of the Ocate Volcanic field, north-central New Mexico: Geological Society of America Bulletin, v. 96, p. 296-312.

Novak, S.W. and Bacon, C.R., 1986, Pliocene volcanic rocks of the Coso Range, Inyo County, California: U.S. Geological Survey Professional Paper 1383, 44 p.

Ormerod, D.S., Hawkesworth, C.J., Rogers, N.W., Leeman, W.P., Menzies, M.A., 1988, Tectonic and magmatic transitions in the Western Great Basin: Nature, v. 333, p. 349-353.

Scott, R.B., Nesbitt, R.W., Dasch, E.J. and Armstrong, R.L., 1969, A strontium isotope evolution model for Cenozoic magma genesis, eastern Great Basin, U.S.A.: Bulletin Volcanologique, v. , p. 1-26.

Smith, E.I., 1984, Geologic map of the Boulder Beach Quadrangle, Nevada: Nevada Bureau of Mines and Geology Map 81

Smith, E.I., Eschner, E., Feuerbach, D.L., Naumann, T.R., and Sewall, A., 1987, Mid-Tertiary extension in the eastern Basin and Range Province, Nevada and Arizona: The Las Vegas Valley-Detrital Wash transect: Geological Society of America, Abstracts with Programs, v. 19, no. 7, p. 848-849.

Smith, E.I., Schmidt, C.S., and Mills, J.G., 1988, Mid-Tertiary volcanoes of the Lake Mead area of southern Nevada and Northwestern Arizona: in Weide, D.L., and Faber, M.L., This Extended Land, Geological Journeys in the southern Basin and Range, Geological Society of America, Cordilleran Section Field Trip Guidebook; UNLV Department of Geoscience, Special Publication No. 2, p. 107-122.

Smith, E.I., Feuerbach, D.L., Naumann, Terry, and Mills, J.G., 1990, Geochemistry and evolution of mid-Miocene igneous rocks in the Lake Mead area of Nevada and Arizona: Geological Society of America, Special Paper "The Nature and Origin of Cordilleran Magmatism.", Anderson, J.L. editor.

Stormer, J.C., Jr., and Nicholls, J., 1978, XLFRAC: a program for the interactive testing of magmatic differentiation models: Computers and Geoscience, v. 4, p. 143-159.

Taylor, S.R., and McLennan, S.M., 1985, The Continental Crust: its Composition and Evolution, Blackwell Scientific Publications.

Thompson, R.A., Dungan, M.A. and Lipman, P.W., 1986, Multiple differentiation processes in Early-Rift Calc-Alkalic volcanics, northern Rio Grande Rift, New Mexico: Journal of Geophysical Research, v. 91, no. B6, p. 6046-6058.

Thompson, K.G., 1985, Stratigraphy and petrology of the Hamblin-Cleopatra volcano, Clark County, Nevada (M.S. thesis): Austin, University of Texas, 306pp.

Weber, M.E., and Smith, E.I. 1987, Structural and geochemical constraints on the reassembly mid-Tertiary volcanoes in the Lake Mead area of southern Nevada: Geology, v. 15, p. 553-556.

Wilshire, H.G., Meyer, C.E., Nakata, J.K., Calk, L.C., Shervais, J.W., Nielson, J.E. and Schwarzman, E.C., 1988, Mafic and ultramafic xenoliths from volcanic rocks of the southwestern United States: U.S. Geological Survey Professional Paper 1443, 177 p.

Zindler, A. and Hart, S., 1986, Chemical geodynamics: Annual Review of Earth and Planetary Science: v. 14, p. 493-557.

MAGMATISM, EXTENSIONAL TECTONICS AND SEDIMENTATION IN THE LAKE MEAD AREA, NEVADA AND ARIZONA: A NEW MODEL

(Eugene I. Smith)

INTRODUCTION

In the last several years there has been considerable progress in understanding large-scale late-Tertiary extension in the Lake Mead area of Nevada and Arizona. Longwell (1974), Anderson (1973), and Bohannon (1984) considered strike-slip faults (Lake Mead fault zone and the Las Vegas Valley shear zone) as the major structures that accomodated extension in the Lake Mead area. With the discovery of the Saddle Island detachment fault (Smith, 1982; Choukroune and Smith, 1985; and Duebendorfer et al., 1990) models were developed that considered detachment and strike-slip faults as a coordinated system that acted to accomodate large-scale offset during regional extension (Weber and Smith, 1987; and Guth and Smith, 1987). Duebendorfer and Wallin (1990) incorporated sedimentation into a tectonic model by demonstrating that the red sandstone unit, a sedimentary unit originally described by Bohannon (1984) that lies stratigraphically between the Horse Spring and Muddy Creek Formations, was deposited coevally with block rotation in the upper plate of the Saddle Island fault. With the exception of the model of Weber and Smith (1987), magmatism was not rigorously

considered as part of an extensional model. Recent detailed mapping, geochemistry and geochronology on the igneous rocks of the Lake Mead area (e.g., Smith et al., 1990; Larson and Smith, 1990; Feuerbach and Smith, 1988) in addition to recent studies of tectonics and sedimentation (Duebendorfer and Wallin (1990) now permits the development of a model that integrates magmatism, tectonics and sedimentation.

In this paper, we propose a four stage model for the late-Tertiary (18-4.7 Ma) evolution of the Lake Mead area, Nevada and Arizona that relates extensional style, magmatism and sedimentation. Our model assumes that (1) detachment faults nucleate at high angle and later rotate to low angle due to footwall rebound (Buck, 1988; Wernicke and Axen, 1988), (2) detachment faults in the upper crust may root into ductile shear zones in the lower crust, (3) upper crustal extension may preferentially occur in areas thermally weakened by magmatism, and (4) magmas generated in the lower crust, mantle lithosphere and/or asthenosphere rise through channelways (faults, joints) to the upper crust and surface.

MAGMATISM, EXTENSION AND SEDIMENTATION

Stage 1 (18-12 Ma)

Regional extension was reflected by moderate volume calc-alkaline intermediate volcanism and plutonism that produced the River Mountains volcano and subjacent Wilson Ridge pluton, and deposition of Horse Spring sediments in broad fault bounded basins (Smith et al., 1990; Bohannon, 1984) (Figure 1). Faulting at basin margins did not

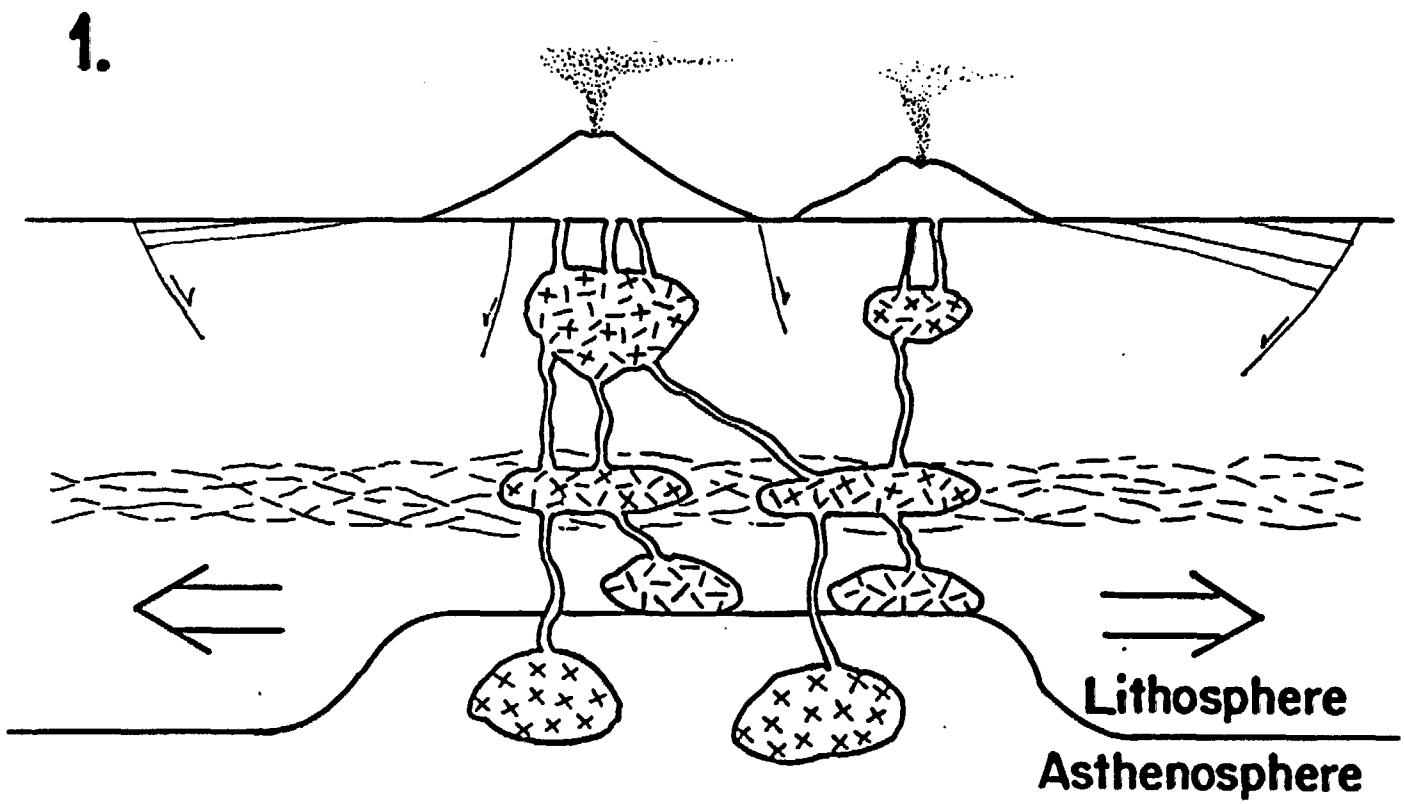

Figure 1. Intermediate calc-alkaline magmatism is accompanied by lower crustal ductile extension in the Lake Mead area of Nevada and Arizona. Alkali basalt commingles with crustal felsic melts to produce hybrid magmas. The River Mountain volcano and the Wilson Ridge Pluton were formed during this stage. Evidence for extension in the upper crust is limited to broad fault bounded basins and intermediate composition volcanoes. Thick sections of sediments accumulated in basins adjacent to volcanoes (X pattern = basalt, dashed pattern = felsic melt, x and dash = hybrid melts).

appreciably tilt either sedimentary or volcanic sections (Duebendorfer and Wallin, 1990). Igneous rocks show abundant textures and isotopic and chemical evidence that indicate magma commingling and considerable residence time in the crust (Larson and Smith, 1990). We suggest that basin formation and magmatism in the Lake Mead area may reflect ductile extension in the lower crust that is directly tied to detachment faulting and block rotation 30 km to the east (Gold Butte-Salt Spring-Cyclopic detachment system; Fryxell and Duebendorfer, 1990; Cascadden and Smith, 1991).

Stage 2 (12 Ma)

Upper crustal extension jumped to the west forming a high-angle detachment fault (the Saddle Island detachment)(SID) in the Lake Mead area; a region that was thermal weakening by stage 1 magmatism (Figure 2). The detachment may have penetrated into the zone of magma commingling and tapped end-member (rhyolite, granite and basalt) and hybrid magmas. Magma rose along the detachment and related faults and joints forming numerous dikes that cut the Wilson Ridge pluton and River Mountains and low volume volcanic centers in the River Mountains (Feuerbach, 1986; Smith, 1984). Nearly 20% extension in the Wilson Ridge pluton can be accommodated by dike emplacement (Feuerbach, 1986).

Stage 3 (12-9 Ma)

The River Mountain-Wilson Ridge magmatic system was tectonically dismembered by the SID (Weber and Smith, 1987). Pieces of the River Mountains were progressively accreted to the footwall of the SID and tilted as segments of the fault were

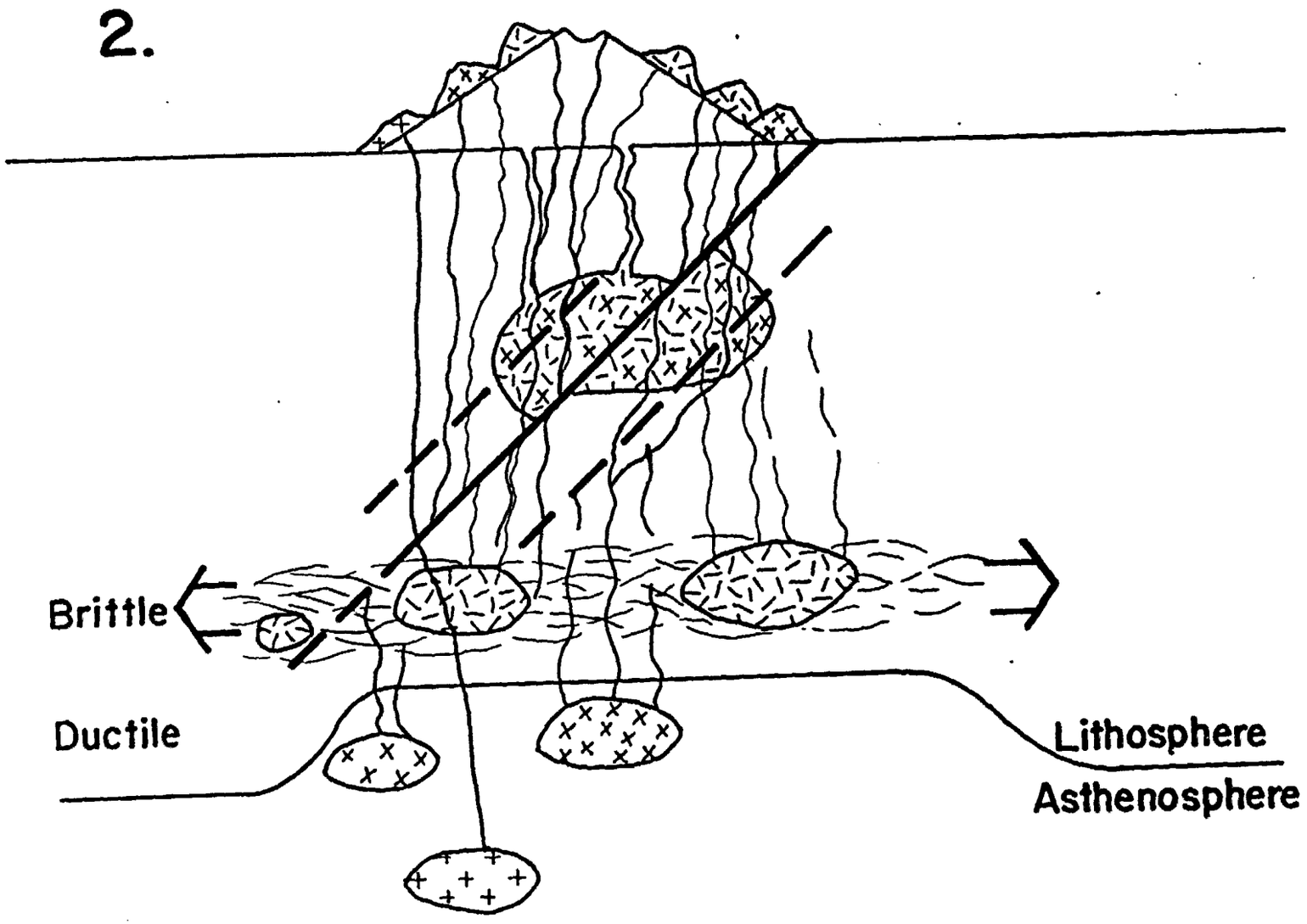

Figure 2. The region that was thermally weakened by earlier magmatism localizes major normal faults. These faults may penetrate into the middle crust to tap end member magma (rhyolite and basalt). During this stage numerous dikes cut the Wilson Ridge pluton and the River Mountain volcanoes, and low-volume volcanoes form on the flanks of the River Mountain volcano.

rotated and abandoned. Nearly 20 km of offset accumulated before the last fragment of the River Mountains was transferred to the footwall of the SID (Figure 3). The present location of the most recently active segment of the SID may be the west boundary of the Frenchman Mountain-River Mountain block. We envision that strike-slip faults such as the Las Vegas Valley and Lake Mead systems separated variably extending terranes and penetrated as deep into the crust as the high-angle detachments. Accordingly, the strike-slip faults may serve as channelways for rising magma. During stage 3, magmatism occurred after significant block rotation, was probably localized by the Las Vegas Valley shear zone and abandoned segments of the detachment, and was low in volume compared to stage 1 activity. These magmas were generated in the lithospheric mantle and show isotopic and petrographic evidence of crustal contamination. Sediments of the red sandstone accumulated in half grabens bounded by abandoned segments of the SID.

Stage 4 (7-4.7 Ma)

High-angle faults cut the SID and penetrated the entire thickness of the crust (Figuer 4). Since crust was cool and rigid, footwall rebound did not occur. Basaltic magma was tapped in the lithospheric mantle (early) and asthenosphere (late) and rose to the surface along high-angle channelways without being contaminated in the crust. Sediments of the Muddy Creek formation accumulated in grabens formed during this stage.

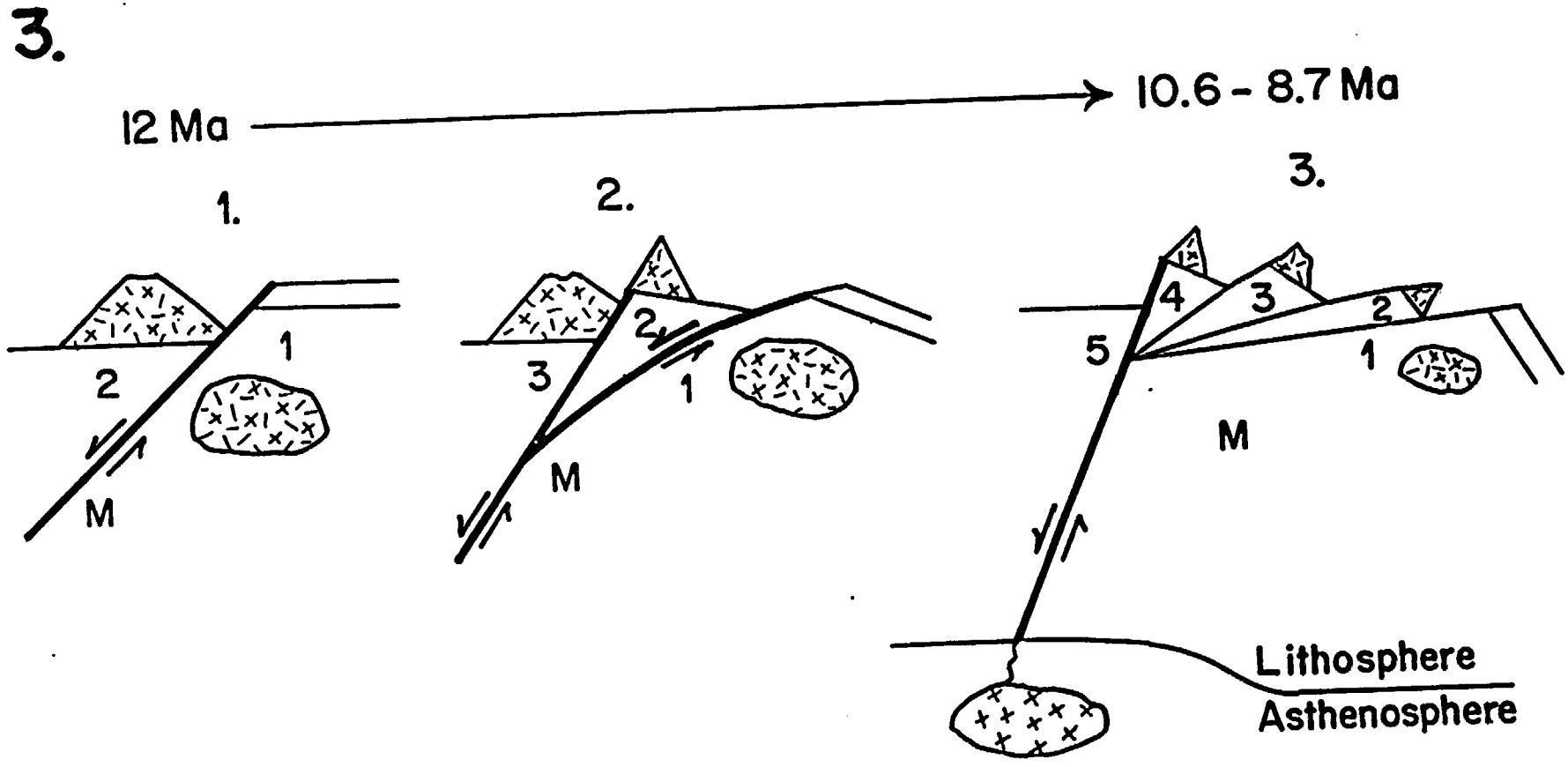

Figure 3. Detachment faults form during the major phase of upper crustal extension and block rotation (1). Volcanoes are separated from their subjacent plutons by evolving detachment system (2 and 3). Sediments accumulate in half grabens in the upper plate of the detachment system. Basalts are tapped and rise along high-angle faults and related strike-slip faults. Basalts magma may be trapped at dip changes on high-angle normal faults and may assimilate crustal material.

4.

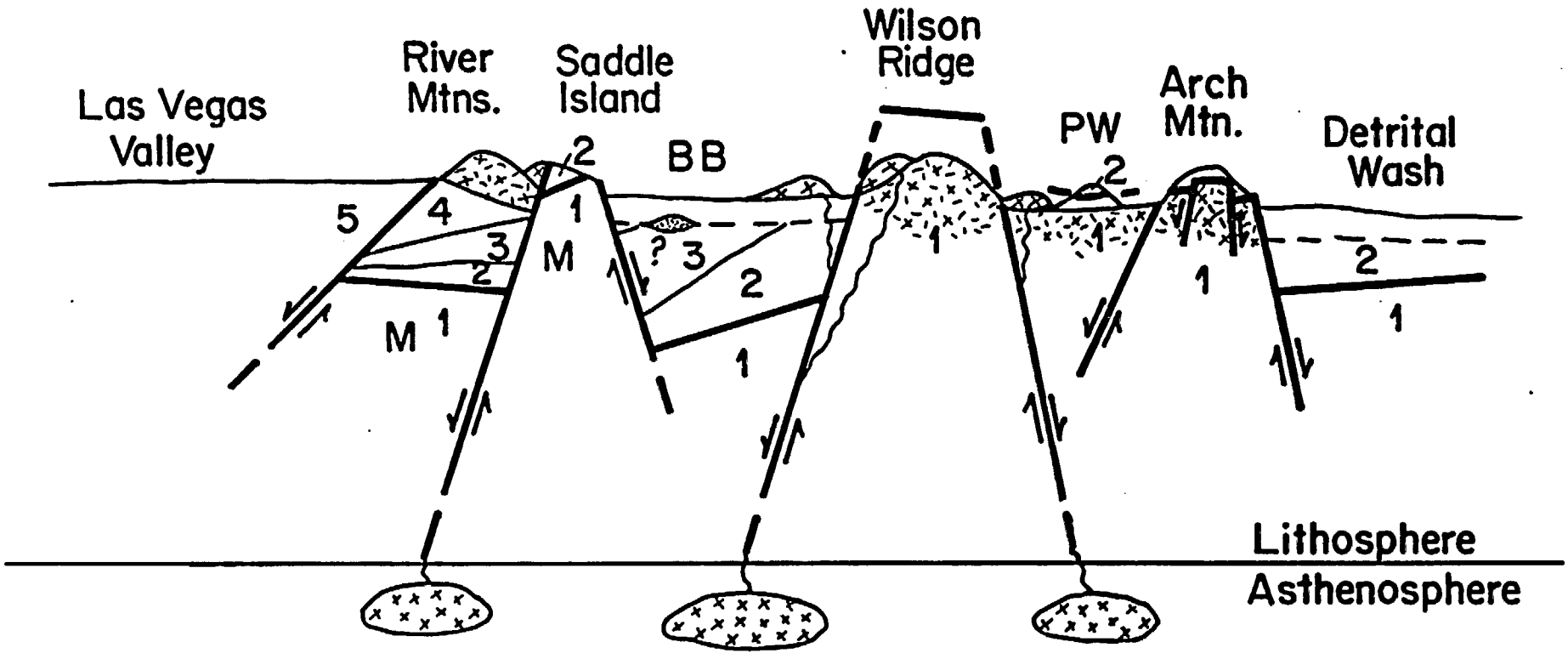

Figure 4. The detachment is cut by numerous high-angle normal faults that form horsts and grabens. Basalts rise quickly from the mantle and/asthenosphere along high-angle faults at depth. Near the surface they may leave the fault and rise along minor faults or joints. Sediments accumulated in grabens.

IMPLICATIONS OF MODEL

Implications of the this model are (1) changes in magmatic composition reflect changes in tectonic style, (2) the largest surge of magmatism occurred prior to significant upper crustal detachment faulting, and (3) the onset of magmatism may be a better guide to the onset of extension than the identification of the youngest tilted unit.

ACKNOWLEDGMENTS

This study was funded by the Nevada Nuclear Waste Project Office.

REFERENCES CITED

Anderson. R.E., 1973, Large-magnitude Late Tertiary strike-slip faulting north of Lake Mead, Nevada: U.S. Geological Survey Professional Paper 794, 18p.

Bohannon, R.G., 1984, Nonmarine sedimentary rocks of Tertiary age in the Lake Mead region, southeastern Nevada and northwestern Arizona: U.S. Geological Survey Professional Paper 1259, 72p.

Buck, W.R., 1988, Flexural rotation of normal faults: Tectonics, v. 7, no. 5, p. 959-973.

Cascadden, T.E. and Smith, E.I., 1991, The eastern boundary of the extensional allochthon in the eastern Basin and Range: volcanic and structural geology of the northern White Hills, Arizona: Geological Society of America, Abstracts with Programs, in press.

Choukroune, Pierre, and Smith, E.I., 1985, Detachment faulting and its relationship to older structural events on Saddle Island, River Mountains, Clark County, Nevada: Geology, v. 13, p. 421-424

Duebendorfer, E.M. and Wallin, T., 1990, Basin development and syntectonic sedimentation associated with kinematically coupled strike-slip and detachment faulting, southern Nevada: Geology, in press.

Feuerbach, D.L., 1986, Geology of the Wilson Ridge pluton; a mid-Miocene quartz monzonite intrusion in the northern Black Mountains, Mohave County, Arizona: M.S. Thesis, University of Nevada, Las Vegas, 79p.

Feuerbach, D.L., and Smith, E.I., 1988, Changes in volcanism during declining stages of regional extension in the Lake Mead area, Nevada and Arizona: Geological Society of America, Abstracts with Programs, v. 20, no. 7, p. 114.

Fryxell, J.E. and Duebendorfer, E.M., 1990, Origin and trajectory of the Frenchman Mountain block, southern Nevada: Geological Society of America, Abstracts with Programs, v. 22, p. 226.

Guth, Peter and Smith, E.I., 1987, Discussion of the paper by Ron and others, "Strike-slip faulting and block rotation in the Lake Mead Fault System", Geology, v. 15, p. 579-580.

Larsen, L.L. and Smith, E.I., Mafic enclaves in the Wilson Ridge Pluton, northwestern Arizona: Implications for the generation of a calc-alkaline intermediate pluton in an extensional environment: Journal of Geophysical Research.

Longwell, C.R., 1974, Measure and date of movement on Las Vegas Valley shear zone, Clark County, Nevada: Geological Society of America Bulletin, v. 85, p. 985-990.

Smith, E.I., 1982, Geology and geochemistry of the volcanic rocks in the River Mountains, Clark County, Nevada and comparisons with volcanic rocks in nearby area: in Frost, E.G., and Martin, D.L. eds., Mesozoic-Cenozoic tectonic evolution of the Colorado River Region, California, Arizona and Nevada: San Diego, California, Cordilleran Publishers, p. 41-54.

Smith, E.I., 1984, Geologic map of the Boulder City quadrangle, Nevada: Nevada Bureau of Mines and Geology, Map 81.

Weber, M.E., and Smith, E.I. 1987, Structural and geochemical constraints on the reassembly mid-Tertiary volcanoes in the Lake Mead area of southern Nevada: Geology, v. 15, p. 553-556.

Wernicke, B.M. and Axen, G.J., 1988, On the role of isostasy in the evolution of normal faults: Geology, v. 16, p. 848-851.

GEOLOGY AND GEOCHEMISTRY OF PLIOCENE BASALTS IN THE REVEILLE RANGE, CENTRAL NEVADA

(Terry Naumann)

ABSTRACT

This paper reports the results of a detailed stratigraphic, petrologic and geochemical investigation of alkali basalts from the Reveille Range, Nevada. Major, trace and rare-earth element geochemistry was determined on 62 samples collected from a stratigraphic section defined on the basis of geologic mapping and K-Ar dating. Alkali-basalt lavas occur as shallow intrusions, domes, flow stacks up to 100 m thick and over 50 dissected cinder cones. Activity spans 3 million years, beginning with alkali basalts and hawaiites erupted between 5.9 and 5.1 Ma (Episode 1), followed by a smaller volume of lava ranging in composition from picrite to trachybasalt that erupted between 4.6 and 3.0 Ma (Episode 2). Explosive eruptions of trachyte and tristanite occurred at 4.4 and 4.2 Ma. Geochemical modeling indicates that lavas formed through a process of partial melting of asthenospheric mantle with small amounts of crustal contamination.

INTRODUCTION

The genesis of magmatic suites in areas of continental extension has been the focus of papers dealing with evolution of the crust and mantle during the extension process. Major and trace element, and isotopic geochemistry are tools to identify the source of the magma either in the asthenospheric or lithospheric mantle, the effects of either upper and/or lower crustal contamination and the initiation and evolution of

mantle plume systems. A way to understand the source and evolution of a continental basaltic system and place constraints on extensional models is to study mafic volcanic rocks than geographically and temporally span the developmental history of the extensional terrane. Each basalt field may provide a snapshot of the extensional mechanism operating at that time. With these objectives in mind, we chose to study the Reveille Range, Nevada (Figure 1).

The basalts of the Reveille Range represent the southern half of a 10 km by 100 km wide, N to N30E trending belt that combined with the Lunar Crater Volcanic Field to the north extends from 37° 45′ to 38° 45′ in the south-central Great Basin (Figure 1). Basement rocks of the Reveille Range consist primarily of ash-flow sheets of Oligocene-Miocene age that along with other minor ash-flow sheets unconformably overly Paleozoic sedimentary rocks in the northern half of the range. The Monotony Tuff (25 Ma), a coarsely devitrified quartz latitic to rhyolitic welded tuff is the most widespread of these units (Ekren et al., 1973).

The Reveille Range forms a west-tilted horst bounded by en-echelon north to northeast striking high-angle normal faults. The west flank of the Reveille Range is bounded by a fault system approximately 20 km long. and the east flank of the range is bounded an east dipping fault system approximately 25 km long.

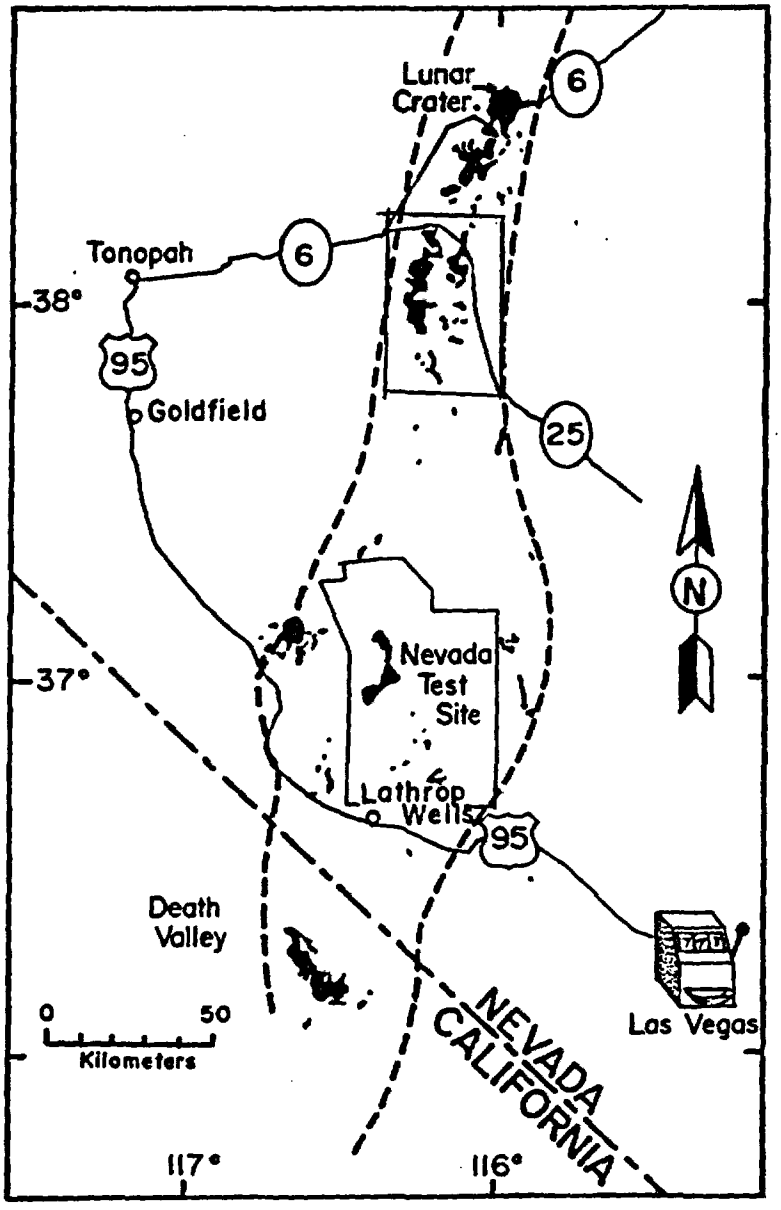

Figure 1. Location of the Reveille Range with respect to other Pliocene and Quaternary volcanic centers in the Lunar Crater-Death Valley volcanic zone. Reveille Range and the location of Figure 2 is outlined by the rectangle.

VOLCANIC CENTERS AND STRATIGRAPHY

Basalts occur as shallow intrusions, domes, flow stacks up to 100 m thick, and over 50 dissected cinder cones. These vents are composed of massively bedded red to brown scoria, cinder, spatter, agglutinated scoria and ash. Dikes (0.5 to 2.0 m wide) are exposed in the dissected cones and in bedrock. Where dikes intrude scoria cones they are arcuate and dip (90 to 20°) towards the vent. Dikes in bedrock pinch and swell and are laterally discontinuous. They cut obliquely across bedrock joints.

Volcanism is divided into three episodes based on field relations, petrology and potassium-argon dating.

EPISODE 1 (5.9 to 5.0 Ma): Basalts of Episode 1 contain megacrysts of plagioclase (up to 40%). Fifty two vents crop out on both the east and west flanks and crest of the range (Figure 2).

EPISODE 2 (4.6 to 3.0 Ma): Basalts of Episode 2 contain abundant megacrysts of augite (up to 40%), amphibole (up to 35%) and plagioclase (<5%) and coarse grained xenoliths of gabbro and dunite (up to 20 cm in length). Fourteen vents crop out on the northeast piedmont and flank of the range (Figure 2).

TRACHYTIC VOLCANISM (4.4 and 4.2 Ma): Trachytic eruptions occurred just prior to the onset of Episode 2 volcanism in the northern Reveille Range. Explosive eruptions of highly evolved trachyte and tristanite magmas containing ferrosillite and hedenbergite, anorthoclase, sanidine and andesine. Eruptions of evolved lavas produced two domes $<0.01\ km^3$ and $0.26\ km^3$ in volume (Figure 2). Initial eruptions at both domes were

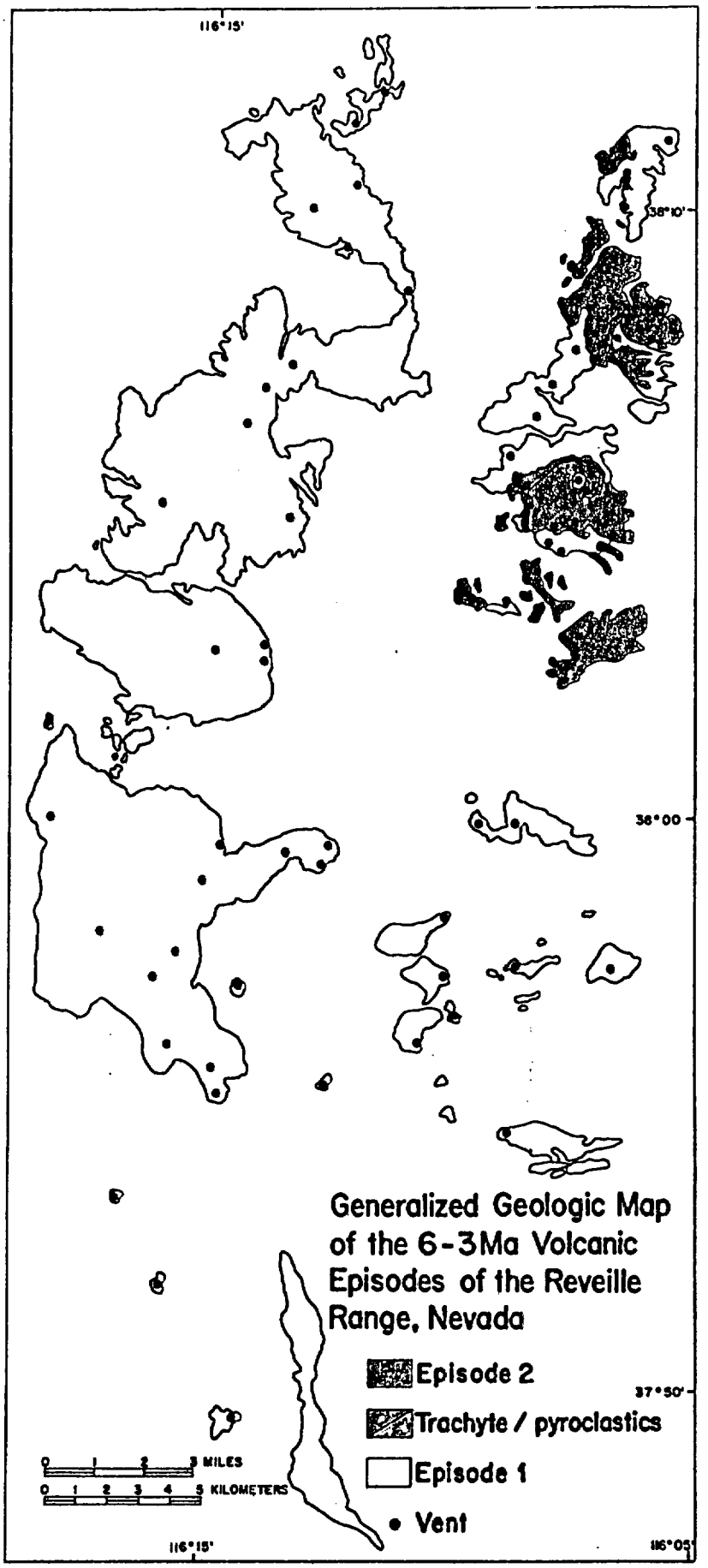

Figure 2. Geological map of Pliocene volcanic rocks in the Reveille Range, central Nevada.

explosive and produced a pyroclastic apron between 2 and 10 m thick that extends up to 5 km from the larger dome. The flanks of the larger dome are composed of stubby flows which originated at or near the summit. This dome is compositionally zoned with trachyte at the base (60% SiO_2) to tristanite at the top (58% SiO_2). Activity at the larger dome can be divided into three separate phases:

(1) Explosive hydromagmatic phase consisting of at least three separate pulses. Deposits consist of hydromagmatically produced pyroclastic surge containing altered pumice, lithic fragments (derived from near surface bedrock units) and ash. These volcaniclastic-pyroclastic deposits represent initial explosive eruptions that preceded the eruption of trachyte flows and include deposits of waterlain ash, debris flows, pyroclastic surge, and air-fall ash and pumice lapilli.

(2) Pumice cone building phase consisting of agglutinated pumice blocks, lithic fragments derived from the underlying tuff units and Episode 1 basalts. These deposits compose the bulk of the dome.

(3) Lava flow phase consisting of trachyte and tristanite lavas that erupted from the summit of the dome and flowed up to 0.5 km down the flanks of the cone.

PETROGRAPHY

Reveille basalts are holocrystaline and contain phenocrysts of olivine, feldspar and diopsidic augite, megacrysts of andesine and labradorite, diopsidic augite and xenoliths of gabbro and dunite. Rocks are mostly unaltered, however, some calcite is present as vein and vesicle

fillings. Episode 1 basalts can be distinguished from Episode 2 in outcrop by a greater abundance of plagioclase megacrysts and lack of augite megacrysts.

Episode 1

Episode 1 basalts have coarse grained intergranular or trachytic (rare) texture. Lavas are porphyritic with a total phenocryst content up to 20 percent (Table 1). Olivine and plagioclase are the major phenocryst phase in all samples. Phenocrysts of olivine are subhedral to euhedral and are commonly iddingsitized. Phenocrysts of plagioclase are euhedral with normal zoning. Diopsidic augite phenocrysts are subhedral with strong dispersion. Plagioclase megacrysts commonly occur in glomeroporphyritic clots that range in size from 5 to 15 cm. They commonly enclose broken grains of olivine and clinopyroxene. Plagioclase megacrysts are euhedral to subhedral, oscillatory zoned from andesine to labradorite and commonly show strong dispersion. Some feldspar megacrysts are partially resorbed and commonly contain abundant inclusions of olivine.

Groundmass phases within Episode 1 basalts include olivine (mostly altered to iddingsite), diopsidic augite, feldspar and opaque Fe-Ti oxides.

Episode 2

Episode 2 basalts are coarse grained with intergranular to subophitic and rare trachytic texture. Episode 2 basalts contain megacrysts of augite up to 4 cm in length and sparse plagioclase (usually broken and resorbed). All samples are porphyritic with total phenocryst content up to 20 percent (Table 1). Olivine, clinopyroxene and plagioclase are the major phenocryst phases. Olivine is euhedral to subhedral and is altered to iddingsite

	EPISODE 1								
	R8-1-10	R8-1-17	R8-1-24	R8-1-28	R8-1-29	R9-1-48	R9-1-57	R9-1-59	R9-3-60
MEGACRYSTS									
feldspar	26.3	15.3	16.3		8	24.6		3.6	3
clinopyroxene									
olivine									
PHENOCRYSTS									
olivine	3.3	6.3	7.6	4	3.6	5.3	3	4.3	8.6
clinopyroxene				1	1	6.3			1
feldspar	17	17.6	23.6	26.6	9	9.6	1	9.3	9
amphibole									
GROUNDMASS									
olivine	3	7.6	5.6	6	6	7.3	10.3	7	7
pyroxene	9.3	24	10.6	8.3	19.6	21	16.6	24	23
feldspar	26.6	16.3	19.6	38.6	16.3	21.3	59	40.6	14.6
amphibole									
opaque	14.3	12.3	14.6	15.6	28.3		9.3	11	17
biotite									
apatite									
VESICLES			1.6		8.3	4	1		
GLASS									

	EPISODE 2								
	R8-1-2	R8-1-5	R8-1-11	R8-1-13	R8-1-27	R8-1-30	R9-1-47	R9-1-55	R9-1-59
MEGACRYSTS									
feldspar						2		1.6	4
clinopyroxene						7			2
olivine									
PHENOCRYSTS									
olivine	4.6	5	6.6	6.6	14.3	2	3.3	4.6	2
clinopyroxene	0.3	1	12.6	0.6	3.3	3			
feldspar	19.6	25.6		13.3	1.3	1		12.6	19.3
amphibole									
GROUNDMASS									
olivine	12.6	12	3.3	12.3	2.7	9.6	16.6	21	9
pyroxene	11.3	7.6	13.6	19.6	49	14	16	26.3	16.3
feldspar	34	35	38	29.6	14.3	26	52.6	13.3	31
amphibole			1	tr					
opaque	17.3	14.3	24	17	14.3	34.6	11	20.3	13
biotite				tr					
apatite			tr						
VESICLES					tr				3
GLASS			tr						

	EVOLVED	
	R8-1-40	R8-1-42
MEGACRYSTS		
feldspar		1
clinopyroxene		
olivine		
PHENOCRYSTS		
olivine		
clinopyroxene	10	9.6
feldspar	61	74
amphibole		
GROUNDMASS		
olivine		
pyroxene		
feldspar		
amphibole		
opaque	10.6	4.6
biotite		
apatite		
VESICLES	16.3	6.6
GLASS	2	3.6

Table 1. Summary of Petrographic Data for Pliocene Volcanic Rocks of the Reveille Range.

along grain boundaries and fractures. Clinopyroxene (diopsidic augite) is subhedral and shows strong dispersion. Oxyhornblende was identified in two samples. Groundmass phases are olivine, pyroxene, opaque Fe-Ti oxides with a trace of biotite and apatite.

Trachyte Lavas

Trachyte lavas are vesicular and porphyritic with approximately 10 percent total phenocrysts. Subhedral to anhedral grains of clinopyroxene (salite to ferrosilite) are the only phenocryst phase. Sanidine is present as aligned microlites and microphenocrysts set in a matrix of colorless to pale green glass.

MINERAL CHEMISTRY

Mineral compositions of basalts and trachytes from the Reveille Range were determined by Dr. Albert Kudo at the University of New Mexico on a JEOL Super Probe.

Ca-Mg-Fe end-member compositions of pyroxene (Figure 7) and Or-Ab-An compositions of feldspar (Figure 8) were plotted for two samples each of Episode 1 basalt, Episode 2 basalt and trachyte. Phenocrysts and groundmass pyroxene from Episode 1 and 2 basalts are diopsidic augite with a narrow range of composition (Figure 7). Clinopyroxenes in the trachytes plot with a range of compositions along the salite-hedenbergite solid solution series and are more Fe-rich than in the basalts of Episodes 1 or 2. CaO content of clinopyroxene from both basalts and trachytes are remarkably similar.

Groundmass plagioclase from Episode 1 basalts plot along the Ab-An solid solution join and are primarily labradorite with minor andesine (Figure 8). A few groundmass

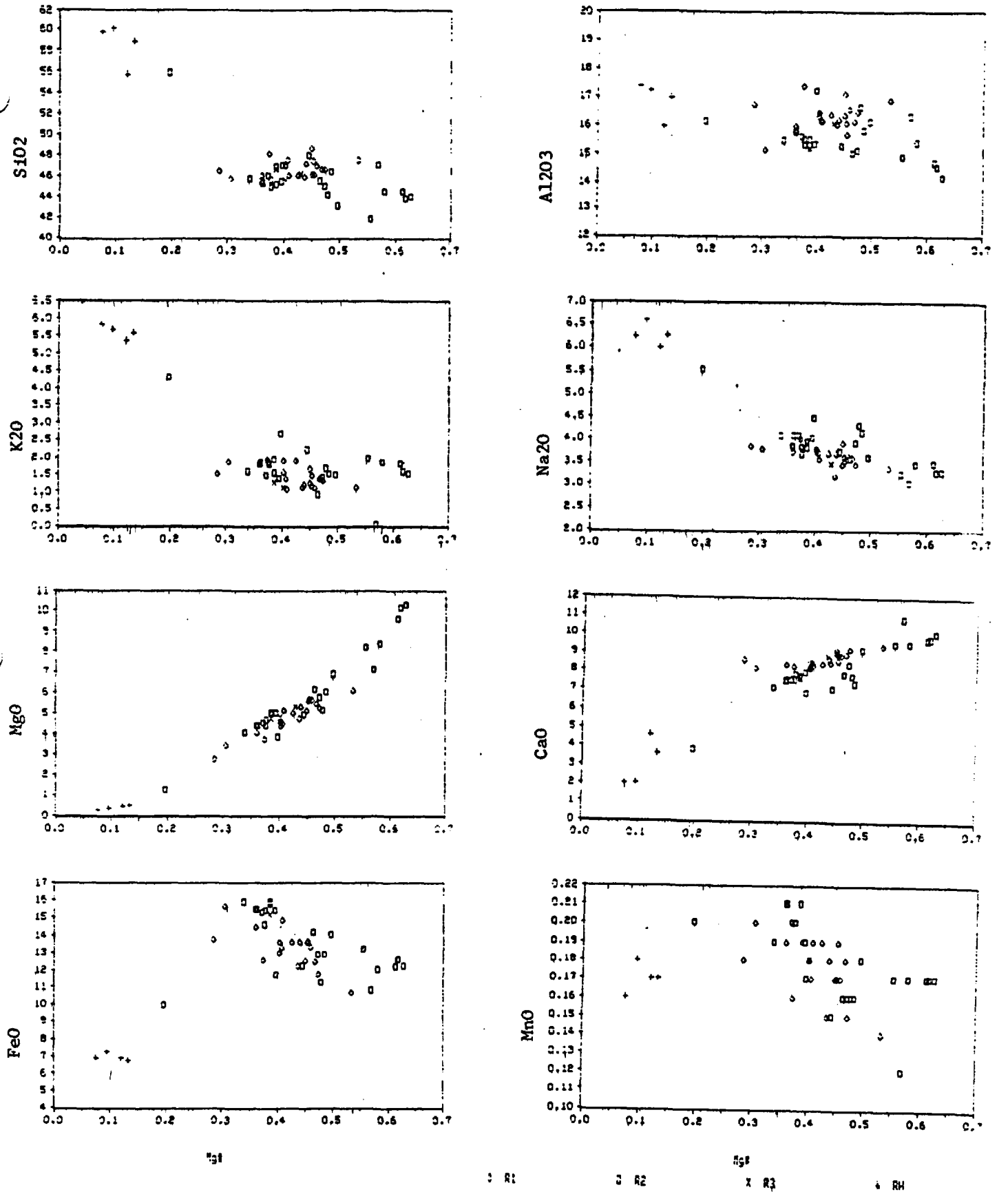

Figure 3. Harker variation diagrams for Pliocene volcanic rocks in the Reveille Range. Diamonds = Episode 1 basalt, squares = Episode 2 basalt, plus signs = trachyte/tristanite domes and flows.

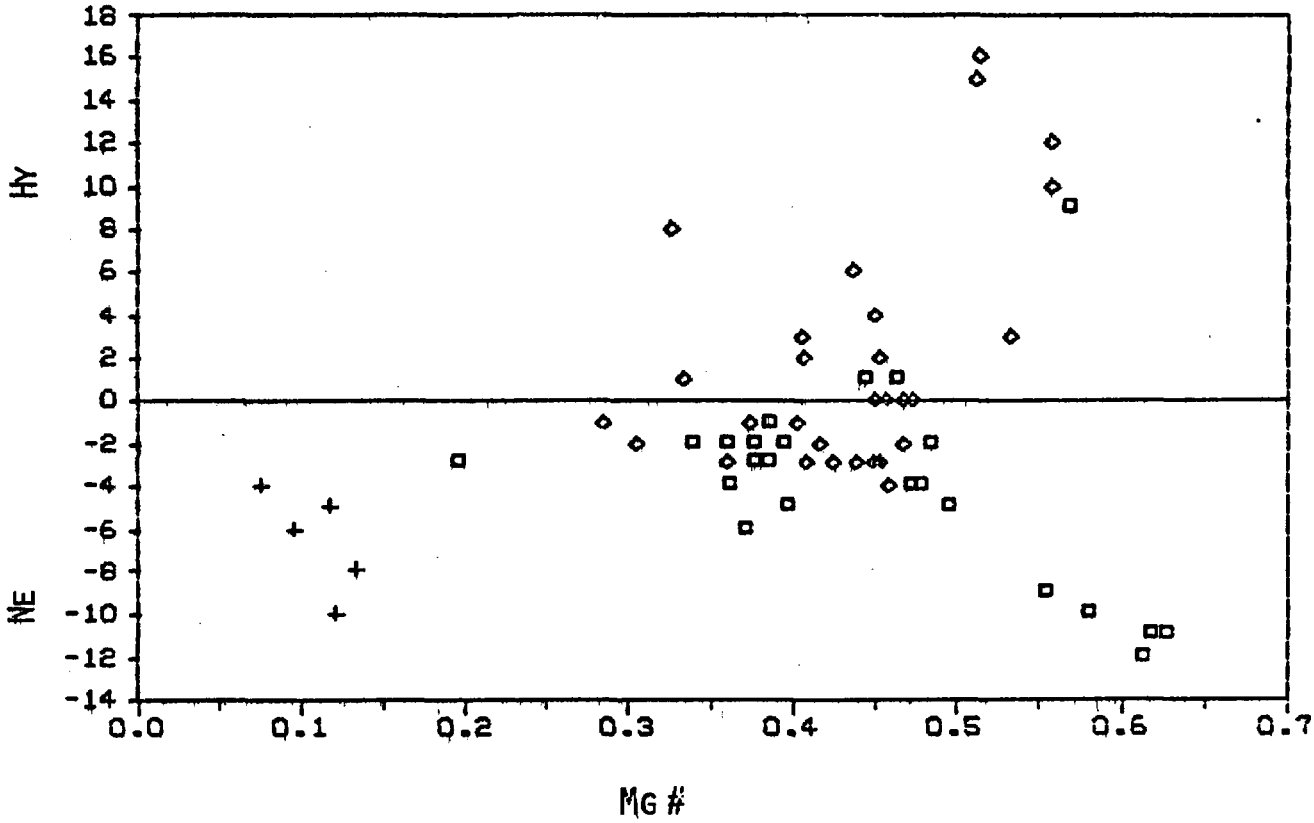

Figure 4, Normative mineralogy vs. Mg# plot for Pliocene volcanic rocks of the Reveille Range. Symbols are defined in the caption to figure 3.

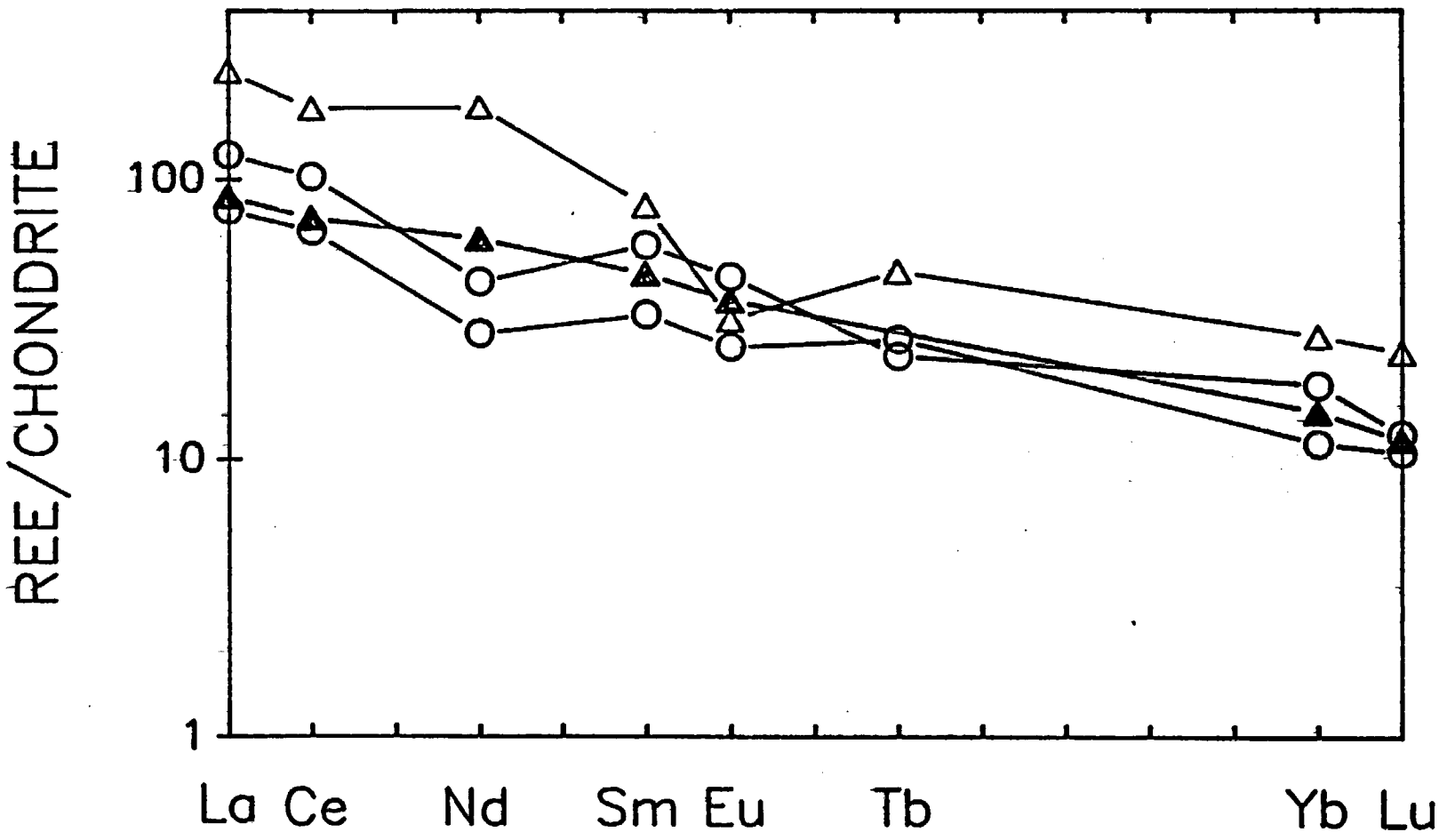

Figure 5. Chondrite normalized rare-earth element plot for Pliocene volcanic rocks in the Reveille Range. Triangles = trachyte, open circles = Episode 1 basalt, filled triangles = Episode 2 basalt.

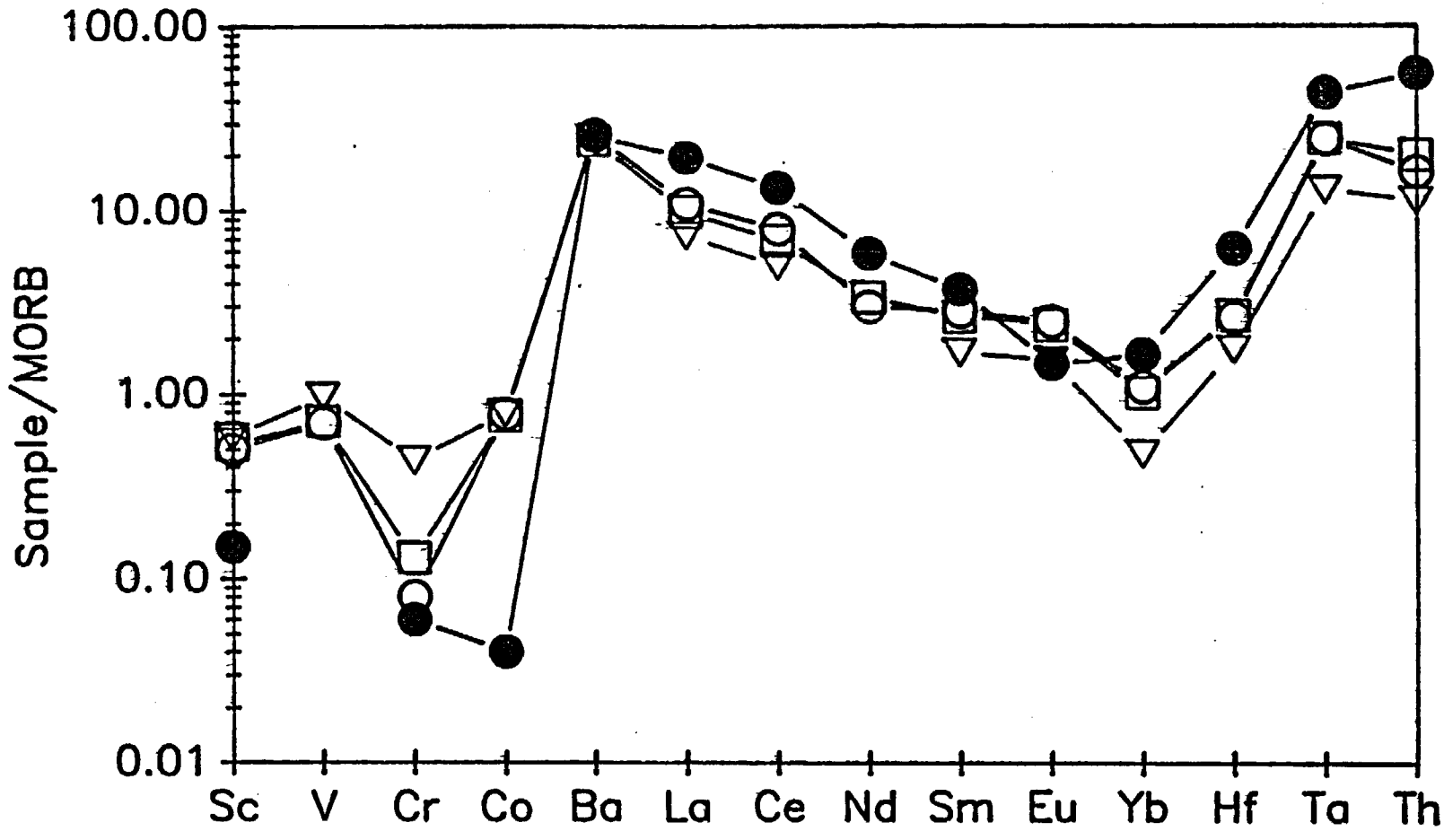

Figure 6. MORB normalized spider diagram for Pliocene volcanic rocks in the Reveille Range. Filled circles and open squares = Episode 2, open circles = Episode 1, upside-down triangles = trachyte.

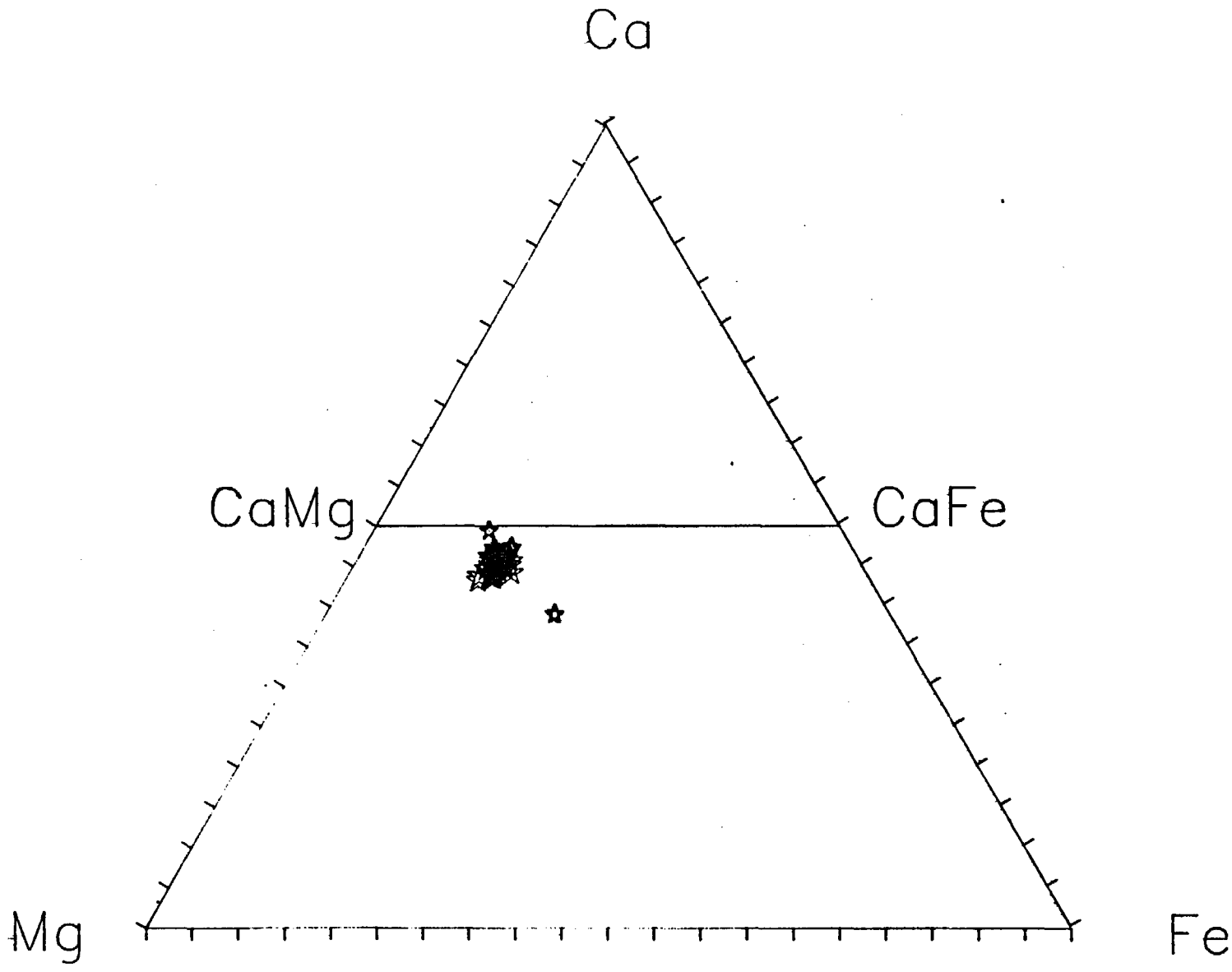

Figure 7a. **Clinopyroxene compositions for Episode 1 basalt 1-17.**

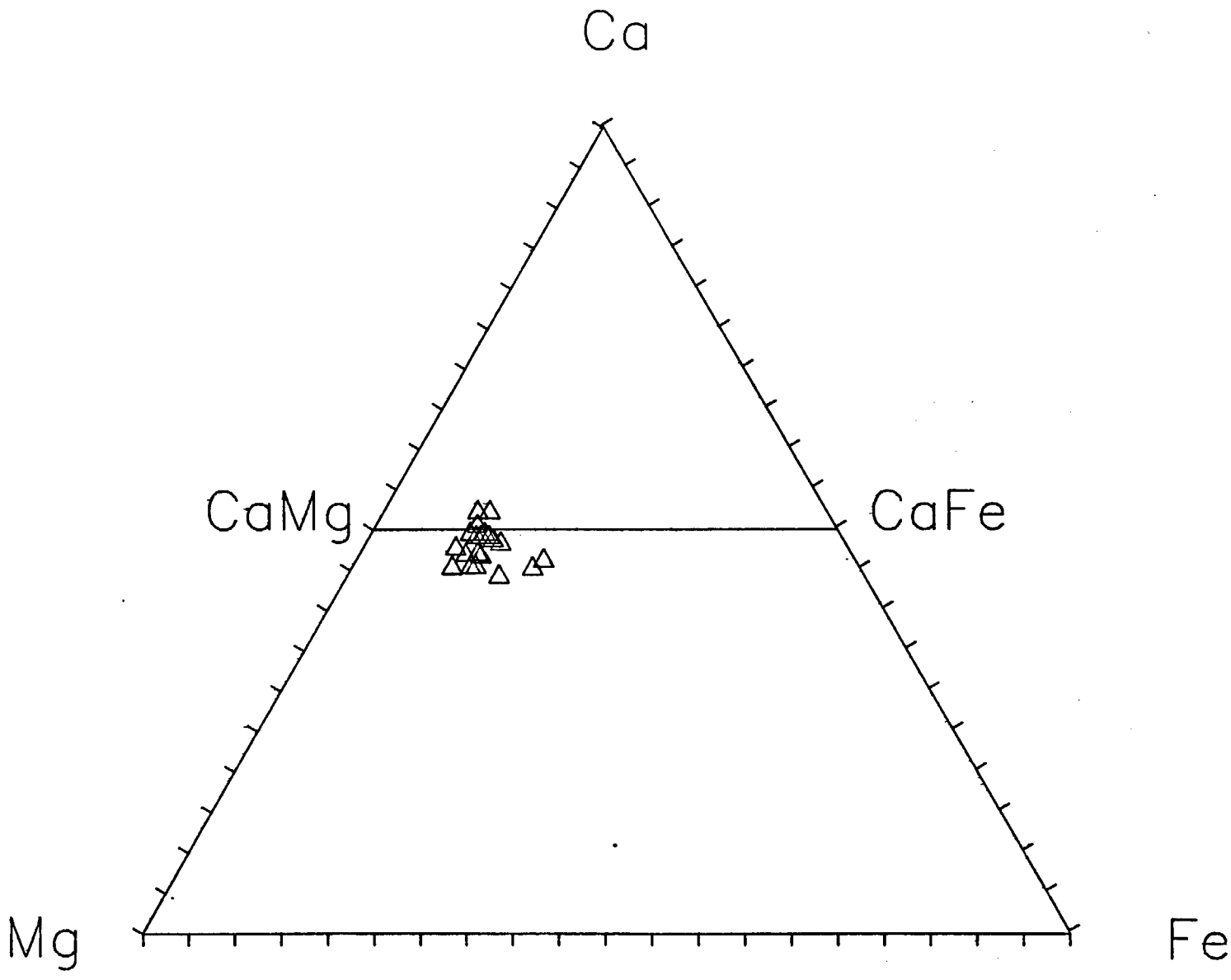

Figure 7b. Clinopyroxene compositions for Episode 2 basalt 2-27.

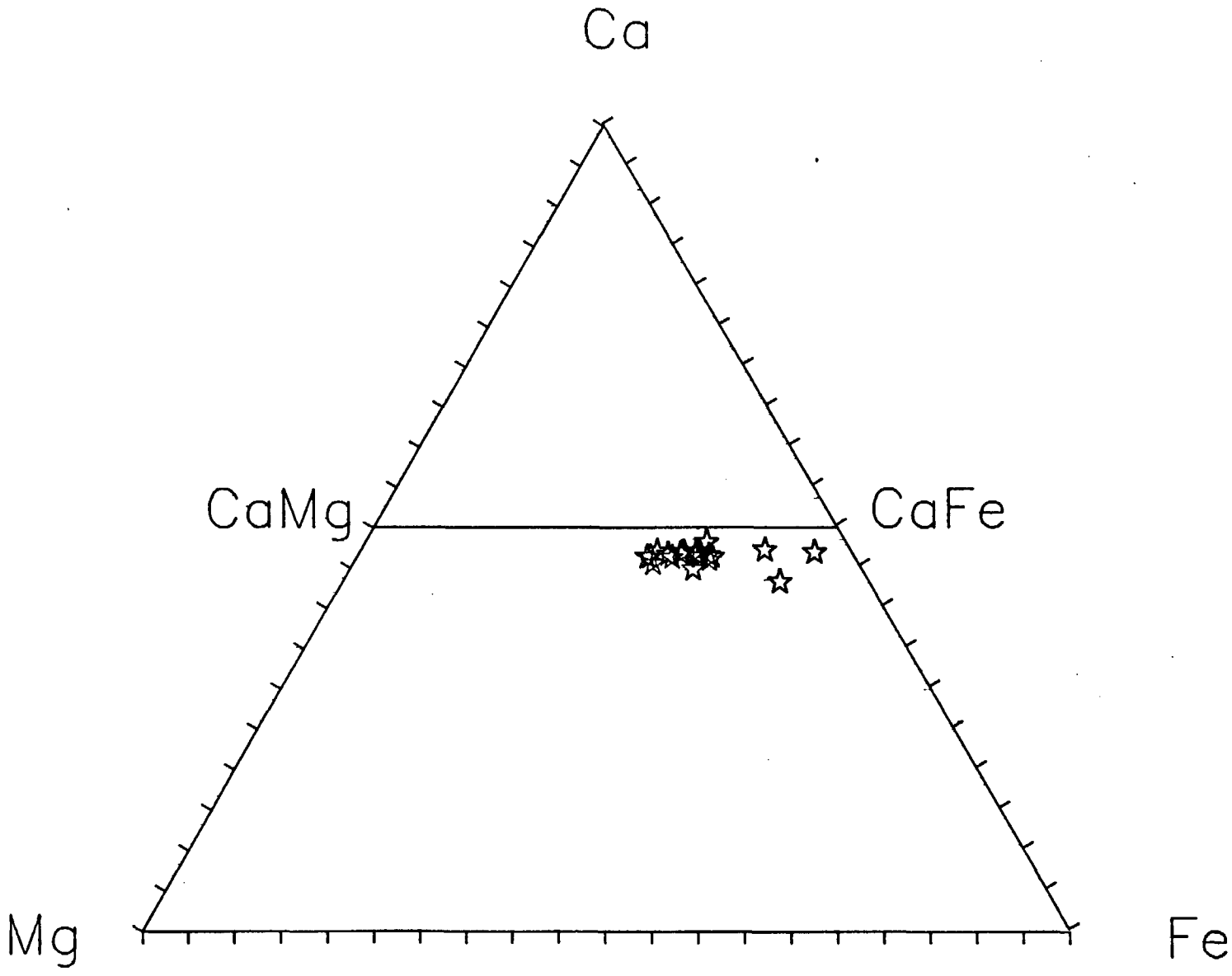

Figure 7c. Clinopyroxene compositions for trachyte 1-41 and 1-42.

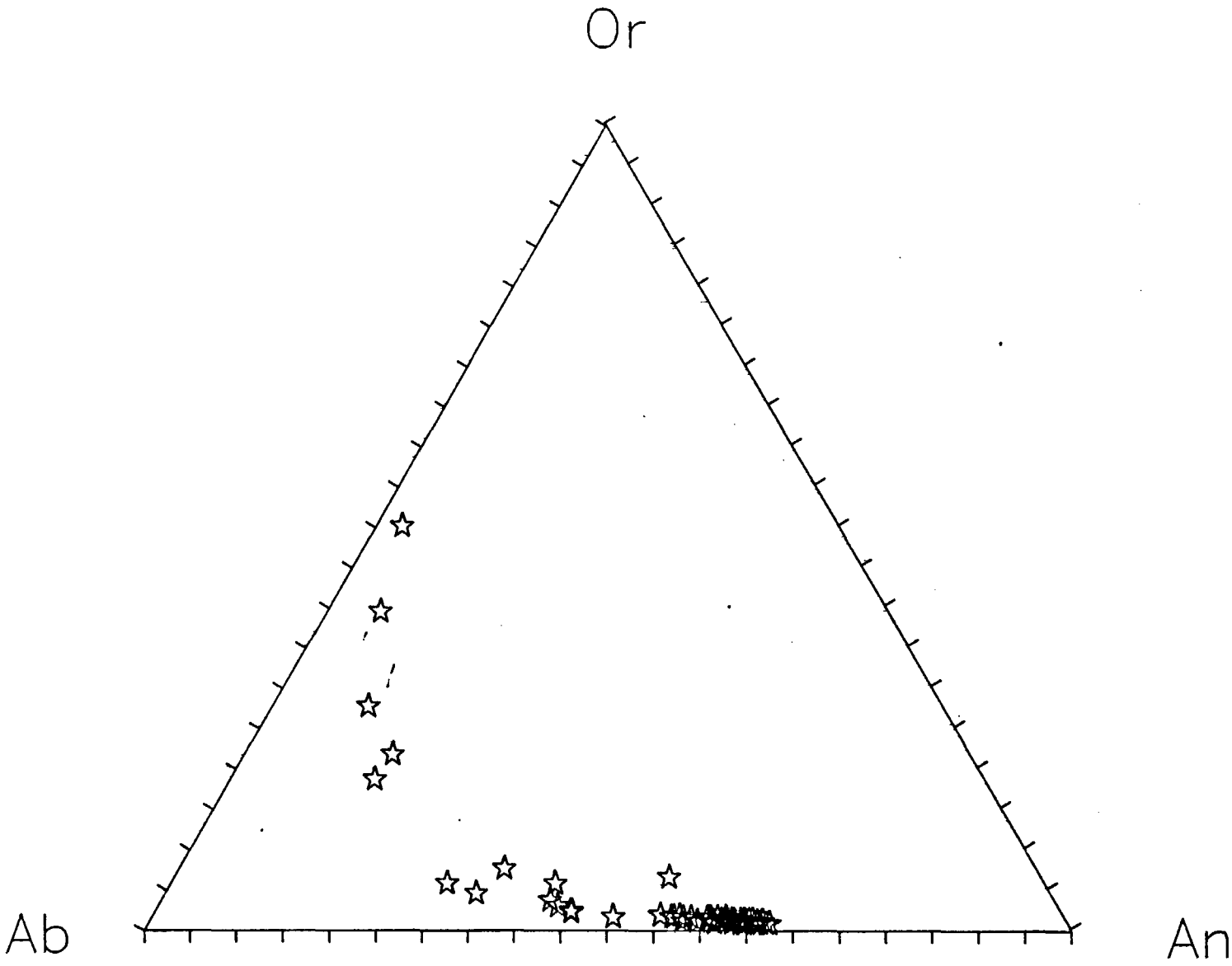

Figure 8a. Feldspar compositions for Episode 1 basalt 1-17.

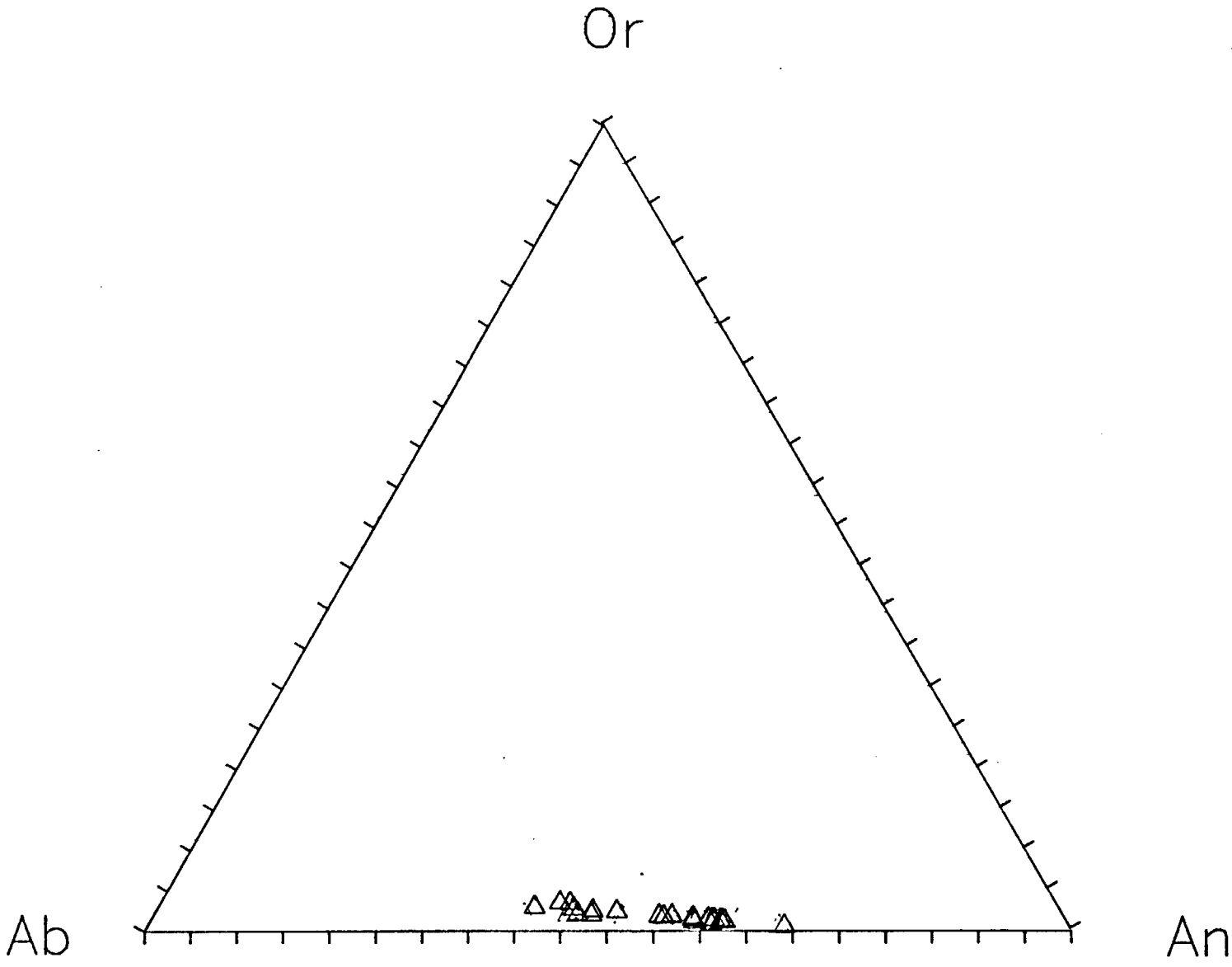

Figure 8b. Feldspar compositions for Episode 2 basalt 2-18.

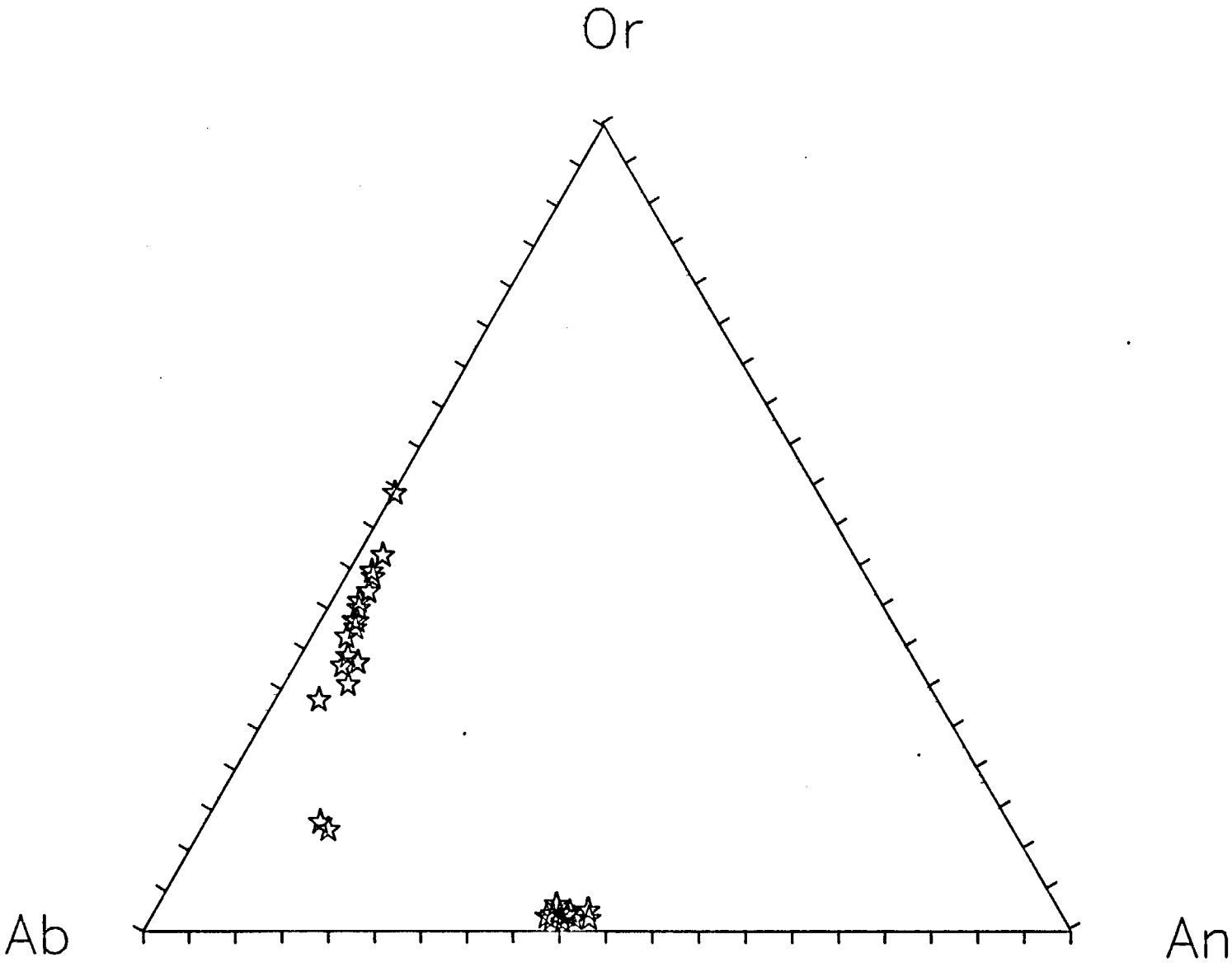

Figure 8c. Feldspar compositions for trachyte 1-41 and 1-42.

feldspars plot within the anorthoclase and sanidine fields. Phenocrysts from Episode 1 are labradorite

Groundmass and phenocrysts of plagioclase in Episode 2 rocks are mostly labradorite with a lesser amount of andesine.

The trachyte dome is compositionally zoned with respect to feldspar. Andesine occurs in the lower section from the pumice cone, and anorthoclase and sanidine occur in the upper part of the section.

GEOCHEMISTRY

Seventy samples were analyzed for major, trace and rare-earth elements. Most are lavas with the exception of one gabbro xenolith. Representative samples were analyzed for Sr, Nd and Pb isotopes.

Analytical methods

Whole rock major element chemistry was determined by Inductively Coupled Plasma (ICP) techniques at Chemex Labs, Inc., Sparks, Nevada. Rare earth elements (REE) and Co, Ta, Hf, Th, V, Sr, Rb, Ba and Sc, were analyzed by Instrumental Neutron Activation Analysis (INAA) at the Phoenix Memorial Laboratory, University of Michigan. The multielement standard BVHO-1 was used as an internal standard.

Chemical Classification

Chemical classification is based on techniques of Irvine and Baragar (1971) and is reviewed in Table 2. All rocks in the northern Reveille Range are alkalic and fall within

either the sodic or potassic series. For this discussion, trachytic rocks of the Hump will be included within Episode 2.

TABLE 2

Chemical Classification of Volcanic Rocks

in the Northern Reveille Range

Episode	# of Samples	Rock Name	Phase
1	26	alkali basalt	dike, flow
1	5	hawaiite	dike, plug
2	5	picrite	plug
2	12	alkali basalt	dike, plug, flow
2	6	hawaiite	flow, plug
2	2	trachybasalt	flow
2	3	tristanite	plug
2	3	trachyte	plug

Reveille Basalts have SiO_2 contents that range from 41 to 56% (Figure 3). Rocks of the first and second episode are both hypersthene and nepheline normative. There is no trend from hypersthene to nepheline normative rocks with time.

Episode 1

These rocks have a narrow chemical range with SiO_2 values ranging from 44 to 48% and except for one hawaiite, all are alkali basalts. Early Episode 1 basalts are higher in Al_2O_3 and CaO, and lower in P_2O_5 while the remaining oxide abundances are similar to the rocks of Episode 2 (Figure 3). Episode 1 basalts are less enriched in the light rare-earth elements (REE) compared to rocks of the Episode 2 (Figure 5). Compared to Mid-ocean ridge basalt

Major element data for Reveille Range

Episode 1

	1-3	1-4	1-7	1-8	1-9	1-10	1-14	1-17	1-24	1-25	1-28	1-29	1-37	1-38	1-39	1-48	1-53	1-56	1-57	1-59	1-60	1-61	1-64	1-66	1-67	1-68	1-69
SiO2	46.58	46.1	46.11	46.02	45.7	46.37	45.81	46.89	47.15	46	46.09	47.47	46.6	47.07	46.92	47.5	46.56	47.36	45.93	45.71	47.36	47.54	48	49.43	47.96	47.87	49.87
Al2O3	16.13	15.68	16.34	15.94	15.16	16.71	16.02	16.54	16.18	16.14	17.37	16.13	17.09	16.3	16.4	16.89	16.46	16.05	16.31	16.21	16.17	15.8	15.96	16.4	15.68	15.09	16
Fe2O3	12.43	13.61	12.44	14.4	15.58	13.72	12.17	13.31	13.52	14.81	12.56	13.23	12.46	13.55	12.92	10.62	11.72	13.52	13.52	14.16	13.25	13.85	13.45	13.42	13.59	15.22	10.3
CaO	8.94	8.92	9.13	8.36	8.14	8.55	8.66	8.86	8.46	8.3	8.2	8.44	8.99	8.21	8.18	9.4	9.19	8.56	8.4	8.94	8.71	8.57	7.94	8.55	7.72	8.95	[illegible]
MgO	5.46	5.67	5.09	4.07	3.4	2.72	4.71	5.63	5.29	5.09	3.74	4.54	5.1	4.55	4.35	6.08	5.25	5.58	5.01	5.05	5.02	5.75	4.58	3.35	5.54	3.66	6.46
Na2O	3.6	3.52	3.43	3.73	3.77	3.84	3.2	3.65	3.67	3.55	4	3.7	3.9	3.77	3.74	3.35	3.42	3.63	3.66	3.89	3.58	3.55	3.73	4.47	3.61	3.61	3.26
K2O	1.36	1.45	1.63	1.81	1.83	1.48	1.11	1.12	1.18	1.05	1.88	1.36	1.24	1.55	1.86	1.1	1.29	1.14	1.06	1.33	1.18	1.33	1.67	2.02	1.59	2.24	1.36
TiO2	2.66	2.83	2.7	3.13	3.58	3.08	2.52	2.91	2.93	3.31	2.75	2.81	2.61	3.08	2.97	2.53	3.12	3.15	3.4	3.51	2.66	2.82	2.97	2.76	2.87	3.17	2.78
MnO	0.18	0.19	0.17	0.19	0.2	0.18	0.15	0.17	0.18	0.19	0.16	0.17	0.17	0.18	0.18	0.14	0.15	0.17	0.19	0.21	0.19	0.2	0.21	0.21	0.19	0.21	0.16
P2O5	0.36	0.38	0.36	0.55	0.61	0.5	0.35	0.44	0.44	0.4	0.74	0.62	0.73	0.61	0.64	0.39	0.48	0.55	0.49	0.76	0.56	0.56	0.68	0.69	0.65	1.09	0.37
LOI	0.55	0.08	1.15	0.88	1.35	2.88	2.41	0.42	0.13	0.61	0.9	1.46	0.65	0.78	1.09	0.84	1.27	0.02	1.12	0.34	0.01	0.52	0.53	0.01	0.01	0.98	-
Total	98.32	98.51	98.62	99.16	99.4	100.1	97.16	99.98	99.18	99.49	100.44	99.98	101.61	99.71	99.31	98.88	98.96	99.81	99.98	99.45	98.59	100.35	99.59	99.59	99.47	100.1	99.77

Episode 2

	1-1	1-2	1-5	1-6	1-11	1-12	1-13	1-15	1-18	1-19	1-22	1-23	1-26	1-27	1-30	1-31	1-32	1-33	1-44	1-46	1-47	1-52	1-54	1-55	1-58
SiO2	45.38	45.28	45.53	44.81	41.79	47.78	45.49	45.68	45.82	45.48	44.3	43.75	44.35	43.91	43.04	46.62	46.11	46.09	46.78	46.31	44.12	44.99	45.38	46.95	45.1
Al2O3	15.72	15.75	15.48	15.28	14.85	15.25	14.99	15.43	15.54	15.46	15.38	14.53	14.66	14.14	16.06	15.14	16.01	16.27	15.5	15.8	16.89	15.11	15.34	17.17	15.29
Fe2O3	15.42	15.42	14.61	15.32	13.15	12.14	14.1	15.8	15.25	14.3	11.99	12.52	12.06	12.13	13.94	16.07	13.99	10.73	15.69	12.83	11.17	12.63	15.35	11.67	15.79
CaO	7.49	7.5	7.54	7.82	9.47	7.08	7.84	7.15	7.55	8.61	9.46	9.8	9.72	10.08	9.15	7.83	9	10.79	7.66	7.36	7.06	9.31	7.92	8.85	7.71
MgO	4.35	4.37	4.37	4.65	8.17	4.87	6.11	4.04	4.53	4.8	8.32	10.14	9.62	10.24	6.06	4.75	5.3	7.07	4.93	6.01	5.12	5.75	5	3.86	4.99
Na2O	3.83	4.09	3.81	3.64	3.21	3.72	3.54	4.07	4.07	3.75	3.42	3.27	3.46	3.27	3.59	3.89	3.44	3.02	3.93	4.12	4.29	3.9	4.01	4.43	3.79
K2O	1.73	1.8	1.8	1.73	1.93	2.16	0.89	1.56	1.41	1.08	1.8	1.56	1.76	1.48	1.44	1.24	0.87	0.01	1.51	1.48	1.63	1.4	1.35	2.63	1.98
TiO2	3.71	3.57	3.37	3.57	4.06	2.5	2.81	3.24	3.47	3.25	2.94	3.11	2.62	2.81	4.29	3.65	3.51	3.99	3.74	3.47	4.02	3.11	4.4	3.57	4.2
MnO	0.21	0.21	0.2	0.2	0.17	0.15	0.16	0.19	0.2	0.18	0.17	0.17	0.17	0.17	0.18	0.19	0.18	0.12	0.21	0.16	0.16	0.16	0.19	0.17	0.21
P2O5	0.62	0.64	0.53	0.53	0.59	0.6	0.44	0.66	0.67	0.47	0.63	0.63	0.62	0.59	1.04	0.8	0.5	0.05	0.56	0.75	0.99	0.61	0.73	0.84	0.6
LOI	0.66	0.3	1.08	0.78	0.01	1.07	0.18	0.01	0.34	1.2	0.79	0.09	0.28	0.41	0.58	0.1	1	0.33	0.3	0.94	3.74	1.43	0.56	1.34	0.9
Total	99.22	99.03	98.31	98.42	97.47	97.07	96.59	97.89	98.9	98.62	99.28	99.62	99.6	99.28	100.25	98.94	99.96	99.29	100.9	99.29	99.6	97.56	100.29	99.58	100.5

Evolved

	1-16	1-40	1-41	1-42	1-43	1-62	1-63	1-65
SiO2	55.77	55.71	59.63	60.14	58.92	59.74	54.76	54.42
Al2O3	16.11	15.93	17.35	17.23	16.94	17.28	16.85	16.52
Fe2O3	9.82	6.86	6.85	7.2	6.74	7.11	8.86	9.12
CaO	3.8	4.6	1.97	2.04	3.62	2.26	8.32	8.23
MgO	1.2	0.47	0.28	0.38	0.52	0.47	4.63	4.81
Na2O	5.53	5.98	6.22	6.58	6.25	6.5	2.72	2.66
K2O	4.28	5.33	5.83	5.68	5.58	5.24	1.76	1.77
TiO2	1.11	0.44	0.45	0.51	0.47	0.51	1.2	1.2
MnO	0.2	0.17	0.16	0.18	0.17	0.18	0.16	0.18
P2O5	0.3	0.17	0.16	0.18	0.11	0.24	0.38	0.39
LOI	0.01	2.57	0.27	1.12	1.64	0.57	0.88	1.45
Total	98.22	98.26	99.4	101.28	101.01	100.15	100.6	100.85

Table 3. Major Element Chemistry for Pliocene Volcanic Rocks of the Reveille Range.

(MORB) (Figure 6), Episode 1 rocks are enriched in Ba, all REE, Hf and Ta and depleted in the transition elements (Sc, V, Cr, Co).

Episode 2

Episode 2 rocks are more chemically diverse than Episode 1 rocks, ranging in SiO_2 from 41 to 56% and include picrite, alkali basalt, hawaiite, trachybasalt, tristanite and trachyte. Episode 2 rocks display higher overall enrichments in the REE (Figure 5). Compared to MORB (Figure 6), Episode 2 rocks are enriched in Ba, the REE, Hf and Ta, and are depleted in the transition elements (Sc, V, Cr, Co).

ISOTOPIC ANALYSIS

Alkali basalts in the Reveille Range show a negative corelation between initial $^{87}Sr/^{86}Sr$ and epsilon Nd that extends from the mantle array to $^{87}Sr/^{86}Sr=0.706$ and epsilon Nd = +1 (Figure 9). Basalts of episode 2 are most primative and lie within the ocean island basalt field (OIB) ($^{87}Sr/^{86}Sr=0.7035$ and epsilon Nd = +3 to +5). Episode 1 basalts have a more radiogenic Sr component ($^{87}Sr/^{86}Sr=0.706$) and are lower in epsilon Nd (+1) than episode 2. Trachyte of the Hump is higher in $^{87}Sr/^{86}Sr$ (0.707) and epsilon Nd (+3) than the associated basalts. All Reveille Range rocks are enriched radiogenically with respect to Pb and cluster about $^{207}Pb/^{206}Pb$ = 15.6, $^{206}Pb/^{204}Pb$ = 19.25 and $^{208}Pb/^{204}Pb$ = 39 (Figures 10 and 11).

The isotopic data has several important implications regarding the formation of Reveille Range basalts. These are:

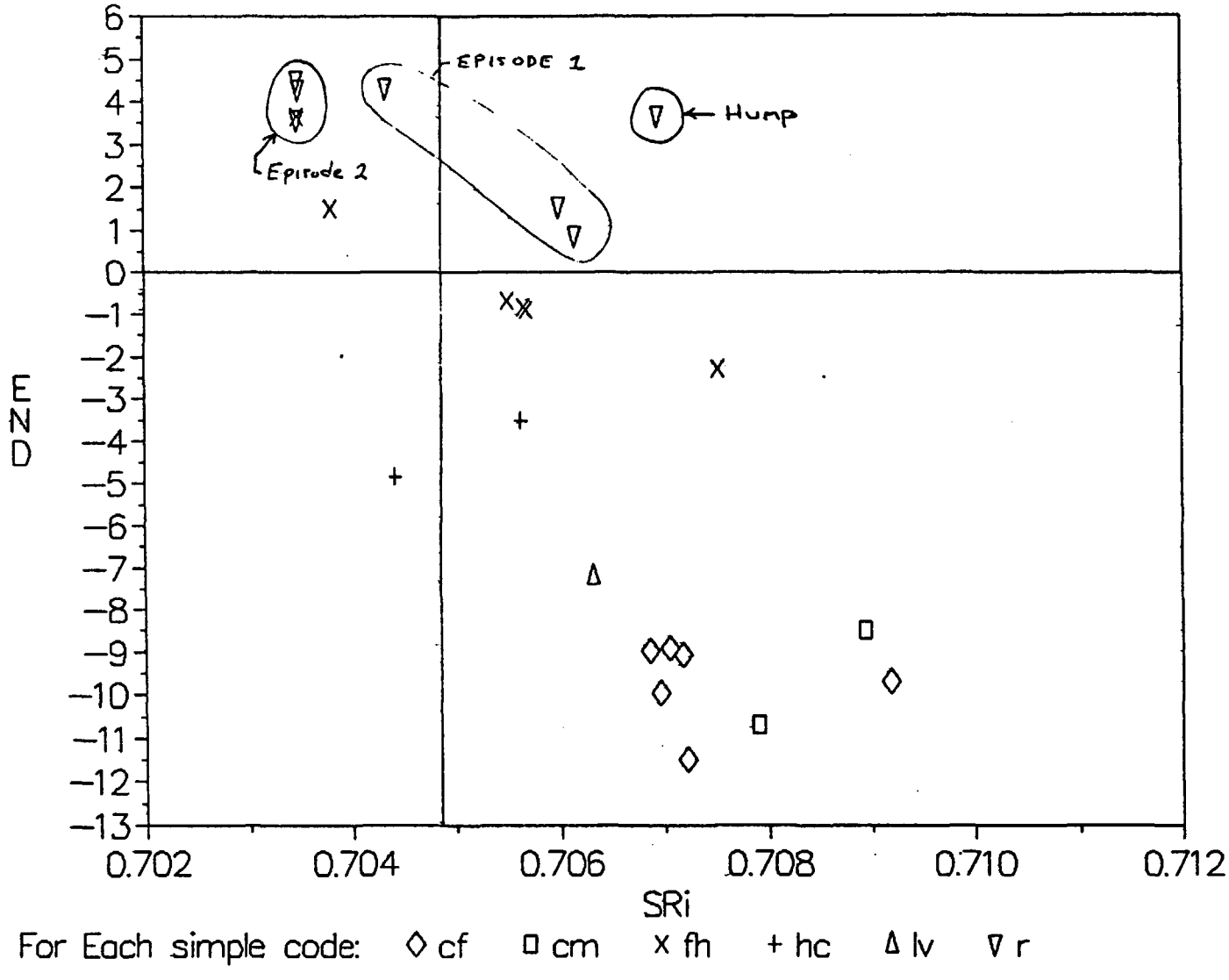

Figure 9. Epsilon Nd-initial $^{87}Sr/^{86}Sr$ plot for basalts in the southern Basin and Range province. Reveille Range basalts and trachytes (circled fields of downward pointing triangles) group into three fields. A low $^{87}Sr/^{86}Sr$ field for episode 1, an intermediate $^{87}Sr/^{86}Sr$ field for episode 2, and a high $^{87}Sr/^{86}Sr$ field for Hump trachyte.

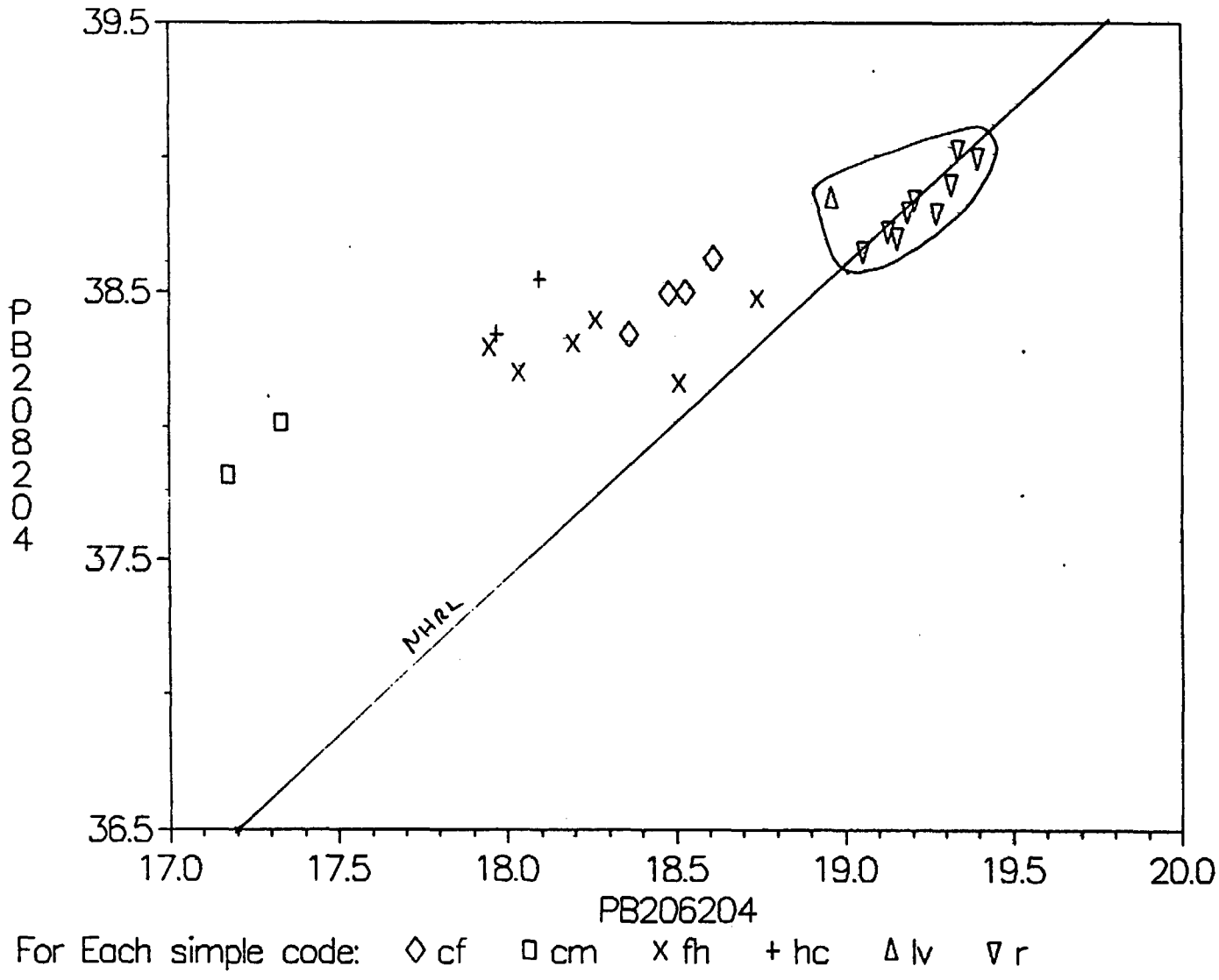

Figure 10. $^{208}Pb/^{204}Pb$ vs. $^{206}Pb/^{204}Pb$ plot for basalts in the southern Basin and Range province. Reveille Range basalts lie on the northern hemisphere reference line (NHRL) and are radiogenic with respect to both $^{208}Pb/^{204}Pb$ and $^{206}Pb/^{204}Pb$.

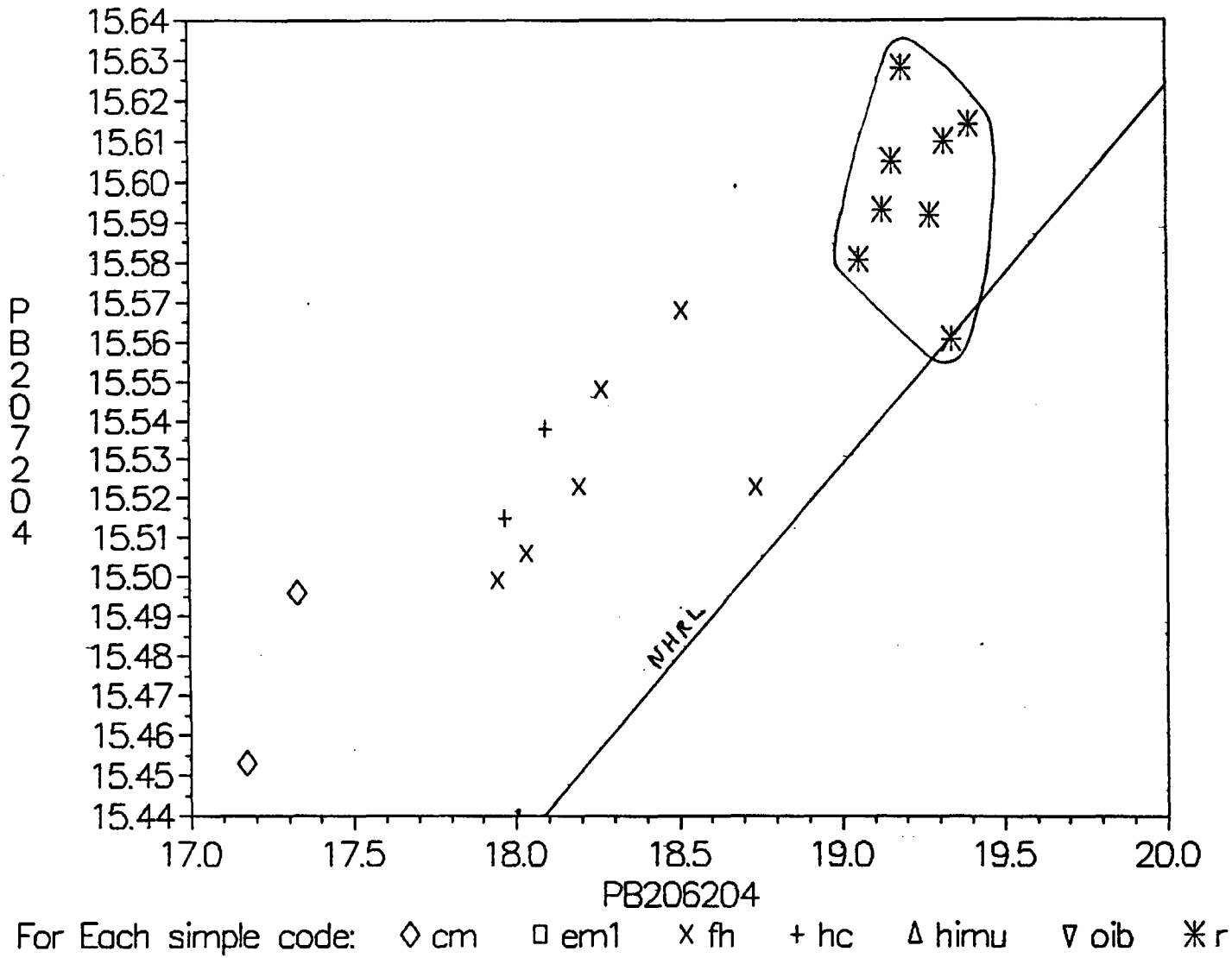

Figure 11. $^{207}Pb/^{204}Pb$ vs. $^{206}Pb/^{204}Pb$ plot for basalts in the southern Basin and Range province. Reveille Range lie on and above the NHRL and are radiogenic with respect to both $^{207}Pb/^{206}Pb$ and $^{206}Pb/^{204}Pb$.

(1) When viewing Pb and Sr systems together all Reveille Range basalts are similiar in composition to the radiogenic HIMU mantle component (Figure 12). This mantle source is characterized by epsilon Nd = +1 to +2, nonradiogenic Sr ($^{87}Sr/^{86}Sr = 0.703$), and enriched Pb values (e.g., $^{206}Pb/^{204}Pb = 19$). HIMU may represent either an isolated mantle reservoir mixed with ancient subducted oceanic crust or metasomatically altered lithospheric mantle (Aibert et al., 1986; Silver et al., 1988; Cooper and Hart, 1990). We suggest that Reveille Range basalts formed by partial melting of such a mantle source.

(2) Episode 1 and 2 magmas may not be cogenetic. Episode 1 may represent magma formed from a more radiogenic HIMU source than episode 2, or magma from a HIMU source contaminated by high U and Rb crust. The latter model is supported by the positive slope of episode 1 basalt on $^{206}Pb/^{204}Pb$ vs. intitial $^{87}Sr/^{86}Sr$, $^{207}Pb/^{206}Pb$ vs. $^{206}Pb/^{204}Pb$, and $^{208}Pb/^{204}Pb$ vs. $^{206}Pb/^{204}Pb$ plots.

(3) Hump trachyte is isotopically distinct from Reveille basalts. Trachyte is enriched in Sr and Pb, but is similar in epsilon Nd ($^{87}Sr/^{86}Sr = 0.707$, $^{206}Pb/^{204}Pb = 19.5$). These observations suggest that (a) Hump trachyte is not related to either episode 1 or 2 basalt by a fractionation process. Fractionation cannot account for the observed differences in Sr and Pb isotopic ratios between trachyte and basalt, since isotopic ratios (initial) are not changed by crystal fractionation. (b) Hump lavas may have formed by crustal contamination of magmas derived from the HIMU source or by independent partial melting and fractionation of a magma produced by melting of a lithospheric source enriched in Sr, Pb but depleted in light rare-earth elements.

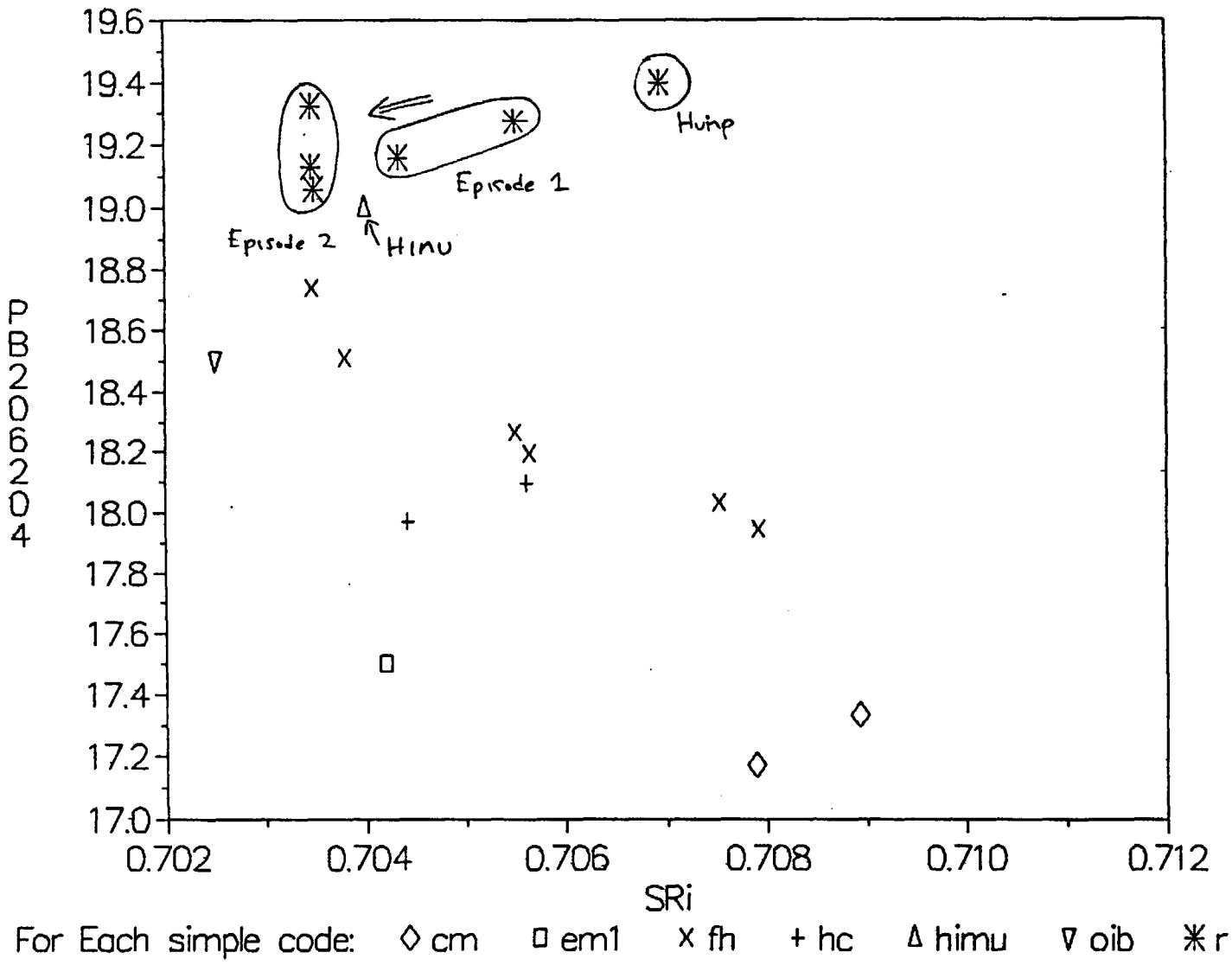

Figure 12. $^{206}Pb/^{204}Pb$ vs. initial $^{87}Sr/^{86}Sr$ plot for basalts in the southern Basin and Range province. Episode 2 basalts are similar in composition to the HIMU mantle component. Episode 1 and Hump lavas represent independent partial melts of the HIMU mantle component mixed with crust. Arrow is a time vector.

REFERENCES

Ekren, E.B., Rogers, C.L. and Dixon, G.L., 1973, Geologic and Bouguer gravity map of the Reveille Quadrangle, Nye County, Nevada: U.S. Geological Survey Miscellaneous Geologic Investigations Map I-806.

THE EASTERN BOUNDARY OF THE EXTENSIONAL ALLOCHTHON IN THE EASTERN BASIN AND RANGE: VOLCANIC AND STRUCTURAL GEOLOGY OF THE NORTHERN WHITE HILLS, ARIZONA.

(CASCADDEN, T. E.)

This summary will be presented as a paper at the Geological Society of America's Cordilleran section meeting in San Francisco (March, 1991).

The northern White Hills lie in the upper plate of the westward-dipping Salt Spring detachment. The upper plate contains 5 east-tilted structural blocks comprised of Miocene basaltic andesite flows (49-54% SiO_2), agglomerates, dacite ash-flow tuffs, megabreccia and fanglomerate. Because each block is isolated and contains only a small part of the stratigraphic section, geochemical data (La, Cr, Hf, Sc, Sr and Co) was used to construct a composite section. The oldest part of the composite section consists of at least 464 meters of basaltic andesite flows and autoclastic breccias. They are overlain by 0-575 meters of coarse monolithologic breccia, in which the dominant clast type is lower plate Precambrian pelite, granite, amphibolite, and mylonite. The breccia forms a discontinuous sheet that extends 12

km west from the detachment in Salt Spring Wash to Squaw Peak and pinches out to the north near Lake Mead. Longwell (1936) described similar deposits in the Virgin Basin (now flooded by Lake Mead). Interbedded with coarse breccia is a dacite ash-flow tuff (94-250 meters thick) that may correlate with a tuff in the northern Black Mountains dated by Faulds (1990) at 16.5 Ma. The upper part of the section consists of 63-627 meters of basaltic andesite, 0-211 meters of poorly consolidated conglomerate, and 50-171 meters of basaltic andesite. Adjacent to the detachment in the eastern White Hills there is a progressive decrease in tilt up section from 30 to 35° near the base to nearly horizontal at the top. Although stratal tilts vary from 10 to 35° in the central and western White Hills, they are uniform within structural blocks.

The Salt Spring detachment may represent a segment of a regional detachment zone that extends from Gold Butte to near Dolan Springs, Arizona (Cyclopic detachment). This fault zone lies 20 km west of the Grand Wash Cliffs and represents both the easternmost boundary of the extensional allochthon and the eastern limit of exposure of Tertiary igneous rocks in the northern Colorado trough. The lack of equivalent igneous rocks in the footwall of the detachment between Salt Spring Wash and the Colorado Plateau may place constraints on either the geometry of the detachment or the pre-extension distribution of volcanic rocks.

APPENDIX I- The Area of Most Recent Volcanism near Yucca Mountain, Nevada: Implications for volcanic risk assessement.

APPENDIX 2- Mid-Miocene volcanic and plutonic rocks in the Lake Mead area of Nevada and Arizona; production of intermediate igneous rocks in an extensional environment.

HIGH LEVEL RADIOACTIVE WASTE MANAGEMENT

VOLUME 1

Proceedings of the International Topical Meeting

Sponsored by the

American Society of Civil Engineers and the
American Nuclear Society

Co-sponsored by the

American Chemical Society
American Geophysical Union
American Institute of Chemical Engineers
American Medical Association
American Society for Quality Control
American Society for Testing and Materials
American Society of Mechanical Engineers
Geological Society of America
Health Physics Society
Institute of Nuclear Materials Management
Society of Mining Engineers

in cooperation with:

U.S. Department of Energy
U.S. Nuclear Regulatory Commission
Edison Electric Institute
Electric Power Research Institute
State of Nevada
National Conference of State Legislatures
Center for Nuclear Waste Regulatory Analysis
University of Nevada Medical School

Hosted by the

University of Nevada, Las Vegas
Howard R. Hughes College of Engineering

Las Vegas, Nevada
April 8-12, 1990

Published by the
American Nuclear Society, Inc.
La Grange Park, Illinois 60525, USA
American Society of Civil Engineers
New York, New York 10017, USA

THE AREA OF MOST RECENT VOLCANISM NEAR YUCCA MOUNTAIN, NEVADA: IMPLICATIONS FOR VOLCANIC RISK ASSESSMENT

Eugene I. Smith, Daniel L. Feuerbach, Terry R. Naumann and James E. Faulds

Center for Volcanic and Tectonic Studies
Department of Geoscience
University of Nevada, Las Vegas
Las Vegas, Nevada 89154
(702) 739-3262

ABSTRACT

The proposed area of most recent volcanism (AMRV) includes all known post-6 Ma volcanic complexes in the Yucca Mountain area and encompasses the four volcanic centers in Crater Flat, the Lathrop Wells cone, several centers in southeast Crater Flat, two centers at Sleeping Butte, and a center at Buckboard Mesa within the moat of the Timber Mountain Caldera. The delineation of high-risk zones for volcanism within the AMRV is an important goal in any risk assessment study. The dimensions and orientation of high-risk zones were based on structural and volcanic chain length data obtained by detailed studies of Plio-Pleistocene volcanic centers in the Yucca Mountain area. Analog studies of Pliocene volcanic centers in the Fortification Hill field (Lake Mead area, Arizona and Nevada) and the Reveille Range (south-central Nevada) were also used to establish the nature of structural control of volcanic vents and to determine the lengths of volcanic chains. Two high-risk rectangles were constructed at each cluster of Quaternary centers. The smaller-dimension rectangle is 12 km long and 1 km wide and is equivalent to the dimensions of the Crater Flat chain. The larger-dimension rectangle is 25 km long and 3 km wide and is equivalent to the dimensions of volcanic chains in the Fortification Hill field and the Reveille Range. Based on geologic studies and the high-risk rectangles, five risk levels were defined with risk level 5 representing the highest relative risk and 1 the lowest. Based on this risk scale, the site of the proposed high-level nuclear waste repository is assigned to risk-category 3.

INTRODUCTION

Volcanic activity has been recognized as a potential hazard for the proposed nuclear waste repository at Yucca Mountain, Nevada.[1] The complex process of evaluating the risk of volcanism is divided into four steps:

(1) understanding Plio-Pleistocene and Quaternary volcanism in the Yucca Mountain area within the context of regional Basin-and-Range volcanism.
(2) defining the area of most recent volcanism (AMRV) in the vicinity of Yucca Mountain. Within the AMRV, the parameters required for hazard studies and volcanic probability calculations such as cone counts, volume-time relationships and the definition of structures controlling volcanism will be determined.
(3) identifying potentially high-risk zones for volcanic activity within the AMRV.
(4) calculation of the probability of eruption within the AMRV and high-risk zones.

Studies of volcanism during the past four years by geologists of the Center for Volcanic and Tectonic Studies (CVTS) have concentrated on developing a regional perspective of volcanism and on providing a detailed understanding of Plio-Pleistocene volcanoes in the immediate vicinity of Yucca Mountain.[2,3,4,5,6,7] Important advances from these studies include the recognition of the recurrence of basaltic volcanism at individual Pliocene vent complexes over periods of up to 400,000 years, refinements in the chronology within volcanic fields and individual volcanic centers, attaining a better understanding of the structural control of volcanism, the recognition of Pliocene intermediate volcanism in the southern Basin-and-Range, and the development of petrogenetic models for basalts and intermediate rocks. This paper will define a geologically reasonable area of most recent volcanism in the Yucca Mountain region and identify potential high-risk zones within this AMRV. Future papers will provide detailed descriptions of individual centers (including geochemistry and geochronology), discuss probability calculations, and describe silicic and intermediate volcanism.

SPATIAL AND TEMPORAL PATTERNS OF POST-6 MA VOLCANISM

In the immediate vicinity of Yucca Mountain,

young basaltic volcanism (3.84 Ma to less than 10,000 years) occurred mainly to the south and west of a series of older basaltic centers (6.5 to 12 Ma).[8,9,10] This observation led Crowe and Perry[10] to suggest a southwest migration of basaltic volcanism in the Yucca Mountain area, a pattern that may reflect an earlier southwest migration of silicic volcanism in the Great Basin. Although, southwest migration of volcanism in the Great Basin between 43 and about 6 Ma is well documented in the literature[11], migration patterns of post-6 Ma basaltic volcanism are not as clear. Figure 1 is derived from a regional survey of post-6 Ma volcanism based on original field studies and a literature search.[9,12,13,14,15,16,17,18,19,20,21] The locations of post-6 Ma basaltic centers in the southern Great Basin and adjacent areas are plotted in three age groups (6 to 4 Ma, 4 to 2 Ma, and less than 2 Ma) (Figure 1 A,B,C). Our regional survey reveals several notable features:

(1) Basaltic volcanism in the Yucca Mountain area is not an isolated phenomenon. It is only a small part of a post-6 Ma volcanic episode that produced a large number of basaltic centers in the southern Great Basin and adjacent areas.

(2) There is no regional-scale migration of post-6 Ma volcanism. Local migration patterns appear to lack regional significance. For example, volcanism in the Yucca Mountain area stepped to the southwest between 6.5 and 3.7 Ma, but during the same time

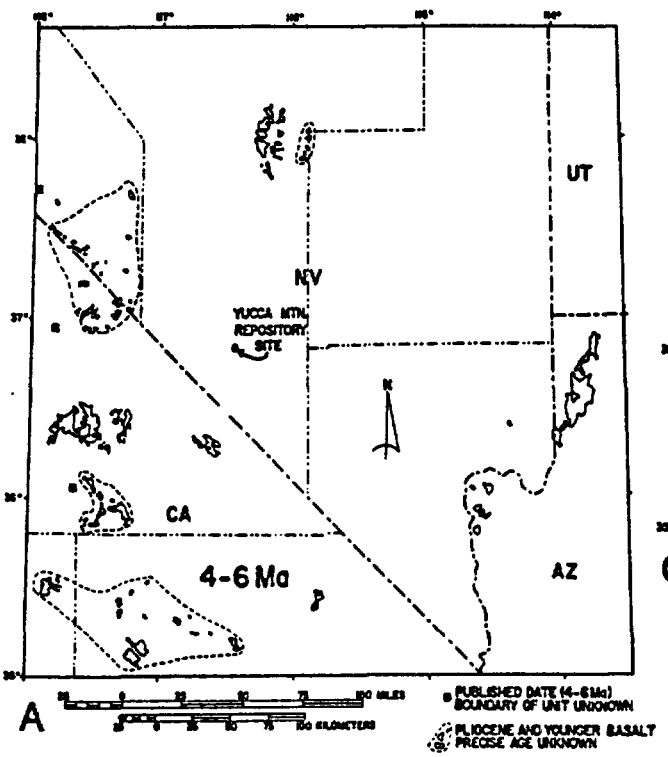

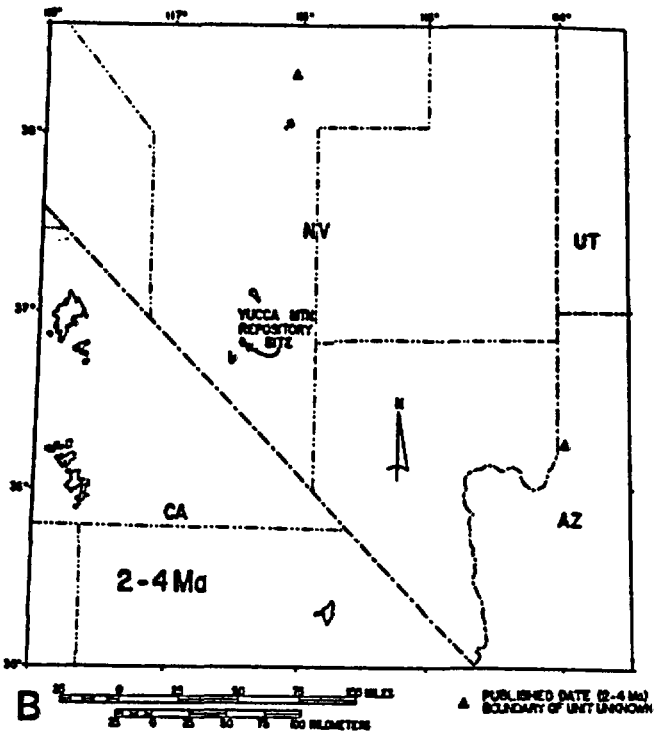

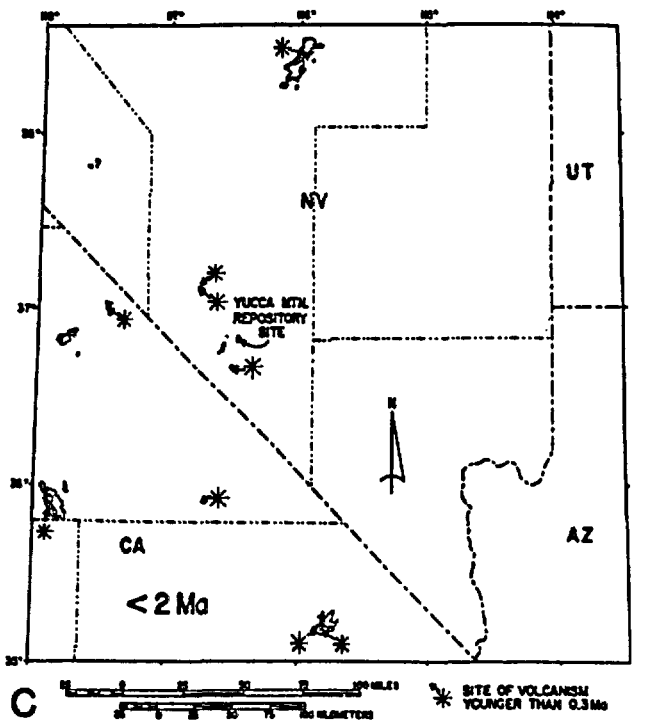

Figure 1. Distribution of Plio-Pleistocene and Quaternary mafic volcanic rocks in the southern Basin-and-Range, Nevada, California and Arizona. Age range is 4 to 6 Ma (A), 2 to 4 Ma (B) and 10,000 years to 2 Ma (C). In A, areas outlined by dashed line are from Luedke and Smith[13] and may contain younger mafic rocks. References for this compilation are in the text.

period volcanism migrated to the east and then to the north in the Reveille and Pancake ranges.

(3) Basaltic centers commonly occur along range margins on the footwalls of range-bounding faults. Flows from these centers commonly cascaded over range margin structures (e.g., in the eastern Reveille Range and the Fortification Hill field). Anderson[22] reported a similar relationship between faults and cinder cones in southwestern Utah. Centers also occur in range interiors, within pre-existing volcanic centers (e.g., the Buckboard Mesa center within the moat of the Timber Mountain caldera), or within basins.

(4) North-northeast, north-northwest or north-striking high-angle normal faults commonly control the location of the volcanic centers. The northeast trend of volcanic centers in the Yucca Mountain area reflects this regional trend. In some cases (e.g., Yucca Mountain), these high-angle faults may not be major structures, as evidenced by moderate to minor amounts of displacement along them. These high-angle faults may bound blocks in the upper plates of regional detachment faults[23] and/or may be associated with pull-apart structures along a strike-slip fault system.[24]

THE AREA OF MOST RECENT VOLCANISM (AMRV)

Selection and Definition of the AMRV

Careful definition of the AMRV is of the utmost importance because it is within this zone that the parameters required for volcanic probability calculations such as volume-time relationships, cone counts, and the definition of structures controlling volcanism will be determined. The first step in selecting volcanic centers for inclusion in the AMRV was to develop a set of selection criteria including age, composition and tectonic setting. Of these criteria, age was the primary factor used to select volcanic centers for inclusion in the AMRV. Tectonic setting was eliminated as a selection criterion, because magma from a mantle source may utilize a variety of existing structures including faults, joints, volcanic vent zones, and/or caldera ring fractures to rise to the surface. Although magma composition is important in evaluating the nature of a volcanic event, composition was eliminated as a criterion, because volcanic risk assessment requires the knowledge of the number of events that occurred over a certain time period regardless of composition. Therefore, the proposed AMRV includes all known post-6 Ma volcanic complexes in the Yucca Mountain area and encompasses the four volcanic centers in Crater Flat, the Lathrop Wells cone, several centers in southeast Crater Flat, two centers at Sleeping Butte, and a center at Buckboard Mesa within the moat of the Timber Mountain Caldera (Figure 2).

Crowe and Perry[10] recently defined the zone of youngest basaltic activity about Yucca Mountain as a narrow northwest trending zone (the Crater Flat Volcanic Zone), extending from several possible buried centers in the Amargosa Valley (aeromagnetic anomalies) through Crater Flat to the Sleeping Butte cones. The AMRV differs from the Crater Flat Volcanic Zone by including the Buckboard Mesa center. Also, because of the uncertain nature and age of the aeromagnetic anomalies in the Amargosa Valley, they were not included in the AMRV.

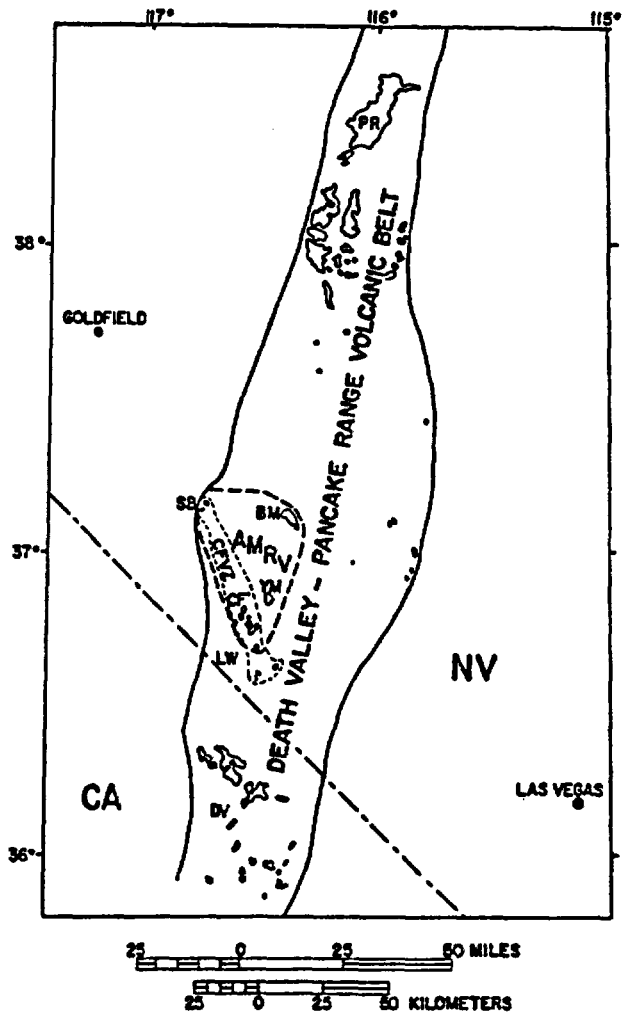

Figure 2. The proposed area of most recent volcanism (AMRV) is outlined by a heavy dashed line and includes the Lathrop Wells cone (LW), Sleeping Butte cones (SB), Buckboard Mesa center (BM) and volcanic centers within Crater Flat (CF). For comparison the Crater Flat Volcanic Zone[10] (dashed line) and the Death Valley-Pancake Range Volcanic Belt[5] (solid line) are shown. PR=Pancake Range. YM=proposed drift perimeter at Yucca Mountain. DV=Death Valley.

Age of Volcanism within the AMRV

Volcanism occurred sporadically in the proposed AMRV over the last 3.84 Ma. The oldest Pliocene volcanism is in southeast Crater Flat (3.84 and 2.53 Ma) and at Buckboard Mesa (2.8 Ma).[7,16] The four volcanoes in central Crater Flat range in age from 1.09 Ma (Black Cone) to 0.785 Ma (Little Cone).[7] Quaternary cones are also located at the Sleeping Butte (0.28 Ma) and Lathrop Wells centers (between 0.3 and 0.01 Ma).[9,16,25] There are no consistent migration trends of volcanism in the AMRV; an observation in agreement with the lack of preferred regional migration patterns for post-6 Ma volcanism.

Structural Control of Volcanism within the AMRV

For this discussion, we concentrate on the group of four cinder cone complexes in the central part of Crater Flat. The cones form a 12-km-long arcuate chain.[8] Details of vent alignment are best observed on Black and Red Cone in the central part of the chain. In the Black Cone complex, the cinder cone is the most prominent topographic feature (about 100 m high and 500 m in diameter), but it may only account for a small volume of flows. A larger volume of basalt erupted from at least 10 vents located north, south and east of Black Cone. These vents are commonly represented by scoria mounds composed of cinder, ash, and large bombs. Vents are aligned along two sub-parallel zones that strike approximately N35E. One zone includes Black Cone and 4 scoria mounds; the other zone lies 300 m to the southeast of Black Cone and contains at least 7 mounds. Dikes exposed in eroded mounds strike northeast and parallel the trend of the vent zones. The Red Cone complex contains three vent zones: two trend approximately N45E and a third zone strikes N50W (Figure 3). As at Black Cone, dike orientation parallels the trend of vent zones. Vent alignments in Crater Flat show a 15 degree clockwise change in orientation from Black Cone in the north to Little Cones in the south. Vent zones within each cone complex project directly toward the adjacent cone complex (Figure 4).

Because the faults that strike into Crater Flat either bound Yucca Mountain on the west or parallel those that fragment Yucca Mountain, we infer that the 12-km-long arc of volcanic centers in Crater Flat was controlled by north-northeast- to northeast-striking faults that are part of the same fault set that disrupts Yucca Mountain.[26,27,28,29] However, vents zones in Crater Flat trend more to the northeast (N35 to N50E) than do faults on the west side of Yucca Mountain (N10 to N20E). Vent zones in Crater Flat may correspond to either high-angle faults that previously underwent significant clockwise rotation or unrotated faults. Structural rotation is suggested by paleomagnetic studies by Rosenbaum and Hudson[23]

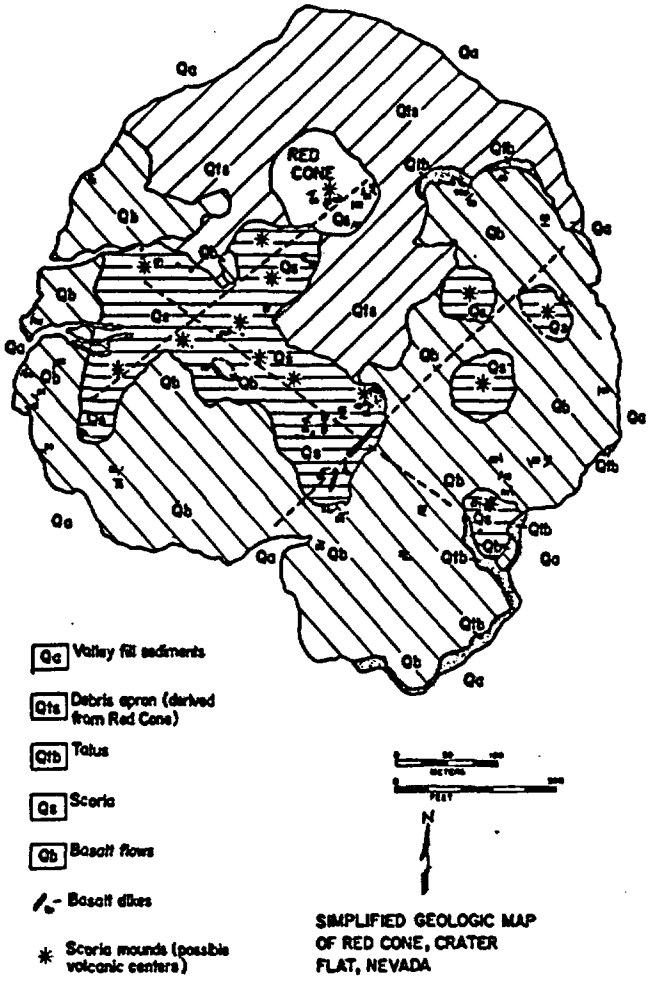

Figure 3. Preliminary geologic map of Red Cone, Crater Flat. Refer to Figure 4 for location of Red Cone.

that demonstrate up to 30 degrees clockwise rotation of the southern part of Yucca Mountain relative to the northern part. Thus, the alignment of vents in Crater Flat, especially the southward progression toward more northeasterly-trending vent zones, may imply that faults controlling vent locations experienced a similar sense and magnitude of rotation to that of Yucca Mountain. Alternatively, several essentially unrotated north- to north-northeast-striking normal faults may have controlled the location of individual cone complexes within Crater Flat, as evidenced by the lack of a significant northeast bend in the strike of major normal faults on Yucca Mountain. The northeast trend of vents within volcanic complexes in Crater Flat may instead reflect the orientation of unrotated faults and/or joints.

The Lathrop Wells cone probably emerged along a splay of the north-northeast-striking Solitario Canyon fault of Scott and Bonk[28]; a major high-angle normal fault that bounds much of Yucca Mountain on the west.

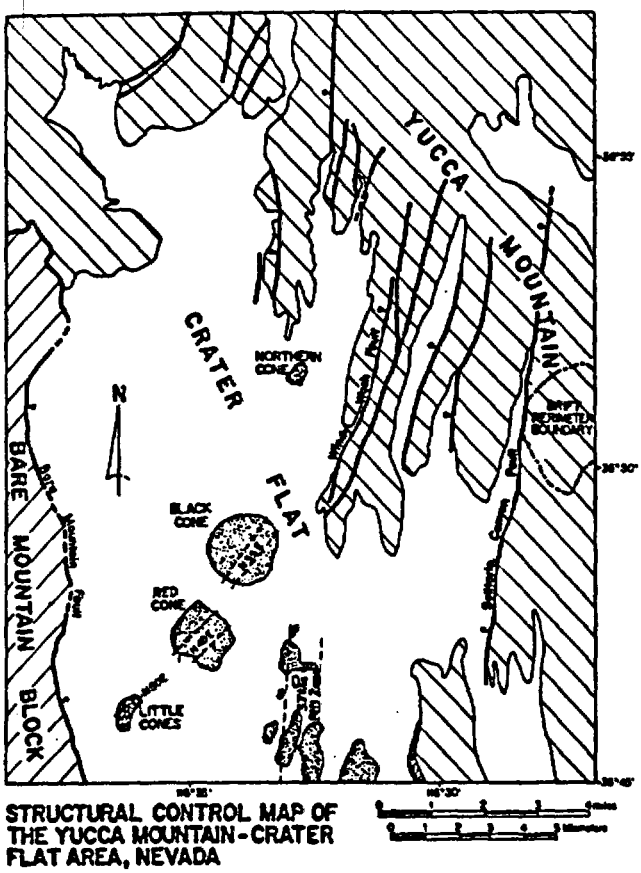

Figure 4. Major volcanic complexes in Crater Flat are depicted by stippled pattern. Map also shows major vent zones and bedrock faults (bar and ball on hanging wall of faults). Southeast sloping diagonal lines = Tertiary volcanic basement. Southwest sloping diagonal lines = Paleozoic basement.

ANALOG STUDIES

Geological analog studies allow inferences to be made about a particular feature (e.g., land form, deposit, structure, volcanic field) by comparison with similar features of known origin. For example, the deposits observed to erupt from a volcano may be used to interpret similar deposits in the geologic record. Volcanic analog studies are helpful in modelling vent geometry, establishing the nature of structural control, determining the lengths of volcanic chains, and establishing the relationship between chemical change and time. A degree of uncertainty is inherent in selecting analogs. This uncertainly can be reduced by developing a set of selection criteria and only choosing features as analogs that meet most or all of the criteria. The following selection criteria were established for analogs of AMRV volcanoes. Analogs should be (1) Plio-Pleistocene or Quaternary in age, (2) in the tectonic setting of the Basin and Range, (3) deeply eroded so that vents are exposed, (4) extinct, and (5) similar in volume to individual centers and also to the entire field. The Fortification Hill field, in the Lake Mead area of Arizona and Nevada, and basaltic volcanoes in the eastern Reveille Range in south-central Nevada satisfy criteria 1 to 4. However, individual eruptions in these fields, with the exception of the youngest eruptions in the Fortification Hill field, have greater volumes (0.03 to 0.6 km^3) than those in the Yucca Mountain area (<0.1 km^3). Therefore, criterion 5 is not satisfied. Nevertheless, we accept these volcanic fields as analogs. The justification for this decision is based on the apparent similarities of vent dimensions and geometry between individual volcanoes in higher volume fields and those in lower volume fields (see discussion below). In the section below, we briefly describe each volcanic field, the timing of eruptions, vent geometry and chain lengths.

Fortification Hill Volcanic Field

The Fortification Hill volcanic field is composed of flows of alkalic basalt that erupted between 5.89 and 4.7 Ma mainly at Fortification Hill, Lava Cascade, Petroglyph Wash and Malpais Flattop (Figure 5).[7] Activity in the field ended with the formation of low-volume alkali basalt centers in northwest Arizona along U.S. 93 and in Petroglyph Wash, and near Boulder Beach, Nevada.[30,31,32,33] The total volume of the field is approximately 3 km^3. Nearly 400 m of erosion by the Colorado River provides an excellent view into the vent systems of Pliocene volcanic complexes.

Fortification Hill basalt crops out south of the Lake Mead fault zone in a north-northwest-trending belt that extends from Malpais Flattop to Fortification Hill, Arizona. Vents occur in three groups (Fortification Hill-Lava Cascade, Petroglyph Wash, and Malpais Flattop), all of which are closely associated with major high-angle faults (Figure 5). Activity was focused at just a few centers along or near these faults.

The Fortification Hill-Lava Cascade group forms a chain of at least 6 vents with a length of 25 km. The chain appears to be controlled by north-northwest-striking faults that bound the west side of the Black Mountains. Vents occur both on the margin and in the interior of the range. At the Lava Cascade, the southernmost volcano of the chain, approximately 0.03 km^3 of lava erupted from a cinder cone near the summit of the Black Mountains in an area nearly devoid of any major faults. Major north-northwest-trending high-angle faults cut the range just to the west of the vent center.[34] Dikes related to the Lava Cascade cut both scoria and Precambrian basement. One dike extends nearly 300 m to the south of the vent complex, two dikes extend 150 m to the north. Dikes vary in width from 5 cm to 1 m, dip steeply, cut foliation in the Precambrian basement rock, and trend north-northwest subparallel to nearby Tertiary high-angle faults (Figure 5). Fortification Hill, the northernmost volcano of the chain, is a steep sided mesa just to the east of Lake Mead. The escarpment that forms the cap of Fortification Hill is composed of over 100 flows (about 0.6 km^3) of olivine basalt and

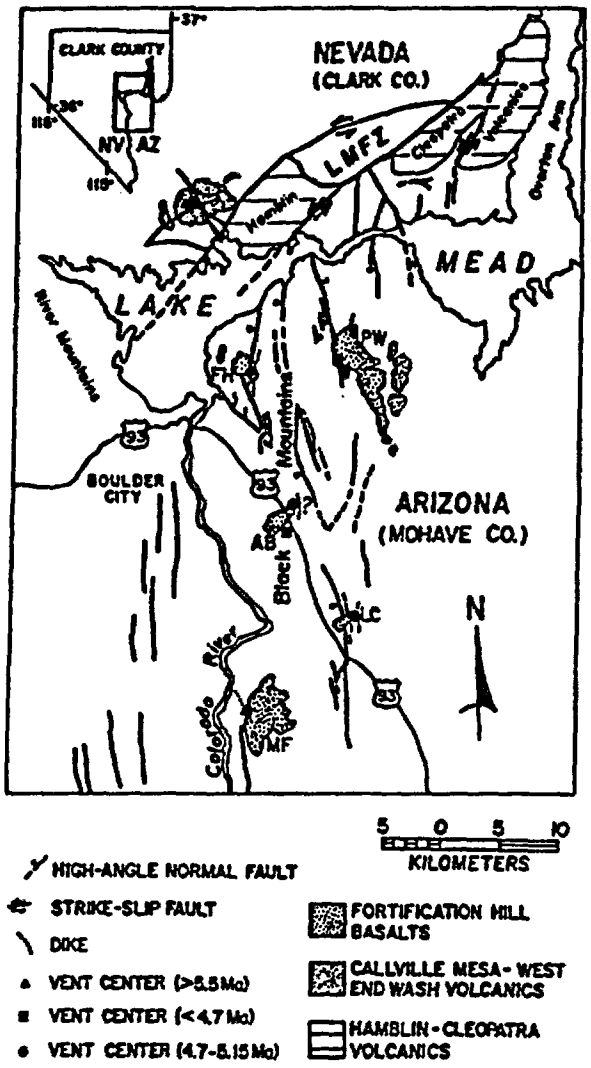

Figure 5. Generalized geologic map of the Fortification Hill volcanic field, Arizona. MF=Malpais Flattop. FH=Fortification Hill. PW=Petroglyph Wash. LC=Lava Cascade. AB=alkali basalt centers. LMFZ=Lake Mead Fault Zone.

scoria.[35] A north-south-trending set of complex cinder cones, which are intruded by dikes and plugs, served as the source for the flows. The Fortification Hill cinder cone complex represents a node of intense volcanic activity along a north-northwest trending en echelon dike system. Dike orientation is coplanar with the mid-Miocene Fortification fault zone which projects beneath Fortification Hill.[35] South of Fortification Hill, dikes extend nearly 6 km as en echelon segments 1 to 2 m wide and 0.5 to 3 km long. The vertical dikes crop out within 100 m of the fault, but rarely occur within the fault zone. Apparently, basalt vented from this dike system only at the Fortification Hill node, and eruptions continued sporatically at this location for at least 10^5 years. The intrusive plugs within the Fortification Hill vent area are elongated parallel to dikes and regional faults. The Fortification Hill-Lava Cascade zone also contains a 4.7 Ma alkali basalt center. This center is associated with dikes, flows and pyroclastic deposits and has a maximum volume of 0.01 km^3. Dikes related to this center vary in length from 0.5 to 1.5 km and in width from 0.5 to 2 meters. It is notable that aspect ratios (length/width) of dikes for this low-volume center are similar to those related to the higher volume eruptions at Fortification Hill and the Lava Cascade.

The Petroglyph Wash group crops out along the east side of the Black Mountains. Basalts of this group erupted from at least two vents. The Malpais Flattop basalts lie to the southwest of the Fortification Hill group and erupted from a northwest-striking dike located approximately 1.5 km west of a major west-dipping, northwest-striking normal fault.[34]

Reveille Range

The Reveille Range is a north-south trending range in south-central Nevada, 80 km east of Tonopah (Figure 6).[7,13,36] Early to late Miocene and Pliocene basalt occurs as intrusive plugs, domes, flows, and eroded cinder cones on the east and west flanks of the range. Vents and dikes are well exposed on the deeply eroded eastern flank of the range. Volcanoes formed along range bounding and range interior faults. Three eruptive episodes of basalt occur in the Reveille Range. The earliest episode (5.9 to 5.1 Ma) is the most voluminous and crops out on both sides of the range. The second episode (4.3 to 3.0 Ma) of basaltic activity is represented by volcanic centers only on the eastern side of the range. The final episode of basaltic activity produced a cinder cone and flows that were deposited on top of second episode lavas.[7]

On the western side of the range, 22 first episode centers form a north-trending chain 35 km long and about 4 km wide. On the eastern side of the Reveille range, 16 volcanic centers of the first episode occur in a narrow north-trending zone, 25 km long and about 4 km wide. Also, 13 volcanic centers of the second episode form a 13 km long and 5 km wide chain that overlaps the chain of first episode centers. Vent alignments are better displayed in the northern Reveille Range; north of latitude 38° 5'.

Timing of Volcanism

Volcanism occurred in the Fortification Hill field between 5.8 and 4.7 Ma. Early and penecontemporanous eruptions of tholeiitic and alkali basalt occurred at Malpais Flattop, Fortification Hill and Petroglyph Wash (5.8 Ma).[7] Activity then shifted to the Lava Cascade (4.7 Ma), and terminated with the emplacement of low-volume alkali basalt centers in the Fortification Hill-Lava Cascade group and near Petroglyph Wash (Figure 5). Thus, during the 1 m.y. history of the field, there was no preferred migration of volcanism. In the Reveille Range, first episode lavas erupted on both sides of the range between 5.9 and

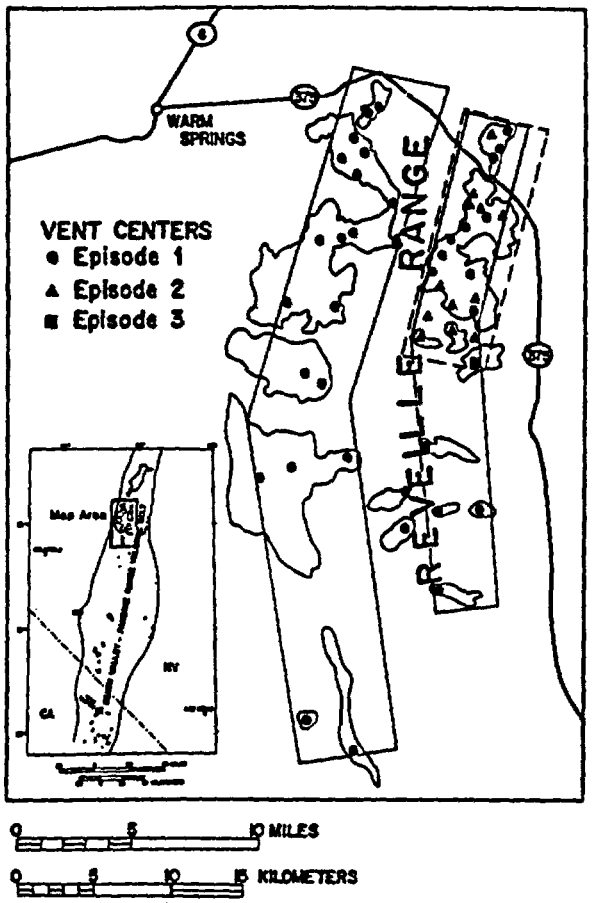

Figure 6. Distribution of post-6 Ma volcanic flows and centers in the Reveille Range, south-central Nevada. Solid lines outline first episode volcanic chains. Dashed lines outline second episode chains.

5.1 Ma.[7,13,37] Volcanism migrated to the eastern side of the range with the eruption of second episode lavas (4.3 to 3.0 Ma) and then northward into the Pancake Range (3.7 to less than 0.1 Ma)(Figure 6).[7,17,19]

Dike Geometry and Chain Dimensions

Dikes in the Fortification Hill field related to both high- and low-volume centers commonly occur in sets that show en echelon geometry. Thickening of dikes toward the surface and sills were not observed. Aspect ratios (width/length) and widths of individual dikes vary from 10^{-2} to 10^{-3} and 0.5 to 2 m respectively. Aspect ratios appear to be independent of the volume of the center with which the dikes are associated. These dimensions are similar to those for dikes worldwide. For example, in Hawaii, dikes range in thickness from less than 0.5 m to 150 m. However, the majority are between 0.5 and 1 m thick.[38] In the southern Great Basin, dike widths range from 0.3 to 4 m and average 1 m[39]. Basic dikes of the central dike swarm in the Shitara district of Japan range in thickness from 1.5 to 3 m and tend to thicken away from magma reservoirs.[40] Fedotov[41] in a study of ascent mechanisms of basaltic magma indicated that aspect ratios for basalt dikes worldwide are typically in the range of 10^{-2} to 10^{-3}. Crowe et al.[40] used the aspect ratios of Fedotov to estimate typical dike lengths based on measured thickness. These observations suggest that dike geometry may be fixed early in the history of a volcanic field. During the subsequent history of the field, new magma may use already established vent systems. If this scenario is correct, then in many volcanic fields, dike dimensions are independent of the volume of magma that has passed through them. On the basis of these arguments we suggest that the Fortification Hill field may be a direct analog in terms of vent geometry to the Quaternary cones in Crater Flat.

A volcanic chain may be defined as an aligned group of temporally related volcanic centers controlled by either a single structure or set of kinematically related structures. In some instances, volcanic chains are not linear but form broad elongated zones. Broad volcanic chains form when eruptions occur along sets of subparallel structures. The width of a volcanic chain may reflect the width of a particular structural zone. For example, eruptions may occur on both sides and in the interior of a range along coplanar structures. The relationship between chain length and the total volume of the magmatic system are presently speculative. For this reason, the length and width measurements obtained from the Fortification Hill and Reveille fields are considered to be the upper bounding limits for this analysis.

The Fortification Hill-Lava Cascade Group forms a chain 25 km long (Figure 5). The chain is composed of at least six centers that occur in either the hanging wall or foot wall of range-bounding faults. During early stages of eruption within the Fortification Hill field, eruptions occurred coevally on both sides of the Black Range. Later, a center developed in the range interior (Lava Cascade). Therefore, the entire range was a potential target for an eruption, even though eruptions near range margins were more common. Chain width can be estimated in three ways: (1) the width of the Fortification Hill-Lava Cascade Chain alone, which is about 3 km (measured by calculating the standard deviation about a regression line fit to vent locations); (2) the distance between the Fortification Hill and Petroglyph Wash vents. Lavas from these centers are similar in composition and are probably related to the same magmatic pulse. This distance is 8 km; (3) the entire width of the range, a distance of about 15 km. This measurement can be defended by arguing that range-bounding and interior high-angle faults are kinematically related[42] and an eruption may occur along any one of these structures. For the purposes of this analog study, we accept the conservative estimate of 3 Km for the chain width.

Chain dimensions in the Reveille range are comparable to those in the Fortification Hill field (30 km by 4 km and 35 km by 5 km) (Figure 6).

Summary of Analog Studies

Analog studies provide useful information about vent geometry, timing of eruptions, and length and width of volcanic chains. The following observations are notable:

(1) There is no preferred migration direction of volcanism in the Fortification Hill field. In the Reveille Range volcanism first shifted to the east and then to the north.
(2) Volcanoes formed mainly along range margins, but in both the Reveille range and in the Fortification Hill field vents formed within the mountain block.
(3) Dike systems are simple and have similar dimensions to those related to low-volume Quaternary systems.
(4) The Fortification Hill-Lava Cascade group within the Fortification Hill field forms a chain 25 Km long and about 3 Km wide. The 3 km width is a conservative estimate. Width may range up to 15 Km. Volcanic chains in the Reveille range display similar dimensions.
(5) Eruptions in the Fortification Hill field occurred at sites of past eruption or along strike of the fault zones that controlled the earlier volcanic centers.

HIGH-RISK ZONES

The delineation of high-risk zones for volcanism within the AMRV is an important goal in any risk assessment study. Our definition of the high-risk zones is based on several criteria and assumptions that were developed in detailed studies of Plio-Pleistocene volcanic centers in the Great Basin and adjacent areas of the Basin and Range. The criteria and assumptions used to establish the high-risk zones within the AMRV are listed below.

1. In the AMRV volcanism was controlled by north- to north-northeast-striking structures.
2. The structures controlling the location of the Crater Flat and Lathrop Wells volcanoes are part of the same set that cut Yucca Mountain.
3. Lengths of volcanic chains vary from 15 to 25 Km. Chain widths vary from about 3 Km to 15 km depending on the width of the fault zone controlling volcanism.
4. Future activity will preferentially occur at sites of past eruptions or along strike of the structural zone controlling volcanism.
5. Future volcanic events in the Yucca Mountain area will occur within the AMRV and will be associated with Quaternary centers in Crater Flat, at Sleeping Butte, or at the Lathrop Wells cone.

We show high risk zones within the AMRV in Figure 7. The rectangles have long axes that parallel regional structure. Two rectangles are placed on each group of Quaternary cones. First, a rectangle with dimensions determined by measurement of the chain of volcanoes within Crater Flat (12 Km long by 1 Km wide). Second, a rectangle with the dimensions of the Fortification Hill-Lava Cascade chain (25 Km long and 3 Km wide). For the purposes of this analysis, the larger rectangle represents an upper bounding limit. According to our assumptions, a future eruption may occur either to the north-northeast or south-southwest of an existing cone or group of cones. Therefore, the high-risk rectangles are centered on the existing volcanoes and their long axes are twice the chain lengths. By constructing the high-risk rectangles in this manner, they may extend outside of the AMRV. This relationship results from the manner in which the AMRV was originally defined (i.e., the area enclosing all post-6 Ma volcanoes in the Yucca Mountain area).

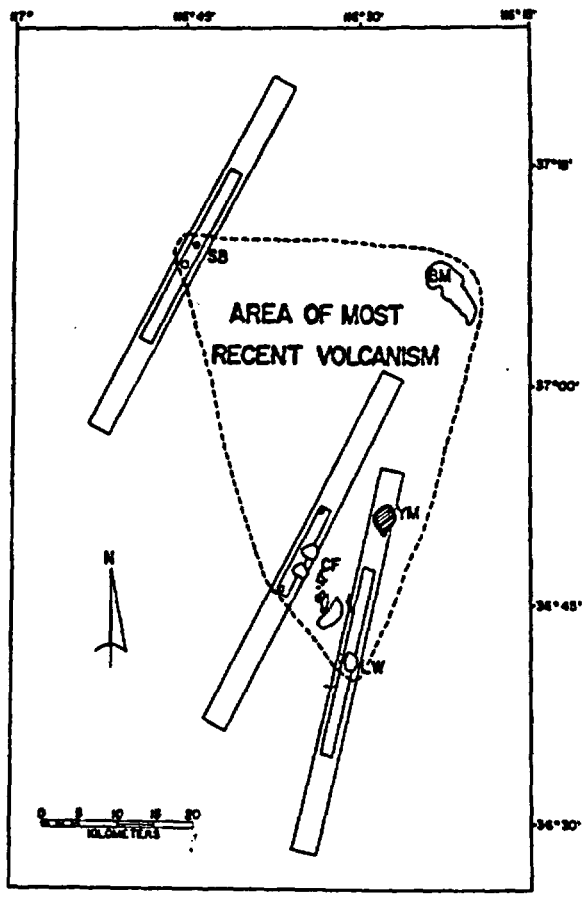

Figure 7. Map outlining the AMRV (solid line) and high-risk zones (rectangles) in the Yucca Mountain area. The construction of the high-risk rectangles is described in the text.

The proposed high-level nuclear waste repository at Yucca Mountain falls within the larger high-risk Lathrop Wells rectangle and just to the east of the high-risk zones constructed for the Crater Flat chain.

Based on the high-risk rectangles and the AMRV, we suggest a qualitative index of volcanic risk for areas within the Yucca Mountain region.

Risk Level Index (from highest to lowest risk index):

5. At or adjacent to an existing Quaternary center.
4. Within the smaller-dimension risk rectangle.
3. Within the larger-dimension risk rectangle.
2. Outside the high-risk rectangles, but within the structural zone controlling the Quaternary center.
1. In other areas of the AMRV.

Based on this risk scale, we assign the site of the proposed waste repository to risk-category 3. At the present time we can not assign quantitative probability values of volcanism for each risk-magnitude zone. Such calculations will be the subject of a future publication.

REFERENCES CITED

1. DEPARTMENT OF ENERGY, "Chapter 1" Site Characterization Plan, Yucca Mountain Site, Nevada Research and Development Area, Nevada DOE/RW-0199, 1 (1988).

2. D. L. FEUERBACH and E.I. SMITH, "Late-Miocene Fortification Hill Basalt, Lake Mead Area, Nevada and Arizona: Source Areas and Conduit Geometry,"Geological Society of America Abstracts with Programs, 19, 376-377 (1987).

3. D. L. FEUERBACH and E. I. SMITH, "Changes in Volcanism During Declining Stages of Regional Extension in the Lake Mead Area, Nevada and Arizona," Geological Society of America Abstracts with Programs, 20, A114 (1988).

4. T. R. NAUMANN and E. I. SMITH, "Compositional Trends Within Late-Cenozoic Alkalic Basalts of the Central Great Basin, Nevada," Geological Society of America Abstracts with Programs, 20, A114 (1988).

5. D. L. FEUERBACH, E. I. SMITH, and M. SHAFIQULLAH, "Structural Control of Pleistocene Volcanism in Crater Flat, Nevada," Geological Society of America Abstracts with Programs, 22 (in press).

6. T. R. NAUMANN, E. I. SMITH, and M. SHAFIQULLAH, "Post-6 Ma Intermediate (Trachytic) Volcanism in the Reveille Range, Central Great Basin, Nevada," Geological Society of America Abstracts with Programs, 22 (in press).

7. E. I. SMITH, D. L. FEUERBACH, T. R. NAUMANN, E. COLE, P. E. DAMON, and M. SHAFIQULLAH, "Plio-Pleistocene Basalts in Clark and Nye Counties, Nevada and Adjacent Areas," Nevada Bureau of Mines and Geology Bulletin (in preparation).

8. D. VANIMAN, B. CROWE, and E. S. GLADLEY, "Petrology and Geochemistry of Hawaiite Lavas From Crater Flat, Nevada," Contributions to Mineralogy and Petrology, 80, 341-357 (1982).

9. B. CROWE, C. HARRINGTION, L. McFADDEN, F. PERRY, S. WELLS, B. TURRIN, and D. CHAMPION, "Preliminary Geologic Map of the Lathrop Wells Volcanic Center," LA-UR-88-4155, Los Alamos National Laboratory (1988).

10. B. M. CROWE and F. V. PERRY, "Volcanic Probability Calculations for the Yucca Mountain Site: Estimation of Volcanic Rates," Focus '89, Nuclear Waste Isolation in the Unsaturated Zone, American Nuclear Society (in press).

11. J. H. STEWART, "Geology of Nevada," Nevada Bureau of Mines and Geology Special Publication 4 (1980).

12. B. CROWE and R. FISHER, "Sedimentary Structures in Base-Surge Deposits With Special Reference to Cross-Bedding, Ubehebe Craters, Death Valley, California," Geological Society of America Bulletin, 84, 663-682 (1973).

13. R. G. LUEDKE and R. L. SMITH, "Map Showing Distribution, Composition, and Age of Late Cenozoic Volcanic Centers in California and Nevada," Miscellaneous Geological Investigations Map I-1090-C, U. S. Geological Survey (1981).

14. N. W. LARSEN, "Chronology of Late Cenozoic Basaltic Volcanism: The Tectonic Implications Along a Segment of the Sierra Nevada and Basin and Range Province Boundary," Ph.D. Dissertation, Brigham Young University (1979).

15. W. A. DUFFIELD, C. R. BACON, and G. B. DALRYMPLE," Late Cenozoic Volcanism, Geochronology, and Structure of the Coso Range, Inyo County, California," Journal of Geophysical Research, 85, 2381-2404 (1980).

16. B. M. CROWE, D. T. VANIMAN, and W. J. CARR, "Status of Volcanic Hazard Studies for the Nevada Nuclear Waste Storage Investigations," LA-9325-MS, Los Alamos National Laboratory (1983).

17. B. D. TURRIN and J. C. DOHRENWEND, "K-Ar Ages of Basaltic Volcanism in the Lunar Crater Volcanic Field, Northern Nye County, Nevada: Implications for Quaternary Tectonism in the Central Great Basin," Geological Society of America Abstracts with Programs, 16, 679 (1984).

18. J. C. DOHRENWEND, L. D. MCFADDEN, B. D. TURRIN and S. G. WELLS, "K-Ar Dating of the Cima Volcanic Field, Eastern Mojave Desert, California: Late Cenozoic Volcanic History and Landscape Evolution," Geology, 12 163-167 (1984).

19. J. C. DOHRENWEND, A. D. ABRAHAMS, and B.D. TURRIN, "Drainage Development on Basaltic Lava Flows, Cima Volcanic Field, Southeast California, and Lunar Crater Volcanic Field, South-Central Nevada," Geological Society of America Bulletin, 99, 405-413 (1987).

20. K. R. STERNLOF, "Structural Style and Kinematic History of the Active Panamint-Saline Extensional System, Inyo County, California," M.S. Thesis, Massachusetts Institute of Technology (1988).

21. L. SERPA, B. DeVOOGD, L. WRIGHT, J. WILLEMIN, J. OLIVER, E. HAUSER, and B. TROXEL, "Structure of the Central Death Valley Pull-Apart Basin and Vicinity From COCORP Profiles in the Southern Great Basin," Geological Society of America Bulletin, 100, 1437-1450 (1988).

22. R. E. ANDERSON, "Hazard Implications of Joint-Controlled Basaltic Volcanism in Southwestern Utah," Geological Society of America Abstracts with Programs, 20, A115 (1988).

23. J. G. ROSENBAUM and M. R. HUDSON, "Paleomagnetic Investigations of Tertiary Structural Rotations at Yucca Mountain," Focus '89, Nuclear Waste Isolation in the Unsaturated Zone, American Nuclear Society (in press).

24. R. A. SCHWEICKERT, "Evidence for a Concealed Dextral Strike-Slip Fault Beneath Crater Flat, Nevada," Geological Society of America Abstracts with Programs, 21, A90 (1989).

25. S. G. WELLS, L. McFADDEN, C. RENAULT, B. D. TURRIN, and B. M. CROWE, "A Geomorphic Assessment of Quaternary Volcanism in the Yucca Mountain Area, Nevada Test Site, Southern Nevada," Geological Society of America Abstracts with Programs, 20, 242 (1988).

26. H. R. CORNWALL and F. J. KLEINHAMPL, "Geology of the Bare Mountain Quadrangle, Nevada," Map GQ-157, U. S. Geological Survey (1961).

27. H. R. CORNWALL, "Geology and Mineral Deposits of Southern Nye County, Nevada," Nevada Bureau of Mines and Geology Bulletin 77 (1972).

28. R. B. SCOTT and J. BONK, "Preliminary Geologic Map of Yucca Mountain, Nye County, Nevada, With Geologic Sections," Open File Report 84-494, U.S. Geological Survey (1984).

29. W. J. CARR, "Volcano-Tectonic Setting of Yucca Mountain and Crater Flat, Southwestern Nevada," *in* M. D. CARR and J. C. YOUNT, "Geologic and Hydrologic Investigations of a Potential Nuclear Waste Disposal Site at Yucca Mountain, Southern Nevada," U. S. Geological Survey Bulletin 1790, 35-49 (1988).

30. R. B. SCOTT, R. W. NESBITT, E. J. DASCH, and R. L. ARMSTRONG, "A Strontium Isotope Evolution Model for Cenozoic Magma Genesis, Eastern Great Basin, U. S. A.," Bulletin Volcanologique 35, 1-26 (1969).

31. I. CAMPBELL and E. T. SCHENK, "Camptonite Dikes Near Boulder Dam, Arizona," American Mineralogist, 35, 671-692 (1950).

32. E. I. SMITH, "Geologic Map of the Boulder Beach Quadrangle, Nevada." Nevada Bureau of Mines and Geology Map 81 (1984).

33. D. L. FEUERBACH, "Geology of the Wilson Ridge Pluton; a Mid-Miocene Quartz Monzonite Intrusion in the Northern Black Mountains, Mohave County, Arizona and Clark County, Nevada," M.S. Thesis, University of Nevada, Las Vegas (1986).

34. R. E. ANDERSON, "Geological Map of the Black Canyon 15' Quadrangle, Arizona and Nevada," Map GQ-1394, U. S. Geological Survey (1978).

35. J. G. MILLS, "The Geology and Geochemistry of Volcanic and Plutonic Rocks in the Hoover Dam 7 1/2 Minute Quadrangle, Clark County, Nevada and Mohave County, Arizona," M.S. Thesis, University of Nevada, Las Vegas (1987).

36. B. D. TURRIN, P. R. RENNE, and J. C. DOHRENWEND, "Temporal Trends in the Chemical Evolution of Megacryst Bearing, Subalkaline-Alkaline Basaltic Lavas From the Lunar Crater Volcanic Field, Nye County, Nevada," Geological Society of America Abstracts with Programs, 17, 414 (1985).

37. B. D. TURRIN, P. R. RENNE, and J. C. DOHRENWEND, "Temporal Trends in the Chemical Evolution of Megacryst Bearing, Subalkaline-Alkaline Basaltic Lavas From the Lunar Crater Volcanic Field, Nye County, Nevada," Geological Society of America Abstracts with Programs, 17, 414 (1985).

38. G. A. MACDONALD and A. T. ABBOTT, Volcanoes in the Sea-The Geology of Hawaii University of Hawaii Press, Honolulu (1970).

39. B. CROWE, R. AMOS, F. PERRY, S. SELF, and D. VANIMAN, "Aspects of Possible Magmatic Disruption of a High-Level Radioactive Waste Repository in Southern Nevada," LA-9326-MS Los Alamos National Laboratory (1982).

40. A. TAKADA, "Subvolcanic Structure of the Central Dike Swarm Associated with Ring Complexes in the Shitara District, Central Japan," Bulletin of Volcanology, 50, 106-118 (1988).

41. S. A. FEDOTOV, "Aspects of Basic Magmas in the Crust and the Mechanism of Basaltic Fissure Eruptions," International Geological Reviews, 20, 33-48 (1978).

42. E. DUEBENDORFER, A. SEWALL, and E. SMITH, "The Saddle Island Detachment: An Evolving Shear Zone in the Lake Mead Area, Nevada," Geological Society of America Memoir (in press).

Geological Society of America
Memoir 174
1990

Chapter 10

Mid-Miocene volcanic and plutonic rocks in the Lake Mead area of Nevada and Arizona; Production of intermediate igneous rocks in an extensional environment

Eugene I. Smith, Daniel L. Feuerbach, and Terry R. Naumann
Department of Geoscience, University of Nevada, Las Vegas, Nevada 89154
James G. Mills
Department of Geology, Monmouth College, Monmouth, Illinois 61462

ABSTRACT

Middle Tertiary volcanic rocks of the Lake Mead field are calc-alkalic to alkalic-calcic and vary continuously in composition from basalt to rhyolite. These volcanic rocks formed during Basin-and-Range extension and are spatially and genetically associated with diorite-to-granite intrusions of the Wilson Ridge pluton. Locally, igneous rocks were subjected to potassium metasomatism.

Field relations and petrography provide evidence of disequilibrium mineral assemblages and liquid-liquid mixing of basalt and granite magmas to form the intermediate rock types of the Lake Mead volcanic field. Evidence of mixing includes incompatible phase assemblages of euhedral olivine, embayed quartz, and sodic plagioclase within andesite flows. Plagioclase occurs in rounded and partially resorbed clusters of equant crystals and commonly displays oscillatory zoning and outer glass-charged zones (fretted texture). Quartz phenocrysts are commonly surrounded by rims of prismatic augite and glass. Fine-grained spheroidal to ellipsoidal inclusions of basalt are common in dacite flows and dikes. Thus, various mixing ratios of olivine basalt and granite end members may be responsible for the textural variations observed in volcanic rocks of the Lake Mead field.

The evolution of the igneous rocks of the Lake Mead field was evaluated by petrogenetic models involving both crystal fractionation and magma mixing. These processes may have operated together to produce the compositional range in volcanic and plutonic rocks of the Lake Mead area. Open-system models provide estimates of the relative importance of the two processes and suggest that mixing was more important in the derivation of andesite and diorite (mass mixed component/mass crystallizing phase R = 0.8 to 2.2) than dacite, quartz monzonite, or granite (R = 0.1 to 0.65).

The calc-alkaline–alkalic-calcic nature of the igneous rocks of the Lake Mead field, and possibly other similar rock suites that formed in the Great Basin during regional extension, may result from magma mixing. Basalts and rhyolites may mechanically mix in various proportions to produce intermediate rock types. The classic bimodal assemblages may only occur where mixing is incomplete or in structural situations where different magma types cannot mix.

Smith, E. I., Feuerbach, D. L., Naumann, T. R., and Mills, J. G., 1990, Mid-Miocene volcanic and plutonic rocks in the Lake Mead area of Nevada and Arizona: Production of intermediate igneous rocks in an extensional environment, *in* Anderson, J. L., ed., The nature and origin of Cordilleran magmatism: Boulder, Colorado, Geological Society of America Memoir 174.

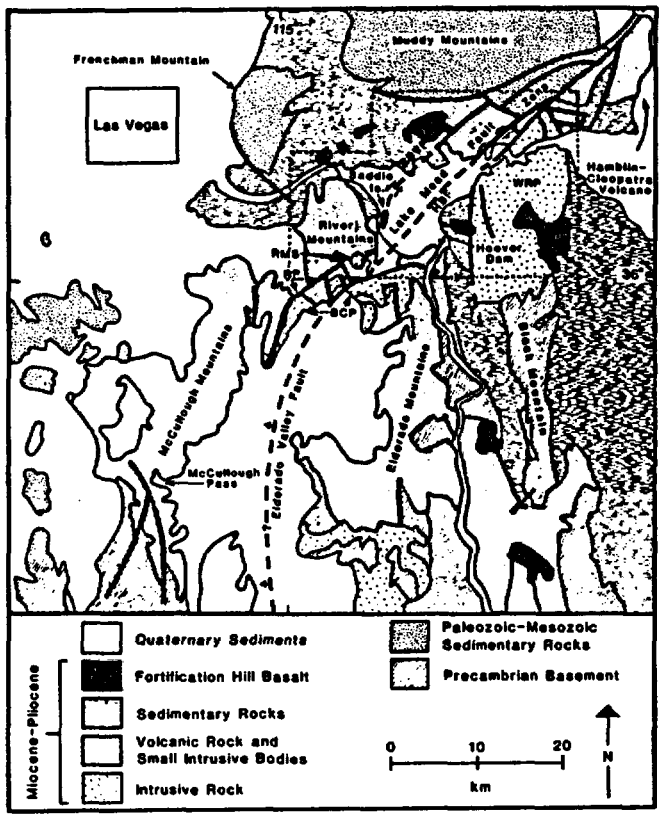

Figure 1. Geologic index map. The Lake Mead volcanic field is outlined by the box and shown in detail in Figure 4. WRP = Wilson Ridge pluton, RMS = River Mountains stock, BCP = Boulder City pluton, RP = Railroad Pass, BSVF = Bitter Spring Valley fault, HBF = Hamblin Bay fault.

INTRODUCTION

In the Lake Mead area of southern Nevada and northwestern Arizona, structural and topographic relief provides a cross section of a mid-Miocene (20 to 12 Ma) volcanic sequence and related subjacent plutons emplaced during Basin-and-Range extension (Fig. 1). Volcanic rocks vary continuously in composition from basalt (47 percent SiO_2) to rhyolite (75 percent SiO_2). Stratovolcanoes in the River, McCullough, Eldorado, and northern Black Mountains are composed mainly of andesite and dacite (56 to 68 percent SiO_2). Basalt and rhyolite are rare and erupted during the last episode of volcanism in the River Mountains (Smith, 1984; Smith and others, 1986). Volcanic rocks are associated with cogenetic diorite to granite intrusions, the Boulder City and Wilson Ridge plutons.

Our approach involves an integrated field, petrographic, and geochemical study of a suite of rocks in the River Mountains–Hoover Dam, and Boulder Wash–Wilson Ridge areas. Petrogenetic models involving both crystal fractionation and magma mixing were developed using the least-squares mass-balance equation of Stormer and Nicholls (1978). Models were refined using techniques proposed by Langmuir and others (1978) and DePaulo (1981) and recently applied to petrologic problems by McMillan and Dungan (1986) and Thompson and others (1986). This suite of rocks, herein named the Lake Mead field, was previously interpreted by Weber and Smith (1987) as a cogenetic suite that evolved independent from volcanic rocks in the McCullough and Eldorado Mountains and the Boulder City pluton.

REGIONAL SETTING

The Lake Mead area of southern Nevada and northwestern Arizona is at the northern end of the Colorado River detachment terrane, a region that was subjected to large-scale extension during mid-Miocene time (Anderson, 1971; Frost and others, 1982; Spencer, 1985; Weber and Smith, 1987) (Fig. 1). Volcanism began in the Lake Mead area at about 20 Ma and continued until about 12 Ma. Basalt at Fortification Hill and at scattered localities near Lake Mead is dated between 4 and 6 Ma and represents the youngest volcanism in the region (Anderson and others, 1972; Feuerbach and Smith, 1987). Tilting, faulting, and detachment of the volcanic section related to the main phase of extension occurred mainly after 14.7 Ma; however, faulting began earlier (15 to 21 Ma) in the River Mountains (Smith, 1982) and in the Hoover Dam area (Mills, 1985).

On the basis of geochemical correlation and geometric reconstructions, Weber and Smith (1987) proposed a model for the prefaulting configuration of volcanoes near Lake Mead. Their model suggested that the River, McCullough, and Eldorado Mountains lie in the upper plate of a west-dipping detachment zone and that prior to mid-Tertiary extensional faulting the Lake Mead area contained three compound stratovolcanoes. These are (1) the River Mountains–Hoover Dam–Boulder Wash volcanoes associated with the Wilson Ridge Pluton (Smith, 1982, 1984; Mills, 1985; Naumann, 1987); (2) the McCullough-Eldorado volcanoes related to the Boulder City and Nelson plutons (Anderson, 1971; Smith and others, 1986); and (3) the Hamblin-Cleopatra volcano associated with an unnamed pluton (Anderson, 1973; Thompson, 1985) (Fig. 2). The stratovolcanoes were assigned to specific plutons on the basis of similarities in trace and rare earth element (REE) distributions (Weber and Smith, 1987). The River Mountains–Hoover Dam–Boulder Wash–Wilson Ridge suite (the Lake Mead field) is characterized by low Ta contents and a negative correlation between total REE concentration and SiO_2 content. The McCullough–Eldorado–Boulder City suite displays high Ta concentrations and a positive correlation between total REE and SiO_2. These characteristics suggest that the two volcanic-plutonic suites formed and evolved independently (Weber and Smith, 1987).

VOLCANIC STRATIGRAPHY AND PETROLOGY

River Mountains

In the River Mountains an andesite-dacite stratovolcano is surrounded by a field of dacite domes and flows. Volcanic activ-

ity occurred in four pulses, each characterized by the eruption of andesite and dacite flows. Flows of the first episode (volcanic rocks of River Mountains; Bell and Smith, 1980) formed the River Mountains stratovolcano at about 13.5 Ma (Fig. 3). Andesite flows cut by dikes and sills of plagioclase-biotite dacite (Table 1 [Tables 1 through 4 located at end of chapter.]) form the flanks of the volcano. A complex pluton of quartz monzonite containing quartz, plagioclase, biotite, and hornblende occupies the core of the stratovolcano (River Mountains stock; Bell and Smith, 1980) (Fig. 4). Volcanic rocks of the second episode (volcanic rocks of Bootleg Wash; Bell and Smith, 1980) exposed only in the southern part of the River Mountains just to the northwest of Boulder City (Fig. 4) contain a basal andesite overlain by a thin volcaniclastic unit that is in turn overlain by plagioclase-, biotite-, and sphene-bearing dacite flows. Dacite contains scattered grains of highly resorbed quartz. The third episode of volcanism formed a broad field of dacite and andesite domes and flows that are associated with thick deposits of breccia and volcaniclastic debris (volcanic rocks of Powerline Road; Bell and Smith, 1980). The last episode of volcanism is characterized by rhyolite and alkali basalt dated at 12 Ma (Anderson and others, 1972). These volcanic rocks erupted from separate centers in the northern part of the River Mountains and mark the first appearance of rhyolite and basalt.

Field evidence for magma mixing and assimilation in the River Mountains includes dacite and quartz monzonite that contain inclusions of pyroxene basalt(?) and/or hornblende andesite, a flow within the Powerline Road section that contains 20 to 40 percent basaltic inclusions, and basaltic inclusions within the River Mountains stock that reach 1 m in diameter.

Hoover Dam

At Hoover Dam, a dacite ash-flow tuff (the tuff of Hoover Dam; Smith, 1984) separates a lower sequence of andesite flows and conglomerate from an upper sequence of dacite flows and breccia, andesite flows, and conglomerate (Fig. 3). The tuff may have erupted from a northwest-trending sag-graben caldera to the northwest of Hoover Dam (Mills, 1985). Because of structural disruption and the Lake Mead reservoir, the form and size of this source area is difficult to document. The following evidence, however, is supportive of a source area for the tuff in the vicinity

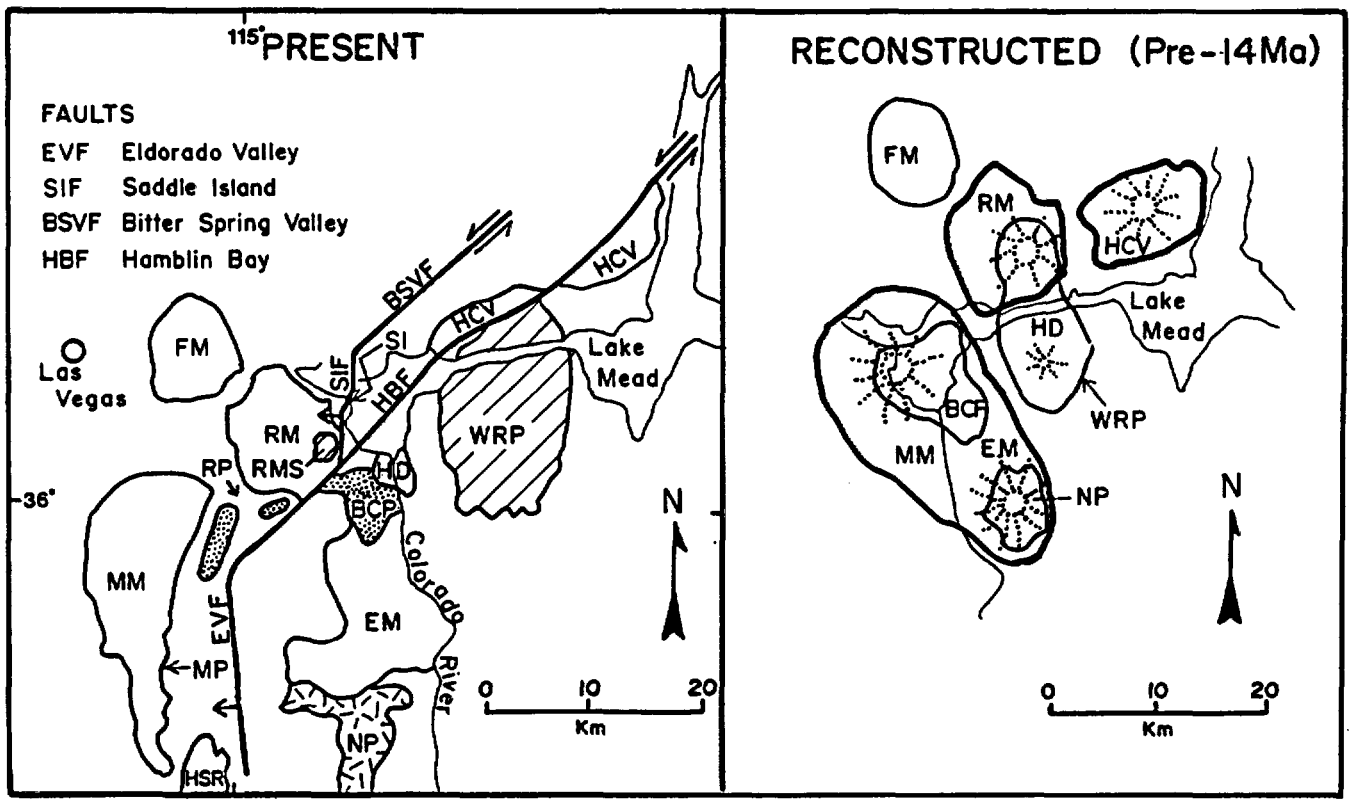

Figure 2. Present geology and proposed reconstruction of the Lake Mead area prior to mid-Miocene extension. In reconstruction, thick solid lines = boundaries of volcanic piles, and thin solid lines = possible extent of subjacent plutons. HSR = Highland Spring Range, FM = Frenchman Mountain, RM = River Mountains, MM = McCullough Mountains, EM = Eldorado Mountains, HD = Hoover Dam volcanic section, HCV = Hamblin-Cleopatra volcano, NP = Nelson Pluton, SI = Saddle Island. Other abbreviations are defined in the caption to Figure 1.

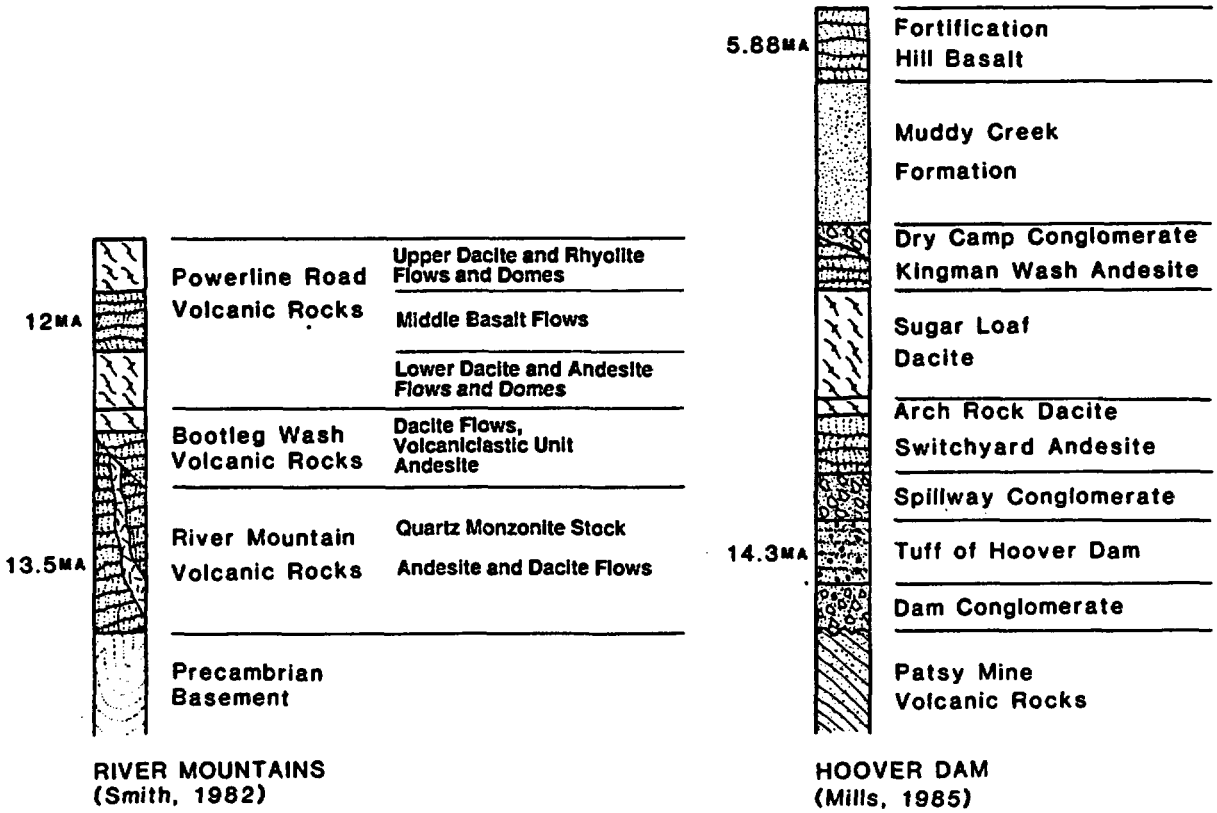

Figure 3. Generalized stratigraphic sections for igneous rocks in the River Mountains and Hoover Dam area.

of Hoover Dam. (1) The tuff of Hoover Dam is restricted in outcrop to a 3-km radius about Hoover Dam (Fig. 4). It is more than 185 m thick at Hoover Dam, but pinches out 1.5 km to the south. (2) To the north and northwest of Hoover Dam, along the south shore of Lake Mead, the tuff is rich in xenoliths of lower-sequence andesite. At Promontory Point (Fig. 4), xenoliths as much as 1 m in diameter compose 75 percent of the tuff. This deposit may represent a megabreccia unit near the west wall of the caldera. (3) Upper-sequence dacite is chemically related to the tuff and may represent post-caldera domes and flows. We envision the eruption of the tuff from a sag-graben or trap-door style caldera. The tuff of Hoover Dam is mineralogically and chemically zoned from dacite (68 percent SiO_2) at its stratigraphic top to andesite (56 percent SiO_2) at its base.

Upper-sequence rocks include a section of dacite flows, breccia, and andesite flows interbedded with conglomerate. The Arch Rock dacite (Mills, 1985) is a flow breccia containing rounded clasts of devitrified dacite. The hornblende-, biotite-, and plagioclase-bearing Sugarloaf dacite (Mills, 1985) has a well-developed basal vitrophyre. The dacite erupted from a large complex dome 1 km south of Hoover Dam. Mafic flows in the upper sequence include the olivine-bearing Switchyard and Kingman Wash andesites (Mills, 1985).

Wilson Ridge pluton

The Wilson Ridge pluton (Anderson, 1978), interpreted as a subvolcanic intrusion related to volcanic centers in the River Mountains and at Hoover Dam (Feuerbach and Smith, 1986), varies in composition from diorite to granite. The mid-Tertiary pluton (13.6 and 15.1 Ma; Anderson and others, 1972) is now exposed in a series of horsts and grabens in the northern Black Mountains (Figs. 1 and 4). During faulting the pluton was tilted 2° to 3° to the north (Feuerbach, 1986). Structural relief provides excellent exposures of a complex composite intrusion composed of at least four intrusive and hypabyssal phases and numerous felsic and mafic dikes (Fig. 4), listed as follows. (1) A *medium-grained phase* is composed of medium- to coarse-grained quartz monzonite to granite, the dominant phase of the Wilson Ridge pluton. This phase contains plagioclase, microcline, orthoclase, quartz, biotite, and hornblende, and minor amounts of sphene, apatite, and zircon (Table 1). (2) A *hypabyssal phase* is formed by monzonite to quartz monzonite containing phenocrysts of plagioclase, orthoclase, quartz, and biotite with subordinate hornblende and zircon. Rocks of this phase crop out in the northern part of the Gilbert Canyon graben and in the Boulder Wash area (Fig. 4). (3) A *diorite phase* is dominated by plagioclase,

hornblende, and biotite with subordinate amounts of orthoclase and trace amounts of sphene, quartz, apatite, and zircon. Diorite is commonly intruded by quartz monzonite along the margins of the pluton, and occurs as inclusions within the pluton (sample 57d). (4) A *red-feldspar granite phase* crops out on Fortification Ridge (Fig. 4) and contains phenocrysts of red to pink orthoclase in a matrix of medium-grained plagioclase, quartz, biotite, microcline, and trace amounts of apatite and zircon (Table 1).

Dikes of granite, granite porphyry, aplite, basalt, and biotite lamprophyre intruded the pluton. Feuerbach (1986) estimated that at least 400 north-trending dikes with an average width of 7 m intruded the core of the pluton and resulted in about 20 percent east-west extension.

Boulder Wash

The Boulder Wash area in the northern Black Mountains (Fig. 4) consists of multiple sheet-like intrusions of quartz monzonite of the Wilson Ridge pluton cut by dikes of dacite, basalt, and biotite lamprophyre. Volcanic rocks in the Boulder Wash area consist of a highly faulted 700-m-thick secton of biotite-plagioclase dacite flows and flow breccias interbedded with flows of pyroxene-olivine andesite containing xenocrysts of quartz and orthoclase. A dacite flow in the eastern part of the volcanic field was dated at 14.2 Ma (Thompson, 1985).

Petrographic and textural evidence of magma mixing is spectacularly developed in the Wilson Ridge pluton and in associated volcanic rocks in the Boulder Wash area (Naumann and Smith, 1987; Naumann, 1987). Evidence includes incompatible phase assemblages of euhedral olivine, embayed quartz, and sodic plagioclase within andesite flows (Naumann and Smith, 1987; Naumann, 1987). Plagioclase occurs in rounded and partially resorbed clusters of equant crystals and commonly displays oscillatory zoning and outer glass-charged zones (fretted texture) (Fig. 5). Quartz phenocrysts are commonly surrounded by rims of prismatic augite and glass (Fig. 5). Dacites contain an identical disequilibrium phenocryst asemblage, but contain biotite rather than olivine. Fine-grained inclusions of basalt are common in dacite flows and dacite dikes within the Wilson Ridge pluton. The inclusions range in size from 2 mm to more than 50 cm and contain phenocrysts of olivine and plagioclase (5 percent total phenocrysts) set in matrix of plagioclase microlites and glass. Elliptical to spherical inclusions commonly have crenulated margins (Fig. 6). Some inclusions have fine-grained margins and coarse-grained vesicular cores (Fig. 6). The presence of fine-grained rims (quench rims) and crenulated margins suggests that these inclusions are quenched "blobs" of mafic magma that crystallized after mixing with the host dacite liquid (Bacon, 1986; Koyaguchi, 1986; Mattison and others, 1986). A continuum of mixing textures exists in the Boulder Wash lavas and related dikes. As the proportion of mafic inclusions decreases, the modal abundance of quartz and sodic plagioclase phenocrysts increases. On the basis of a model by Koyaguchi (1986), we concluded that various mixing ratios of olivine basalt and granite end members are responsible for the textual variations (Naumann and Smith, 1987; Naumann, 1987).

INSTRUMENTAL TECHNIQUES

Whole-rock major-element concentrations were determined by Inductively Coupled Plasma techniques (ICP) at Chemex Labs, Inc. (Sparks, Nevada) and by x-ray fluorescence (XRF) analysis in the Rock Chemistry Laboratory at the University of Nevada, Las Vegas, and in the Department of Geology, Michigan State University. Cr, Ni, Cu, Zn, Rb, Sr, Y, Zr, Nb, and Ba were analyzed by XRF. Rare-earth elements and Sc, Rb, Sr, Ba, Ta, Hf, Zr, U, and Th were analyzed by Instrumental Neutron Activation Analysis (INAA) at the Phoenix Memorial Laboratory, University of Michigan. The multielement standards G-2, GSP-1, BHVO-1, and RGM-1 were used as internal standards. Precision for REE with concentrations of less than 1,000 ppm is 5 percent, except for Nd, Tb, and Yb, which is 10 percent.

MAJOR- AND TRACE-ELEMENT CHEMISTRY

Representative major- and trace-element analyses are shown in Table 2. Harker variation plots show a continuous range of SiO_2 contents from 46 to 77 percent (Fig. 7). Volcanic rocks in the River–Hoover Dam–Boulder Wash sections are mainly calc-alkalic or alkalic-calcic andesites and dacites (Fig. 8), with SiO_2 content varying between 54 and 67 percent. Plutonic rocks have the same geochemical affinities, but are generally more highly evolved (SiO_2 contents up to 77 percent) than their volcanic counterparts (Feuerbach, 1986).

Rocks of the Lake Mead field show decreasing total REE content with increasing SiO_2, and in the River Mountains, each of the four episodes of andesite-dacite volcanism is accompanied by a decrease in total REE content (Figs. 9, 10). Chondrite-normalized REE distribution plots (Fig. 11) in general show light REE depletion with increasing SiO_2. Several curves show small negative Eu anomalies. Distribution curves for samples of the tuff of Hoover Dam are stacked with lower REE contents in the dacitic top of the ash-flow sheet and higher contents at the andesitic base of the unit (Fig. 11C).

METASOMATISM AND ALTERATION

Some samples of igneous rock of the Lake Mead field were strongly affected by K-metasomatism (Table 2). Metasomatism mainly produced changes in the abundances of Na_2O, K_2O, Ba, and Rb (Fig. 7 and Table 2), but did not cause any noticeable lithologic or petrographic changes. Therefore, metasomatized rocks cannot be easily recognized by field or petrographic examination, but must be identified by evaluation of chemical data. A plot of Na_2O vs K_2O (Fig. 9) was used to evaluate the degree of metasomatism for volcanic and plutonic rocks in the Lake Mead field with SiO_2 more than 60 percent. "Normal" unmetasomatized rocks fall within the solid box (Carmichael and others,

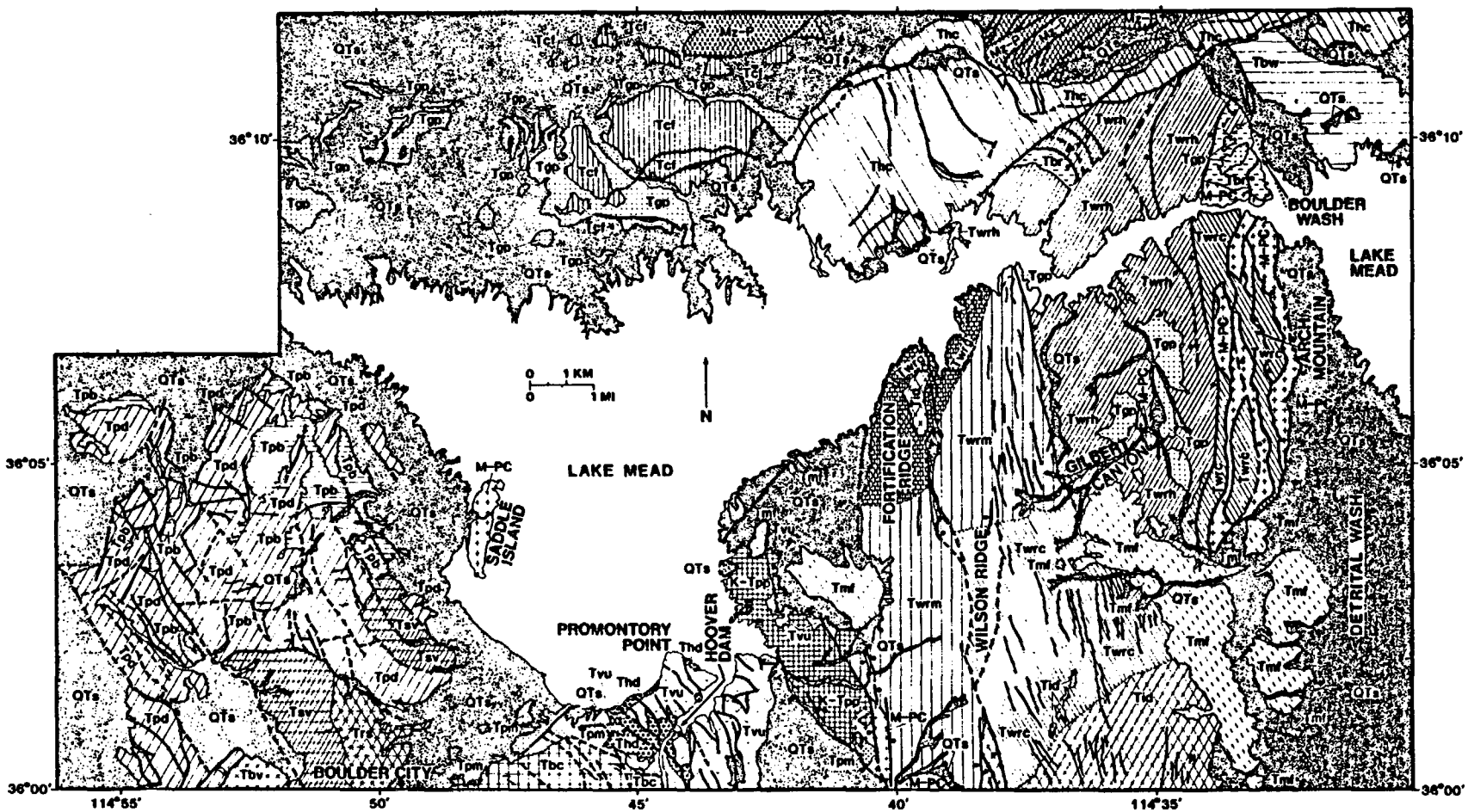
LAKE MEAD
BOULDER WASH
LAKE MEAD
ARCH MOUNTAIN
DETRITAL WASH
GILBERT CANYON
FORTIFICATION RIDGE
WILSON RIDGE
HOOVER DAM
PROMONTORY POINT
SADDLE ISLAND
BOULDER CITY
0 1 KM
0 1 MI
N
36°10'
36°05'
36°00'
114°55'
50'
45'
40'
114°35'

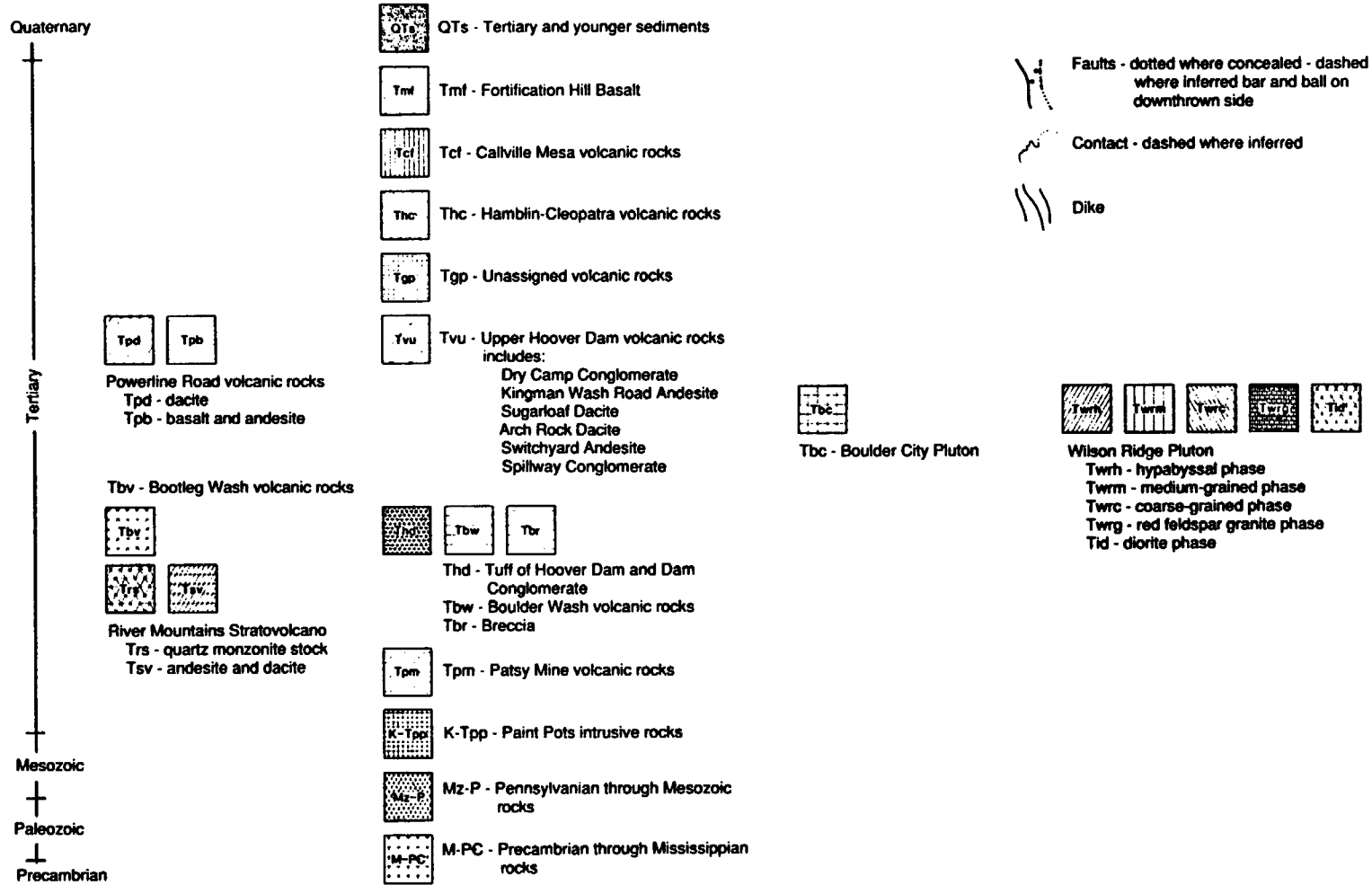

Figure 4. Geologic map of the Lake Mead volcanic field. Geology of the River Mountains is based on Bell and Smith (1980) and Smith (1984). Hoover Dam geology is from Mills (1985). Geology of the Wilson Ridge pluton and Boulder Wash area based on mapping by Feuerbach (1986) and Naumann (1987), respectively.

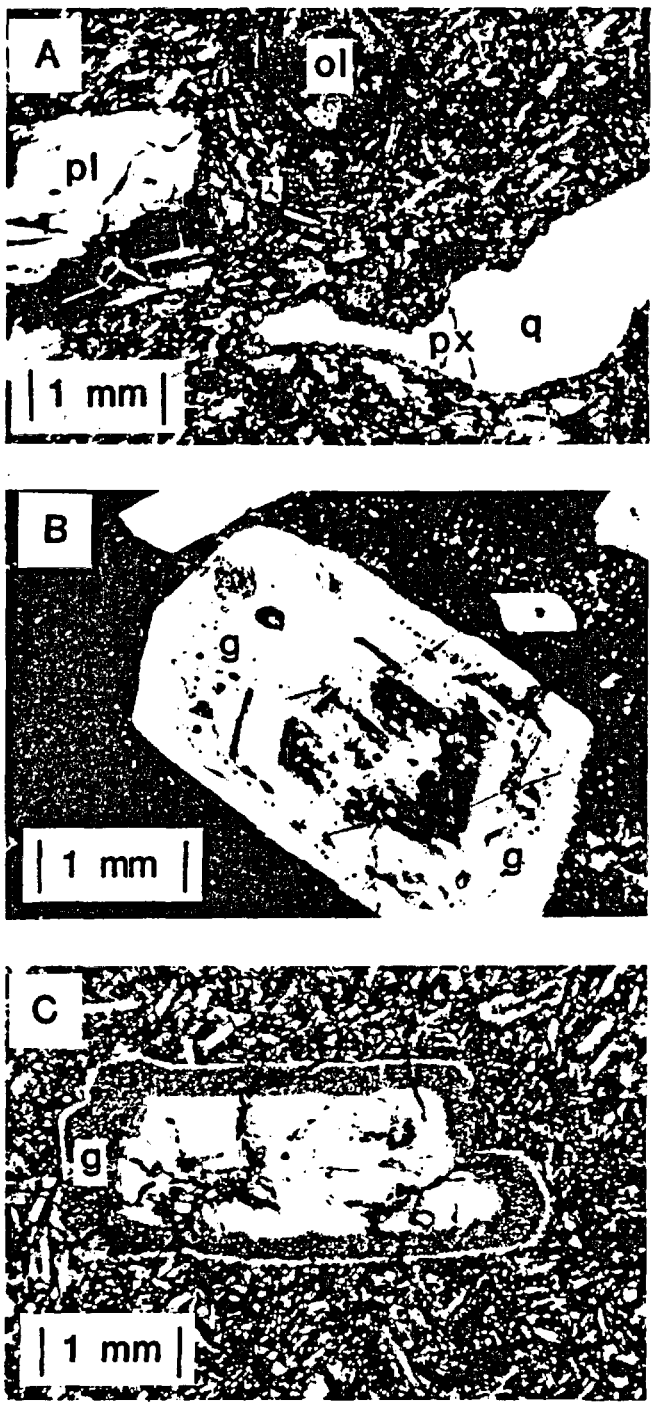

Figure 5. Photomicrographs of disequilibrium phenocrysts in Boulder Wash andesites (polarized light) (Naumann, 1987). A: Euhedral olivine (ol), rounded and partially resorbed sodic plagioclase (pl), and embayed quartz (q) with a rim of granular clinopyroxene (px) in specimen BW1. B: Rounded and partially resorbed, oscillatory zoned, sodic plagioclase with glass-charged zones (g) in specimen BW3. C: Rounded and partially resorbed plagioclase with well-developed glass-charged zones (g) (fretted texture) in specimen BW4.

1974). Note that 74 percent of the rocks of the Lake Mead field plot within the range of "normal" intermediate and felsic igneous rocks. Altered rocks are both high in K_2O and low in Na_2O, and high in Na_2O and low in K_2O. Also note the apparent negative correlation between Na_2O and K_2O contents for metasomatized rocks of the Wilson Ridge pluton. Perhaps this relation indicates that the pluton was, for all practical purposes, a closed system during metasomatism, so that K metasomatism and Na expulsion in one area resulted in Na metasomatism in another, and vice versa. Alteration is also likely in samples with loss on ignition (LOI) values more than 2 percent.

Whenever possible, unaltered samples were used to develop petrogenetic models involving the major elements. However, all samples of the tuff of Hoover Dam and Bootleg Wash volcanic rocks in the River Mountains were strongly affected by K-metasomatism, so the use of altered rocks in modeling differentiation processes for these volcanic suites was unavoidable. Major-element models that use altered rocks should be applied with caution (models 4, 5, 6, 14, and 21; Table 3).

An important concern in the application of REE and trace elements to petrogenetic studies is their mobility during hydrothermal alteration and low-grade metamorphism. Among others, Condie and others (1977), Martin and others (1978), Herrmann and others (1974), Vocke and others (1979), and Ludden and Thompson (1979) concluded that unless alteration or metamorphism was severe, they do not produce significant changes in either the abundances or distributions of the REE. Also, Hildreth and Mahood (1985) indicated that Sc, Ti, REE, Zr, Hf, Nb, Ta, and Th are relatively immobile during the alteration of volcanic rocks and are useful elements for correlating strongly altered tuffs. The relative immobility of Sc and the REE in igneous rocks of the Lake Mead field is demonstrated by their moderate to high correlation with SiO_2 on Harker variation diagrams (Fig. 7), and by REE patterns and distributions that lack selective enrichment or depletion of specific REE elements or element groups (light vs. heavy REE) (Fig. 11). Therefore, igneous rocks of the Lake Mead field should have REE and Sc abundances indicative of the original unaltered rock. Models that use these elements realistically constrain evolutionary trends and are probably not affected by secondary processes.

DIFFERENTIATION MODELS

Introduction

We evaluate open-magma system evolutionary paths for the River Mountains and Hoover Dam volcanics and Wilson Ridge pluton using both Rayleigh fractionation and magma mixing.

Major elements were modeled by using the program XLFRAC (Stormer and Nicholls, 1978). XLFRAC solves a series of linear least-squares mass-balance equations to determine the proportions of added or subtracted phases required to produce a fractionated rock from a given parent. Distribution coefficients for basalts and rhyolites are average values reported in Arth (1976). Mineral compositions used in models are from Deer and

others (1972) and Thompson (1985) (Table 4). Mineral analyses from Thompson are from andesites and dacites of the Hamblin-Cleopatra volcano. These mineral analyses were used for major-element models, because the rocks of the Hamblin-Cleopatra volcano are petrographically and chemically similar to volcanic rocks of the Lake Mead field. Also, the Hamblin-Cleopatra volcano is temporally and spatially related to igneous rocks of the Lake Mead field (Weber and Smith, 1987).

Parent rocks

Our major- and trace-element open-system mixing models use compositions of basalt from the northern River Mountains (218) and high-silica granite of the Wilson Ridge pluton (WR57 and WR59) as parental compositions. The basalt and high-silica granites were chosen because they are the most mafic and felsic rocks, respectively, in the Lake Mead area, and lack obvious mixing textures. Also, basalt is similar in mineralogy to basalt inclusions within dikes that cut the Wilson Ridge pluton.

River Mountains

Six models provided reasonable matches between the observed and calculated compositions of differentiated andesitic magma (Table 3). Because many samples showed evidence of K-metasomatism and/or alteration, models were accepted if the value of the sum of squares of the residuals (r) was less than 10. Models 10 to 15 involve both mixing of Wilson Ridge granite and fractionation to produce andesite from basalt. Fractionation of plagioclase and clinopyroxene as well as mixing are required in models 10–12. Models 14 and 15 involve olivine, clinopyroxene, and plagioclase, as well as the addition of Wilson Ridge granite. Note that fractionation alone produces unacceptably high r values (Model 13). Between 20 and 58 percent fractionation is required by models that involve mixing, whereas 52 percent fractionation is required without mixing. R values (mass mixed-component/mass crystallizing phase) vary between 0.76 and 2.24.

Three models provided reasonable matches for the evolution of dacite from andesite. Models 1 and 2 require 41 percent fractionation of hornblende and plagioclase and the addition of 19.8 to 30.1 percent Wilson Ridge magma (WR57 or WR59) (R = 0.48–0.73). Forty-five percent fractionation is required without mixing (model 3). In the Bootleg Wash suite, models 4 and 5, which derive dacite from andesite, require 29 percent fractionation of hornblende and plagioclase and the addition of Wilson Ridge pluton (R = 0.30–0.46). Derivation of dacite from andesite in the Powerline Road section (models 7–9) also requires removal of hornblende and plagioclase (41 to 44 percent) and the addition of Wilson Ridge pluton (R = 0.24–0.69). These models are consistent with modal differences between parent and daughter, except that clinopyroxene is a phase in the andesite (1 percent), but in models that include clinopyroxene as a fractionating phase, XLFRAC requires that it be added to, not subtracted from, the andesite to form dacite.

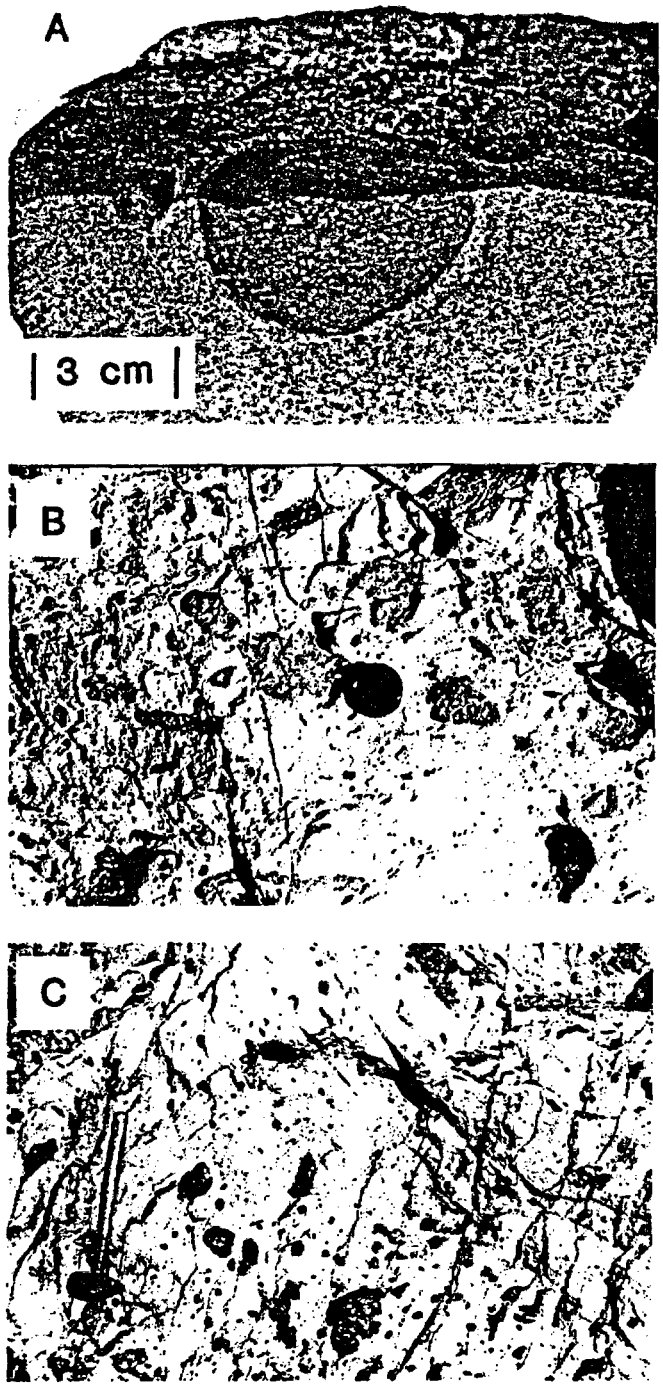

Figure 6. Basalt inclusions in Boulder Wash dacite flows and dikes within the Wilson Ridge pluton (Naumann, 1987). A: Cut surface of an ellipsoidal basalt inclusion in dacite showing fine-grained rim and coarser-grained core. B: Ellipsoidal basalt inclusions in dacite dikes within the Wilson Ridge pluton. C: Basalt inclusion with crenulate margins in a Boulder Wash dacite flow.

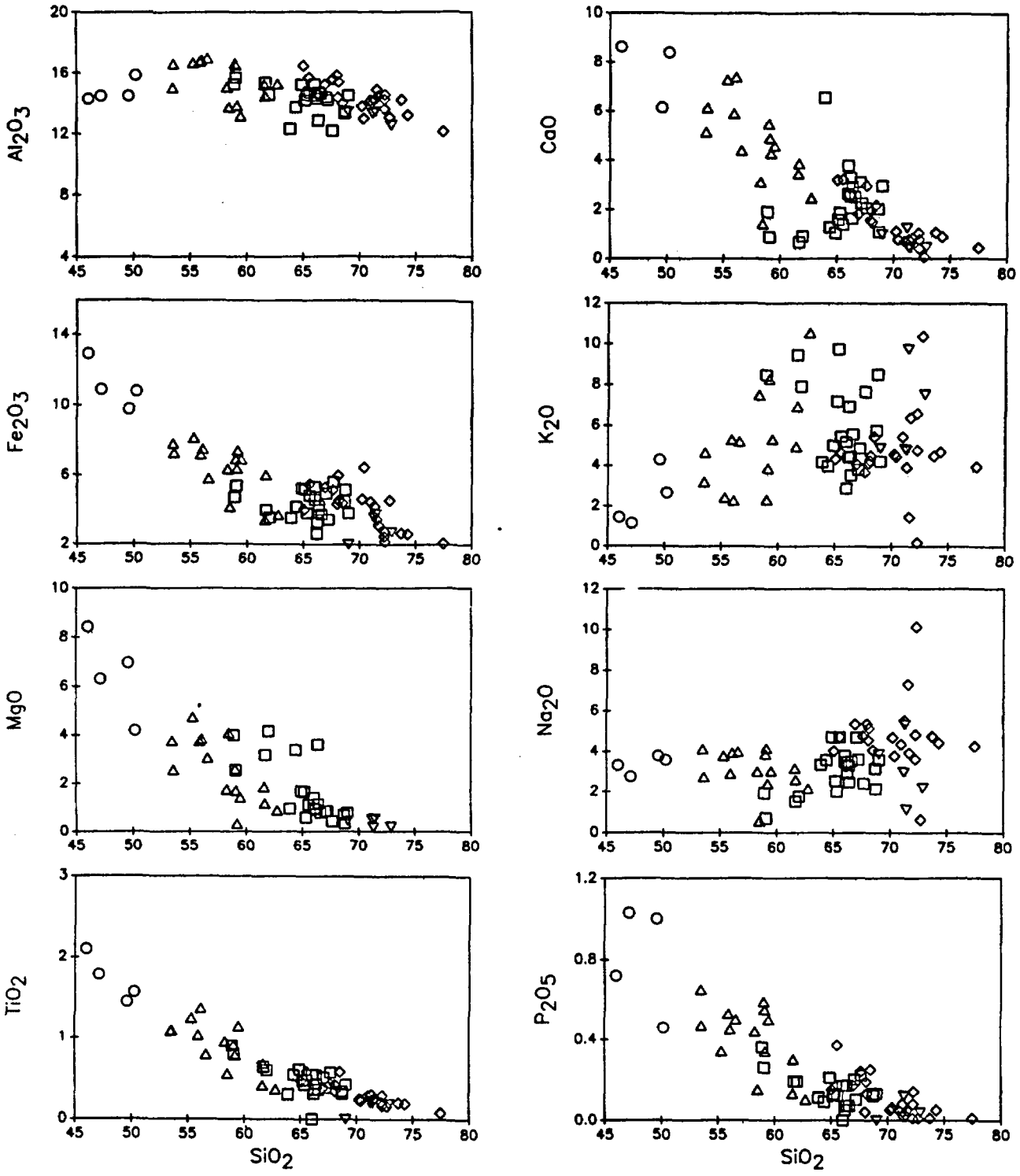

Figure 7 (this and facing page). Harker variation diagrams for volcanic and plutonic rocks of the Lake Mead field. Concentrations of oxides are in weight percent and elements in parts per million. Triangle = andesite, diamond = granite, circle = basalt, downward-pointing triangle = rhyolite, box = dacite.

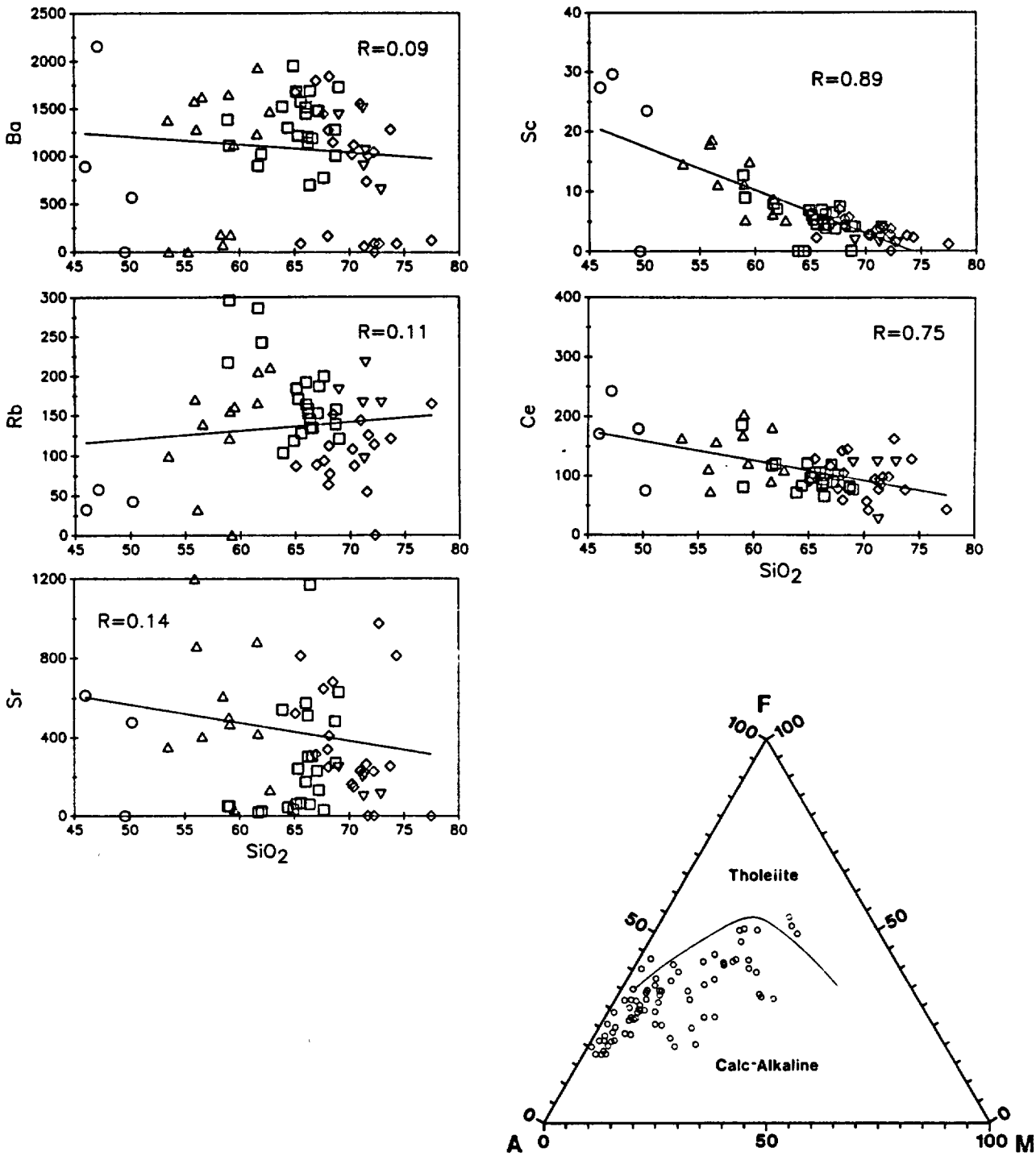

Figure 8. Volcanic and plutonic rocks of the Lake Mead field are calc-alkalic based on an AFM plot. The boundary line between tholeiitic and calc-alkalic fields is from Irvine and Baragar (1971).

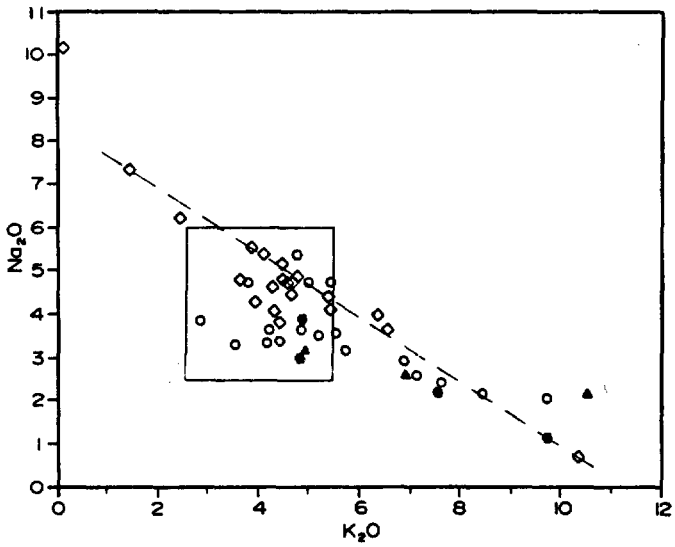

Figure 9. Na_2O vs. K_2O plot for volcanic and plutonic rocks of the Lake Mead field with $SiO_2 > 60$ percent. Rocks with "normal" alkali (Na_2O and K_2O) contents should fall within the box. The box was constructed from chemical data for unaltered rocks with $SiO_2 > 60$ percent listed in Carmichael and others (1974). The dashed line represents a possible metasomatic mixing line between rocks with high K and rocks with high Na. Filled upward-pointing triangles = andesite, circles = dacite, diamonds = granite, and filled hexagons = rhyolite.

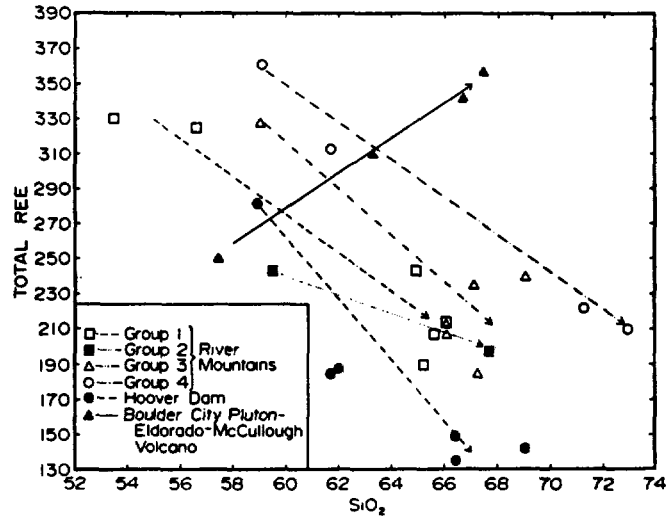

Figure 10. Total REE (La, Ce, Nd, Sm, Eu, Tb, Yb, Lu) vs. SiO_2 plot for volcanic rocks of the River Mountains and Hoover Dam. Each of the four episodes of andesite-dacite volcanism in the River Mountains was accompanied by a decrease in total REE content. Volcanic rocks in the Hoover Dam area also show a negative correlation between total REE content and SiO_2. For comparison, igneous rocks of the McCullough–Eldorado–Boulder City area display a positive correlation between total REE content and SiO_2 concentration.

Hoover Dam

No fractionation or mixing models were successful in modeling the range of compositions observed within the Hoover Dam Tuff or between andesite and dacite flows. Even though extreme K-metasomatism contributes to the large errors, the lack of success of these models cannot be attributed entirely to the effect of this alteration. Trace-element models (discussed below) suggest that processes other than fractional crystallization may be responsible for the observed compositional range in the tuff. The differentiation path between dacite representing the most evolved part of the tuff of Hoover Dam and Sugarloaf dacite were successfully modeled by fractionation of plagioclase, biotite, and hornblende (F = 0.23) (Model 21, Table 3).

Wilson Ridge

We tested two evolutionary paths using XLFRAC for the Wilson Ridge pluton. First, we evaluated the possibility that diorite (57d) was produced by fractionation of plagioclase, olivine, and clinopyroxene from basalt (218) and the addition of Wilson Ridge granite. About 30 percent fractionation is required with mixing (R = 1.04). Second, we evaluated the derivation of Wilson Ridge granite (WR33) from diorite (57d). Models involving mixing provided the best fit but required the subtraction of quartz, a requirement that is not supported by rock modes. Fractionation of hornblende, biotite, orthoclase, and quartz from diorite to form granite without mixing provides a model that agrees with the modal difference between rock types (Model 16, Table 3).

Trace-element models

Models derived from the major elements were refined by use of REE and Sc. If magma mixing is an important differentiation process, samples will fall on a hyperbolic curve on a ratio-ratio plot and on linear trends on companion plots (plots of the ratios of the denominators against one of the original ratios; Langmuir and others, 1978). In addition, each sample should maintain its position relative to adjacent samples regardless of the elements plotted. End-member compositions can be approximated on ratio-ratio plots because the hyperbola will become asymptotic to the X and Y coordinates at ratios that approximate the elemental ratios of the end members (Langmuir and others, 1978). Differentiation processes were evaluated using the trace elements La, Sc, Ce, and Yb.

Samples from the River Mountains, Hoover Dam, and Boulder Wash plot close to a hyperbolic mixing curve on a Ce/Yb-La/Sc plot (Fig. 12), calculated by using two widely separated points (218-basalt and 226-dacite) and applying the equations in Langmuir and others (1978). The hyperbolic trend on this diagram is suggestive of magma mixing, but data scatter indicates that other processes such as fractionation are involved in magmatic evolution. For example, crystal fractionation may ex-

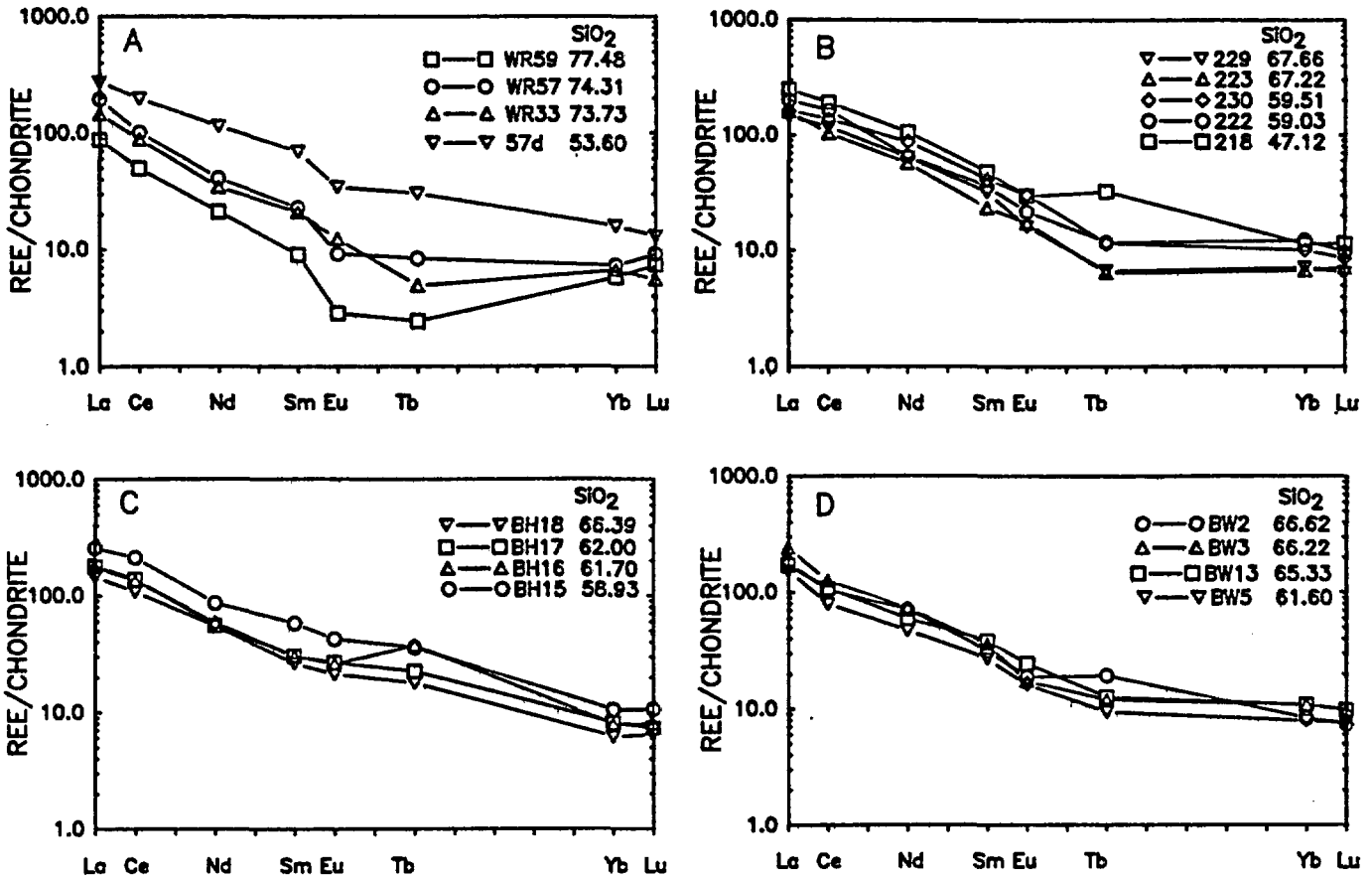

Figure 11. Chondrite normalized REE plots for volcanic and plutonic rocks of the Lake Mead field. A: Wilson Ridge pluton. B: River Mountains. C: Tuff of Hoover Dam. D: Boulder Wash. Note that REE contents in general decrease with increasing SiO_2.

plain higher Ce/Yb than predicted by the mixing line, because fractional crystallization of observed phases results in lower bulk distribution coefficients for Ce than for Yb.

To evaluate the relative importance of mixing and fractionation, Ce and Yb were modeled using Rayleigh fractionation and techniques that determine the change of the concentration of an element as a system undergoes concurrent mixing and fractionation (Depaulo, 1981; Thompson and others, 1986). This element pair was chosen because distribution coefficients are readily available (Arth, 1976). Each area within the Lake Mead field was considered separately. Major-element models were refined to account for the presence of sphene (<1 percent) in the mode of most andesites, dacites, and granites. Bulk distribution coefficients used for each model were calculated using proportions of phenocryst phases determined from the major-element models (Table 3).

For the River Mountains, samples fall on a crude linear trend between basalt (218) and high-silica granite (WR57) (Fig. 13). Note that andesite end members of each River Mountain suite fall below a mixing curve drawn between 218 and WR57; dacite end members fall above or just below this curve. We first evaluated models that derive the andesites from basalt (218). Neither fractionation nor mixing models alone predict the Ce/Yb ratio of the andesites. Evolution paths calculated using the equations of DePaulo (1981) radiate from the basalt end member and were calculated by assuming certain values of R (mass of mixed component/mass of crystallized component) and allowing F (mass of magma/initial mass of magma) to vary. The evolution paths for R = 1.5 provide the best fit to the differentation path between basalt (218) and andesite (226 and 222). R = 1.5 to 2.0 is required to match the differentiation path from basalt (218) to Bootleg Wash andesite (230). These values agree well with R values of 0.76 to 2.12 predicted by major-element models (Table 3).

Models deriving the River Mountain and Powerline Road dacites (227 and 223) from andesites 226 and 222, respectively, indicate that R = 0.6 for the River Mountain section and 0,9 for the Powerline Road section (Fig. 13). These values are similar to those predicted by the major-element models. The Bootleg Wash differentiation path shows a sharp increase in Ce/Yb. The evolution path calculated using Rayleigh fractionation models is essentially identical to the differentiation path, suggesting that the

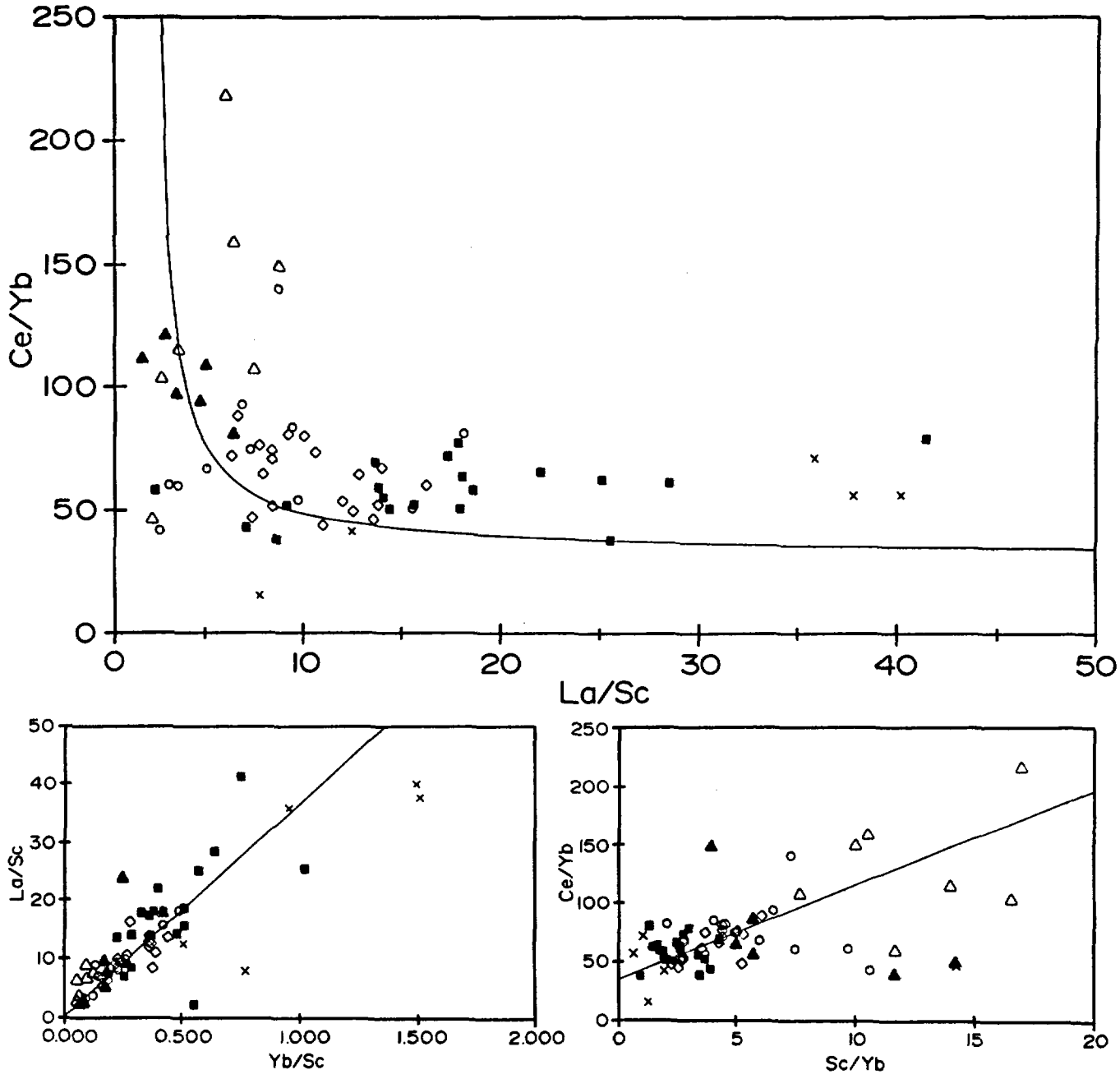

Figure 12. Ce/Yb vs. La/Sc plot and companion plots for igneous rocks of the Lake Mead field. Circle = andesite, X = rhyolite, open triangle = basalt, filled triangle = diorite, diamond = dacite, and filled box = granite.

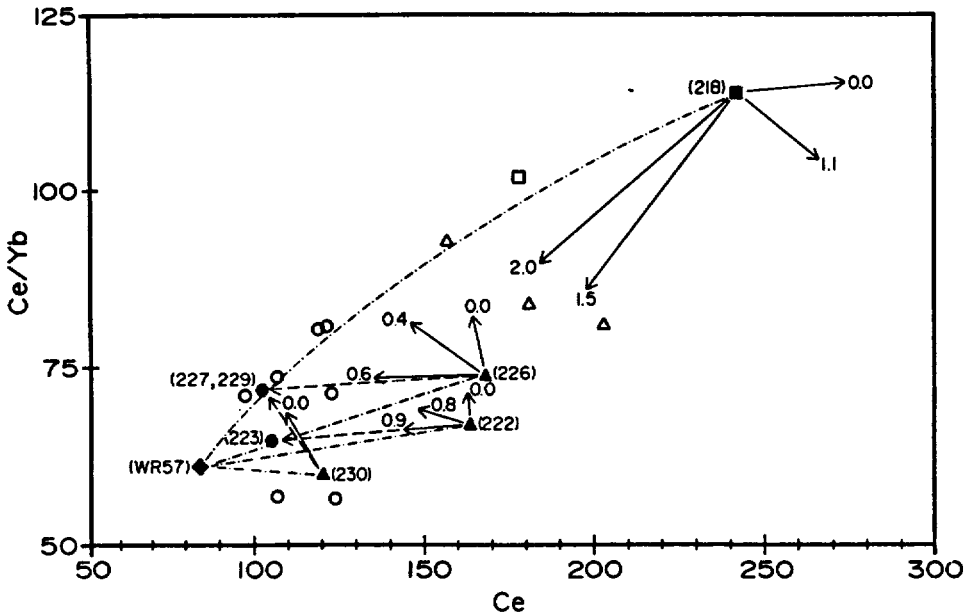

Figure 13. Observed and model differentiation paths for the River Mountains plotted on a Ce/Yb vs. Ce diagram. Filled symbols are rocks used in models. Open symbols represent other specimens. Square = basalt, diamond = Wilson Ridge pluton specimen WR57, triangles = andesites, circles = dacite. Dash-dot curves are two-component mixing curves calculated by using the equations in Langmuir and others (1978). Dashed lines are observed differentiation paths. Solid lines with arrows are differentiation paths calculated using the equations of DePaulo (1981). The number at the tip of each arrow is the R value for each model (R = mass of mixed component/mass crystallizing phase).

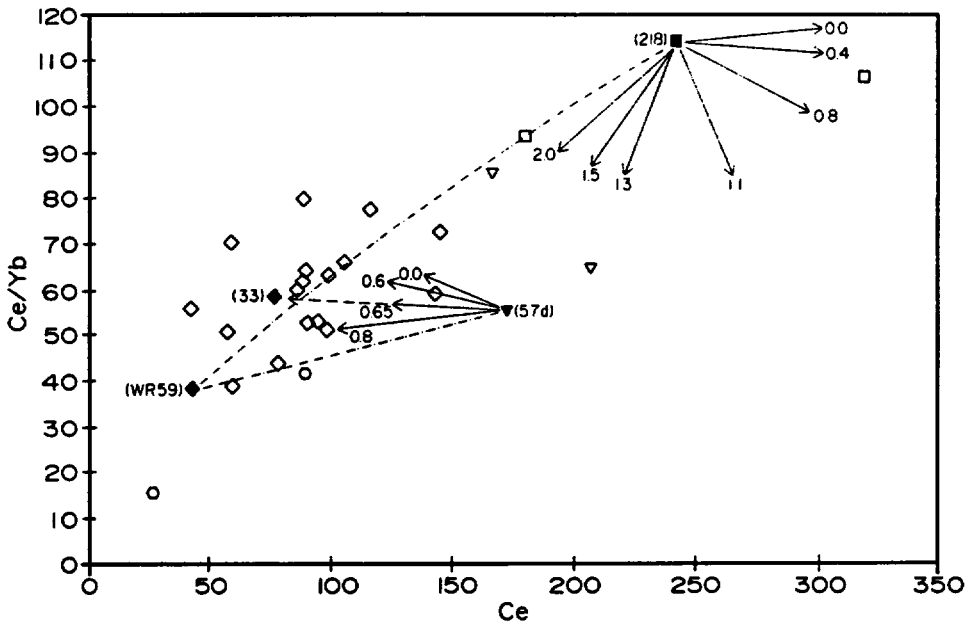

Figure 14. Observed and model differentiation paths for the Wilson Ridge pluton plotted on a Ce/Yb vs. Ce diagram. Filled symbols are rocks used in models. Open symbols represent other specimens. Diamonds = granite, downward-pointing triangles = diorite. Other symbols are defined in the caption to Figure 13.

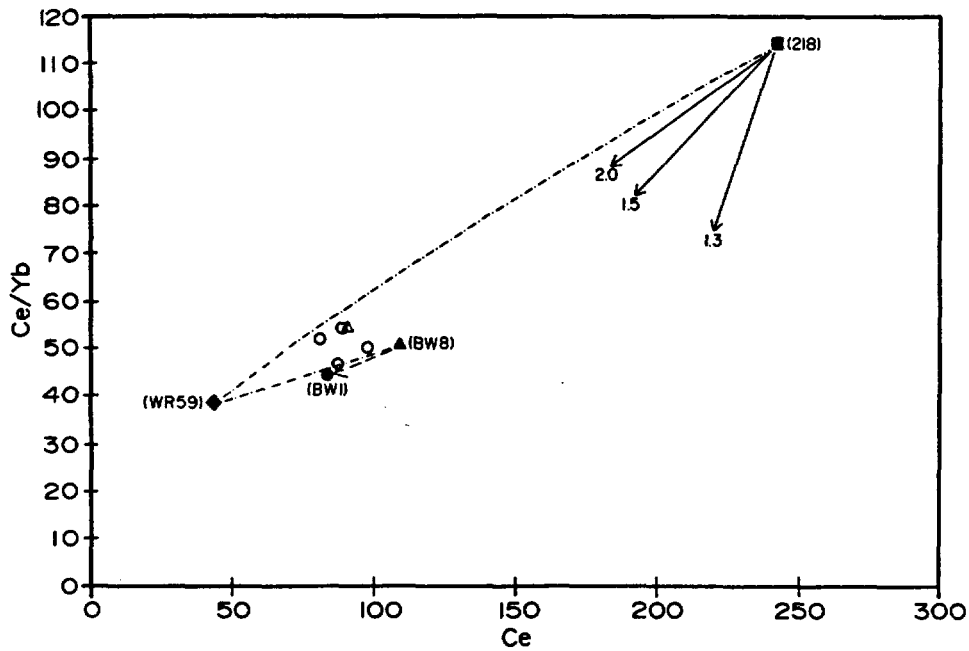

Figure 15. Observed and model differentiation paths for the Boulder Wash area plotted on a Ce/Yb vs. Ce diagram. Filled symbols are rocks used in models. Open symbols represent other specimens. Symbols and lines are defined in the caption to Figure 13.

dacite formed by 34 percent fractionation of hornblende, plagioclase, and sphene from andesite (230).

Models for the Wilson Ridge pluton suggest that diorite (57d) can be derived by 30 percent fractionation of clinopyoxene and plagioclase from basalt magma having the composition of sample 218 and mixing with high-silica granite (WR59) (R = 1.5) (Fig. 14). Modeling suggests that granite represented by sample WR33 may be produced from diorite (sample 57d) by 40 percent fractionation and mixing with high-silica granite (R = 0.65). Models for the Wilson Ridge pluton and related volcanic rocks in the Boulder Wash area produce similar results, except that mixing alone may have formed the Boulder Wash dacites (Fig. 15).

Rayleigh fractionation was unsuccessful in modeling the compositional variation observed within the tuff of Hoover Dam. Evolution paths trended toward higher Ce/Yb and higher Ce. Successful models involving fractionation and mixing with high-silica granite magma (WR57) (R = 0.8) were only obtained by using sphene as a fractionated phase. Sphene is not found in the mode, so these models are invalid. On the other hand, because both andesite and dacite of the tuff fall close to the mixing line, mixing of high-silica magma with andesite may be the dominant differentiation process. Other differentiation processes such as Soret diffusion (Hildreth, 1981) may also be operating. A more detailed study of the tuff of Hoover Dam is required to resolve problems regarding its evolution.

Summary

Magma evolution in the Lake Mead field was complex and probably involved episodic and/or coeval fractional crystallization, magma mixing, crustal assimilation, and partial melting. Models based on trace element confirm that concurrent and/or episodic mixing and fractionation are the dominant differentiation processes. Open-system models provide estimates of the relative importance of the two processes and suggest that mixing was more important in the derivation of the andesites and diorites (R = 0.8 to 2.2) than in the formation of dacite, quartz monzonite, or granite (R = 0.1 to 0.65).

PRODUCTION OF INTERMEDIATE COMPOSITION IGNEOUS ROCKS IN AN EXTENSIONAL ENVIRONMENT

Lipman and others (1972) and Christiansen and Lipman (1972) suggested that the change from calc-alkalic intermediate volcanism to a bimodal rhyolite-basalt suite marked the change from regional compression to extension. Even though bimodal suites form during periods of extension in the Basin and Range province (e.g., Suneson and Lucchitta, 1983), recent work suggests that volcanism before and during the main pulses of extension is mainly calc-alkalic or alkalic-calcic with basaltic-andesite, andesite, and dacite predominating (Eaton, 1982; Anderson,

1973; Elston and Bornhorst, 1979; Smith, 1982; Otton, 1982). The tectonic transition between regional compression and extension may pass without affecting the nature of magmatic activity. Our observations suggest that the combined effect of mixing of basalt and granite parental magmas and crystal fractionation results in magma compositions with many of the characteristics of a calc-alkalic or alkalic-calcic suite (Fig. 8) formed during plate convergence. In the Lake Mead area, basalt and high-silica granite (rhyolite) are inferred to be parental magmas, so, if mixing was prevented, a bimodal suite may have resulted. The occurrence of a bimodal suite may therefore be more a function of the tectonic "state" of the crust rather than some primary petrogenetic process. If fractures dip steeply and penetrate to deep levels of the crust, magma may rise to the surface along these zones of weakness without mixing, and bimodal or dominantly basaltic volcanism may predominate. Alternately, if extension results in shallow faults (e.g., detachment structures), magma may rise until encountering a low-angle fault zone, where it may spread laterally and accumulate. In this structural scenario, the opportunity for magma mixing may be high, and intermediate volcanism may predominate.

In the Lake Mead field, basalt and high-silica granite (rhyolite) mixed to produce intermediate calc-alkalic igneous rocks prior to detachment faulting (20 to 13.4 Ma), but did not erupt until 4 to 12 Ma, when deeply penetrating high-angle faults tapped unmixed magma (Smith and others, 1987; Feuerbach and Smith, 1987). Basaltic volcanism occurred mainly in the northern River Mountains, in the Fortification Hill area, and to the southeast of Hoover Dam (Campbell and Schenk, 1950; Anderson, 1973; Feuerbach and Smith, 1987). Therefore, in the Lake Mead field, there was a delay of as long as 8 m.y. between the initial generation of bimodal magmas and bimodal volcanism. The transition from calc-alkalic to dominantly basaltic volcanism in the Lake Mead area reflects a change in structural style during regional extension, and not a fundamental change from regional compression to extension.

ACKNOWLEDGMENTS

We thank the staff of the Phoenix Memorial Laboratory, University of Michigan for completing the REE analyses. Financial support by the Department of Energy to the Phoenix Memorial Laboratory through the University Research Reactor Assistance Program and Reactor Facility Cost Sharing Program made this work possible. Much of our mapping covered areas studied earlier by R. E. Anderson and C. E. Longwell. We especially thank R. E. Anderson for his continuing help and encouragement of our studies in the Lake Mead area. R. Cullers, R. E. Anderson, and R. Scott provided helpful reviews. We thank Allen Glazner for providing us with a manuscript based on a thesis by R. Turner describing magma mixing in a mid-Tertiary volcanic section in the Castle Mountains, California. Their work provided the stimulus for our evaluation of the importance of mixing process in the petrogenesis of the volcanic and plutonic rocks of the Lake Mead field.

TABLE 1. MODAL COMPOSITIONS OF REPRESENTATIVE PHENOCRYSTS OF VOLCANIC ROCKS AND MODAL COMPOSITIONS OF PLUTONIC ROCKS, LAKE MEAD VOLCANIC FIELD

	Number of Specimens	Quartz	Plag.	Microcline	Kspar	Biotite	Hn	Cpx	Ol	Ap	Zircon	Sphene	Opaque	Matrix
Hoover Dam volcanic rocks (Mills, 1985)														
Tuff of Hoover Dam														
Top	3	-	31	-	-	7	2	tr	-	-	-	-	-	54
Base	2	-	26	-	-	3	-	2	-	-	-	-	-	63
Switchyard Basalt	3	-	5-15	-	-	-	-	3-5	-	-	-	-	-	80-92
Arch Rock Dacite	2	-	5-15	-	-	3	1-2	-	-	-	-	-	-	80-91
Surgarloaf Dacite	2	-	3-15	-	-	2-4	2	-	-	-	-	-	-	79-93
Wilson Ridge Pluton (Feuerbach, 1986)														
Quartz Monzonite (WR57)	1	17	41	8	22	7	3	-	-	tr	tr	tr	tr	-
Red-feldspar Granite	2	26	34	2	32	4	-	-	-	tr	tr	tr	2	-
Diorite (33d)	1	1	30	-	4	7	1	-	-	tr	tr	1	2	-
Granite (WR59)	1	49	24	2	22	1	-	-	-	-	-	-	tr	-
Diorite (57d)	1	-	61	-	4	10	23	-	-	tr	tr	tr	2	-
Boulder Wash volcanic rocks (Naumann, 1987)														
Dacite (BW1)	1	5	24	-	-	6	-	-	-	tr	-	tr	1	64
Andesite (BW6)	1	tr	31	-	1	-	-	14	4	tr	-	-	-	50
River Mountains igneous rocks (Smith, unpublished data)														
River Mountains stock	5	18	22	-	-	8	2	-	-	-	-	-	5	45
River Mountains dacite	18	-	35	-	-	2	-	-	-	tr	-	tr	1	62
River Mountains andesite	13	-	35	-	-	-	3	-	-	-	-	tr	1	61
Bootleg Wash dacite	5	tr	30	-	-	9	-	-	-	-	-	1	tr	60
Powerline Rd dacite	24	-	37	-	-	15	5	-	-	-	-	-	tr	55
Powerline Rd basalt (218)	1	-	5	-	-	-	-	10	2	-	-	-	tr	83

Notes: The top of the tuff of Hoover dam contains 4% andesite and basalt xenoliths, and base 6%. Modes are average values. Hn = hornblende, cpx = clinopyroxene, ol = olivine, ap = apatite, Kspar = K-feldspar, and tr = trace. Point counts based on at least 500 points per slide.

TABLE 2. CHEMICAL ANALYSES OF REPRESENTATIVE VOLCANIC AND PLUTONIC ROCKS FROM THE LAKE MEAD VOLCANIC FIELD

	Hoover Dam Volcanics				Hoover Dam Tuff			
Oxide	DHD 84-3	DHD 84-4	AHD 84-2	AHD 84-5	THD BH-15	THD BH-16	THD BH-17	THD BH-18
SiO_2	66.4	69.0	55.9	56.1	58.9	61.7	62.0	66.4
Al_2O_3	14.7	14.5	16.7	16.8	15.2	15.4	14.6	12.9
Fe_2O_3	4.2	3.8	7.2	7.5	4.7	4.0	3.6	4.0
CaO	2.9	3.0	5.9	7.4	1.9	0.7	0.9	1.6
MgO	1.1	0.8	3.7	3.8	4.0	3.2	4.2	3.6
Na_2O	3.3	3.6	2.9	3.9	1.9	1.5	1.8	2.5
K_2O	3.6	4.2	5.3	2.3	8.5	9.4	7.9	4.5
TiO_2	0.4	0.4	1.0	1.4	0.9	0.6	0.6	0.5
MnO	0.1	0.0	0.2	0.1	0.1	0.3	0.1	0.1
P_2O_5	0.1	0.1	0.5	0.5	0.4	0.2	0.2	0.2
LOI	3.4	0.5	1.2	0.8	2.4	2.6	2.4	1.7
Total	100.8	100.3	100.9	100.8	99.2	99.6	99.4	98.1
Trace elements in ppm								
La	62.7	56.0	54.9	47.5	84.4	58.1	59.2	47.9
Ce	66.1	77.9	111.3	73.6	185.8	117.4	120.9	94.3
Nd	33.6	30.5	29.7	13.2	51.6	35.5	33.3	32.8
Sm	4.9	7.2	4.5	1.3	10.4	5.5	5.5	4.8
Eu	1.0	1.0	2.0	1.7	2.9	1.8	1.9	1.5
Tb	0.8	1.0	4.4	3.4	1.7	1.8	1.1	0.8
Yb	1.1	1.5	1.8	1.8	2.1	1.6	1.6	1.2
Lu	0.3	0.4	0.3	0.2	0.4	0.3	0.3	0.2
U	14.9	7.8	12.1	22.5	4.6	3.6	3.0	2.6
Th	13.5	15.3	11.3	6.9	19.8	17.0	16.3	12.8
Hf	4.2	4.6	5.8	5.2	8.1	5.8	6.5	5.1
Ba	1690	1730	1580	1280	1384	901	1024	699
Rb	134	121	170	32	217	296	242	145
Sr	1170	630	1200	860	50	18	24	59
Ta	1.2	1.2	1.1	1.4	1.3	1.2	1.3	1.0
Sc	3.9	4.1	17.9	18.6	12.7	7.9	7.1	6.2

Major elements in weight percent.
Total iron as Fe_2O_3
AHD = Hoover Dam andesite
DHD = Hoover Dam dacite
s = Specimen used in models

NA = not analyzed or not detected.
THD = Tuff of Hoover Dam

TABLE 2. CHEMICAL ANALYSES OF REPRESENTATIVE VOLCANIC AND PLUTONIC ROCKS FROM THE LAKE MEAD VOLCANIC FIELD (continued)

	Wilson Ridge Pluton				s									
Oxide	GWR WR368	GWR WR46	GWR WR53	GWR WR55	GWR WR57	GWR WR58	GWR WR62	GWR WR63	GWR WR67	GWR WR56	GWR WR71	GWR WR65	GWR WR72	GWR WR36
SiO_2	68.2	68.5	72.3	68.1	74.3	67.0	70.2	71.3	72.7	65.6	71.7	71.3	71.6	71.0
Al_2O_3	15.4	14.0	14.6	14.4	13.2	15.2	13.8	14.2	13.1	15.7	14.4	14.2	14.9	14.2
Fe_2O_3	4.6	4.4	2.8	6.0	2.6	5.3	4.7	4.2	4.6	5.5	3.1	3.6	3.5	4.5
CaO	1.5	2.2	0.4	2.0	0.9	1.8	1.1	0.8	0.1	3.2	0.8	0.5	0.7	0.7
MgO	1.0	1.1	0.6	1.0	0.4	0.9	0.5	1.0	0.2	1.5	0.3	0.2	0.7	0.6
Na_2O	5.2	4.1	10.1	4.6	4.4	5.4	4.7	5.5	0.6	4.7	3.9	5.3	7.3	4.4
K_2O	4.5	5.5	0.2	4.3	4.7	4.1	4.6	3.9	10.4	4.7	6.4	4.8	1.5	5.4
TiO_2	0.4	0.6	0.3	0.3	0.2	0.4	0.2	0.3	0.2	0.6	0.3	0.2	0.3	0.3
MnO	0.0	0.1	0.0	0.0	0.0	0.0	0.0	0.0	0.0	0.0	0.0	0.0	0.0	0.0
P_2O_5	0.1	0.3	0.1	0.2	0.1	0.2	0.1	0.1	0.0	0.4	0.1	0.0	0.0	0.1
LOI	0.1	0.2	0.4	0.1	0.1	0.0	0.0	0.7	0.3	0.2	1.1	0.2	0.7	0.1
Total	101.0	100.8	101.7	101,0	100.9	100.3	99.9	102.0	102.1	102.1	102.1	100.3	101.1	101.2
Trace elements in ppm														
La	88.9	97.9	66.7	46.6	64.2	80.9	48.2	49.7	62.6	64.2	58.3	17.4	54.0	55.8
Ce	105.7	145.8	90.3	59.8	88.6	117.0	57.6	59.3	89.8	88.6	98.6	26.7	89.8	95.4
Nd	41.0	61.0	21.2	26.2	24.4	34.2	19.0	18.3	25.1	24.4	37.9	10.5	18.7	38.1
Sm	6.5	8.6	4.4	4.7	4.1	6.5	3.4	4.0	4.4	4.1	5.6	2.1	4.5	5.0
Eu	1.4	1.6	0.8	1.0	0.6	1.3	0.7	0.8	0.7	0.6	1.1	0.4	1.0	1.0
Tb	0.5	1.1	0.5	0.4	0.4	0.5	0.9	0.8	0.3	0.4	0.5	0.3	0.4	0.4
Yb	1.5	2.0	1.4	1.6	1.4	1.5	1.1	0.9	1.1	1.4	1.9	1.7	1.5	1.8
Lu	0.4	0.4	0.3	0.3	0.3	0.3	0.2	0.3	0.2	0.3	0.3	0.3	0.3	0.2
U	16.9	15.2	17.2	11.1	18.8	11.9	10.3	11.3	20.5	18.8	1.6	2.4	0.8	2.4
Th	20.1	18,9	16.8	11.7	21.0	15.4	16.3	17.2	19.1	21.0	16.0	17.2	12.2	16.9
Hf	5.9	8.1	5,4	4.8	4.9	5.5	3.6	5.3	4.1	4.9	4.9	5.5	4.3	4.9
Ba	1840	1146	1989	1274	811	1796	1021	1702	975	811	1008	903	736	1554
Rb	77	151	NA	112	129	89	108	78	164	129	125	96	54	143
Sr	410	680	NA	249	NA	314	163	NA	NA	NA	NA	99	264	230
Ta	1.7	1.9	1.4	1.3	2.2	1.4	1.5	1.5	1.3	2.2	1.5	1.2	1.1	1.4
Sc	4.0	5.7	3.7	5.4	2.3	4.5	2.7	3.6	1.5	2.3	4.1	2.2	3.9	3.6

Major elements in weight percent.
Total iron as Fe_2O_3.
AHD = Hoover Dam andesite.
DHD = Hoover Dam dacite.
s = Specimen used in models.
NA = not analyzed or not detected.
THD = Tuff of Hoover Dam
GWR = Wilson Ridge granite or quartz monzonite
DWR = Wilson Ridge diorite

TABLE 2. CHEMICAL ANALYSES OF REPRESENTATIVE VOLCANIC AND PLUTONIC ROCKS FROM THE LAKE MEAD VOLCANIC FIELD (continued)

	Wilson Ridge Pluton		s	s					s			
Oxide	GWR WR57	GWR WR67	GWR WR33	GWR WR59	GWR WR106	GWR WR114	GWR WR120	DWR WR74	DWR 57d	DWR 39d	DWR WR107	GWR WR121
SiO_2	67.6	71.5	73.7	77.5	68.0	72.2	65.1	59.7	53.6	57.0	55.9	53.3
Al_2O_3	15.6	13.4	14.2	12.1	15.8	14.3	16.5	19.1	15.4	15.6	17.4	17.6
Fe_2O_3	5.2	3.8	2.7	2.1	4.4	2.5	4.0	6.2	8.9	6.6	6.4	7.6
CaO	3.0	0.4	1.1	0.4	1.6	1.0	3.2	4.7	5.5	6.7	4.2	6.7
MgO	1.2	0.6	0.6	0.1	1.0	0.5	1.5	1.7	4.5	6.5	2.8	3.5
Na_2O	4.8	1.1	4.8	4.3	5.4	3.6	4.0	6.1	4.6	4.7	5.2	3.7
K_2O	3.7	9.7	4.5	4.0	4.1	6.6	4.4	2.6	3.0	2.2	4.2	3.3
TiO_2	0.4	0.2	0.2	0.1	0.4	0.2	0.5	0.7	1.1	0.7	0.8	1.4
MnO	0.0	0.0	0.0	0.0	0.0	0.0	0.1	0.1	0.2	0.1	0.1	0.1
P_2O_5	0.2	0.1	0.0	0.0	0.0	0.0	0.2	0.2	0.8	0.3	0.5	0.4
LOI	0.0	0.6	0.3	0.2	0.4	0.2	0.2	.0.4	1.8	1.5	1.6	0.4
Total	101.8	101.5	102.0	100.7	101.2	101.2	99.5	101.4	99.4	101.8	99.0	98.0
Trace elements in ppm												
La	49.7	51.9	47.9	28.8	10.3	69.8	58.6	206.5	90.5	50.3	105.0	54.0
Ce	79.0	89.5	77.1	43.6	143.2	99.2	91.2	328.1	173.2	79.0	167.1	76.4
Nd	31.9	35.2	20.5	12.6	43.4	24.5	38.1	101.0	68.2	39.0	52.7	NA
Sm	5.9	5.1	3.8	1.6	0.8	4.5	6.1	13.6	12.5	7.3	11.2	8.4
Eu	1.4	1.0	0.8	0.2	1.6	0.9	1.4	3.5	2.4	2.0	2.6	2.1
Tb	0.5	0.5	0.2	0.1	0.5	0.4	0.7	1.3	1.4	1.2	1.3	1.1
Yb	1.8	2.1	1.3	1.2	2.4	1.6	1.7	2.2	3.1	1.6	2.0	2.0
Lu	0.3	0.3	0.2	0.3	0.0	0.3	0.3	0.3	0.4	0.2	0.3	0.4
U	1.4	2.2	1.9	4.2	0.2	2.1	1.0	NA	2.4	NA	2.0	1.0
Th	10.0	13.7	13.5	25.1	18.9	18.9	8.8	17.0	14.4	4.5	11.0	7.0
Hf	5.1	4.6	4.3	3.3	7.7	5.2	5.0	10.4	7.8	4.0	6.0	5.0
Ba	1448	1063	1281	123	166	1045	1679	2830	1339	1055	1883	1632
Rb	93	217	121	164	64	113	87	63	126	77	70	54
Sr	646	212	254	NA	339	227	524	1660	415	778	663	505
Ta	1.3	1.2	1.1	1.7	1.4	1.3	1.0	0.9	1.8	0.6	0.9	1.3
Sc	7.1	4.2	2.6	1.1	4.4	2.8	6.4	8.7	17.9	22.7	11.1	22.7

Major elements in weight percent.
Total iron as Fe_2O_3.
AHD = Hoover Dam andesite.
DHD = Hoover Dam dacite.
s = Specimen used in models.
NA = not analyzed or not detected.
THD = Tuff of Hoover Dam.
GWR = Wilson Ridge granite or quartz monzonite.
DWR = Wilson Ridge diorite.

TABLE 2. CHEMICAL ANALYSES OF REPRESENTATIVE VOLCANIC AND PLUTONIC ROCKS FROM THE LAKE MEAD VOLCANIC FIELD (continued)

River Mountains																
	s			s						s	s	s	s			
Oxide	PB 218	PB 219	DP 220	DP 223	DP 271	RP 348	RP 349	AP 346	AP 347	AP 222	DB 229	AB 230	AB 226	MR 231	DR 229	DR 272
SiO_2	47.1	46.0	67.1	67.2	66.0	72.9	71.2	59.1	61.7	59.0	67.7	59.5	53.5	64.9	65.2	56.6
Al_2O_3	14.5	14.3	14.4	14.2	14.5	12.6	13.3	16.5	14.5	16.6	12.2	13.1	15.0	15.2	14.2	17.0
Fe_2O_3	10.9	12.9	5.0	3.5	4.6	2.7	1.8	6.4	6.0	6.9	5.6	6.9	7.8	5.3	5.2	5.8
CaO	11.2	8.6	3.1	2.3	3.8	0.5	1.3	4.9	3.9	5.5	2.1	4.6	5.2	1.0	1.6	4.4
MgO	6.3	8.4	0.9	0.9	1.0	0.2	0.5	1.7	1.2	2.6	0.4	1.4	3.8	1.7	1.7	3.0
Na_2O	2.8	3.3	4.7	3.6	3.5	2.2	3.0	4.2	2.6	3.9	2.4	3.0	4.1	4.7	2.5	4.0
K_2O	1.2	1.5	3.8	4.9	5.2	7.5	4.8	3.9	6.9	2.3	7.7	5.3	3.2	5.0	7.2	5.2
TiO_2	1.8	2.1	0.5	0.4	0.5	0.2	0.2	0.9	0.7	0.9	0.6	1.1	1.1	0.6	0.5	0.8
MnO	0.1	0.2	0.1	0.1	0.1	0.0	0.1	0.1	0.1	0.1	0.0	0.1	0.1	0.1	0.1	0.1
P_2O_5	1.0	0.7	0.2	0.1	0.2	0.0	0.0	0.6	0.3	0.6	0.2	0.5	0.7	0.2	0.1	0.5
LOI	2.3	1.7	0.3	3.0	1.0	0.1	4.4	0.2	1.7	1.0	0.8	3.3	4.7	0.8	1.3	1.4
Total	99.2	99.8	100.0	100.0	100.4	99.0	100.8	98.8	99.8	99.4	99.6	98.9	99.1	99.4	99.5	98.8
Trace elements in ppm																
La	107.6	75.9	64.7	52.4	55.0	55.6	59.5	93.5	82.1	81.7	47.7	53.6	74.5	63.0	49.9	75.9
Ce	242.4	170.9	119.3	90.7	105.4	124.5	124.5	203.5	181.5	167.9	102.6	120.3	163.6	121.6	97.6	157.2
Nd	117.7	44.2	41.3	34.2	37.0	22.4	29.1	50.6	37.6	63.3	38.5	56.5	75.5	49.3	35.6	77.9
Sm	15.5	9.1	5.6	4.2	5.6	3.7	4.6	7.5	7.2	8.7	5.8	7.5	10.6	5.6	4.5	9.1
Eu	3.9	2.7	1.4	1.2	1.3	1.0	1.0	1.9	1.9	2.0	1.1	2.1	2.5	1.4	1.1	2.2
Tb	3.0	2.0	0.9	0.3	1.2	0.4	0.4	0.9	0.4	1.5	0.3	0.5	0.7	0.1	0.2	1.1
Yb	2.1	1.7	1.5	1.3	1.6	2.2	2.2	2.5	2.2	2.3	1.4	2.0	2.4	1.5	1.4	1.7
Lu	0.4	0.3	0.3	0.2	0.3	0.3	0.3	0.4	0.3	0.4	0.2	0.3	0.4	0.3	0.3	0.3
U	6.4	8.7	9.9	9.1	7.6	3.9	3.6	2.1	2.0	4.6	3.0	2.6	2.0	NA	1.3	1.3
Th	13.2	7.7	18.5	17.6	15.4	31.2	26.3	19.3	18.6	14.9	14.8	10.8	20.7	14.2	15.8	15.7
Hf	8.1	6.4	4.7	4.8	4.7	4.9	4.5	9.2	6.7	7.3	4.1	5.1	6.6	5.5	4.5	5.8
Ba	2155	891	1484	1477	1517	650	1510	2740	1930	1650	774	1121	1376	1950	1683	1625
Rb	58	33	152	187	163	166	166	155	205	121	199	161	99	118	184	139
Sr	1205	614	230	131	175	110	200	470	420	504	30	33	351	33	60	405
Ta	1.5	1.6	0.9	1.2	1.1	15.3	14.6	15.1	11.1	1.0	1.2	1.1	0.9	1.0	0.9	1.1
Sc	29.6	27.4	6.5	3.8	6.9	1.5	1.5	5.2	8.7	11.2	7.5	14.9	14.6	6.9	5.9	11.0

Major elements in weight percent.
Total iron as Fe_2O_3.
PB = Powerline Road basalt.
DP = Powerline Road dacite.
s = Specimen used in models.
DR = Dacite of the River Mountains stratavolcano.
NA = not analyzed or not detected.
AP = Powerline Road andesite.
DB = Bootleg Wash dacite.
AB = Bootleg Wash andesite.
MR = Quartz monzonite of the River Mountains stock.
AR = Andesite of the River Mountains stratovolcano.

TABLE 2. CHEMICAL ANALYSES OF REPRESENTATIVE VOLCANIC AND PLUTONIC ROCKS FROM THE LAKE MEAD VOLCANIC FIELD (continued)

Boulder Wash											
	s						s				
Oxide	ABW BW5	ABW BW8	ABW BW4	ABW BW10	ABW BW6	BBW BW12	DBW BW1	DBW BW2	DBW BW3	DBW BW13	DBW BW27
SiO_2	61.6	62.8	55.3	53.6	50.2	47.9	66.2	66.6	66.2	65.3	68.8
Al_2O_3	15.2	15.3	16.7	16.6	15.9	16.1	14.3	14.6	14.5	14.5	13.4
Fe_2O_3	3.4	3.7	8.1	7.3	10.8	4.5	3.3	3.8	2.6	3.8	5.2
CaO	3.5	2.5	7.3	6.1	8.4	10.0	3.3	2.5	2.6	1.9	1.1
MgO	1.8	0.9	4.7	2.5	4.2	1.2	0.9	0.8	0.9	0.6	0.3
Na_2O	3.2	2.1	3.8	2.7	3.6	3.4	2.9	3.5	3.4	2.0	2.1
K_2O	5.0	10.5	2.4	4.7	2.7	7.4	6.9	5.6	4.5	9.7	8.5
TiO_2	0.4	0.4	1.2	1.1	1.6	1.1	0.4	0.4	0.3	0.4	0.3
MnO	0.1	0.1	0.1	0.1	0.1	0.2	0.1	0.1	0.1	0.1	0.1
P_2O_5	0.1	0.1	0.3	0.5	0.5	0.4	0.1	0.1	0.1	0.1	0.1
LOI	5.7	1.4	1.7	3.5	0.4	7.5	1.5	0.2	4.3	0.9	0.1
Total	99.9	99.6	101.7	98.6	98.3	99.7	99.8	98.1	99.3	99.3	100.0
Trace elements in ppm											
La	59.3	79.0	NA	NA	50.2	69.3	53.1	54.2	57.6	65.5	34.6
Ce	90.6	109.3	NA	NA	75.3	109.2	84.1	88.7	87.8	98.4	81.5
Nd	42.3	43.5	NA	NA	53.2	40.4	29.7	33.4	29.4	32.0	5.2
Sm	5.7	6.5	NA	NA	8.4	8.4	6.1	5.6	5.3	6.3	1.0
Eu	1.3	1.2	NA	NA	2.1	2.0	1.2	1.2	1.1	1.2	0.4
Tb	0.9	0.6	NA	NA	1.4	1.1	1.0	0.5	0.5	0.4	1.6
Yb	1.7	2.2	NA	NA	1.7	1.8	1.9	1.6	1.9	2.0	0.2
Lu	0.3	0.3	NA	NA	0.4	0.4	0.3	0.3	0.3	0.3	1.8
U	1.1	1.9	NA	NA	1.1	1.4	1.8	2.1	1.5	2.3	NA
Th	13.9	18.0	NA	NA	5.1	9.3	13.7	14.6	13.5	16.4	13.1
Hf	4.9	5.7	NA	NA	4.5	4.8	5.1	5.4	4.8	5.5	4.1
Ba	1232	1472	NA	NA	569	1067	1140	1187	1206	1216	1006
Rb	166	211	NA	NA	43	113	158	135	153	170	157
Sr	883	132	NA	NA	479	351	303	304	513	241	270
Ta	1.6	1.2	NA	NA	1.6	1.4	1.4	1.3	1.3	1.6	1.0
Sc	6.1	5.1	NA	NA	23.4	21.5	4.9	4.5	4.3	5.3	4.1

Major elements in weight percent.
Total iron as Fe_2O_3.
ABW = Boulder Wash andesite.
DBW = Boulder Wash dacite.
s = Specimen used in models.
NA = not analyzed or not detected.
BBW = Boulder Wash basalt.

TABLE 3. MAJOR ELEMENT MODELS

Model Number	Phases added or subtracted* cpx	hn	plag	ol	kspar	qtz	biotite	mixed component	R	T	r
1 RM(226-227)	.....	28.70	12.30	.....	.....	.....	.....	30.1(WR57)	0.73	0.41	1.69
2	.....	29.30	12.00	.....	.....	.....	.....	19.8(WR59)	0.48	0.41	1.90
3	.....	32.90	12.10	.....	.....	.....	.....	.....	.....	0.45	3.37
4 RM(230-229)	.....	16.10	13.60	.....	.....	.....	.....	13.3(WR57)	0.46	0.29	1.94
5	.....	16.30	12.60	.....	.....	.....	.....	8.7(WR59)	0.30	0.29	2.02
6	.....	18.50	12.10	.....	.....	.....	.....	.....	.....	0.31	2.40
7 RM(222-223)	.....	22.80	19.20	.....	.....	.....	.....	28.1(WR57)	0.69	0.41	5.29
8	.....	23.90	20.40	.....	.....	.....	.....	10.4(WR59)	0.24	0.44	5.45
9	.....	25.70	22.60	.....	.....	.....	.....	.....	.....	0.48	5.57
10 RM(218-226)	19.45	.....	0.54	.....	.....	.....	.....	42.4(WR57)	2.12	0.20	7.26
11	16.58	.....	5.7 An	.....	.....	.....	.....	28.9(WR57)	0.76	0.38	2.71
	.....	.....	+15.7 Ab	.....	.....	.....	.....	.....	.....	.....	.....
12	26.70	+32.3	3.6 An	.....	.....	.....	.....	48.0(WR57)	0.83	0.58	1.37
	.....	.....	+21.4 Ab	.....	.....	.....	.....	.....	.....	.....	.....
13	33.00	.....	18.50	.....	.....	.....	.....	.....	.....	0.52	55.70
14 RM(218-230)	7.30	.....	22.60	18.40	.....	.....	.....	53.3(WR59)	1.11	0.48	11.57
15 RM(218-222)	23.20	.....	.....	0.96	.....	.....	.....	53.8(WR57)	2.24	0.24	3.84
16 WR(57-33)	.....	34.60	.....	.....	+10.52	+22.9	.....	.....	.....	0.40	3.61
17	.....	25.70	.....	.....	+13.2	2.40	.....	188 (WR59)	4.95	0.38	3.52
18 WR(218-57)	20.30	.....	25.90	9.90	.....	.....	.....	.....	.....	0.56	34.40
19	21.70	.....	8.47	.....	.....	.....	.....	.....	.....	0.32	6.85
20	20.80	.....	8.90	.....	.....	.....	.....	31.3(WR57)	1.04	0.30	6.14
21 HD(BH10-84-4)	.....	5.00	15.00	.....	.....	.....	3.00	.....	.....	0.23	2.10

R = mass ratio of the mixed component/crystallizing phase
T = total phenocrysts relative to initial mass of magma
r = sum of squares of the residuals
*All numbers are negative except those values preceded by + sign.

TABLE 4. MINERAL COMPOSITIONS USED IN MAJOR ELEMENT MODELS

Oxides in weight percent	Hornblende*	Biotite†	Biotite*	Andesite†	Labradorite†	Orthoclase†	Quartz†	Clinopyroxene*	Olivine*
SiO_2	43.5	39.14	36.14	58.1	52.96	64.46	99.99	51.83	38.00
Al_2O_3	11.29	13.1	12.88	26.44	29.72	18.55	0	2.29	0.02
Fe_2O_3	13.05	17.99	16.38	0	0	0.14	0	7.75	22.12
CaO	11.17	1.64	0.00	7.84	13.28	0.17	0	20.28	0.12
MgO	12.77	12.65	13.77	0	0	0.00	0	16.40	39.11
MnO	2.65	0.7	0.98	6.7	4.21	0.49	0	0.35	0.01
K_2O	0.73	6.55	8.39	1.1	0.1	16.07	0	0.00	0.00
TiO_2	3.55	4.27	7.27	0.00	0	0.00	0	0.63	0.00

*Mineral analyses from volcanic rocks of the Hamblin-Cleopatra volcano (Thompson, 1985).
†Mineral analyses from Deer and others (1972).

REFERENCES CITED

Anderson, R. E., 1971, Thin skin distension in Tertiary rocks of southeastern Nevada: Geological Society of America Bulletin, v. 82, p. 42–58.

——, 1973, Large-magnitude late Tertiary strike-slip faulting north of Lake Mead, Nevada: U.S. Geological Survey Professional Paper 794, 18 p.

Anderson, R. E., 1978, Geologic map of the Black Canyon 15° quadrangle, Arizona and Nevada: U.S. Geological Survey map GQ–1394.

Anderson, R. E., Longwell, C. R., Armstrong, R. L., and Marvin, R. F., 1972, Significance of K-Ar ages of Tertiary rocks from the Lake Mead region, Nevada–Arizona: Geological Society of America Bulletin, v. 83, p. 273–287.

Arth, J. G., 1976, Behavior of trace elements during magmatic processes; A summary of theoretical models and their applications: U.S. Geological Survey Journal of Research, v. 4, no. 1, p. 41–47.

Bacon, C. R., 1986, Magmatic inclusions in silicic and intermediate volcanic rocks: Journal of Geophysical Research, v. 91, no. B6, p. 6091–6112.

Bell, J. W., and Smith, E. I., 1980, Geological map of the Henderson Quadrangle, Clark County, Nevada: Nevada Bureau of Mines and Geology Map 67, scale 1:24,000.

Campbell, I., and Schenk, E. T., 1950, Camptonite dikes near Boulder Dam, Arizona: American Mineralogist, v. 35, no. 9–10, p. 671–692.

Carmichael, I.S.E., Turner, F. J., and Verhoogen, J., 1974, Igneous petrology: New York, McGraw Hill Book Company, 739 p.

Christiansen, R. L., and Lipman, P. W., 1972, Cenozoic volcanism and plate-tectonic evolution of the western United States; 2, Late Cenozoic: Philosophical Transactions of the Royal Society of London, series A, v. 271, p. 249–284.

Condie, K. C., Viljoen, M. J., and Kable, E.J.D., 1977, Effects of alteration on element distributions in Archaean tholeiites from the Barberton greenstone belt, South Africa: Contributions to Mineralogy and Petrology, v. 64, p. 75–89.

Deer, W. A., Howie, R. A., and Zussman, J., 1972, An introduction to the rock forming minerals: London, Longman Group Limited, 528 p.

DePaulo, D. J., 1981, Trace element and isotopic effects of combined wall-rock assimilation and fractional crystallization: Earth and Planetary Science Letters, v. 53, p. 189–202.

Eaton, G. P., 1982, The Basin and Range Province; Origin and tectonic significance: Annual Review of Earth and Planetary Sciences, v. 10, p. 409–440.

Elston, W. E., and Bornhorst, T. J., 1979, The Rio Grande rift in context of regional post-40 m.y. volcanic and tectonic events, *in* Riecker, R. E., ed., Rio Grande Rift; Tectonics and magmatism: Washington, D.C., American Geophysical Union, p. 418–438.

Feuerbach, D. L., 1986, Geology of the Wilson Ridge pluton; A mid-Miocene quartz monzonite intrusion in the northern Black Mountains, Mohave County, Arizona and Clark County, Nevada [M.S. thesis]: Las Vegas, University of Nevada, 79 p.

Feuerbach, D. L., and Smith, E. I., 1986, The mid-Miocene Wilson Ridge pluton; A subvolcanic intrusion in the Lake Mead region, Arizona and Nevada: EOS (Transactions of the American Geophysical Union), v. 67, no. 44, p. 1262.

——, 1987, Late Miocene Fortification Hill basalt, Lake Mead area, Nevada and Arizona: Source area and conduit geometry: Geological Society of America Abstracts with Programs, v. 19, p. 376–377.

Herrmann, A. G., Potts, M. J., and Knake, D., 1974, Geochemistry of the rare earth elements in spillites from the oceanic and continental crust: Contributions to Mineralogy and Petrology, v. 44, p. 1–16.

Hildreth, W., 1981, Gradients in silicic magma chambers; Implications for lithospheric magmatism: Journal of Geophysical Research, v. 86, p. 10153–10192.

Hildreth, W., and Mahood, G., 1985, Correlation of ash-flow tuffs: Geological Society of America Bulletin, v. 96, p. 968–974.

Irvine, T. N., and Baragar, W.R.A., 1971, A guide to the chemical classification of the common volcanic rocks: Canadian Journal of Earth Sciences, v. 8, p. 523–548.

Koyaguchi, T., 1986, Textural and compositional evidence for magma mixing and its mechanism, Abu volcano group, southwestern Japan: Contributions to Mineralogy and Petrology, v. 93, p. 33–45.

Langmuir, C. H., Vocke, R. D., Jr., Hanson, G. H., and Hart, S. H., 1978, A general mixing equation with applications to Icelandic basalts: Earth and Planetary Science Letters, v. 37, p. 380–392.

Lipman, P. W., Prostka, H. J., and Christiansen, R. L., 1972, Cenozoic volcanism and plate-tectonic evolution of the western United States; 1, Early and middle Cenozoic: Philosophical Transactions of the Royal Society of London, series A, v. 271, p. 217–248.

Ludden, J. N., and Thompson, G., 1979, An evaluation of the behaviour of the rare-earth elements during weathering of sea-floor basalt: Earth and Planetary Science Letters, v. 43, p. 85–92.

McMillan, N. J., and Dungan, M. A., 1986, Magma mixing as a petrogenetic process in the development of the Taos Plateau Volcanic Field, New Mexico: Journal of Geophysical Research, v. 91, no. B6, p. 6029–6045.

Martin, R. F., Whitley, J. E., and Wooley, A. R., 1978, An investigation of rare-earth mobility; Fenitized quartzite Borralan complex, N.W. Scotland: Contributions to Mineralogy and Petrology, v. 66, p. 66–73.

Mattison, S. R., Vogel, T. A., and Wilband, J. T., 1986, Petrochemistry of the silicic-mafic complexes at Vesturhorn and Austurhorn, Iceland; Evidence for zoned/stratified magma: Journal of Volcanology and Geothermal Research, v. 28, p. 197–223.

Mills, J. G., 1985, The geology and geochemistry of volcanic and plutonic rocks in the Hoover Dam 7½ Quadrangle, Clark County, Nevada, and Mohave County, Arizona [M.S. thesis]: Las Vegas, University of Nevada, 119 p.

Naumann, T. R., 1987, Geology of the central Boulder Canyon Quadrangle, Clark County, Nevada [M.S. thesis]: Las Vegas, University of Nevada, 68 p.

Naumann, T. R., and Smith, E. I., 1987, Evidence for magma mixing in Mid-Tertiary volcanic rocks, Lake Mead region, southern Nevada: Geological Society of America Abstracts with Programs, v. 19, p. 435–436.

Otton, J. K., 1982, Tertiary extensional tectonics and associated volcanism in west-central Arizona, *in* Frost, E. G., and Martin, D. L., eds., Mesozoic-Cenozoic tectonic evolution of the Colorado River region, California, Arizona, and Nevada: San Diego, California, Cordilleran Publishers, p. 143–157.

Smith, E. I., 1982, Geology and geochemistry of the volcanic rocks in the River Mountains, Clark County, Nevada, and comparisons with volcanic rocks in nearby areas, *in* Frost, E. G., and Martin, D. L., eds., Mesozoic-Cenozoic tectonic evolution of the Colorado River region, California, Arizona, and Nevada: San Diego, California, Cordilleran Publishers, p. 41–54.

——, 1984, Geological map of the Boulder Beach Quadrangle, Nevada: Nevada Bureau of Mines and Geology Map 81, scale 1:24,000.

Smith, E. I., Schmidt, C. S., and Weber, M. E., 1986, Mid-Tertiary volcanic rocks of the McCullough Range, Clark County, Nevada: Geological Society of America Abstracts with Programs, v. 18, p. 187.

Smith, E. I., Eschner, E., Feuerbach, D. L., Naumann, T. R., and Sewall, A., 1987, Mid-Tertiary extension in the eastern Basin and Range Province, Nevada and Arizona; The Las Vegas Valley–Detrital Wash transect: Geological Society of America Abstracts with Programs, v. 19, p. 848–849.

Stormer, J. C., Jr., and Nicholls, J., 1978, XLFRAC: A program for the interactive testing of magmatic differentiation models: Computers and Geoscience, v. 4, p. 143–159.

Suneson, N. H., and Lucchitta, I., 1983, Origin of bimodal volcanism, southern Basin and Range province, west-central Arizona: Geological Society of America Bulletin, v. 94, p. 1005–1019.

Thompson, K. G., 1985, Stratigraphy and petrology of the Hamblin-Cleopatra

volcano, Clark County, Nevada [M.S. thesis]: Austin, University of Texas, 306 p.

Thompson, R. A., Dungan, M. A., and Lipman, P. W., 1986, Multiple differentiation processes in early-rift calc-alkalic volcanics, northern Rio Grande Rift, New Mexico: Journal of Geophysical Research, v. 91, no. B6, p. 6046–6058.

Vocke, R. D., Hanson, G. N., and Gruenenfelder, M., 1979, The effects of low temperature metasomatism on REE distributions in the Roffna Gneiss, Switzerland: EOS (Transactions of the American Geophysical Union), v. 60, p. 425.

Weber, M. E., and Smith, E. I., 1987, Structural and geochemical constraints on the reassembly mid-Tertiary volcanoes in the Lake Mead area of southern Nevada: Geology, v. 15, p. 553–556.

MANUSCRIPT SUBMITTED AUGUST 26, 1987.
REVISED MANUSCRIPT SUBMITTED JANUARY 4, 1988
MANUSCRIPT ACCEPTED BY THE SOCIETY FEBRUARY 7, 1989

Printed in U.S.A.